University of Stavanger

FACULTY OF SCIENCE AND TECHNOLOGY

MASTER'S THESIS

Study Program/ Specialization: Structures and Materials	Spring semester, 2021 Open / ~~Confidential~~
Author: Bo Wang and Yuping Zhong	
Supervisor: Associate Prof. Yanyan Sha	
Title of master's thesis: Analysis of a semi-submersible floating offshore wind turbine subjected to ship collisions	
Credits (ECTS): 30	
Key words: Floating offshore wind turbine, ship collision, strain rate, reinforced concrete structure, dynamic response	Number of Pages:135 Stavanger, June, 2021

Abstract

Wind energy has enormous potential in reducing greenhouse emissions and curbing global warming. The number of installed offshore wind turbines has been continuously growing worldwide in recent years. Since offshore farms are usually located near the coast and close to the main traffic routes, they are at the risk of collisions with ships, which usually causes casualties and severe economic losses. Therefore, it is essential to analyze the structural responses of the wind turbine subjected to ship collision. However, there is limited literature about floating offshore wind turbine (FOWT) collisions with the ship, especially the semi-submersible floating offshore wind turbine. In order to fill the knowledge gap, a series of local and global numerical analyses are conducted in this thesis to study the collision between a semi-submersible FOWT and the vessel.

The LIFES50+ OO-Star wind floater is modelled in LS-DYNA for the local analyses. The local analyses focus on the structural responses, such as force-displacement relationship, structural deformations, effective stress as well as plastic strain. Numerous scenarios, such as various thick walls of concrete wall (0.5 m and 1 m concrete walls), initial speeds of the ship (2.5 m/s, 5 m/s, 7.5 m/s, 10 m/s), collision angles (0 degrees and 45 degrees), collision positions (top, top1, still water level and bottom) and strain rates of ship shell (has or does not have strain rate), are conducted for the local impact analyses. The results show that the ship with an initial speed of 2.5 m/s can destroy the 0.5 m concrete wall, and the ship with an initial speed of 10 m/s can damage the 1 m concrete wall. When the forecastle of the ship is higher than the top of a column, the ship can damage the concrete wall with a 7.5 m/s initial speed. When a bulb of the ship with the initial velocity of 5 m/s impacts the conical structure of the column, the conical structure can be destroyed. When the ship with an initial velocity of 7.5 m/s impacts the 1 m concrete wall, the ship can be fractured on the side. In addition, when ship and concrete are under the strain rate, the strength of concrete and ship can be improved significantly. Moreover, the force-displacement curves from the results of local analyses are applied to the subsequent global analysis.

The DTU 10 MW wind turbine and LIFES50+ OO-Star wind floater are modeled in OrcaFlex for global analyses. The eigenfrequency and free decay tests are carried out for model verification. Depending on the wind turbine condition (parked or operating), ship's type (8800-

ton supply vessel or 20000-ton shuttle), collision type (head-on bow or sideway), collision direction, collision location, collision speed, multiple scenarios are conducted. As a result, the nacelle acceleration, tower stress, tower clearance, strain energy, force and displacement, and mooring force are obtained. The nacelle acceleration, in general, exceeds the limitation in both parked conditions and operating conditions. Since the tower stress and mooring force may exceed the limit, wind turbines are more dangerous when hit by the ship under operating conditions. The impact of the simple and fine force-displacement curves is discussed, and the finer curve shall be used to obtain more accurate results. In addition, the influence of collision location, including horizontal offset and vertical offset, is investigated. The situation is safer when the collision is not centric, or the ship impacts the wind turbine with only the forecastle or bulb. At last, the collision in the cut-out conditions is also carried out.

Acknowledgement

We would like to give our sincere gratitude to our supervisor, Associate Prof. Yanyan Sha, for his guidance, extraordinary patience, and consistent encouragement during the master's thesis. He provided us with necessary materials, advice of great value, and inspiration for new ideas.

Special thanks should go to the technical staff of Orcina Ltd for their great help and professional advice about OrcaFlex. We would like to thank our dear friends and classmates during our two year's study here. You really make Stavanger a wonderful place to stay. Finally, we thank our parents for their unconditional love and encouragement. Without their support, we would not have the opportunity to study at the University of Stavanger and complete this thesis.

Table of contents

Innholdsfortegnelse

List of figures

List of tables

Nomenclature

Variable	Unit	Description
a_i	kg	Added mass of installation
a_s	kg	Added mass of approaching vessel
A	m^2	Rotor swept area
c		Reduced buckling coefficient
C		Damping matrix
C_d		Drag coefficient
C_m		Mass coefficient
c_p		Power coefficient
D	m	Diameter of tower
d	m	Radius of mooring chain
E	Pa	Young's modulus
$E_{s,i}$	J	Strain energy of installation
$E_{s,s}$	J	Strain energy of vessel
E_s	J	Strain energy
E_v	J	approaching ship energy
F	N	External loads
F_x^{2D}	N	Morrison force
f_c'	MPa	Static Uniaxial Compressive Strength
f_c	MPa	Dynamic Tensile Strength
f_{cs}	MPa	Static Compressive Strength
f_{cu}	MPa	Static Cube Strength
f_e	Pa	Elastic buckling strength of an unstiffened circular cylindrical shell
f_t	MPa	Dynamic Tensile Strength
f_{ts}	MPa	Static Tensile Strength
f_y	MPa	Steel Yield Strength
R	m	Cylinder radius
t	cm	Thickness
U	m/s	Flow velocity
$\dot{U}$	m/s^2	Flow acceleration
u	m/s	Wind speed

v_i	m/s	Speed of installation
v_s	m/s	Speed of approaching vessel
V	m/s	Velocity of ship and installation after collision
v		Passion ratio
$\ddot{x}$	m/s^2	Nodal acceleration
$\dot{x}$	m/s	Nodal velocity
x	m	Nodal displacement
Z_l		Curvature parameter
$\dot{\varepsilon}$		Strain Rate
$\sigma_{eq,cr}$	Pa	Characteristic buckling strength of a shell
$\sigma_{x,sd}$	Pa	Design axial stress
$\sigma_{b,sd}$	Pa	Design bending stress
σ_{xE}	Pa	Elastic buckling strength for axial force
σ_{bE}	Pa	Elastic buckling strength for bending moment
σ_y	Pa	Yield strength for material
$\sigma_{eq,E}$	Pa	Design equivalent von mises stress
η		Coefficient
λ_{eq}		Coefficient
ψ		Coefficient
ξ		Coefficient
ρ	kg/m^3	Density

Abbreviation

Abbreviation	Full name
ALS	Accidental Limit State
CoM	Center of Mass
DIF	Dynamic Increasing Factor
DoF	Degree of freedom
DTU	Technical University of Denmark
DWT	Deadweight Tonnage
FEA	Finite Element Analysis
FEM	Finite Element Method
FOWT	Floating Offshore Wind Turbine
LCBS	Large-scale Composite Bumper System
MSL	Mean Sea Level
OSV	Offshore Supply Vessel
OWT	Offshore Wind Turbine
RC	Reinforced Concrete
rpm	Rounds per minute
SWL	Still water level
ULS	Ultimate Limit State

Chapter 1 Introduction

1.1 Wind energy

As one of the renewable energy sources with enormous potential, wind power plays a key role against global warming and counterbalances greenhouse gas emissions. The EU is committed to climate neutrality by 2050. According to WindEurope, Europe's wind farms generated 458 TWh of electricity in 2020, meeting 16% of the electricity demand in Europe (EU27+UK). Denmark is the country with the highest share of wind energy in their electricity mix with 48%, followed by Ireland (38%), Germany (27%), the UK (27%), Spain (22%), and Portugal (25%). Wind energy has been continuously increasing in the last few decades. According to IEA, in 2019, onshore wind electricity generation increased by an estimated 12% and is expected to increase to 3749 TWh by 2030 (IEA, 2020). Offshore wind electricity increased rapidly in recent years, with an increase of 32% in 2017 and 20% in 2018, and it is expected to increase to 606 TWh by 2030 (IEA, 2020). IEA's analysis showed that the best close-to-shore offshore wind sites could provide almost 36000 TWh globally per year, nearly equal to global electricity demand in 2040.

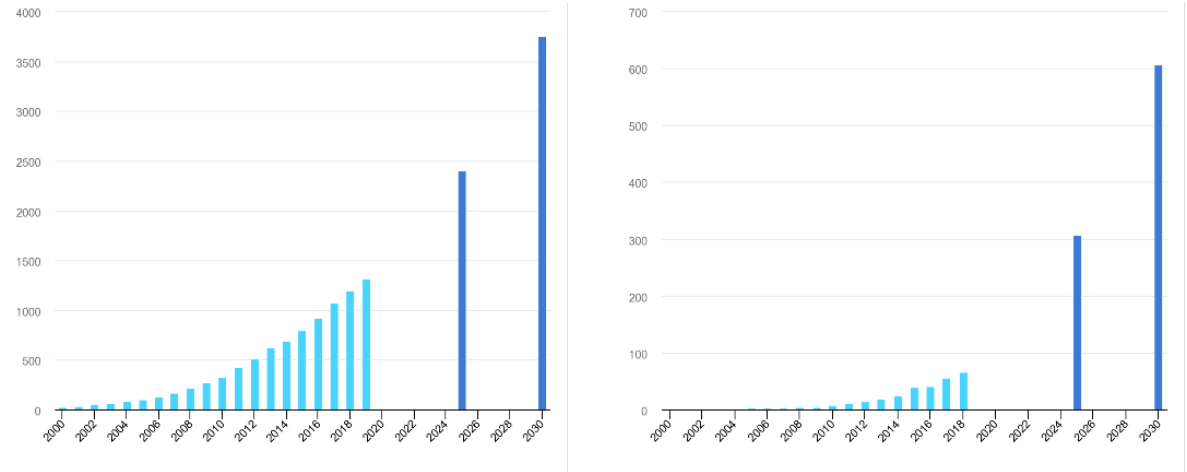

Figure 1-1: Onshore (left) and offshore (right) wind power generation Scenario, 2000-2030 (IEA, 2020)

Wind energy installation in Europe decreased by 6% compared to 2019 due to the covid-19 pandemic, 14.7 GW of new wind capacity added in 2020. The Netherlands installed the most wind power with a capacity of 1.98 GW in 2020, followed by Germany (1.65 GW), Norway (1.53 GW), Spain (1.4 GW), and France (1.32 GW). The installed capacity of wind power in Europe has now reached 220 GW by the end of 2020.

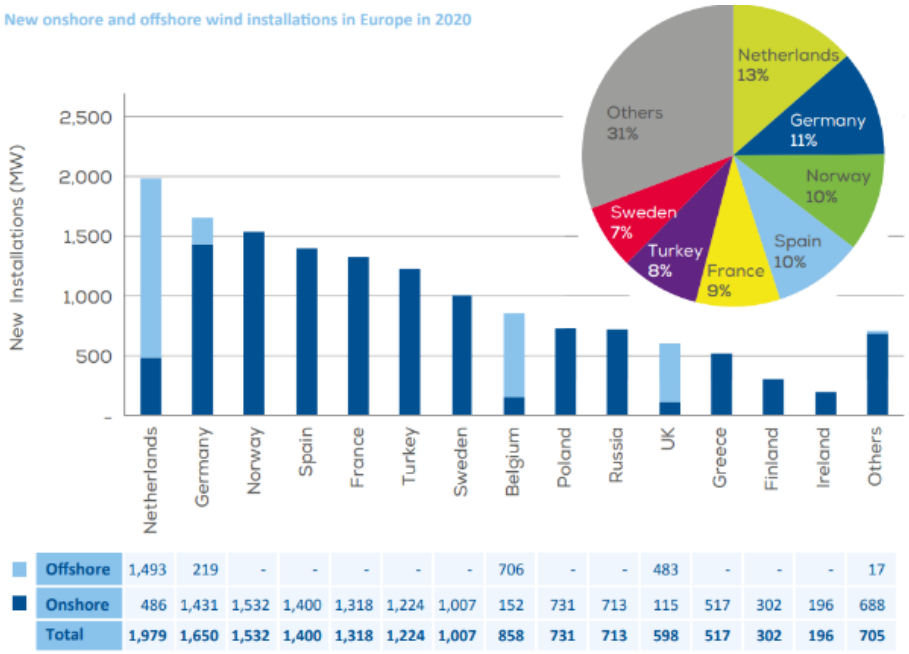

Figure 1-2 New onshore and offshore wind installation in Europe in 2020 (WindEurope, 2020)

Europe added 11.8 GW onshore wind power capacity during 2020, accounting for 80% of the new installed capacity. Norway installed the most onshore wind power capacity in 2020 (1.5 GW), followed by Germany (1.4 GW), Spain (1.4 GW), and France (1.3 GW). Europe now has 194 GW of installed onshore wind power capacity.

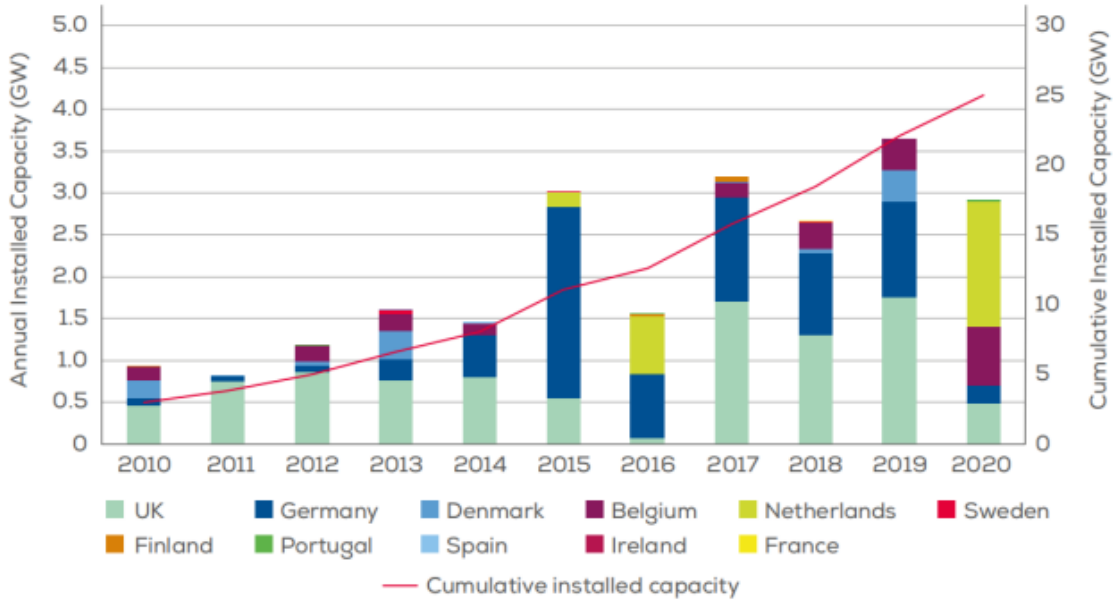

Figure 1-3 Annual offshore wind installation in Europe by country (left axis) and cumulative capacity (right axis) (WindEurope, 2020)

Europe added 2.9 GW of offshore wind power capacity during 2020, a 20% decrease in 2019, the Netherlands installed the most offshore wind power capacity in 2020 (1.49 GW), accounting for 75% of the new installation, followed by Belgium (706 MW), the UK (483 MW) and Germany (219 MW). Europe saw 356 new offshore wind turbines connected to the grid for electricity generation, nine new wind farms completed in 2020, and one wind farm has been partially grid-connected and will be fully commissioned in 2021. In addition, the construction work of six other wind farms has started. The total installed offshore wind capacity in Europe is now 25 GW, 5402 wind turbines, and 116 offshore wind farms across 12 countries have been grid-connected. The UK has the largest offshore wind capacity in Europe, accounting for 42% of all installations. This is followed by Germany (31%), the Netherlands (10%), Belgium (9%), and Denmark (7%).

In 2021-2025, Europe is expected to install 105 GW of new wind power. The UK is expected to install the most wind energy with a capacity of 18 GW, most of which will be offshore. Germany is expected to add a similar amount of wind power, most of which will be onshore. This is followed by France, Sweden, and the Netherlands.

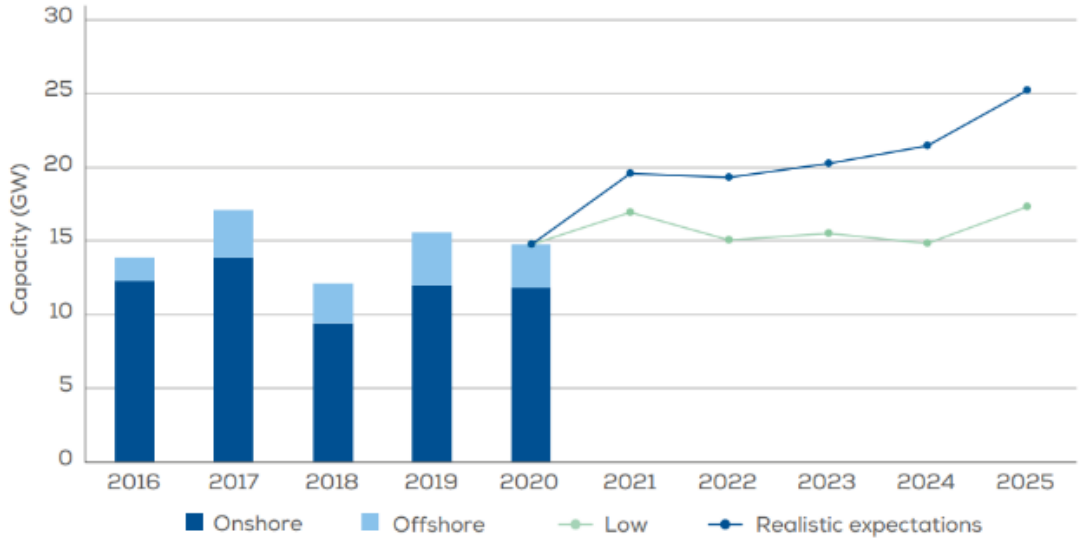

Figure 1-4 2021-25 new onshore and offshore wind installation in Europe (WindEurope, 2020)

Offshore wind power is growing rapidly. Europe is expected to install 29 GW of new offshore wind over the next five years, and the annual installation rate will almost double from 3 GW to 5.8 GW. According to the Offshore Renewables Energy Strategy (ORES), the EU's ambition to build 300 GW of offshore wind by 2050 (Ramírez et al., 2020). Figure 1-5 shows offshore

wind turbine is going further and bigger. Onshore wind turbine usually has a limited size due to matter of space and blade transportation. Besides, the average wind speed is generally larger for offshore. The limited size and lower wind speed result in less electricity production. As shown in Equation (1-1), a doubling of the rotor diameter and wind speed leads to a four-times and eight-time increase in power output, respectively. Moreover, visual and noise issues also limit the onshore wind turbine. Compared with the onshore wind turbine, the offshore wind turbine has greater wind speed and larger size. In 2020, the average power rating of newly installed wind turbines in Europe was 3.3 MW for onshore and 8.2 MW for offshore. Finland installed the most powerful onshore wind turbines with an average rating of 4.5 MW. The Netherlands and Belgium had the most powerful new offshore turbines with an average rating of 8.7 MW.

$$P = \frac{1}{2} C_P \rho A u^3 \tag{1-1}$$

Where, P is power extracted from the airflow, C_p is power coefficient, A is the rotor swept area, and u is wind speed.

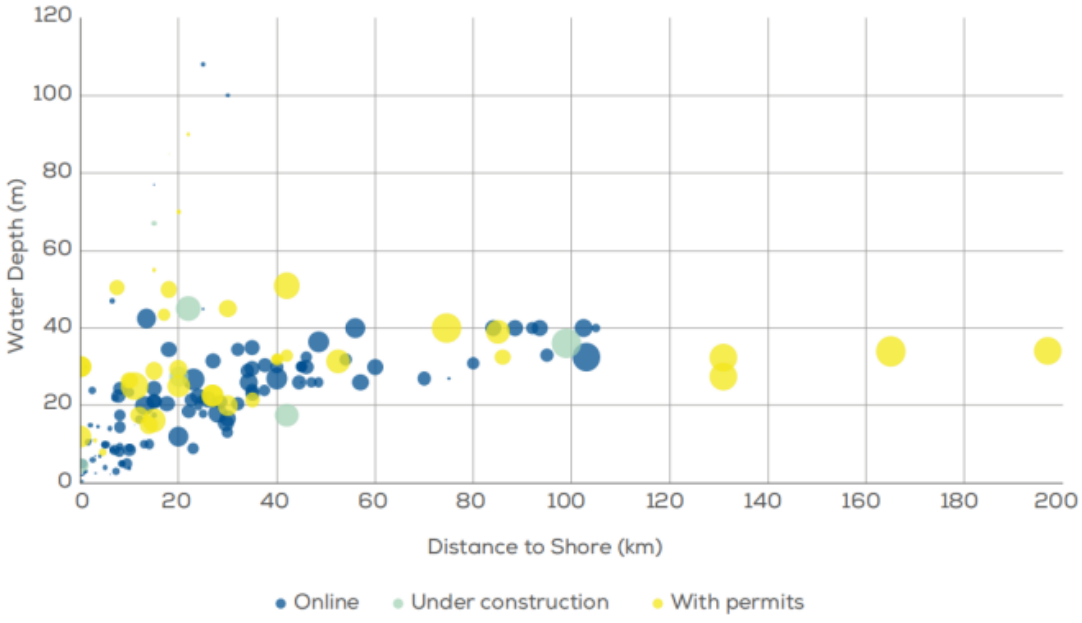

Figure 1-5 Average water depth and distance to shore of all offshore wind farms in Europe, the size of the bubble indicates the overall capacity of the site (WindEurope, 2020)

Offshore wind turbines have been continuously growing in power. Since 2015 turbines have grown at a constant 16% rate. Turbine orders in 2020 already show a trend towards the next generation in size, with turbines ranging from 10 to 13 MW for projects coming online after 2022 (Ramírez et al., 2020). Floating wind turbine is a new trend for offshore wind, with 30

MW Hywind project in Scotland and 24 MW Atlantic project in Portugal, Europe is the global technology leader for floating offshore wind turbine with a capacity of 62 MW by the end of 2020, accounting for 83% of the global floating wind capacity. Though it represents a small share of total offshore installations, it has enormous potential according to WindEurope that Europe has an exceptionally high potential for floating wind turbine with a capacity of 4000 GW, it is expected that 7 GW and 150 GW of floating offshore wind can be installed in Europe by 2030 and 2050, respectively, as many as one-third of all offshore wind installation could be floating.

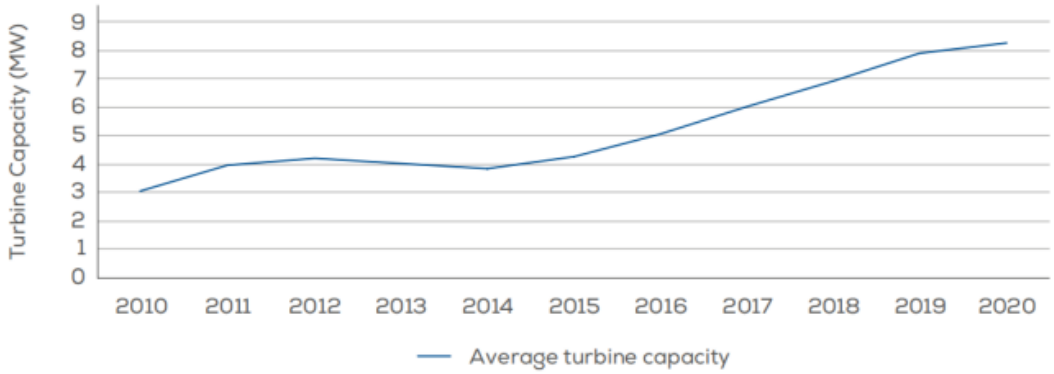

Figure 1-6 Yearly average of newly installed offshore wind turbine rated capacity (WindEurope, 2020)

1.2 Offshore wind turbine

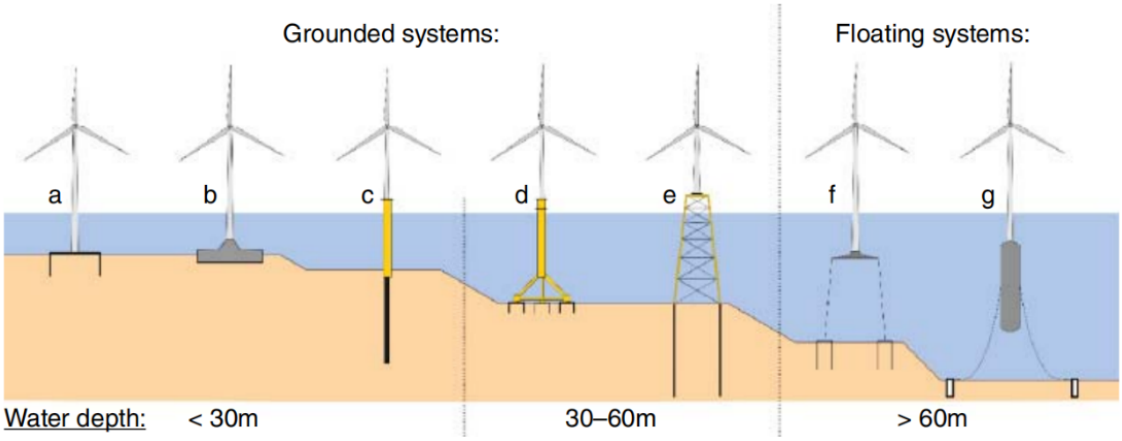

Figure 1-7 Offshore wind turbine substructure system (Bhattacharya, 2019)

The offshore wind turbine can be categorized as the grounded system and floating system. Bottom-fixed wind turbine dominant when water depth less than 60 m. Monopile, gravity-based and suction caissons are primally used for water depth less than 30 m, for water depth

between 30 and 60 m, jackets, tripods are used. The floating system, such as semi-submersible, spar-buoy, tension leg platform, is mainly used when water depth larger than 60 m, cost is the main aspect be considered because it increases sharply for the grounded system.

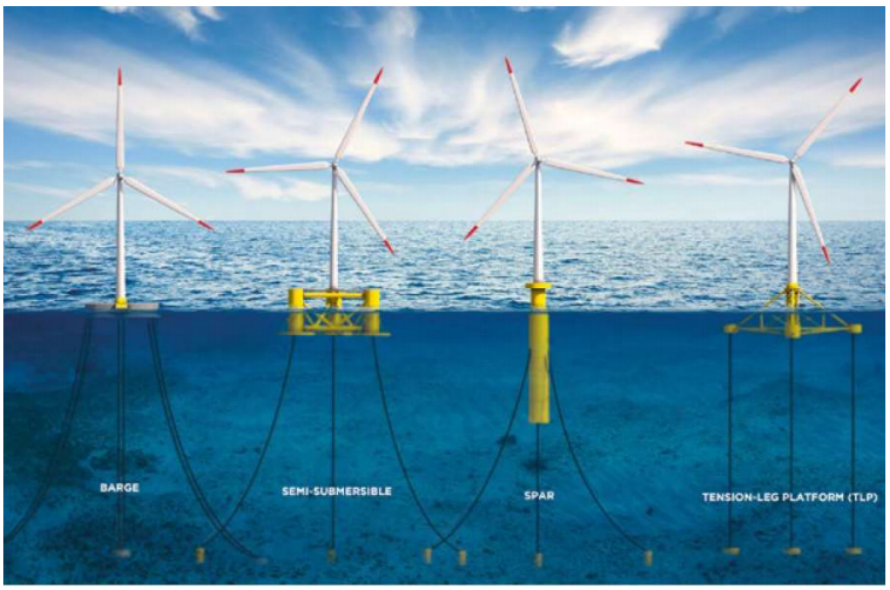

Figure 1-8 Floating wind turbine concepts (WindEurope, 2018)

Spar-buoy has excellent stability, and its simple hull geometry design is amenable to serial fabrication processes and easy to manufacture, but its deep draft requires deep water location and limits its application in shallow water. Figure 1-9 shows the Hywind Scotland, developed by Equinor, has a draught of 78 m.

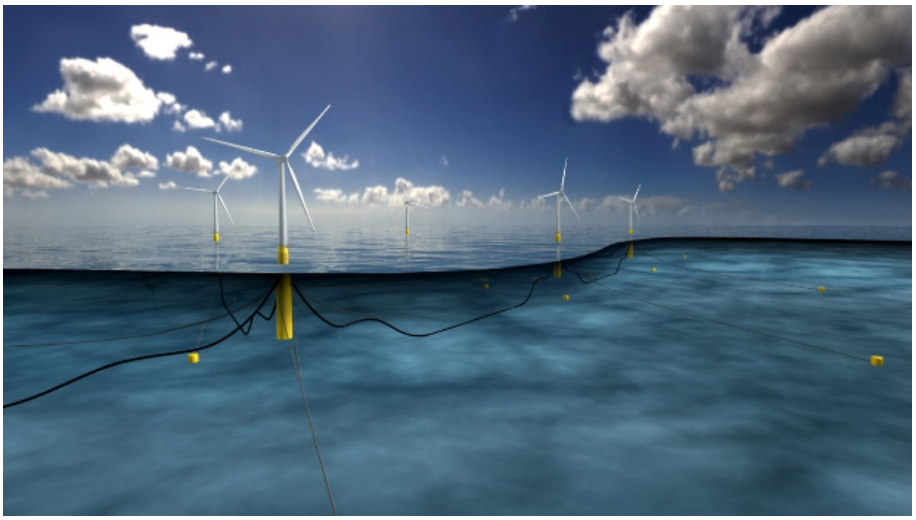

Figure 1-9 Hywind Scotland (Hywind)

Semi-submersible can operate in shallow water depth compared with spar-buoy. Its onshore assemble characteristics make it easy for installation, but it requires high structural mass to

provide sufficient buoyancy and stability, besides, the structure is complex and difficult to manufacture. One example of a submersible floater is the OO-Star wind floater developed by Olav Olsen, shown in Figure 1-10.

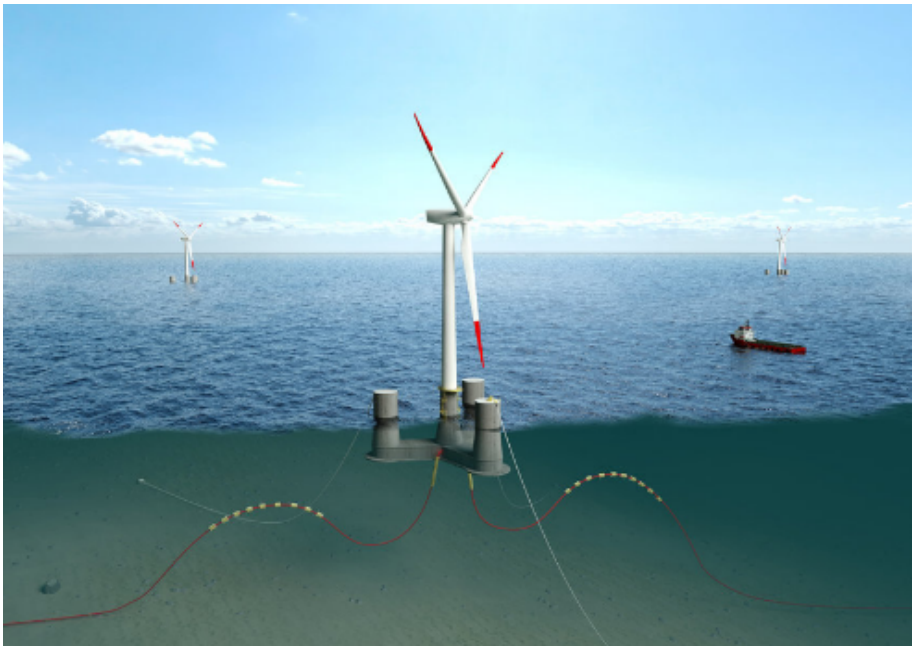

Figure 1-10 The OO-Star wind floater (Olav Olsen, 2017).

The tension-leg platform has excellent stability and low structural mass and can also be assembled onshore. However, the mooring line and anchor system bear the high load and the installation process is challenging.

1.3 Literature review

Floating wind turbines are exposed to the risk of vessel collision. The wind turbine accidents can be significant, resulting not only in technical failures and financial losses, but also and more severely, human injuries and deaths. On 23 April 2020, a collision between a crew transfer vessel and wind turbine was reported at Borkum Riffground offshore wind farm in the German North Sea, resulting in 3 persons injured, including one seriously, and serious damage to the vessel (offshorewind.biz, 2020). Another collision accident between a fishing vessel and wind turbine was reported in 2016 on the Cumbrian coast, resulted in one man injured and the vessel sink (offshorewind.biz, 2016).

The number of collisions has been increasing during the last few decades. 115 collisions in total have been reported on the Norwegian continental shelf with varying degrees of severity

since 1982 and 26 collisions have been reported in the period 2001-2010. Although there was no loss of lives has been reported, the economic loss has been significant (Kvitrud, 2011). According to a report by Caithness Windfarm Information Forum (2021), 737 incidents were reported from UK offshore windfarms during 2016 alone and 44% of medical emergencies were turbine related. The number of wind turbine accidents increases year by year as more and more wind turbines are built. 865 offshore accidents were recorded during 2019, numbers of recorded accidents increase from an average of 57 accidents per year from 2001-2005 inclusive to 184 accidents per year from 2016-2020 inclusive, as shown in Figure 1-11.

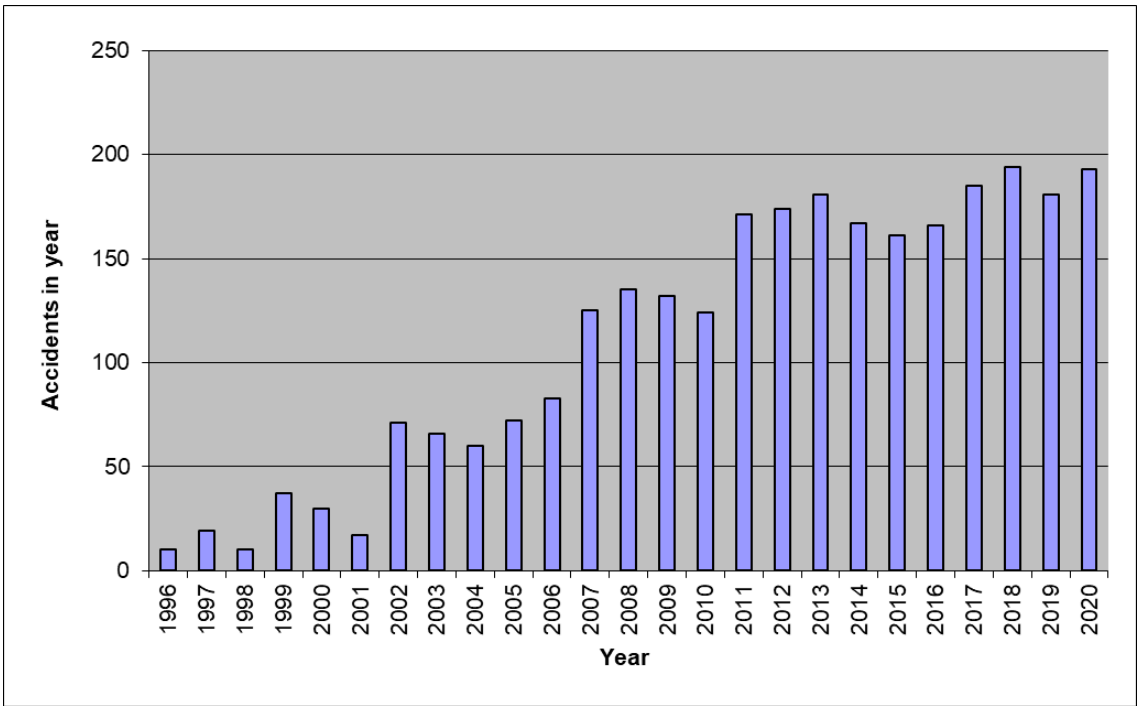

Figure 1-11 Accidents per year (Caithness Windfarm Information Forum, 2021)

Offshore wind turbines are exposed to hazards associated with collisions with either commercial ships or infield support vessels passing closely at high speeds. According to an analysis on wind turbine accidents conducted by Asian (2016), collision is one of the main reasons for wind turbine accidents. Many analyses have been carried out on collisions between the vessel and offshore wind turbine.

Some platforms of FOWT are made entirely of reinforced concrete (RC). Reinforced concrete structure has outstanding characteristics such as corrosion resistance, simple construction and low cost. The collision incidents between ships and offshore installations have been widely studied. Minorsky (1958) did pioneering research on ship-ship collision. The empirical force-

deformation relationship and energy absorption curve are established through experiments. The codes of AASHTO and Eurocode for bridge structure and the code of NORSOK for the offshore structure contain formulae to analyze the ship collision loads. In recently years, nonlinear finite element software, such as LS-DYNA and ABAQUS, have been widely used for offshore collision analysis.

Sha (2019) researched the structural response to simulate the ship forecastle impact bridge. The design considerations of the bridge resisting the collision load of the ship forecastle are discussed from the simulation results. An effective reinforcement way takes advantage of improving the impact resistance of steel bridges. Fang (2016) analyzed the performance evaluation of a large-scale composite bumper system (LCBS) for bridge piers against ship collision. The simulation results showed that LCBS could effectively increase the collision time of the ship and bridge and reduce the peak value of collision forces to non-destructive level, thus leading to a good effect in energy dissipation. The LCBS is a good and effective system against collision between ships and bridges.

Nevertheless, the ship collision against RC structure learning is limited, particularly in the cases of offshore wind turbine (OWT). Furnes and Amdahl (1980) addressed supply ships impacted reinforced concrete walls with similar geometrical and mechanical properties for the oil and gas platforms. It is mentioned that offshore shell structures with thicknesses of more than 0.5 m are not easy to suffer high damage levels when the ship hulls are significantly lower than the stiffness. Moreover, supply vessels with displacements of 2500 t and a velocity from 0.5 m/s to 2 m/s are safe to structures. A 2500 tons ship-tripod wind turbine collision was studied by Han (2019). the damage of the tripod's fender and the dynamic response of offshore wind turbine under the protection of the fender were investigated. The maximum impact force, energy absorbed, the maximum bending moment of the fender, von mises stress, plastic strain, and the thickness of material layer were analyzed. It was found that the aluminum foam fender has a better anti-collision function and the thickness of the material layer makes the difference for the fender of the tripod.

Ding et al. (2014) studied the dynamic response of bucket foundation offshore wind turbine collided by a ship of 5000 deadweight tonnage (DWT) at the speeds of 0.5 m/s, 1 m/s, 1.5 m/s, and 2 m/s. Hao and Liu (2014) investigated and compared the anti-impact performance of three

foundations: monopile, tripod, and jacket. A series of cases were conducted in LS-DYNA. It was found that the jacket has the best comprehensive anti-impact performance because it produces the minimum collision force, damage area, nacelle acceleration as well as moderate bending moment, and steel consumption among the three. Le Sourne (2015) and Bela (2017) investigated the response of offshore wind turbine impacted by a ship, rigid and deformable ship are considered in the articles. It was found that when the OWT is collided with a deformable ship, the deformations of the OWT are 2 times smaller than that of a rigid ship. In addition, the behavior of the wind turbine is highly sensitive to wind loads, in some cases, the wind turbine may collapse when the impact speed is only 3 m/s, and in the worst case, it may fall directly on the ship, posing a real threat to the people on board.

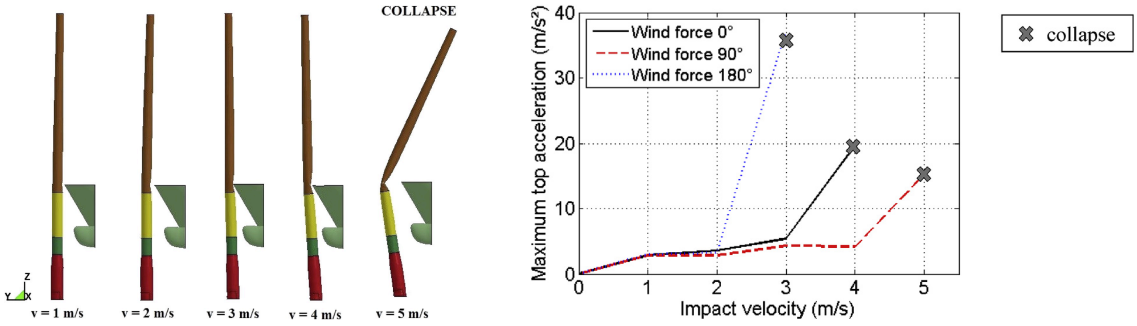

Figure 1-12 Deformed shape of the OWT (Bela, 2017)

Song et al. (2021) studied a monopile-supported 5 MW offshore wind turbine impacted by a 4600-ton ship, a total of 36 cases were conducted. Wind load and direction were considered in this article. It was found that impact velocity and wind direction have a significant impact on the wind turbine response. For wind directions of 0 degrees and 90 degrees, the tower falls into the sea at an impact velocity of 2 m/s. However, the tower fall onto the ship at an impact velocity of 3 m/s for a wind direction of 180 degree, which can be regarded as the most dangerous case because the following impact between the nacelle and the ship deck may cause casualties. The collapse of the tower was caused by structural buckling under the combined load effects of ship impact, wind load, and wind turbine gravity. Ice load also shall be considered according to DNVGL-ST-0119. Song (2019) and Zhou (2019) also investigated the collision between the offshore wind turbine and drifting sea ice.

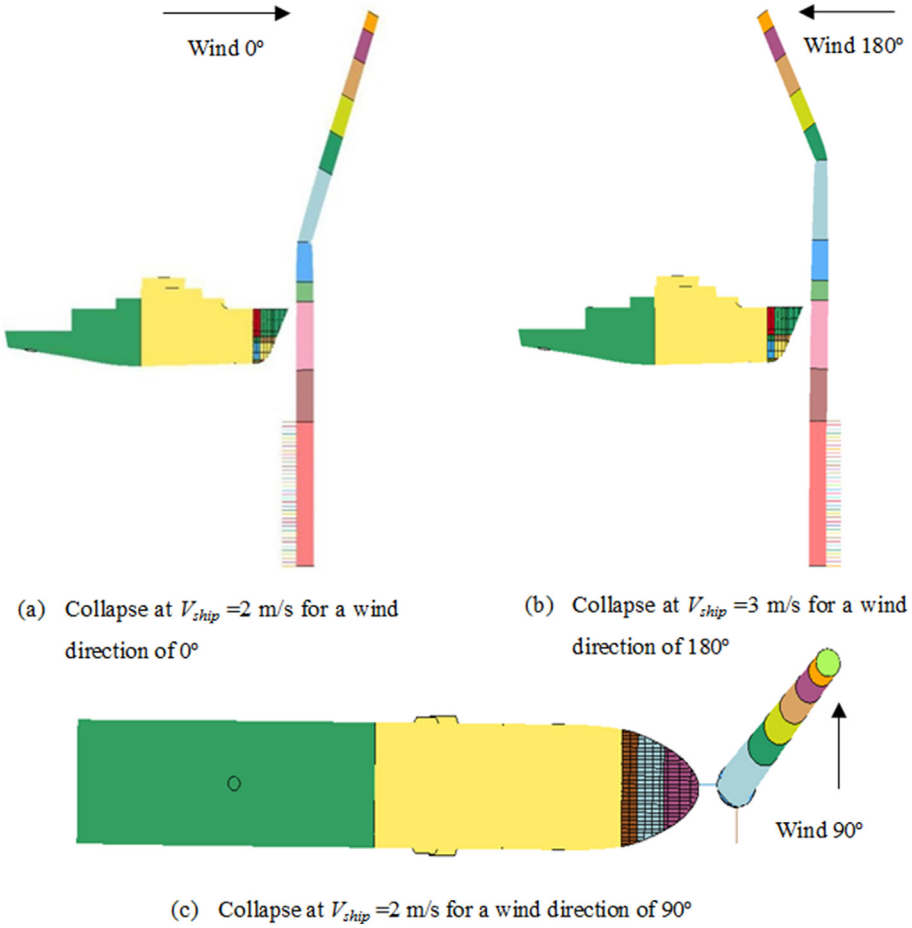

Figure 1-13 Collapse of the OWT (Song et al., 2021)

Pire et al. (2017, 2018) studied a jacket-supported offshore wind turbine impacted by a supply vessel with a mass of 6000 tons. Two types of vessel bows, non-bulbous and bulbous, were considered in this article, as shown in Figure 1-14.

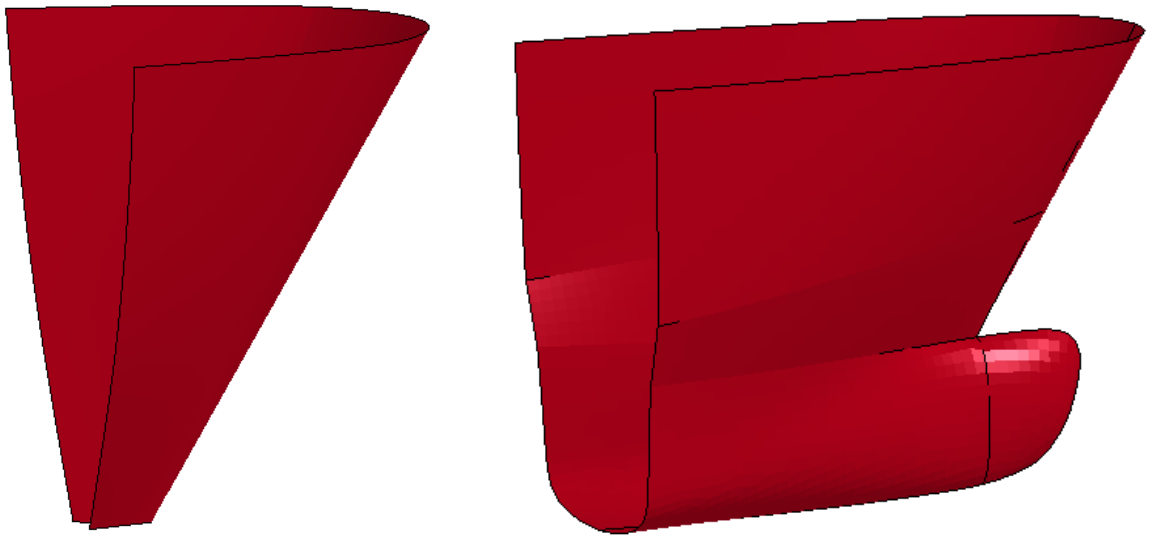

Figure 1-14 Non-bulbous and bulbous bow model (Pire, 2017)

Moulas et al. (2017) investigated monopile-supported and jacket-supported wind turbine stricken by a 4000-ton vessel. Both head on bow collision and sideway collision were considered in this article. Depending on collision direction, collision angle, ship's type, and impact speed, 44 scenarios in total were conducted in ABAQUS. It was found that collision energy is one of the most influencing factors. Most of the research focuses on low-energy collisions. Amdahl and Holmås (2011) studied a jacket foundation offshore wind turbine collided by a high-energy ship. A Suezmax tanker with a mass of 190000 tons drifts to the 5 MW wind turbine at the speed of 2 m/s, which gives kinetic energy more than 500 MJ. He found that the tower may fall toward the ship, and the nacelle may drop onto the ship deck, as shown in Figure 1-15.

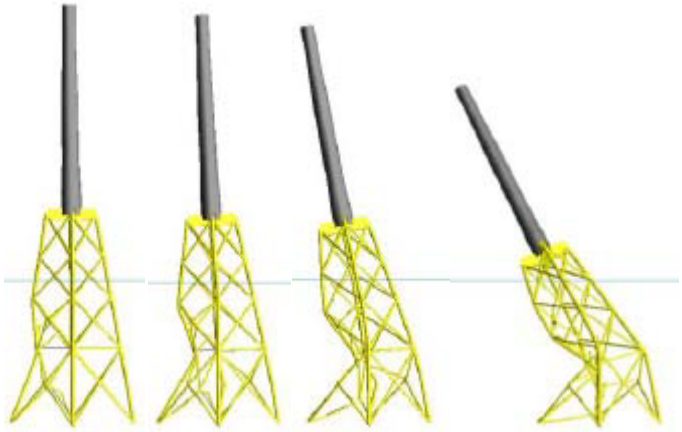

Figure 1-15 Collapse mode of jacket (Amdahl and Holmås, 2011)

The papers above analyzed the collision between the bottom fixed OWT and the vessel. There is limited literature about floating wind turbine collision with the ship (Yu, 2018). Compared with the bottom fixed OWT, there are some unique characteristics in the collision between FOWT and the vessel. First, hydrodynamics is essential for the FOWT, and it has a significant impact on the FOWT motion. Second, The FOWT will drift after the collision, and part of the vessel's kinetic energy will be transferred to the FOWT. Third, Mooring lines are used for station-keeping of the FOWT, thereby it is important to analyze its ability to hold the FOWT. Echeverry et al. (2019) investigated a spar floating offshore wind turbine impacted by a 200000-ton container ship and 6000-ton offshore supply vessel (OSV). It is found that collision with an OSV seems to be most dangerous because the OSV has a displacement comparable to that of the FOWT, it transfers a huge amount of kinetic energy into internal energy, compared to the container ship. Plastic indentation in the collided area, the beamlike elastic response of the overall FOWT, plastic deformation near the ballast level, surge displacement, and turning

pitch moment is the main deformation modes of FOWT. Compared with the bottom-fixed offshore wind turbine, the effect of hydrodynamic force is important when studying the ship-FOWT collision as the floater external dynamics controls the FOWT response. Zhang et al. (2021) studied the dynamic response analysis of a 5 MW spar-type floating wind turbine impacted by a ship and proposed a mathematical model for the external mechanism of the ship-FOWT collision scenario. Three collision cases in still water condition, wave-only condition, and wave-wind combined condition were carried out. To minimize the damage of offshore wind turbines caused by ship impact, Liu et al. (2015) proposed a crashworthy device that contains a rubber blanket and an outer steel shell. The crashworthy device can help to lessen the maximum collision force and nacelle acceleration by absorbing ship energy with structure deformation.

Chapter 2 Theory

This chapter introduces the basic theory, including the finite element method, the software introduction (LS-DYNA and OrcaFlex), external mechanics, internal mechanics, dissipation of strain energy, force-deformation curve, and dynamic equations of motion.

2.1 Finite element method

The finite element method (FEM) has been widely applied in engineering and science. It is a computational tool to solve engineering and scientific problems including fields of heat transfer, fluid flow, structural analysis, mass transport, and electromagnetic potential etc. The process of FEM is given in Figure 2-1. The method takes advantage of mesh generation techniques for dividing a complex problem into small elements to imply the problems. In this paper, finite element models are built to analyze the structural behavior of the floating wind turbine.

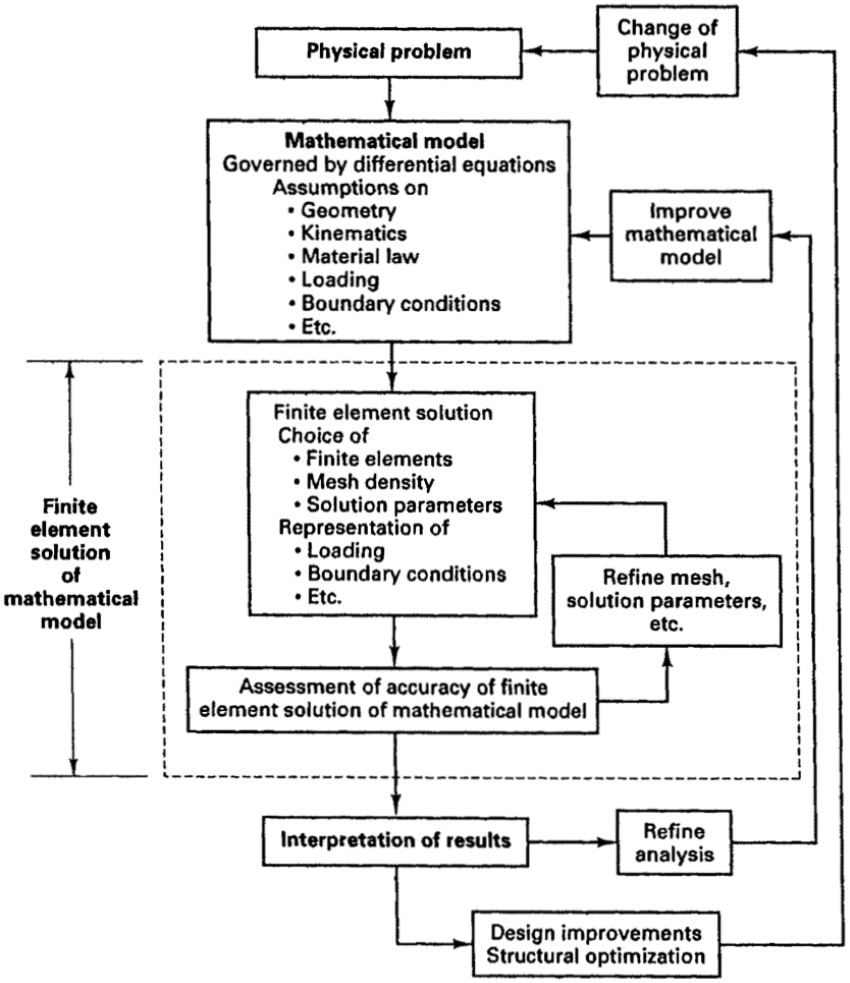

Figure 2-1 The process of finite element analysis (Bathe, 2014)

2.2 Theory of collision

Ships collide with offshore structures is one of the major hazards. Various design codes about ship collision have been established and widely used, such as NORSOK and Eurocode. For example, a comprehensive design standard for calculating accidental loads caused by ship collision from DNV-RP-C204 (2010) was proposed, American Bureau of Shipping (2013) analyzed the unexpected situations encountered during the installation, and the analysis of collision events is based on the simplified empirical model brings up by Minorsky, VU (1958).

In order to study the accident limit state of ship collision, nonlinear finite element technique is used to gain the structural response. These methods consider the use of finite element models of ships and specific devices under study. This paper is about a floating wind turbine, and how they interact by assuming specific contact characteristics.

There are two mechanisms to analyze the collision process. One is external mechanics, which focuses on how much energy has been dissipated into strain energy. The other is internal mechanics, which deals with how the energy dissipated in the impacted and impacted parts is distributed.

For external mechanics, the main principles for calculating how much energy is dissipated as strain energy are momentum conservation and energy conservation (DNV-RP-C204, 2010). The conservation of momentum and energy are shown in Equations (2-1) and (2-2).

$$(\mathrm{m_s} + \mathrm{a_s})\mathrm{v_s} + (\mathrm{m}_i + \mathrm{a}_i)\mathrm{v}_i = (\mathrm{m_s} + \mathrm{a_s} + \mathrm{m}_i + \mathrm{a}_i)\mathrm{V} \tag{2-1}$$

$$\frac{1}{2}(\mathrm{m_s} + \mathrm{a_s})\mathrm{v_s^2} + \frac{1}{2}(\mathrm{m}_i + \mathrm{a_b})\mathrm{v}_i^2 = \frac{1}{2}(\mathrm{m_s} + \mathrm{a_s} + \mathrm{m}_i + \mathrm{a}_i)\mathrm{V}^2 + \mathrm{E_s} \tag{2-2}$$

Where, E_s is strain energy, m_s is mass of approaching vessel, m_i is mass of installation, a_s is added mass of approaching vessel, a_i is added mass of installation, v_s is speed of approaching vessel, v_i is speed of installation, V is velocity of ship and installation after collision.

It is assumed here that the ship and FOWT have the same velocity after collision, that is, V. Then strain energy E_s can be calculated. The strain energy consumed by the ship and FOWT is equal to the total area under the load-deformation curve shown in Figure 2-2.

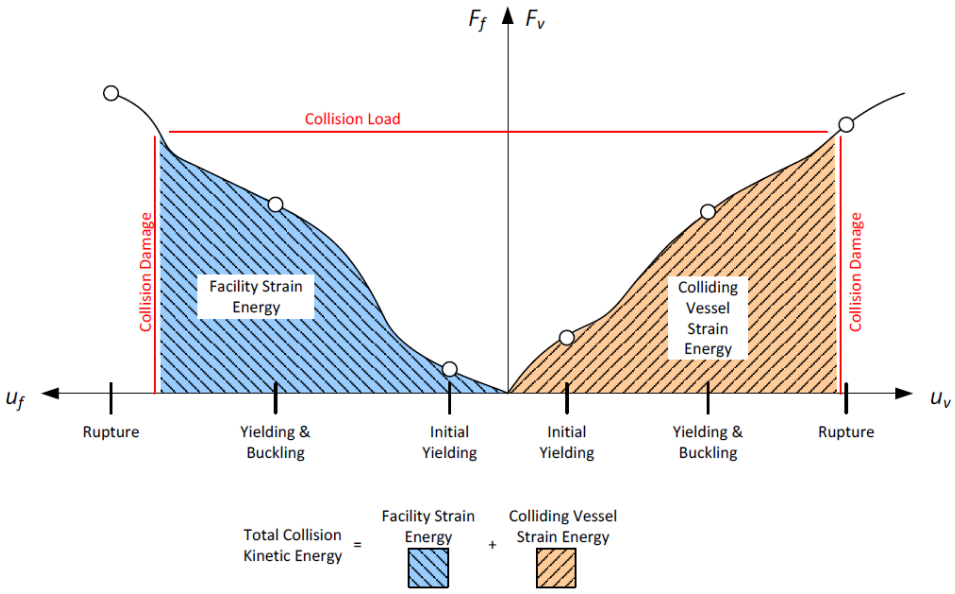

Figure 2-2 Dissipation of strain energy in ship and FOWT (A. B. S., 2013)

The energy balance of ship collision can be expressed as Equation (2-1).

$$E_s = E_{s,s} + E_{s,i} = \int_0^{W_{s,max}} R_s \, dw_s + \int_0^{W_{d,max}} R_d \, dw_d \tag{2-1}$$

Kinetic energy is usually a characteristic of ship collision, which is affected by ship mass, speed, and the added mass. Restricted by collision conditions, kinetic energy may be dissipated in the form of strain energy or retained in the form of kinetic energy. Generally, large plastic deformation will occur in the event of collision, in addition, the vessel, the installation or both are destroyed (DNV-RP-C204, 2010).

How the dissipated energy is distributed is solved in Internal Mechanism. According to DNV-RP-C204 (2010), there are three design stages: strength design, ductility design and shared-energy design shown in Figure 2-3. In the *strength design zone*, ships dissipate far more the energy than that of the FOWT, which means that ships deform greatly, but the FOWT does not. In this stage, the platform can be regarded as a rigid body, but it may lead to excessive reinforcement of the floater. In the *ductility design zone*, contrary to the strength design, the FOWT contributes most of the dissipated energy and has a relatively large plastic deformation, while ships can be regarded as rigid bodies with small deformation. In the *shared-energy design zone*, both ships and installation contribute to energy dissipation and have a large deformation, which is the most reasonable condition.

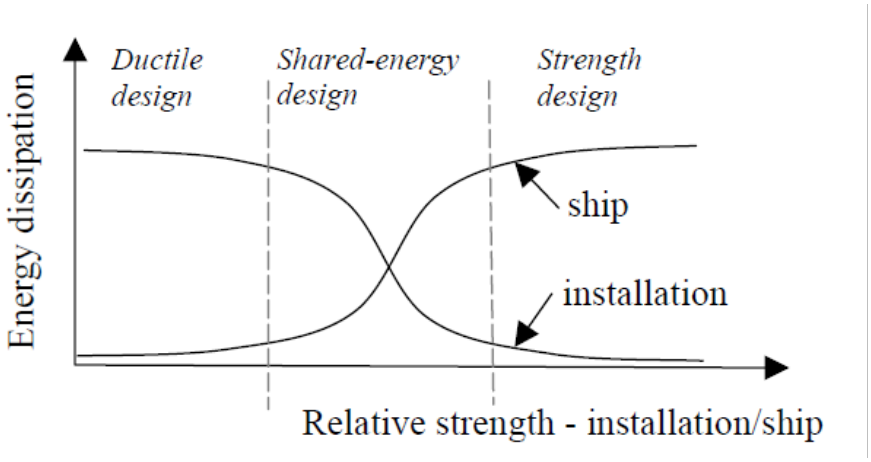

Figure 2-3 Energy dissipation for strength, ductile and shared-energy design (DNV-RP-C204, 2010)

2.3 The recommended force-deformation curve

A particularly interested result is the force-deformation relationship when study the collision mechanism. Depending on the structural characteristics, different ships have different interactions with the installations. On the other hand, the nature of the interaction between two objects has an important influence on these results. According to DNV-RP-C204 (2010), the recommended force-deformation curves are shown in Figure 2-4, Figure 2-5 and Figure 2-6.

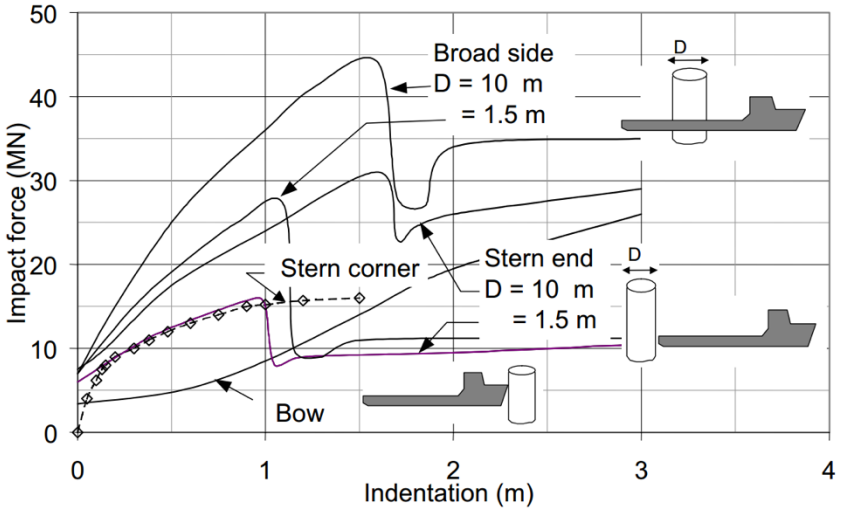

Figure 2-4 Recommended force-deformation curves for the standard vessel with a displacement of 5000 tons in beam, bow and stern impacts (DNV-RP-C204, 2010)

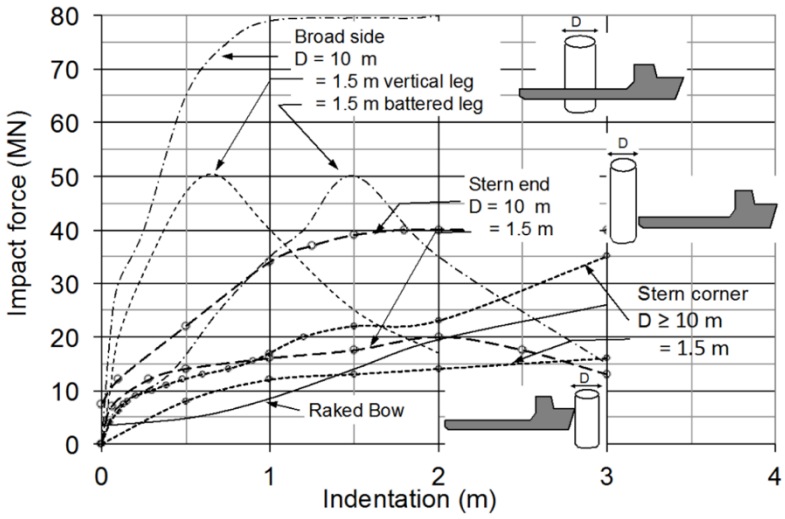

Figure 2-5 Recommended force-deformation curves for standard design vessels with displacements of 6500-10,000 tons in beam, bow and stern impacts (DNV-RP-C204, 2010)

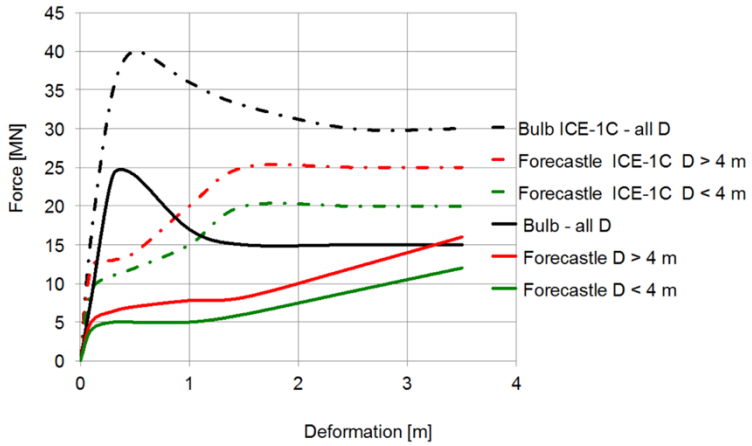

Figure 2-6 Force-deformation relationships for bow impacts from supply vessels with displacements of 5,000-10,000 tons, standard bulbous bows with no ice reinforcement and with ICE-1C class. (DNV-RP-C204, 2010)

2.4 Dynamic equations of motion

The dynamic response of structure to external load can be expressed by dynamic equilibrium equation, which can be written as Equation (2-2).

$$M\ddot{x} + C\dot{x} + Kx = F \qquad (2\text{-}2)$$

Where, M is mass matrix, C is damping matrix, K is stiffness matrix, $\ddot{x}$ is nodal acceleration, $\dot{x}$ is nodal velocity, x is nodal displacement respectively, F is external loads.

Chapter 3 Modelling of DTU 10 MW wind turbine and OO-Star wind floater

3.1 DTU 10 MW wind turbine

The DTU 10 WM reference wind turbine is, in general, a traditional three-bladed, upwind wind turbine with a rated rotor speed of 9.6 rounds per minute (rpm). The gearbox ratio is 50:1 and the generator inertia about the medium-speed shaft is 1500.5 kgm^2. The blades have prebend to ensure tower clearance. Key parameters are summarized in Table 3-1.

Table 3-1 Key parameters of the DTU 10 MW wind turbine

Parameter	DTU 10 MW
Rotor Orientation	Clockwise rotation-upwind Variable speed, Collective pitch
Cut-in wind speed (m/s)	4
Cut-out wind speed (m/s)	25
Rated wind speed (m/s)	11.4
Rated power (MW)	10
Number of blades	3
Rotor diameter (m)	178.3
Hub diameter (m)	5.6
Hub height (m)	119
Minimum rotor speed (rpm)	6
Maximum rotor speed (rpm)	9.6
Gearbox ratio	50
Hub overhang (m)	7.1
Shaft tilt angle (deg)	5
Rotor pre-cone angle (deg)	2.5
Blade prebend (m)	3.332
Rotor mass (kg)	227962
Nacelle mass (kg)	446036
Tower mass (kg)	628442

3.1.1 Blade

The thickness of the blades is relatively high in order to increase the moment of inertia and thereby increase the stiffness and challenge the aerodynamics. The minimum and maximum thickness of DTU wind turbine blades are 24.1% and 60%, respectively. The wind load on the blades consists of lift load and drag load, the lift load rotates the blade while the drag load bends the tower. Figure 3-1 to Figure 3-3 display the lift coefficient, drag coefficient, and moment coefficient of DTU 10 MW wind turbine blades. Figure 3-4 shows wind turbine blade parameters, including chord length, twist angle, and blade thickness along the blade span. As Figure 3-5 shows, the blade's tip is bent to increase the tower clearance.

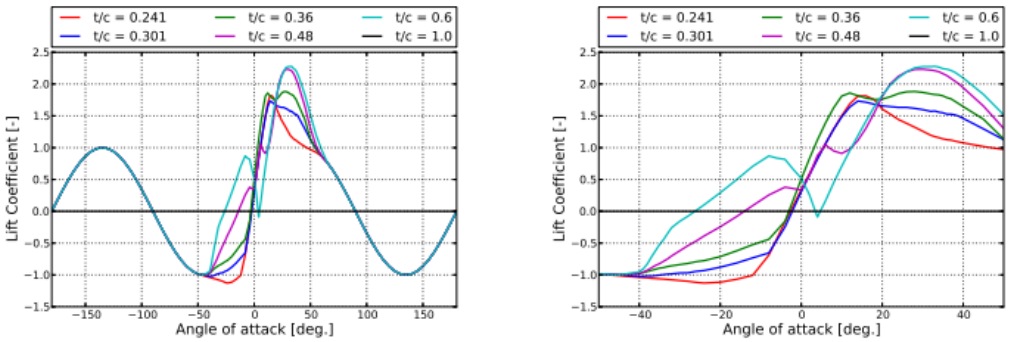

Figure 3-1 Lift coefficient of the DTU 10 MW blades (Bak et al., 2013)

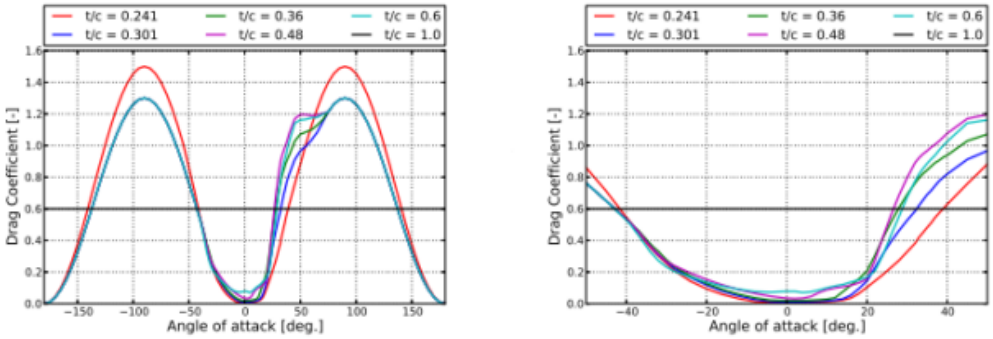

Figure 3-2 Drag coefficient of the DTU 10 MW blades (Bak et al., 2013)

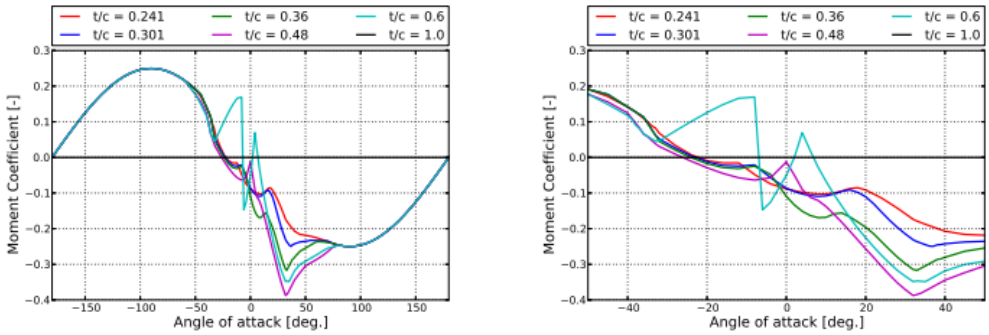

Figure 3-3 Moment coefficient of the DTU 10 MW blades (Bak et al., 2013)

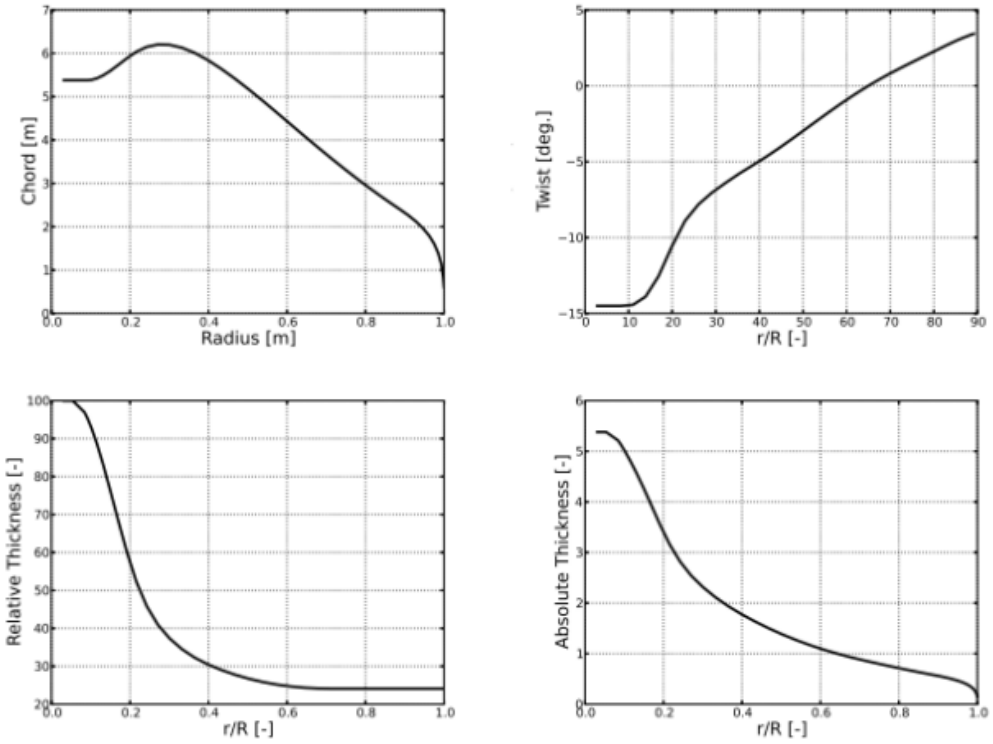

Figure 3-4 The DTU 10 MW wind turbine parameters vs normalized blade span (Bak et al., 2013)

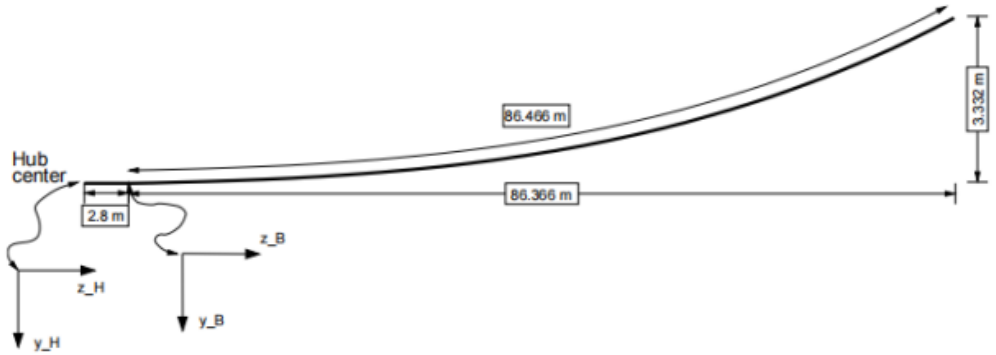

Figure 3-5 Prebend shape of the DTU 10 MW wind turbine blade (Bak et al., 2013)

3.1.2 Hub and nacelle

The hub of DTU 10 MW is placed 119 m above the ground and 7.07 m upwind of the tower centerline, the yaw bearing is placed at the top of the tower with a tilt of 5 deg and the vertical distance along the yaw axis from yaw bearing to the shaft is 2.75 m, this gives a distance along the shaft from hub center to the yaw axis of 7.1 m. The hub has a mass of 105,520 kg and inertia of 325,671 kgm^2. The nacelle has a mass of 446,036 kg and the center of mass (CoM) is located 2.45 m above the tower and 2.678 m downwind of the tower, which gives inertia of

7,326,346 kgm^2 about the yaw axis. The rotor radius is 89.166 m, and the hub diameter is 5.6 m. The nacelle and hub properties are summarized in Table 3-2.

Table 3-2 Mass property of the DTU 10 MW wind turbine

Property	Value
Rotor mass (kg)	230,717
Hub mass (kg)	105,520
Hub CoM (m, m, m)	(-7.07,0,119)
Hub inertia (kgm^2)	325,671
Nacelle mass (kg)	446,006
Nacelle CoM (m, m, m)	(2.678,0,118.08)
Nacelle inertia (kgm^2)	7,326,346
Vertical distance along yaw axis from yaw bearing to shaft (m)	2.75
Distance along shaft from hub center to yaw axis (m)	7.07
Distance along shaft from hub center to main bearing (m)	2.7
Hub inertia about low-speed shaft (kgm^2)	325,671
Nacelle CoM location above yaw bearing (m)	2.45

3.1.3 Tower

The tower is made of steel S355, as defined in the European standard DIN EN 10025-2, the material properties are summarized in Table 3-3

Table 3-3 Material properties of tower

Property	Value
Young's modulus (GPa)	210
Poisson's ratio	0.3
Mass density (kg/m^3)	8500
Minimum yield strength (MPa)	355

The tower has a length of 115.36 m and a mass of 628,442 kg. It consists of 10 conical sections, where the wall thickness is constant, and the inner and outer diameter increases linearly in each section. The outer diameter of the tower is 8.3 m at the bottom (h = 0 m), decreases linearly to

5.5 m at the top (h=115.63) and the wall thickness decreases from 38 mm at the bottom to 20 mm at the top. Table 3-4 shows the wall thickness distribution.

Table 3-4 The wall thickness distribution of the tower

Height (m)	Outer diameter (m)	Wall thickness (mm)
0	8.3	38
11.5	8.0215	38
11.501	8.0215	36
23	7.7431	36
23.001	7.7430	34
34.5	7.4646	34
34.501	7.4646	32
46	7.1861	32
46.001	7.1861	30
57.5	6.9076	30
57.501	6.9076	28
69	6.6292	28
69.001	6.6291	26
80.5	6.3507	26
80.501	6.3507	24
92	6.0722	24
92.001	6.0722	22
103.500	5.7937	22
103.501	5.7937	20
115.63	5.5	20

3.2 LIFES50+ OO-Star wind floater

3.2.1 Platform

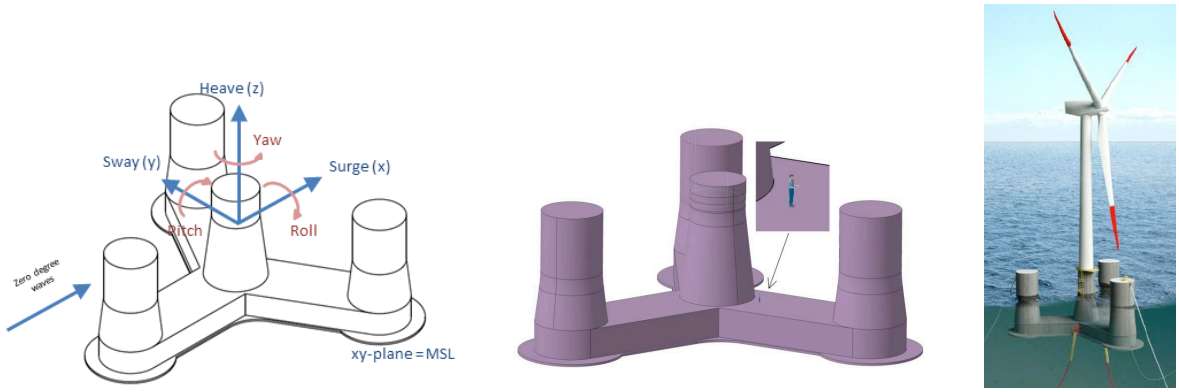

Figure 3-6 LIFES50+ OO-Star wind floater (Yu et al., 2017)

LIFES50+ OO-Star wind floater, as shown in Figure 3-6, is designed by Dr. techn. Olav Olsen AS as an innovative solution to meet the demand for the offshore floating wind turbine. The floater is able to support heavy wind turbines in harsh environmental conditions and can be placed in areas that are not suitable for bottom-fixed wind turbines. It is suitable for wind turbines of 12-15 MW.

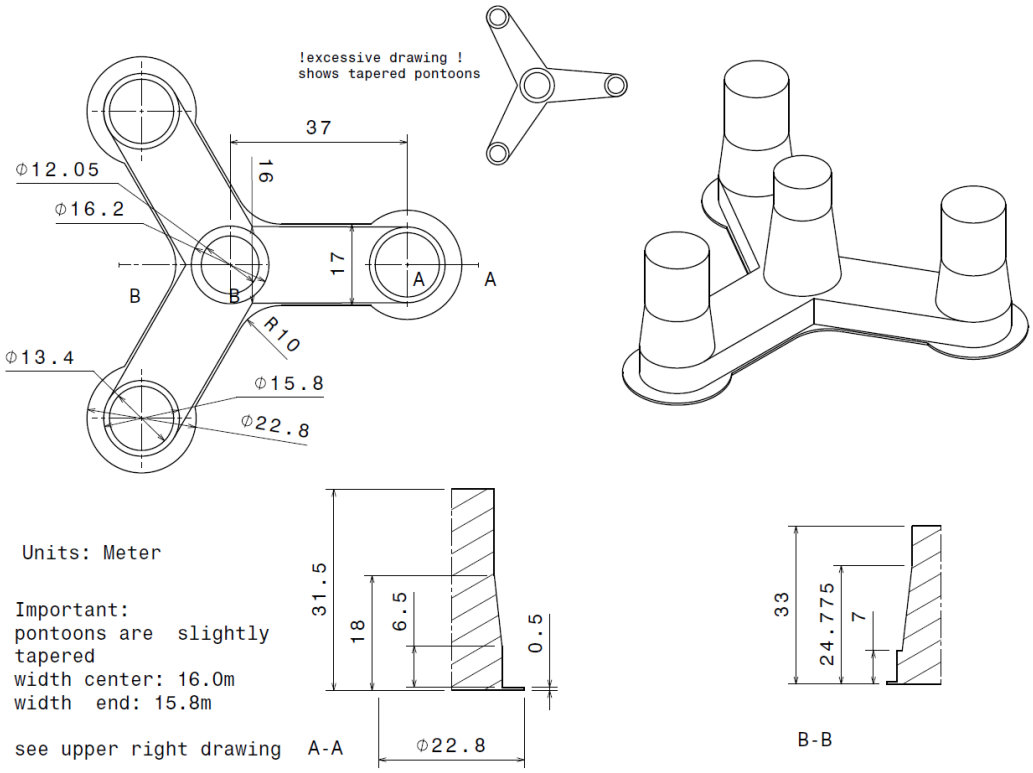

Figure 3-7 LIFES50+ OO-Star wind floater main dimensions (Yu et al., 2017)

The main dimensions of the OO-Star wind floater are shown in Figure 3-7. The substructure of the offshore floating wind turbine includes 3 outer columns, 1 central column, 1 star-shaped pontoon, and 1 slab. Columns are placed on the pontoon and the slab is attached under the pontoon. The distance between the outer column and central column is 37 m. The horizontal pontoon elements connecting the columns have a width of 16 m and a height of 7 m. The slab has a width of 17 m, adding 0.5 m on each side, and the curvature radius below the central column is 10 m. The upper part of the central column has a diameter of 12.05 m and a length of 13.5 m. The lower part of the central column has a tapered shape with a length of 11 m and a diameter of 16.2 m at the bottom, decreasing linearly to 12.05 m at the top. The upper part of the outer column has a diameter of 13.4 m and a length of 13.5 m. The lower part of the outer column has a tapered shape with a length of 11 m and a diameter of 15.8 m at the bottom, decreasing linearly to 13.4 m at the top. The circular portions of the heave plates below the outer columns have a diameter of 22.8 m.

The overall mass of the platform is 21,709 tones. The mass moments of inertia about CoM are 9.43×10^9 kgm² about the x-axis and y-axis, and 1.63×10^{10} kgm² about the z-axis. Key parameters of the floater are summarized in Table 3-5. Important structural properties for individual members are listed in

Table 3-6.

Table 3-5 LIFES50+ OO-Star wind floater platform parameters including ballast

Property	Value
Overall substructure mass excluding tower, and mooring (kg)	2.1709×10^7
CoM below MSL (Mean Sea Level) (m)	15.225
Substructure roll inertia about CoM (kgm^2)	9.43×10^9
Substructure pitch inertia about CoM (kgm^2)	9.43×10^9
Substructure yaw inertia about CoM (kgm^2)	1.63×10^{10}
Tower base interface above MSL (m)	11.0
Draft at equilibrium position with moorings (no thrust) (m)	22.0
Displaced water volume (m^3)	23509
Center of buoyancy below MSL (m)	14.236

Table 3-6 LIFE50+ OO-Star wind floater distributed structural properties

Section	Radius (m)	Mass density (kg/m)	Element length (m)	EA (N)	EIy (Nm^2)	EIz (Nm^2)	GJ (Nm^2)
Pontoon	-	1.73×10^5	21.1	6.39×10^{11}	5.53×10^{12}	1.97×10^{13}	1.05×10^{13}
Outer Column Lower	7.9	1.4×10^5	7	5.81×10^{11}	2.2×10^{13}	2.2×10^{13}	1.83×10^{13}
Outer Column Conical Part	-	9.28×10^4	11.5	5.36×10^{11}	1.62×10^{13}	1.62×10^{13}	1.35×10^{13}
Outer Column Upper	6.7	4.55×10^4	13.5	4.9×10^{11}	1.04×10^{13}	1.04×10^{13}	8.64×10^{12}
Central Shaft Lower	8.1	1.17×10^5	7	8.82×10^{11}	2.69×10^{13}	2.69×10^{13}	2.24×10^{13}
Central Shaft Conical Part	-	8.73×10^4	17.775	7.39×10^{11}	1.84×10^{13}	1.84×10^{13}	1.53×10^{13}
Central Shaft Upper	6.025	5.76×10^4	8.225	5.96×10^{11}	9.88×10^{12}	9.88×10^{12}	8.23×10^{12}

Morrison equation, consisting of inertia force and drag force, is given by:

$$F_x^{2D} = (1 + C_m)\rho\pi R^2 \dot{U} + \frac{1}{2}\rho C_d 2\mathrm{RU}|U| \tag{3-1}$$

Where, C_m is the mass coefficient, C_d is the drag coefficient, ρ is the fluid density, R is the radius, U is flow velocity and $\dot{U}$ is flow acceleration.

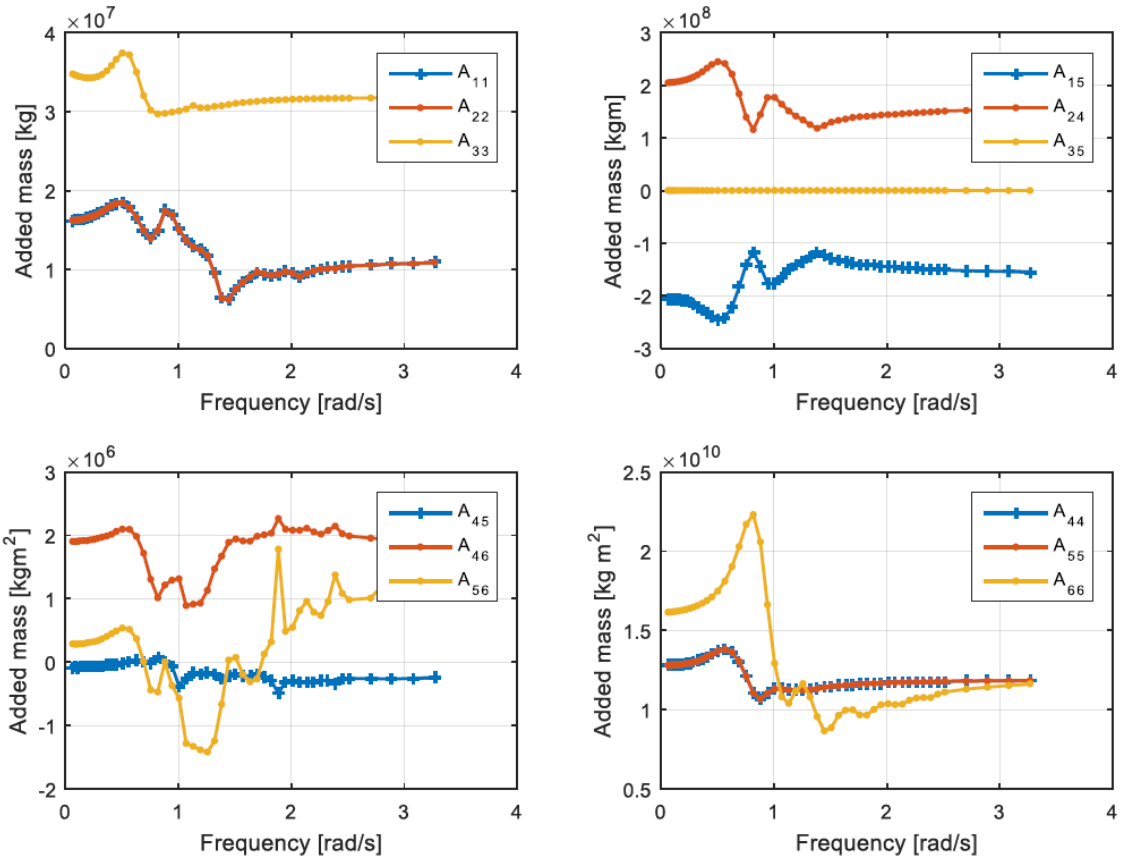

Figure 3-8 LIFES50+ OO-Star wind floater hydrodynamic added mass (Yu et al., 2017)

The added mass of the floater is displayed in Figure 3-8 LIFES50+ OO-Star wind floater hydrodynamic added mass (Yu et al., 2017). For the drag coefficient, the cylinder upper section of the central column, with a diameter of 12.05 meters, has a drag coefficient of 0.729. The conical lower section has a variable diameter between 12.05 and 16.2 m, resulting in a variable drag coefficient between 0.729 and 0.704. The cylinder upper sections of the three outer columns, with a diameter of 13.4 meters, has a transversal drag coefficient of 0.720. The tapered bottom section of the three outer columns, has a variable diameter between 13.4 m and 15.8 m, resulting in a variable drag coefficient between 0.720 and 0.706. The pontoon legs have a rectangular cross-section, with a width of 17 m and a height of 7 m, has a drag coefficient of 2.05. The outer heave plate has an area of 368.57 m^2 and a drag coefficient of 10, the Central heave plate has an area of 125.14 m^2 and a drag coefficient of 2.05 (Pegalajar-Jurado et al., 2018).

3.2.2 Mooring system

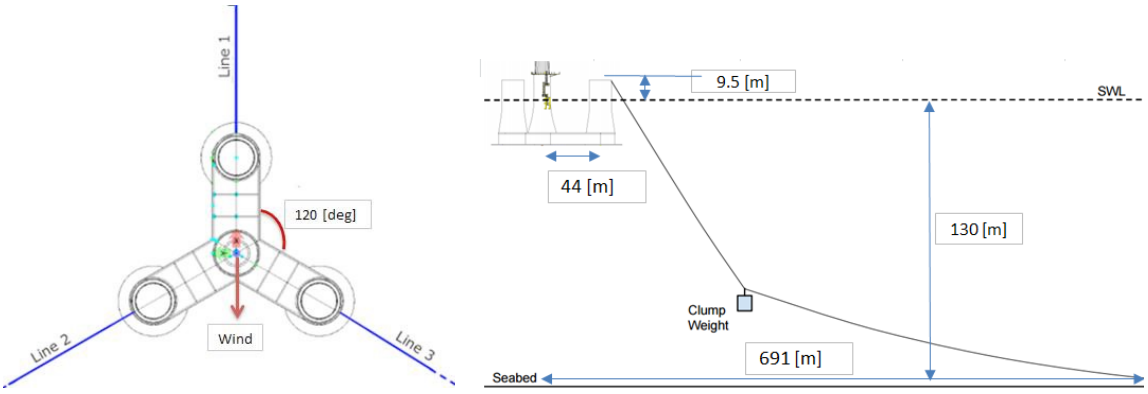

Figure 3-9 LIFES50+ OO-Star wind floater mooring line arrangement in the top view (left) and side view (right) (Yu et al., 2017)

Figure 3-9 shows the layout of the mooring system of the floating wind turbine. The mooring system consists of three chains and three clumps. Each chain has a length of 703 m and a diameter of 0.137 m, and the horizontal angle between the two chains is 120 deg. Each clump has a mass of 50 tons and is attached to the mooring line, dividing the mooring line into two sections. The upper section has a length of 118 m and is connected to the fairlead, which is 9.5 m above the still water level (SWL). The lower section is anchored to the seabed and has a length of 585 m. The material properties are equal for the upper segment and lower segment. Important parameters of the mooring system are summarized in Table 3-7. The number of segments is set to 80 for the lower part and 20 for the upper part in OrcaFlex.

Table 3-7 LIFE50+ OO-Star wind floater mooring system properties

Property	Value
Number of lines	3
Angle between adjacent lines (degree)	120
Equivalent total mass in water of the clump mass (kg)	50000
Unstretched mooring line length, upper part (m)	118
Unstretched mooring line length, lower part (m)	585
Vertical position of fairleads above MSL (m)	9.5
Radius to anchors from platform centerline (m)	691
Anchor position below MSL (m)	130
Radius to fairleads from platform centerline (m)	44
Initial vertical position of clump mass below MSL (m)	90.45
Initial radius to lump mass from centerline (m)	148.6
Pretension (N)	1.67×10^6
Equivalent weight per length in water (N/m)	3200.6
Extensional stiffness EA (N)	1.506×10^9
Hydrodynamic added mass coefficient	0.8
Hydrodynamic drag coefficient	2.0
Physical chain diameter (m)	0.137

3.3 Modeling for local analysis

In LIFES50+ Project, the OO-Star wind floater was investigated and optimized in the first stage, and the basic structural characteristics were determined by (Yu et al., 2017). The main dimensions of the platform are shown in Figure 3-7. The OO-Star wind floater has a central and three outer columns. The outer columns have the highest probability of being hit by a ship when the ship isn't aware of the wind floater or has failed. Based on this situation, the local analysis is focused on the outer columns.

3.3.1 Initial design

According to the LIFES50+ Project, the column's thickness, reinforcements, and material types are unavailable. In this paper, the thickness of column's wall is assumed to be 0.5 m and 1 m, respectively. Figure 3-10 exhibits the geometric dimension of the 1 m thick wall. The upper part of the column is more likely to collide with ships, so the simulation of local mainly studies the upper part. In addition, the details of reinforcement design are introduced in chapter 0. The model is demonstrated in Figure 3-10. The concrete columns are concrete grade 60 (C60) and the steel bars are B500c.

3.3.2 Reinforcement design and column model

The OO-Star wind floater is installed in sea depths ranges from 50 m to 200 m. According to Eurocode 2 (2004), the design working life is selected as 100 years from environmental conditions. The cover depth can be calculated by Equation (3-2).

The concrete cover:

$$C_n = C_m + \Delta C_{dev} \tag{3-2}$$

Where, C_n is nominal cover, C_m is minimum cover, C_{dev} is allowance in design for deviation.

The key parameters are summarized in Table 3-8. The steel reinforcement of concrete columns consists of two layers of steel rebars. The longitudinal reinforcement is 40 mm in diameter, and the transverse reinforcement is 24 mm in diameter. The outer and inside cover depths are 65 mm and 60 mm, respectively. For the 0.5 m column, the outer spacing of longitudinal rebar is 208 mm and inside is 197 mm, the spacing of transverse steel bar is 200 mm. For the 1 m column, the outer spacing of longitudinal steel bars and transverse rebars are 173 mm and 200 mm separately, inside spacings for longitudinal and transverse rebars are 150 mm and 200 mm.

Table 3-8 Reinforcement parameter

	Thickness of wall (m)		Number of bars	Spacing (mm)	Diameter of bar (mm)	Cover depth (mm)
Longitudinal	0.5	Outer	200	208	40	65
		Inside	200	197	40	60
	1	Outer	240	173	40	65
		Inside	240	150	40	60
Transverse	0.5	Outer	123	200	24	65
		Inside	123	200	24	60
	1	Outer	123	200	24	65
		Inside	123	200	24	60

The geometry of the column with a thickness of 1 m is shown in Figure 3-10, and the column with a thickness of 0.5 m is similar. The concrete part of the column is modeled in Inventor and meshed in LS-PrePost, and the steel bars are modeled and meshed in LS-PrePost. The mesh size is 80 mm.

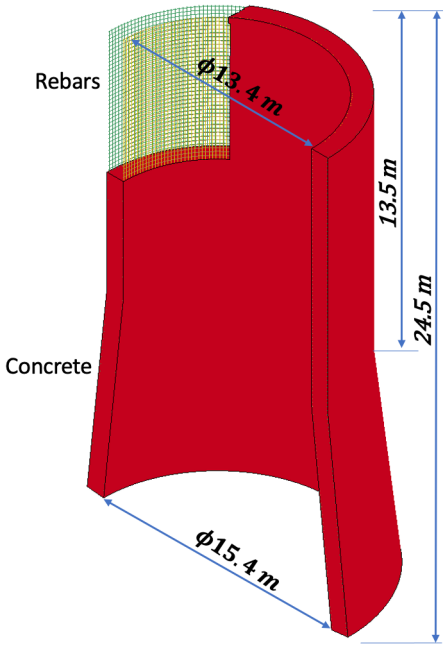

Figure 3-10 FEM model of 1 m thick wall

3.3.3 Ship model

Figure 3-11shows the ship model provided by Prof. Yanyan Sha, which is based on container ship with the displacement of 20,000-tons. The added mass of ship bow is 10% (N-003, 2017). The container ship model has a height of 16.67 m, a width of 26.4 m, and a length of 20.4 m.

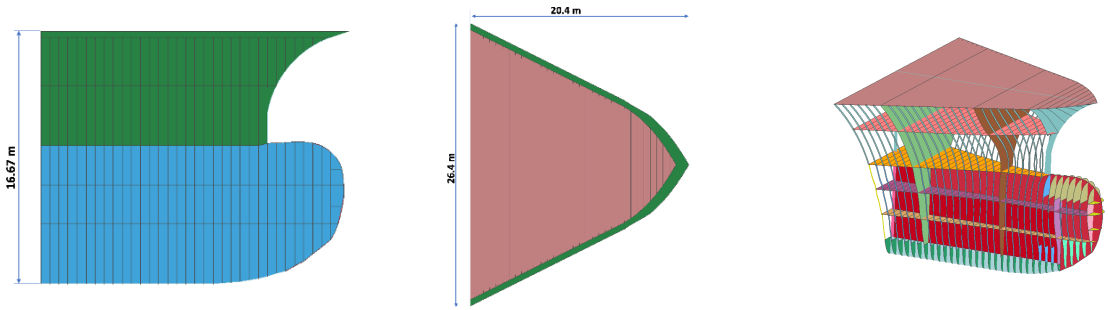

(a) (b) (c)

Figure 3-11 The FEM model of the ship: (a) left view; (b) top view; (c) internal structure

3.4 Modelling and verification for global analysis

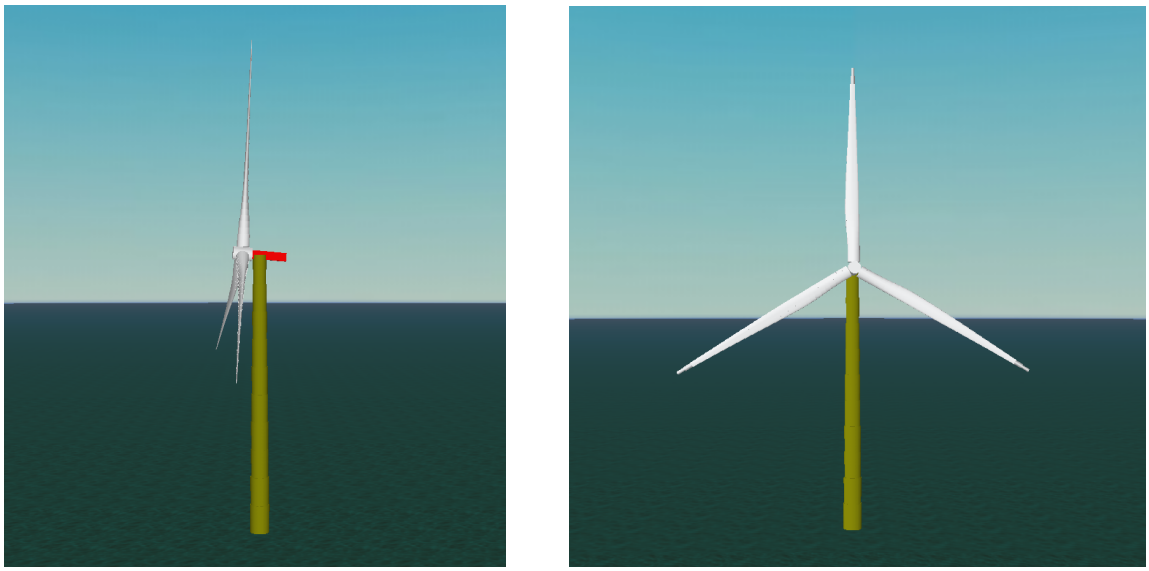

Figure 3-12 Assembled wind turbine in OrcaFlex

The DTU 10 MW wind turbine is modeled in OrcaFlex, both the turbine blades and assembled wind turbine in OrcaFlex are verified by conducting modal tests and comparing with the corresponding values in the DTU 10 MW wind turbine report.

3.4.1 Modal test of an isolated blade

Table 3-9 Comparison of natural frequencies for an isolated wind turbine blade

mode	DTU 10 MW (Hz)	OrcaFlex model (Hz)	Deviation (%)
1st flap mode	0.61	0.61	0
1st edge mode	0.93	0.95	2.15
2nd flap mode	1.74	1.73	-0.57
2nd edge mode	2.76	2.85	3.26
3rd flap mode	3.57	3.53	-1.12
3rd edge mode	5.69	5.79	1.6

First, a model test is carried out for an isolated blade. Table 3-9 summarizes and compares natural frequencies from OrcaFlex analysis for an isolated blade with the DTU 10 MW wind turbine report. The first three flap and edge modes are of importance and analyzed. The deviation is calculated and relatively small, less than 5%, which means the modeling of the turbine blade is verified.

3.4.2 Modal test of the assembled wind turbine and tower

Second, a modal test for assembled wind turbine including blades and tower is carried out, the blades and tower would interact and affect the eigenfrequency when assembled. The bottom of the tower is fixed, as shown in Figure 3-12. Table 3-10 summarizes and compares natural frequencies between OrcaFlex analysis for the assembled wind turbine with the DTU 10 MW wind turbine report. The first five modes of the assembled wind turbine are crucial and analyzed. The deviation is relatively small, the maximum deviation is 7.27%, but less than 10% and the absolute deviation is just 0.04 Hz. This demonstrates that the modeling of the assembled wind turbine is correct.

Table 3-10 Comparison of natural frequencies for assembled wind turbine and tower

Mode	DTU 10 MW (Hz)	OrcaFlex model (Hz)	Deviation (%)
1st tower fore-aft mode	0.25	0.25	0
1st tower side-side mode	0.25	0.26	4
1st asymmetric with yaw	0.55	0.59	7.27
1st asymmetric with tilt	0.59	0.62	5.08
1st collective flap mode	0.63	0.62	-1.59

3.4.3 Decay test

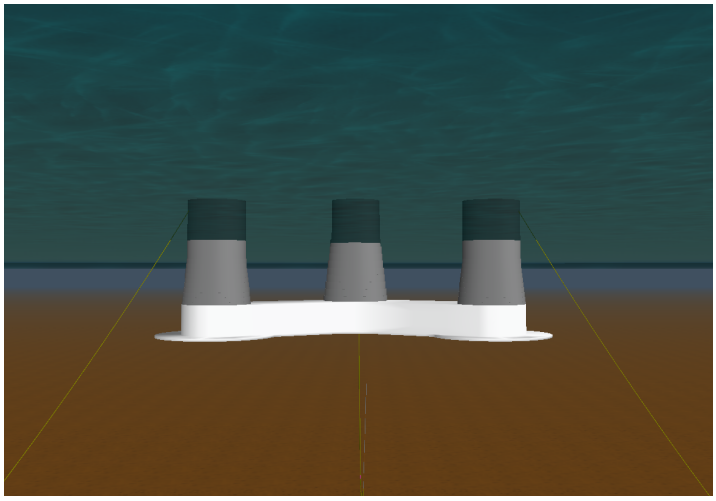

Figure 3-13 LIFES50+ OO-Star wind floater model in OrcaFlex

Figure 3-13 shows the LIFES50+ OO-Star wind floater in OrcaFlex and Table 3-11 summarized the key parameters of the floater, including the mass and moments of inertia, and compared with the corresponding value from the LIFES50+ D4.2 report. The deviation is calculated and quite small, less than 5%, which indicates that the modeling is correct.

Table 3-11 Comparison of key parameters between OrcaFlex model and LIFES50+ Report (Yu et al., 2017)

Property	LIFES50+ Report	OrcaFlex model	Deviation (%)
Overall substructure mass excl. tower and mooring (kg)	2.171×10^7	2.17×10^7	0.32%
Floater roll inertia about CM (kgm^2)	9.43×10^9	9.39×10^9	-0.41
Floater pitch inertia about CM (kgm^2)	9.43×10^9	9.39×10^9	-0.39
Floater yaw inertia about CM (kgm^2)	1.63×10^{10}	1.5×10^{10}	-4.6

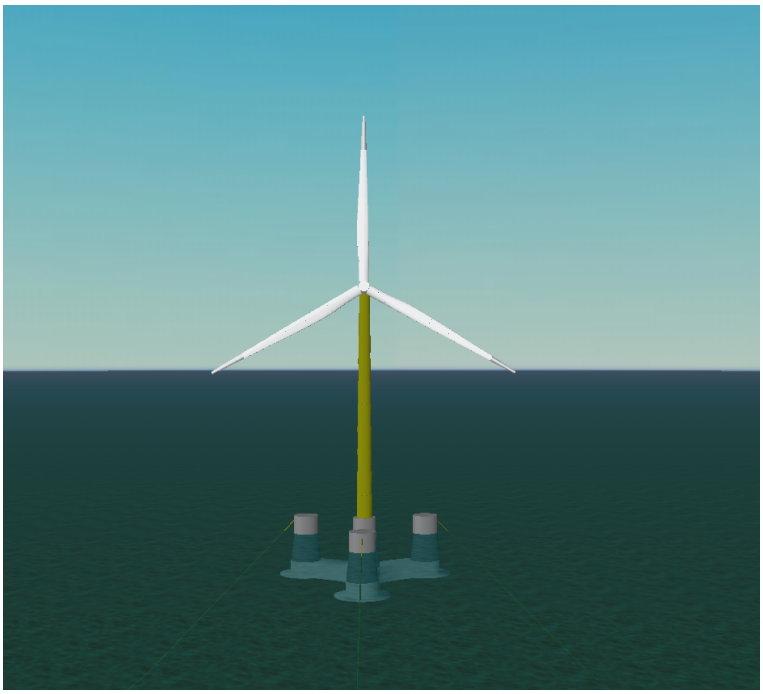

Figure 3-14 The assembled floating wind turbine

The LIFES50+ OO-Star wind floater is assembled with DTU 10 WM wind turbine and then free decay test is carried out in OrcaFlex. First, the statics calculation is performed to obtain the equilibrium position of the wind turbine, a small offset is observed because of imperfect balance between global mass and net buoyancy, moreover, the tower-top CM is not aligned with the tower axis. For each decay test case, an initial displacement is introduced in the corresponding degree of freedom (DoF) and the rest of DoFs are set as the equilibrium position, then the system is left to decay to its equilibrium position.

Table 3-12 Comparison of natural period

Property	LIFES50+report (s)	OrcaFlex model (s)	Deviation (%)
Natural period surge	185.2	187	0.97
Natural period heave	20.92	20.5	-2.01
Natural period pitch	31.65	34	7.42
Natural period yaw	103.09	99	-3.97

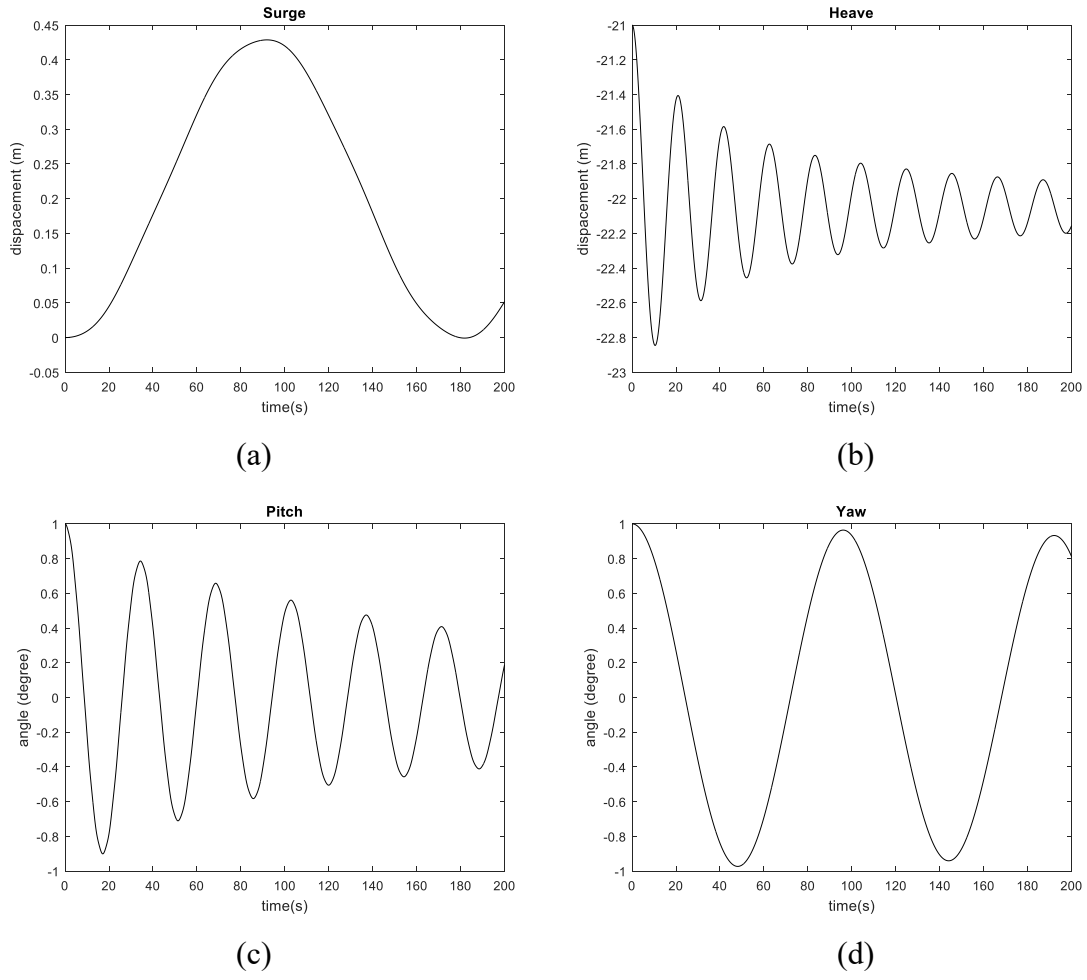

Figure 3-15 Time history of free decay test, (a) surge, (b) heave, (c) yaw, (d) pitch

Table 3-12 summarizes and the natural periods for assembled floating wind turbine and compares with the corresponding value from the LIFES50+ D4.5 report. Figure 3-15 shows the decay test of the floating wind turbine. The deviation is calculated and relatively small. The maximum difference is 7.42%, less than 10%, which demonstrates that the modeling is correct.

The collision analysis between FOWT and the vessel consists of local analysis and global analysis. Figure 3-16 shows the flow chart of collision analysis. The local analysis is performed in LS-DYNA, and global analysis is conducted in OrcaFlex. Multiple scenarios are conducted in both local and global analysis. The force-displacement curves obtained in local analysis are used in global analysis.

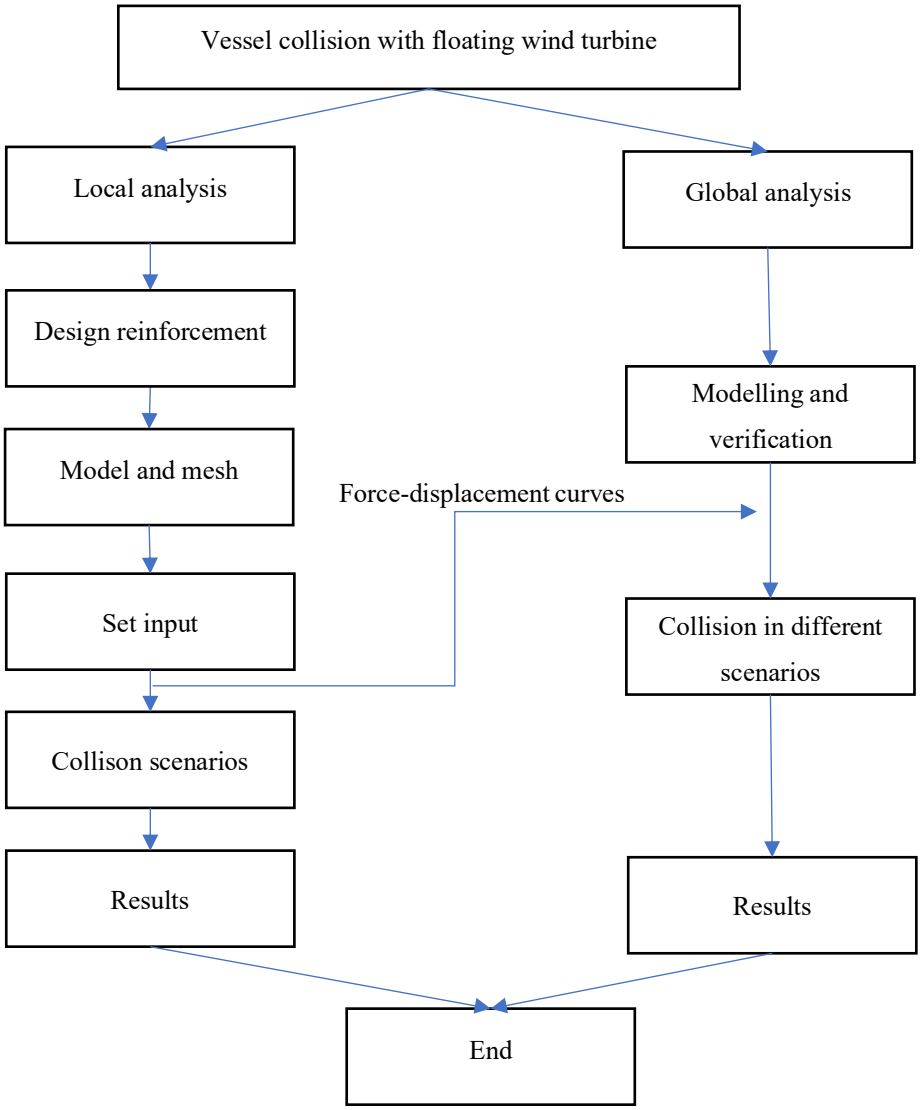

Figure 3-16 Flow chart of collision analysis between floating wind turbine and vessel

Chapter 4 Local simulations and results

In this chapter, the local numerical simulations of ship collision with wind turbine column are introduced. The local structural deformations and damage are investigated in LS-DYNA. The establishment of the model has been mentioned in chapter 3.3. LS-DYNA is a general finite element program, which is used to analyze the static and dynamic responses of structures (including structures coupled with fluids) with large deformation (Hallquist, 2006). The origin of LS-DYNA can be traced back to 1976, which was developed in Lawrence Livermore National Laboratory.

4.1 Collision analysis setup

The velocity of the ship is set to two modes: a constant velocity and an initial velocity. The ship is set at a constant velocity of 7.5 m/s impacts the column at still water level. The force-displacement curve is plotted showing in chapter 5.4.1 (Figure 5-4) to analyze the global simulation. Its function is to make sure the ship will not reduce the velocity during experiencing the collision. On the other hand, in the remaining cases, the speed of the ship is set as the initial speed.

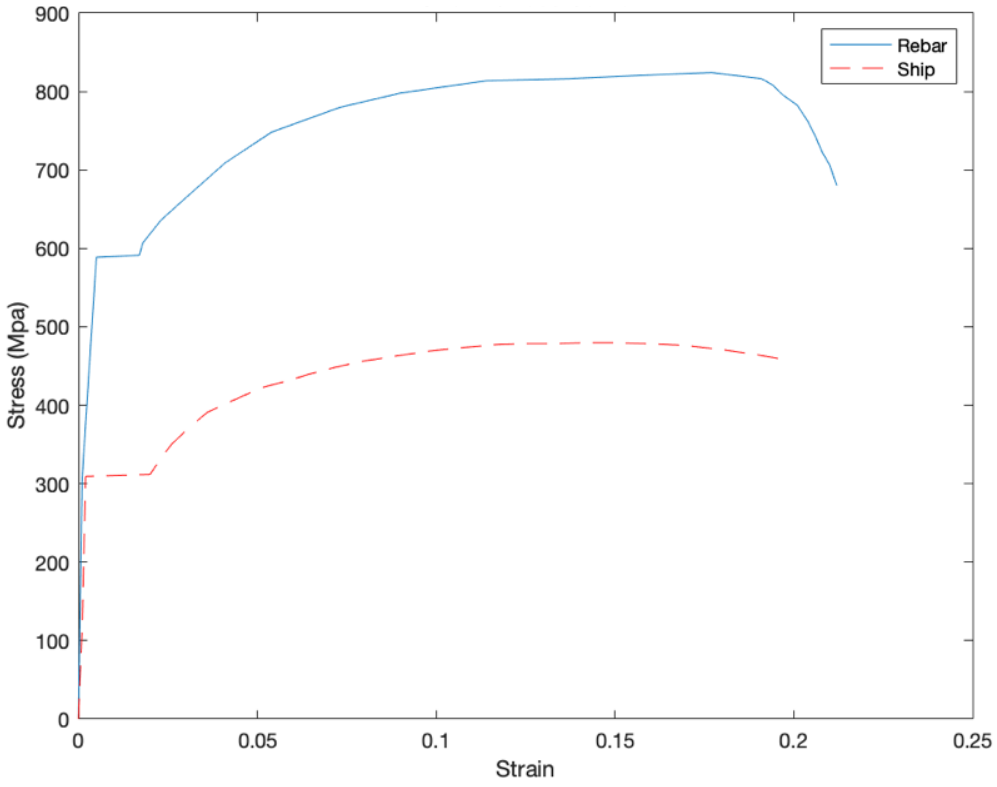

Figure 4-1 Stress–strain curves for the steel material in the rebar (Papadopoulos, 2007) and the ship (Mander, 1988)

Table 4-1 Material properties of the steel and concrete

Material	LS-DYNA model	Input parameter	Magnitude
Rebar	*MAT_PIECEWISE_LINEAR_PLASTICITY	Mass density	7850 kg/m^3
		Young's modulus	200 GPa
		Poisson's ratio	0.3
		Yield stress	580 MPa
Concrete	*MAT_CONCRETE_DAMAGE_REL3	Mass density	2400 kg/m^3
		Poisson's ratio	0.2
		Unconfined strength	60 MPa
Ship	*MAT_PIECEWISE_LINEAR_PLASTICITY	Mass density	7800 kg/m^3
		Young's modulus	200 GPa
		Poisson's ratio	0.3
		Yield stress	275 Mpa

The details of materials and models are shown in Table 4-1. The concrete is modelled by **MAT_72R3 in LS-DYNA*, it can well simulate the damage of concrete under impact and collision loads. This material model has been widely used to simulate the dynamic behavior of concrete, including plasticity and damage softening after failure. The elastic-plastic material model **MAT_PIECEWISE_LINEAR_PLASTICITY* is used to simulate steel bars and ships. The ship is made of ordinary low carbon steel with a yield stress of 275 MPa. The reinforcing bars are made of high strength steel strand with yield stress of 580 MPa (B500c). The stress-strain curves of S275 (ship) and B500c (reinforcements) are given in Figure 4-1. The strain rate effect is considered in chapter 4.7. Because the reinforcements steel bars are the high strength steel and are not so important than the concrete, rebars don't take into account the strain rate effect of reinforcements. In other cases in chapter 4.3 to 4.6, only the strain rate for concrete is considered. The rebars and concrete connection is employed by the **LAGRANGE_IN_SOLID* model. Contact modeling in LS-DYNA provides a method to deal with the interaction between

disjoint parts. This is achieved by setting different algorithms according to the type of contact the user wants. In this paper, the mutual contacts of ship have been employed the **AUTOMATIC_SINGLE_SURFACE* while the ship with floater adopted **AUTOMATIC_SURFACE_TO_SURFACE*. The initial speeds of the ship are 10 m/s, 7.5 m/s, 5 m/s and 2.5 m/s for 1 m thick wall in x-direction. For 0.5 m thick wall the initial velocities of the ship are 7.5 m/s, 5 m/s and 2.5 m/s. The initial velocities are given to the whole part of the ship by using **INITIAL_VELOCITY_GENERATION.*

The boundary conditions of the ship and column are indicated in Figure 4-2, the black elements are boundary elements and the ship part is only allowed to move in the x-direction.

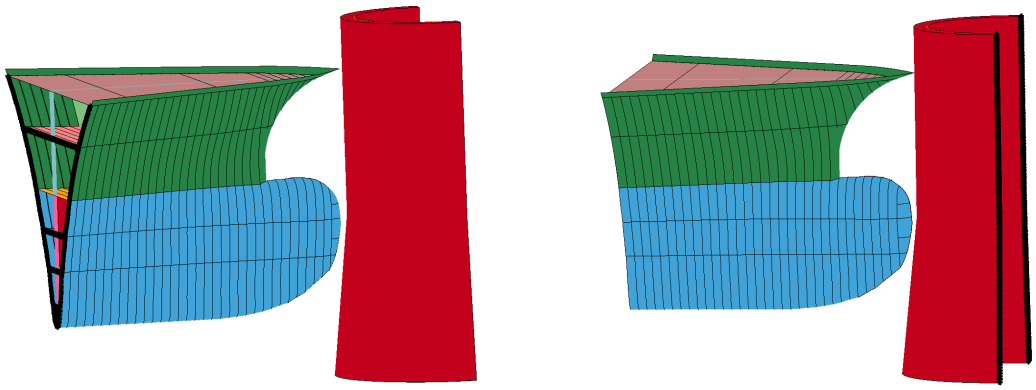

Figure 4-2 Boundary conditions of the ship (left) and column (right)

4.2 Collision scenarios

This section introduces the scenarios of collisions between the ship and concrete wall. All parameter changes such as different wall thicknesses, initial velocities, angles, positions and strain rates are given in Table 4-2. The setups of thickness wall, different velocities and strain rates are mentioned in the chapter 4.1, Figure 4-3 demonstrates that the ship with an initial velocity of 7.5 m/s impacts 1 m thick wall at various position. The scenarios of effect of angle shows in Figure 4-4 and it is considered the 0 and 45 degrees, when the ship with an initial velocity of 7.5 m/s impacts still water level of 1 m thick wall.

Table 4-2 Collision scenarios

Case	Velocity of ship (m/s)	Position	Angle (degree)	Thickness of wall (m)	Strain rate
1	2.5	SWL	0	0.5	Concrete-yes
2	5	SWL	0	0.5	Concrete-yes
3	7.5	SWL	0	0.5	Concrete-yes
4	2.5	SWL	0	1	Concrete-yes
5	5	SWL	0	1	Concrete-yes
6	7.5	SWL	0	1	Concrete-yes
7	10	SWL	0	1	Concrete-yes
8	7.5	Top	0	1	Concrete-yes
9	7.5	Top1	0	1	Concrete-yes
10	7.5	Bottom	0	1	Concrete-yes
11	7.5	SWL	45	1	Concrete-yes
12	7.5	SWL	0	1	Ship-yes
13	7.5	SWL	0	1	Without strain rate
14	2.5	Bottom	0	1	Concrete-yes
15	5	Bottom	0	1	Concrete-yes

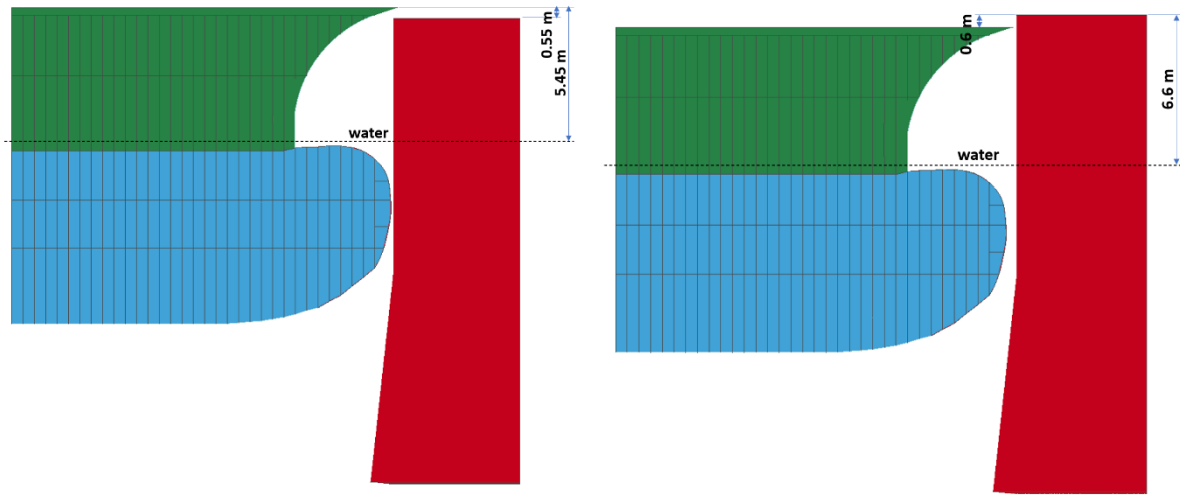

(a) (b)

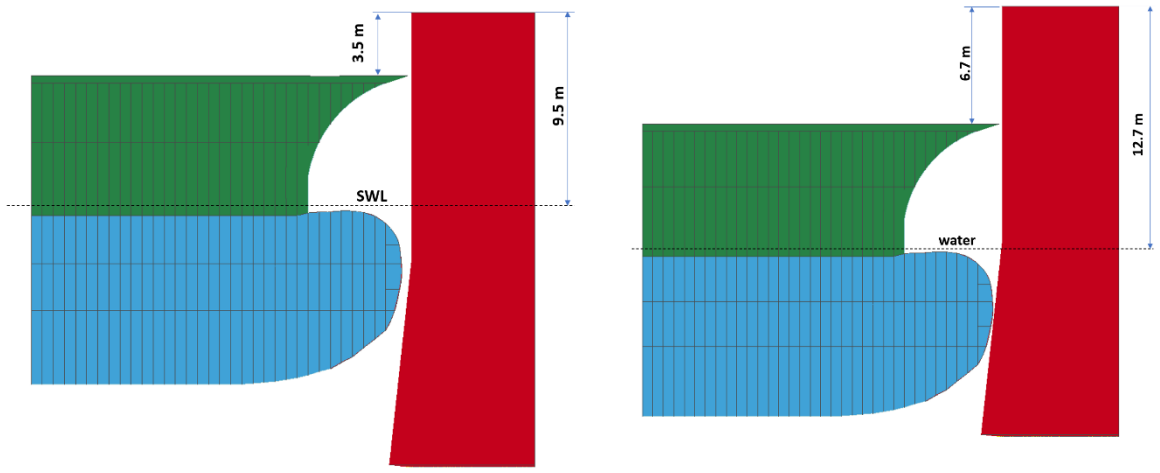

(c) (d)

Figure 4-3 Collision scenarios of the ship with an initial velocity of 7.5 m/s impacts different position of 1 m thick wall. (a) When the water level is high, only the bulb of the ship impacts the wall (Top); (b) the ship impacts the top of the wall (Top1); (c) the ship impacts the wall at the still water level (SWL); (d) the ship impacts the top of the wall (Bottom)

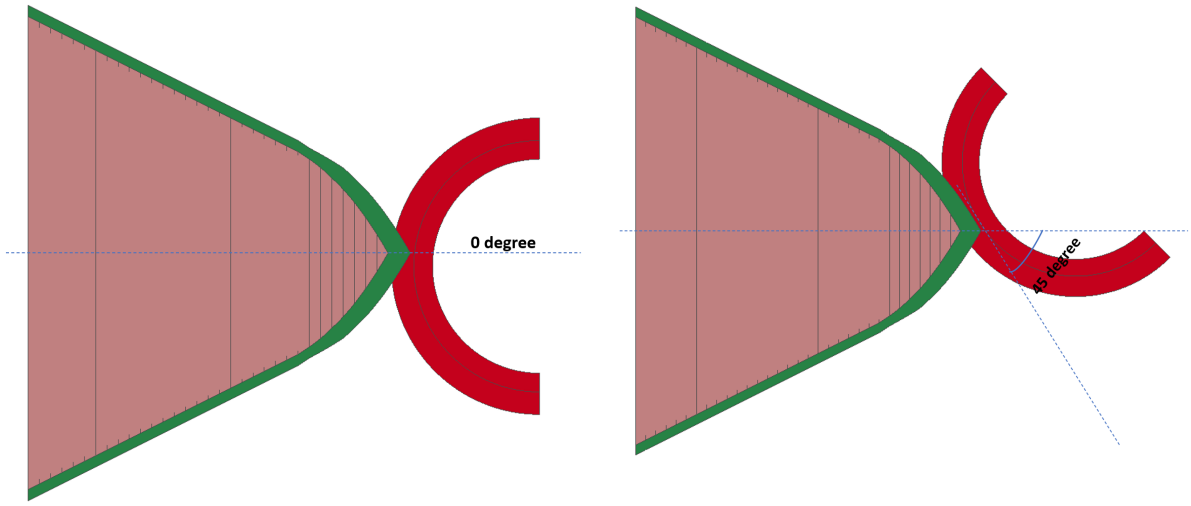

Figure 4-4 Collision scenarios of the ship when the ship with an initial velocity of 7.5 m/s impacts the 1 m thick wall at 0 degrees (left) and 45 degrees (right)

4.3 Effect of wall thickness

In this situation, the ship with an initial velocity of 7.5 m/s impacts SWL of the different thicknesses of walls at 0 degree.

4.3.1 Force-displacement curve

The force-deformation curve of the bulb and forecastle of ship crashing with column is shown in Figure 4-5. In the comprehensive analysis, the force from bulb of the ship is greater than that from the forecastle, and the force of the ship hitting a wall with a thickness of 1 m is greater than that impacting a wall with a thickness of 0.5 m. The peaks correspond to the failure of the bulb tip and the forecastle for blue line, respectively. And other obvious peaks and valleys in the force-displacement curve are due to the continuous collapse of the bulb and forecastle fractured.

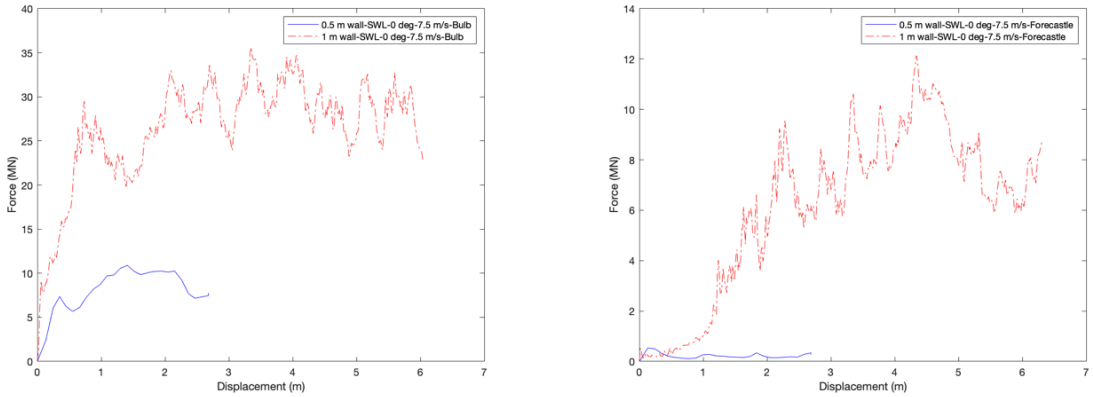

Figure 4-5 Force-displacement curve for bulb (left) and forecastle (right) of the ship when the ship with an initial velocity of 7.5 m/s impacts SWL of the different thicknesses of walls at 0 degree.

4.3.2 Total internal energy curve

Figure 4-6 shows the change of internal energy when the ship impacts the wall of different thickness. When ship with an initial velocity crashes into the 1 m thick wall, the total internal energy of ship increases value of 200 MJ obviously, and the total internal energy of concrete wall increases value of 0.25 MJ. The ship is obviously damaged, but the wall is not damaged. However, for the collision between the ship and 0.5 m thick wall, the situation is reversed.

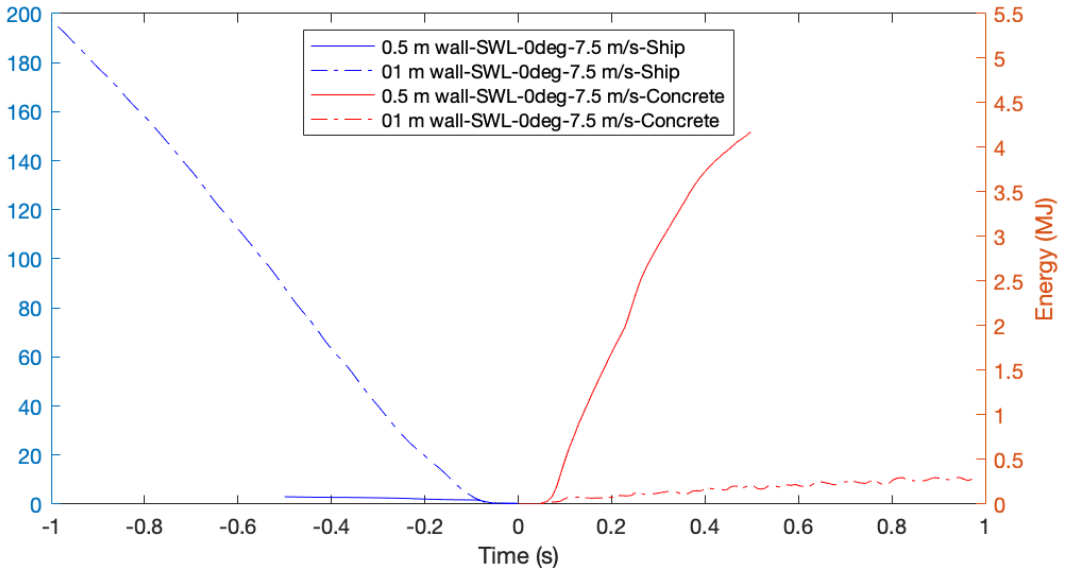

Figure 4-6 Internal energy (including eroded internal energy) of the ship and wall when the ship with an initial velocity of 7.5 m/s impacts 0.5 m and 1 m thick wall on SWL at 0 degree.

4.3.3 Structural deformation

(a)

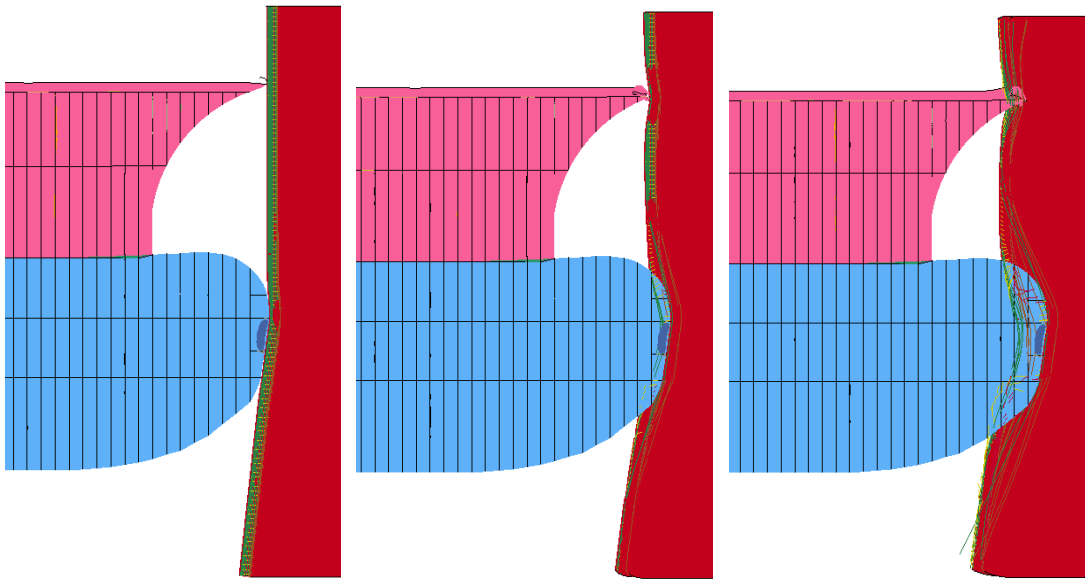

0.1 s 0.3 s 0.5 s

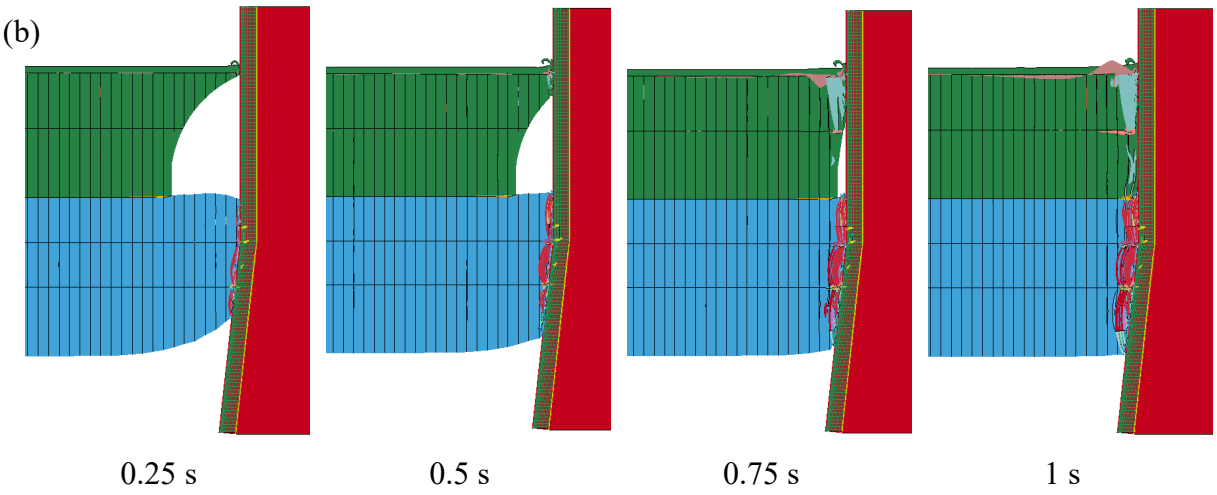

Figure 4-7 Structural deformation of ships and walls at different times, when ship with an initial velocity of 7.5 m/s impacts (a) 0.5 meters and (b) 1 m thick wall

Figure 4-7 illustrates the structural deformation of ships and concrete walls when the ship impacts different wall thickness. In the beginning, the 0.5 m thick wall doesn't fracture but then the concrete broke and the deformation of steel bars gradually increased. For 1 m thick wall, the ship deforms greatly, but concrete is not damaged.

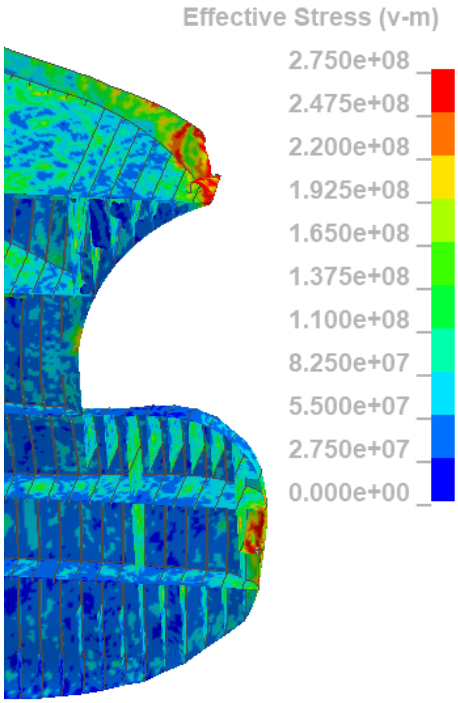

Figure 4-8 Structural deformation of the ship when the ship with an initial velocity of 7.5 m/s impacts SWL of 0.5 m thick wall at 0 degrees. The time is 0.5 s

For 0.5 m thick wall, the stress of ship shows in the Figure 4-8. The stress focuses on the tip of the bulb and forecastle. During the collision, the forecastle of the ship is deformed, but the bulb isn't deformed because the 0.5 m thick wall is damaged. For 1 m thick wall, the stress of ship shows in the Figure 4-9. As time goes on, the bow and forecastle have been continuously deformed and destroyed.

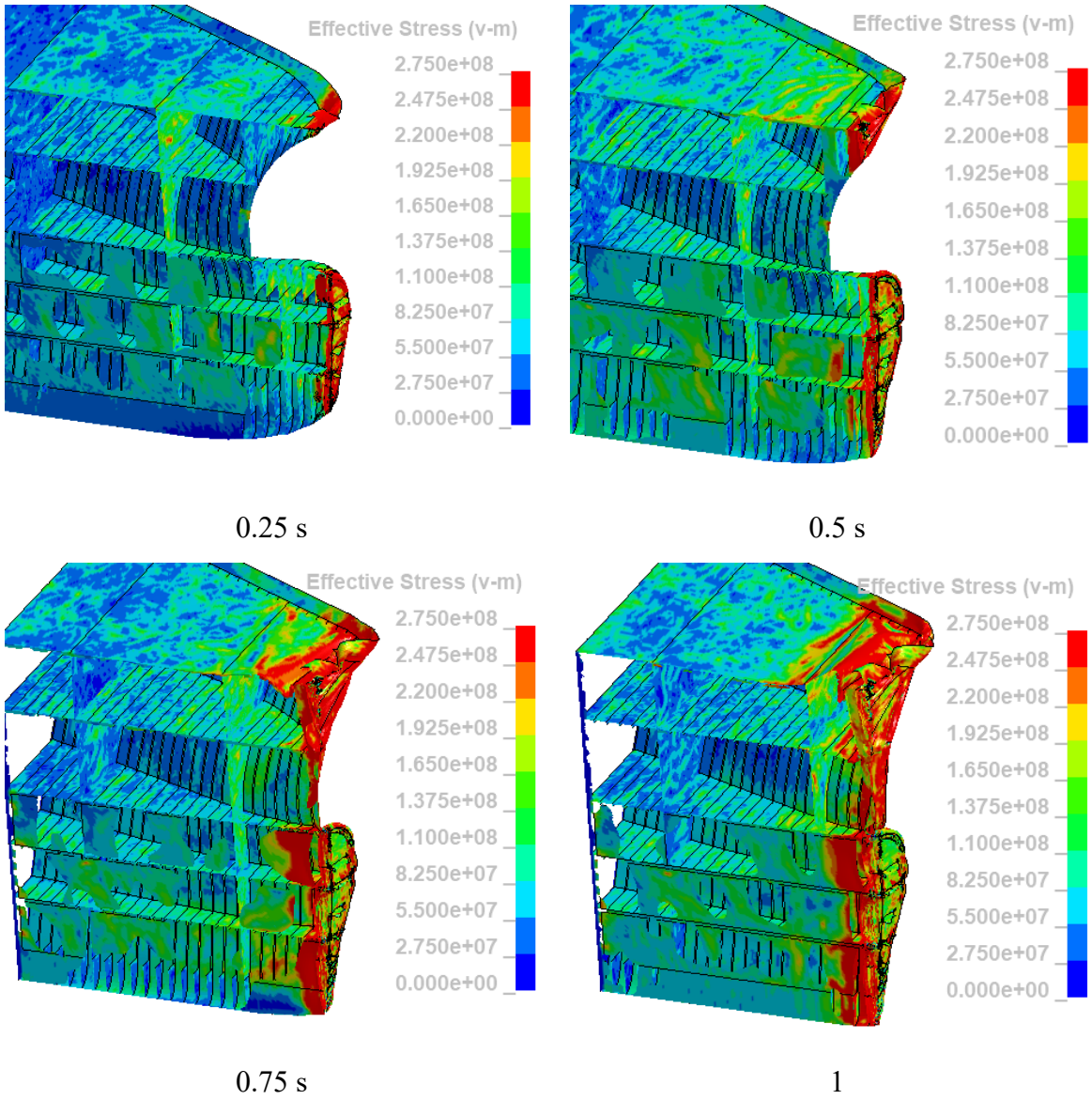

Figure 4-9 Time-varying structural deformation of the ship when the ship with an initial velocity of 7.5 m/s impacts SWL of 1 m thick wall at 0 degrees.

The displacement contours in ship direction and strain contour of the concrete wall are demonstrated in Figure 4-10. The ship is damaged after contacting with concrete. The strength of 0.5 m thick wall is not capable to bear the collision load, and it is easy to be broken. The strain is mainly concentrated in the contact part between ship and concrete, and there are

obvious strain changes but no displacement on both sides of the contact surface. The strain on both sides could be since the upper part of the column is round, and the lower part is conical. The deformation of the transverse reinforcement at the junction pulls the longitudinal reinforcement, which causes the strain in the side of wall.

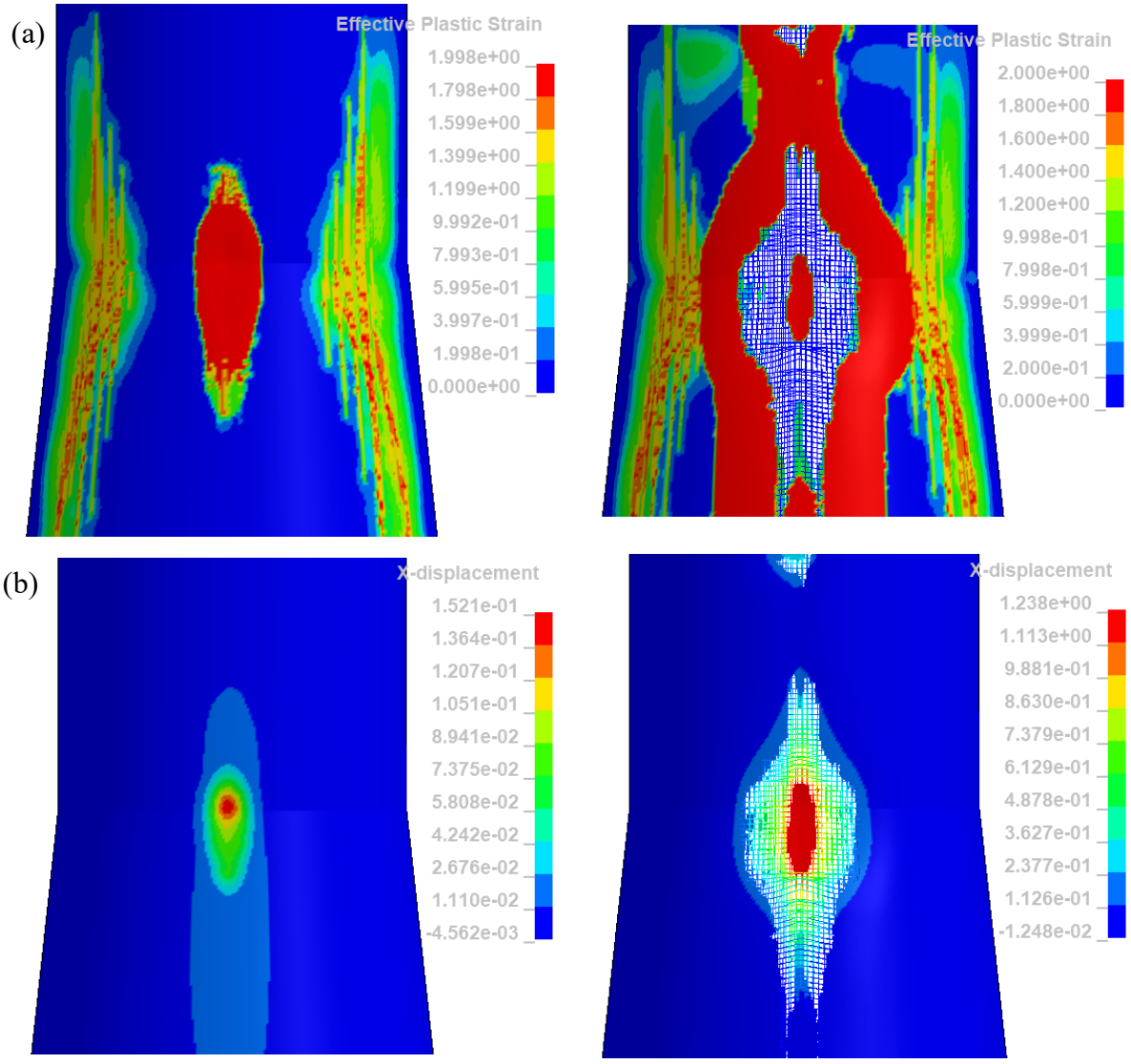

Figure 4-10 Concrete wall of time-varying (a) strain contours and (b) displacement in ship direction contours, when ship with an initial velocity of 7.5 m/s impacts SWL of 0.5 m thick wall at 0 degrees.

Figure 4-11 shows the concrete strain contours changing with time when the ship with an initial velocity of 7.5 m/s impacts the 1 m thick wall. At first, the contact area is small because of the ship deformation small. Then the ship continued to deform, the contact area gradually increases.

In the end, contact area doesn't change but the ship keeps deforming. Compared with Figure 4-10 and Figure 4-11, the 0.5 m thick wall is more easily damaged than 1 m thick wall.

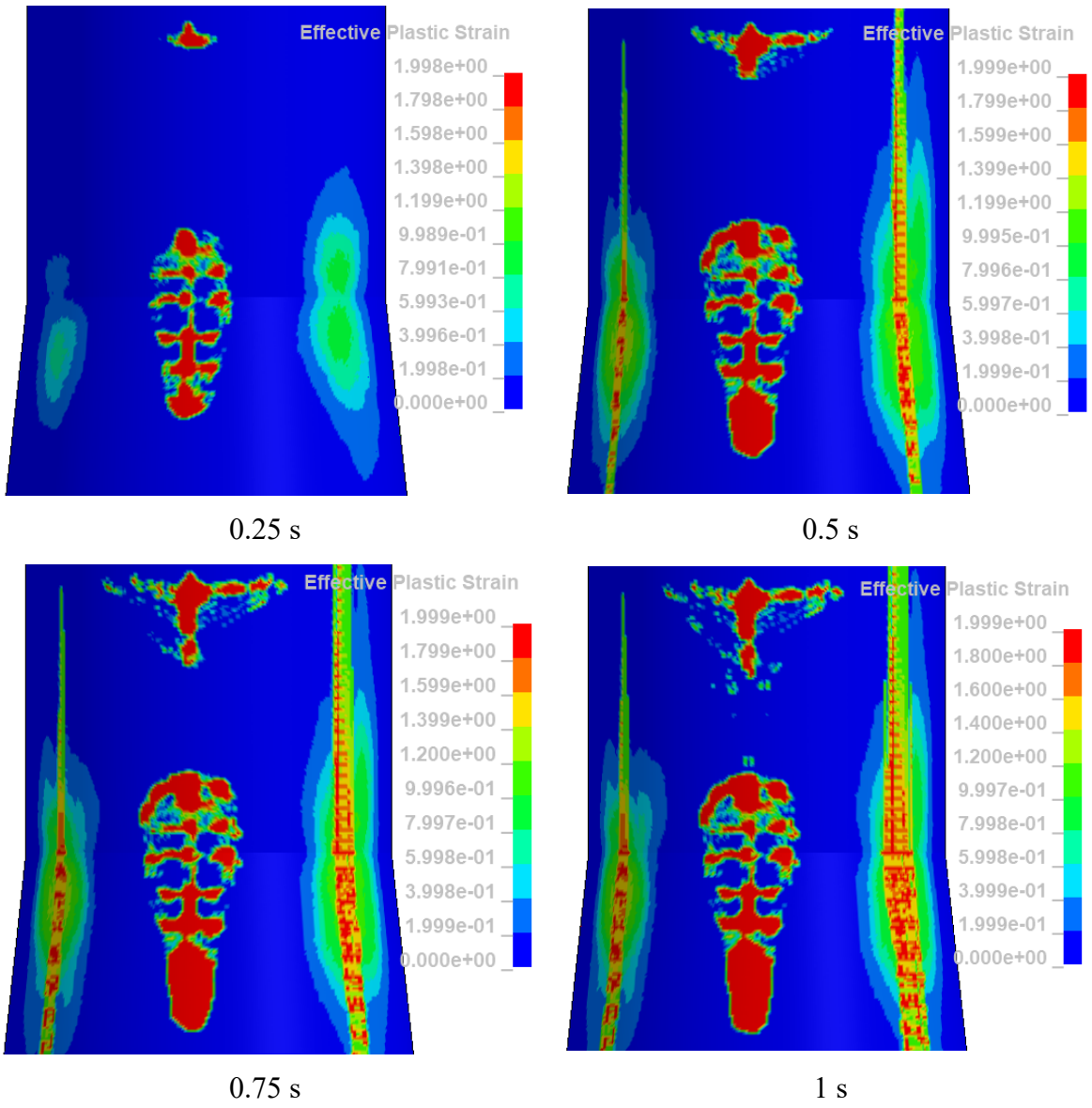

Figure 4-11 Time-varying strain contours of concrete wall, when ship with an initial velocity of 7.5 m/s impacts SWL of 1 m thick wall at 0 degrees.

4.4 Effect of impact speed

In this section, the ship with different initial velocities impacts SWL of the different thicknesses of walls at 0 degree. The initial velocities of ship are 2.5 m/s, 5 m/s and 7.5 m/s for 0.5 m thick wall and 2.5 m/s, 5 m/s, 7.5 m/s and 10 m/s for 1 m thick wall.

4.4.1 Impact on SWL

4.4.1.1 Force-displacement curve

The force-deformation curve of the bulb and forecastle of ship crashing with wall is shown in Figure 4-12 and Figure 4-13. For the 0.5 m thick wall, the different initial velocities do not affect the force of the forecastle. All the forces of the bulb increase to the first peaks, the concrete wall is damaged. Due to the collision failure of concrete surface, a small fall occurred. The peaks and valleys in the force curves due to the continuous collapse of the reinforcement fractured.

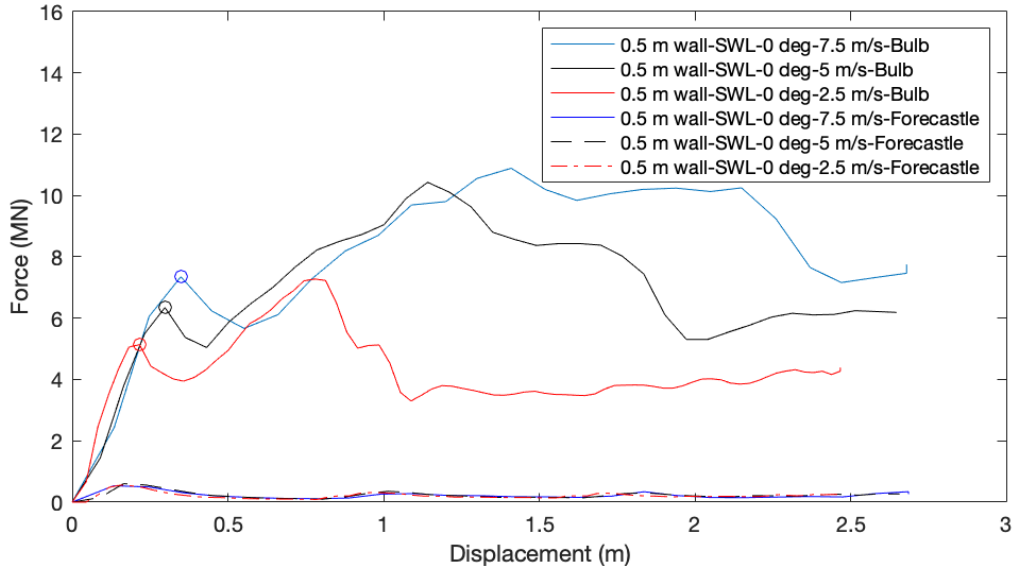

Figure 4-12 Force-displacement curves of ship bulb and forecastle at various initial ship velocities impacts SWL of 0.5 m thick wall at 0 degrees. (The O on the line is damage point)

For the 1 m thick wall, the forces of the bulb are far greater than the forces of the forecastle. At the first peak, all curves are basically the same, and then the curve of 1 m wall-SWL-0 deg-10 m/s-Bulb reaches the first peak and lags other cases of bulb. The curve of 1 m wall-SWL-0 deg-2.5 m/s-Bulb and the curve of 1 m wall-SWL-0 deg-2.5 m/s-Forecastle pass through the peaks and valleys, and then the forces become 0 because of the rebound of ship.

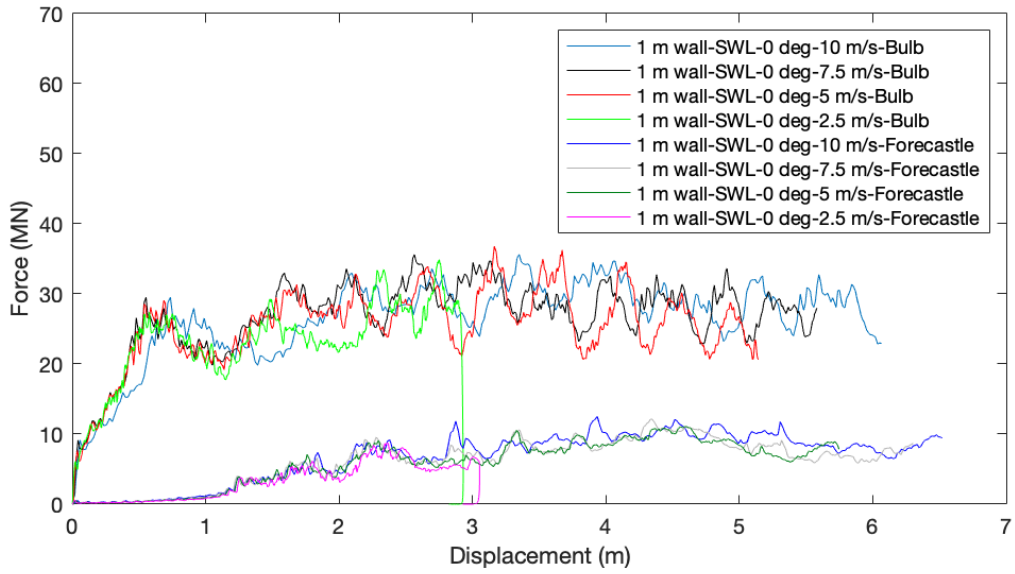

Figure 4-13 Force-displacement curve of ship bulb and forecastle at various ship initial velocities impacts SWL of 1 m thick wall at 0 degrees.

4.4.1.2 Total internal energy curve

Figure 4-14 shows the total internal energy of ships and concrete walls at various ship initial velocity impacting on the 0.5 m thick wall. The ship and concrete wall have the same abscissa but different ordinance. The blue ordinate is the total internal energy of the ship, and the red ordinate is the total internal energy of the concrete wall. For all the 0.5 m thick wall cases, the total internal energies of the concrete walls are larger than that of ships because of damage to the concrete wall. Moreover, the greater the speed, the greater the total internal energy.

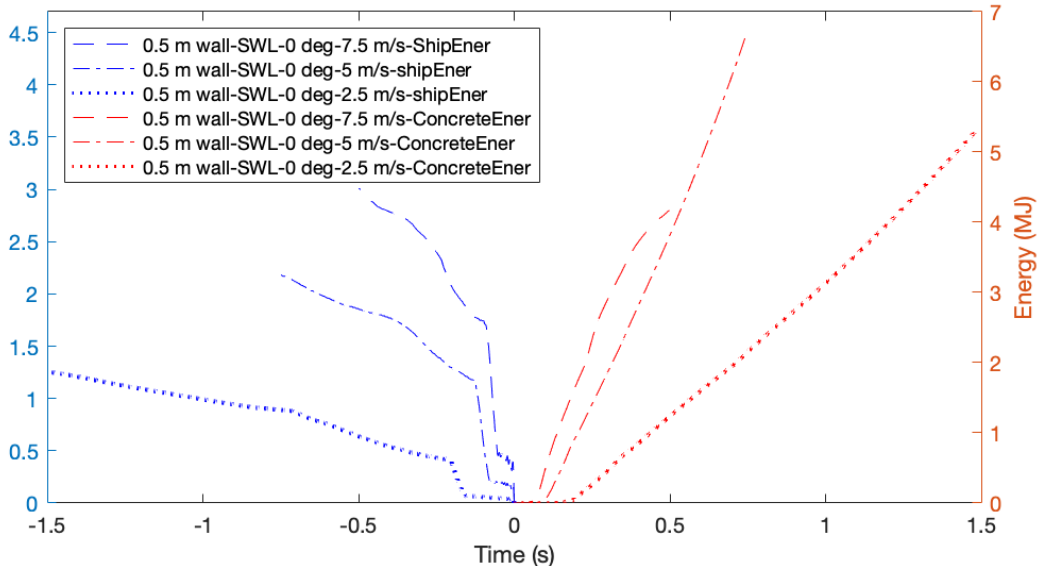

Figure 4-14 Internal energy (including eroded internal energy) of ship and concrete wall at various ship initial velocities impacts SWL of 0.5 m thick wall at 0 degrees.

Figure 4-15 demonstrates the change of total internal energy of the ship and wall when the ship with various initial velocities impacts the 1 m thick wall. The ship and concrete wall have the same abscissa but different ordinance. The blue ordinate is the total internal energy of the ship, and the red ordinate is the total internal energy of the concrete wall. The concrete internal energy of the case of 1 m wall-SWL-0 deg-10 m/s is the largest among all the 1 m thick wall, because the larger the velocity, the larger the total internal energy, and the greater damage to the concrete wall.

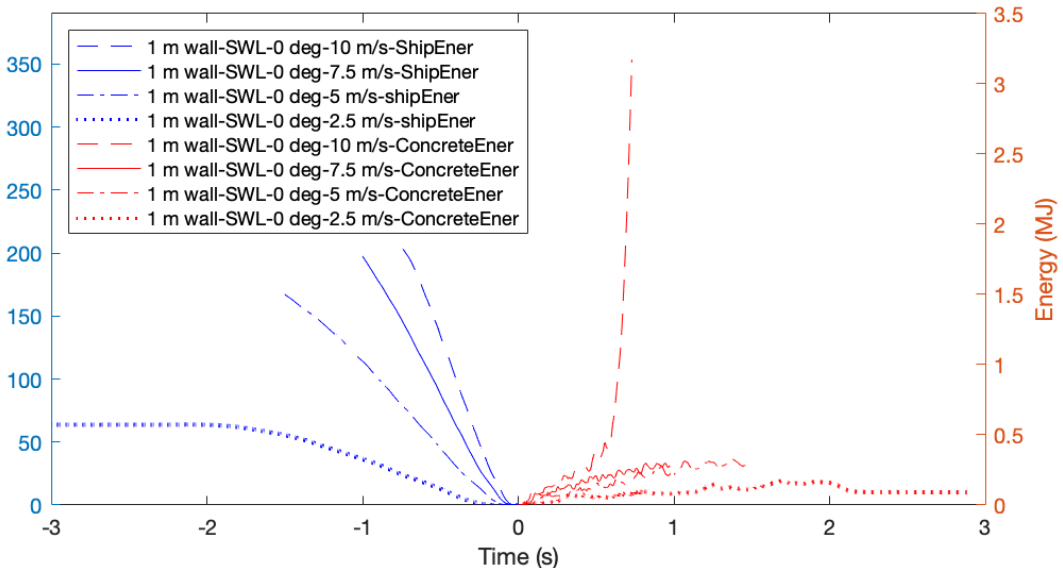

Figure 4-15 Internal energy (including eroded internal energy) of ship and concrete wall at various ship initial velocities impacts SWL of 1 m thick wall at 0 degrees.

4.4.1.3 Structural deformation for 0.5 m thick wall

Figure 4-16 shows the structural deformation of the ship when it with different initial velocities impacts the 0.5 m thick wall. The ship's bulb is not significantly deformed. The stress is just at the tip of the bulb. The pointed shape of forecastle is damaged. Figure 4-17 demonstrates the concrete wall's displacement in the ship direction when the ship with a different initial velocity impacts the 0.5 m thick wall. The concrete wall is damaged in all scenarios of 0.5 thick wall. Therefore, a 0.5 m thick wall is not enough to against the collision.

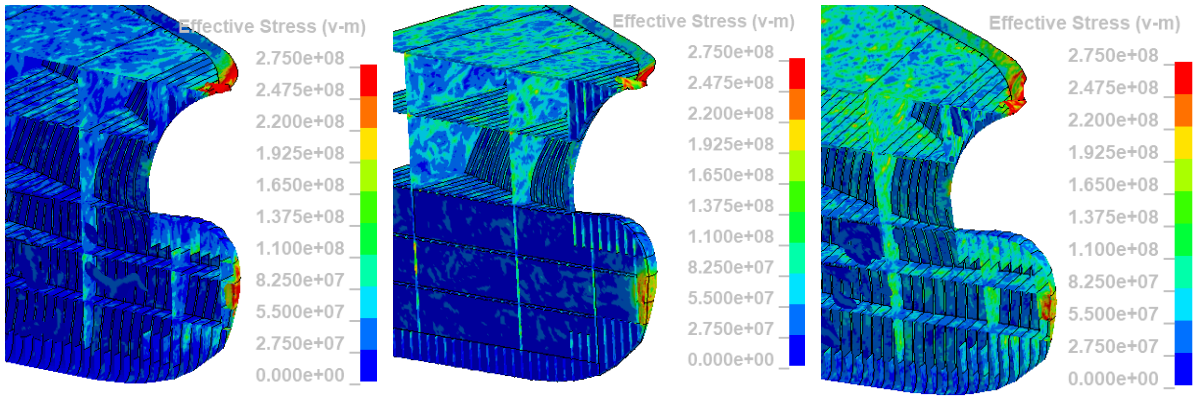

(a) (b) (c)

Figure 4-16 Structural deformation of the ship when a ship with an initial velocity of (a) 2.5 m/s at 1.5 s, (b) 5 m/s at 0.74 s and (c) 7.5 m/s at 0.5 s impacts SWL of 0.5 m thick wall at 0 degrees.

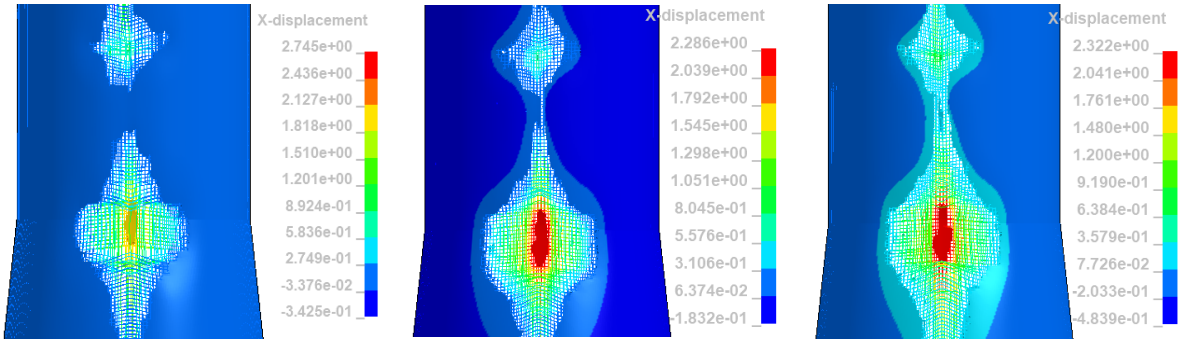

(a) (b) (c)

Figure 4-17 Displacement contours of the concrete wall in ship direction when ship with an initial velocity of (a) 2.5 m/s at 1.5 s, (b) 5 m/s at 0.74 s and (c) 7.5 m/s at 0.5 s impacts SWL of 0.5 m thick wall at 0 degrees.

Figure 4-18 shows the stress contours of the reinforcement when the ships with different initial velocities impact 0.5 m thick walls. The greater the velocity, the greater the deformation and stress of the steel bars. Hence, the greater the ship's speed, the more dangerous the column will be in collision.

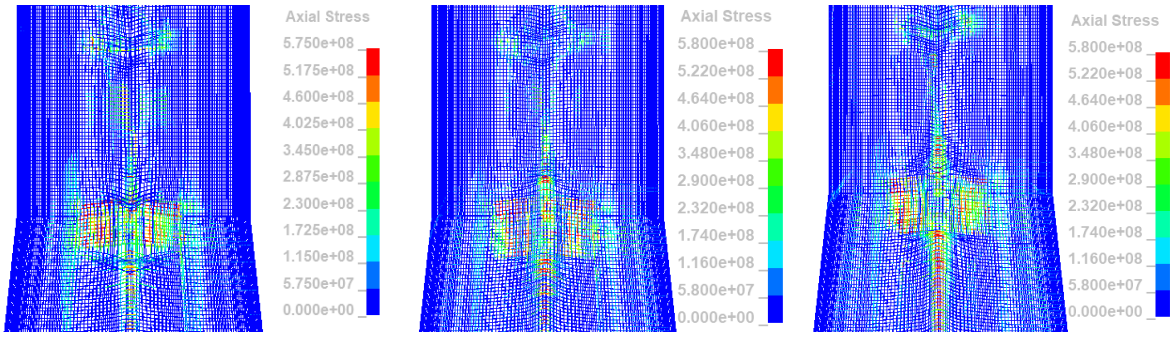

(a) (b) (c)

Figure 4-18 Stress contours of the steel rebars when ship with an initial velocity of (a) 2.5 m/s at 1.5 s, (b) 5 m/s at 0.74 s and (c) 7.5 m/s at 0.5 s impacts SWL of 0.5 m thick wall at 0 degrees.

4.4.1.4 Structural deformation for 1 m thick wall

Figure 4-19 shows structural deformation of the ships with a different initial velocity impacts 1 m thick walls. With the increase of velocities from 2.5 m/s to 10 m/s, the greater the damage of the ships.

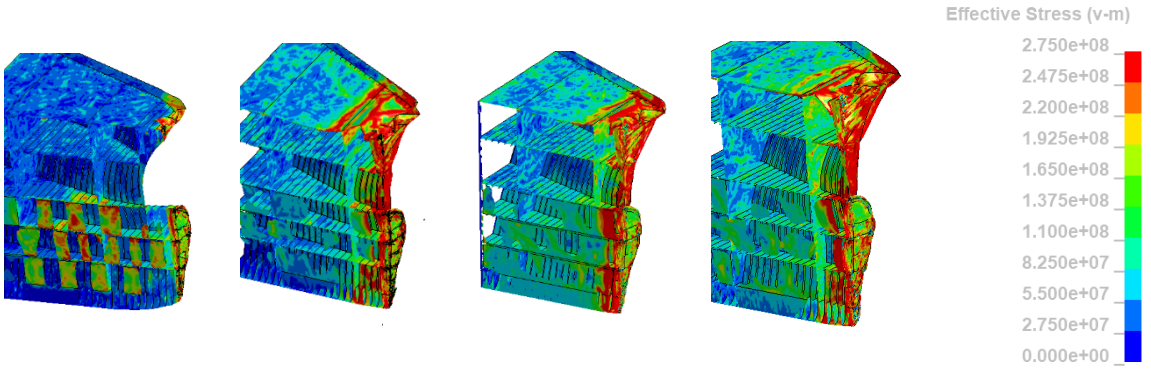

(a) (b) (c) (d)

Figure 4-19 Structural deformation of ship when the ship with an initial velocity of (a) 2.5 m/s at 3 s, (b) 5 m/s at 1.5 s, (c) 7.5 m/s at 1 s and (d) 10 m/s at 0.75 s impacts SWL of 1 m thick wall at 0 degrees.

Figure 4-20 shows the stress contours of the reinforcement when the ships with a different initial velocity impact 1 m thick walls. When the velocity is within the range of 2.5 m/s to 7.5 m/s, the concrete is not damaged, and the contact area is the same size. When the velocity of the ship increased to 10 m/s, the concrete is damaged. Figure 4-21 demonstrates the displacement contours of the concrete wall in ship direction, when the ships with a different initial velocity impact 1 m thick walls. With the increased velocity, the displacement in the ship direction is greater. If the concrete is damaged, the displacement of wall is huge than the

intact concrete wall. When ship velocity is 7.5 m/s and 10 m/s, the displacement in the ship direction is 0.0132 m and 0.699 m, respectively. Therefore, the greater the ship's velocity, the more dangerous the column in the event of a collision. 1 m thick wall is safer than 0.5 m thick wall.

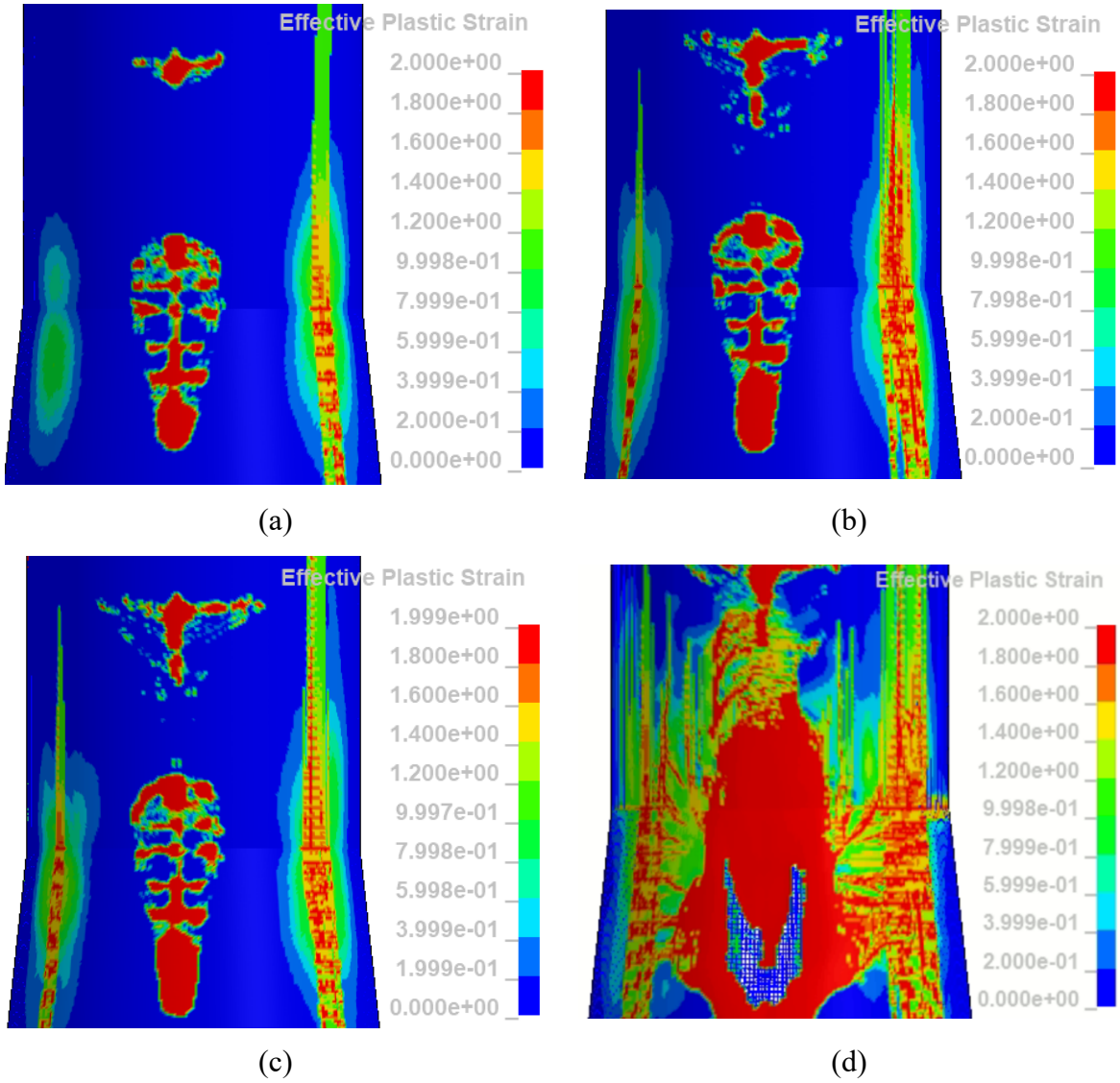

Figure 4-20 Strain contours of the concrete wall when with an initial velocity of (a) 2.5 m/s at 3 s, (b) 5 m/s at 1.5 s, (c) 7.5 m/s at 1 s and (d) 10 m/s at 0.75 s impacts SWL of 1 m thick wall at 0 degrees.

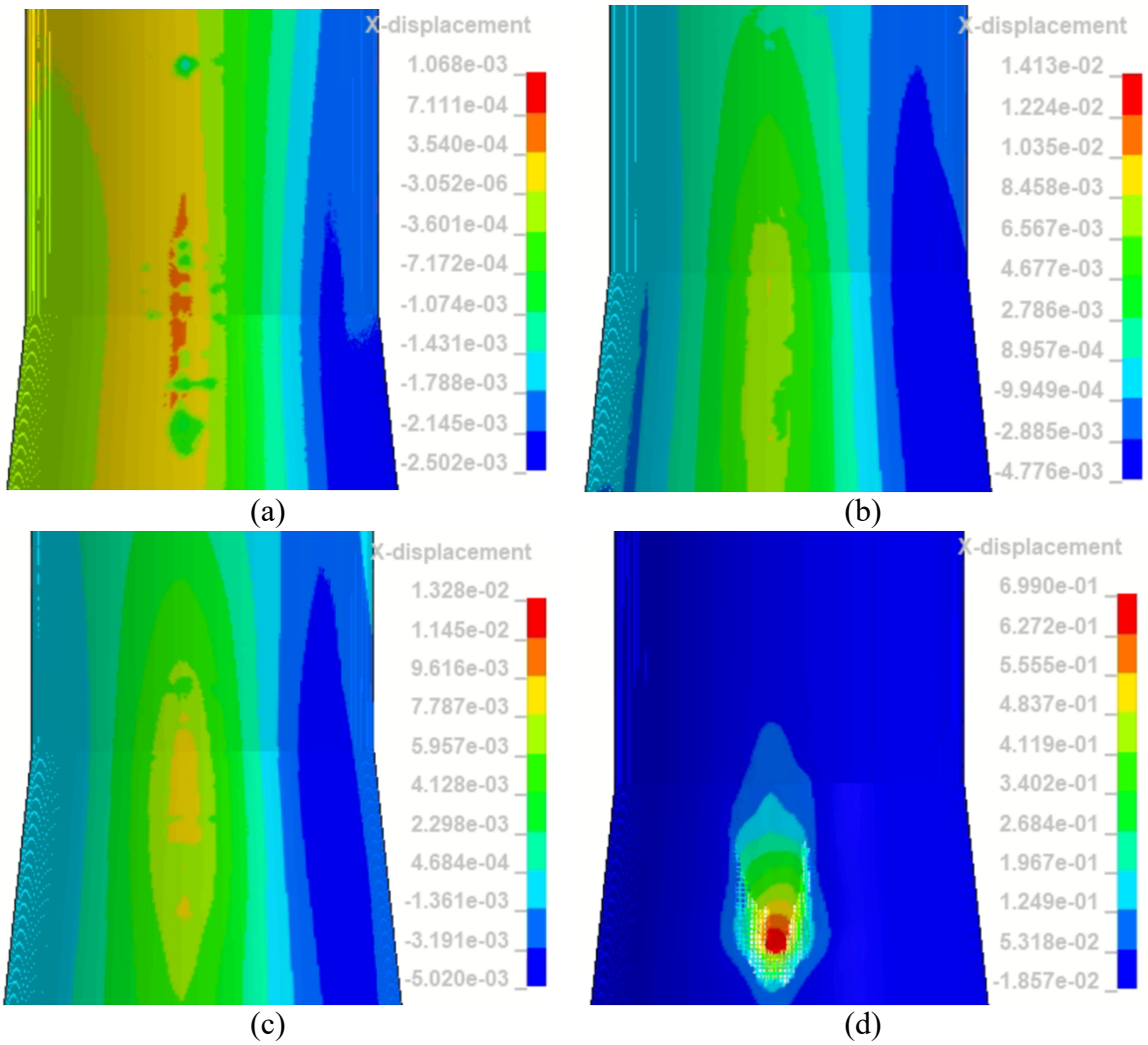

Figure 4-21 Displacement contours of the concrete wall in ship direction when the ship with an initial velocity of (a) 2.5 m/s at 3 s, (b) 5 m/s at 1.5 s, (c) 7.5 m/s at 1 s and (d) 10 m/s at 0.75 s impacts SWL of 1 m thick wall at 0 degrees.

4.4.2 Impact on bottom

In chapter 4.5, the bottom of the concrete wall is broken because of the conical shape. This part will compare the influence of velocities on the conical shape of the bottom of the concrete wall. The initial velocities of ship are 7.5 m/s, 5 m/s and 2.5 m/s respectively.

4.4.2.1 Force-displacement curve

Figure 4-22 shows the force-displacement curve of ship bulb and forecastle at initial different ship velocities impacts bottom of 1 m thick wall at 0 degrees. The curve of the 1 m wall-Bottom-0 deg-7.5 m/s-Bulb is larger than other curves for the high speed of the ship damages the bottom of wall. The curve of the 1 m wall-Bottom-0 deg-5 m/s-Bulb goes up until the top,

and then up and down keeping the plan trend. The concrete wall is broken at the peak of the curve, and the up and down because of the ship and rebars deformation. The curve of the 1 m wall-Bottom-0 deg-2.5 m/s-Bulb increases gradually, after reaching the peak value, it goes down and the displacement retreats. Due to the ship with low initial velocity hitting the bottom of wall, the energy dissipated and bounced back. All forces of forecastle are smaller than those force of bulbs. The greater velocity of ship, the greater the force. After energy dissipation, the ship with an initial velocity of 2.5 m/s bounds back. Hence, the high-speed is dangerous for the bottom of wall.

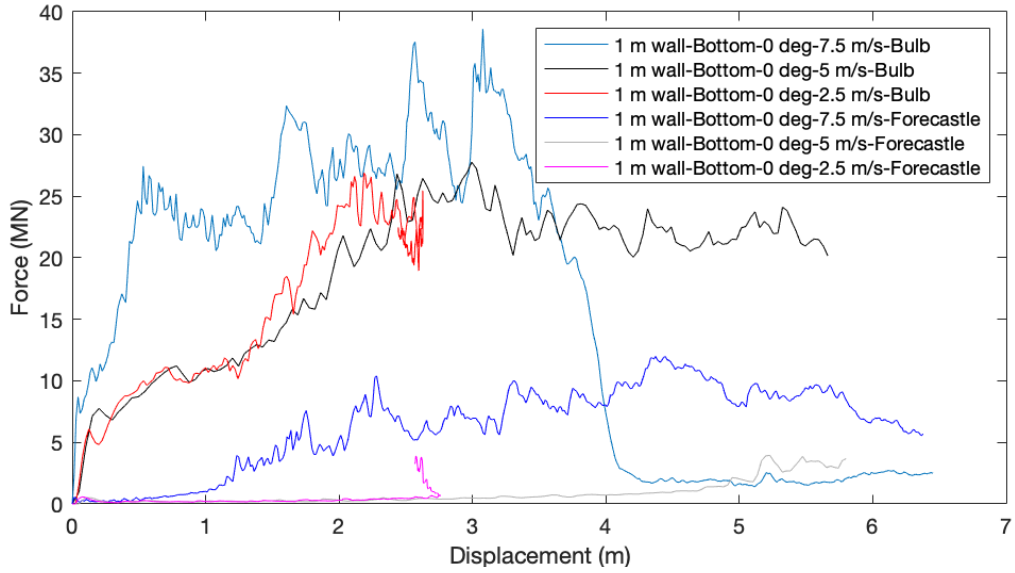

Figure 4-22 Force-displacement curve of ship bulb and forecastle at initial different ship velocities impacts bottom of 1 m thick wall at 0 degrees.

4.4.2.2 Total initial energy

When ships with different initial ship speeds hit the bottom of a 1 m thick wall at an angle of 0 degrees, the internal energy (including eroded internal energy) of the ship and concrete wall is shown in Figure 4-23. The total internal energy of the ship is greater than that of concrete wall. With the change of time, the total internal energy curves of the ship and concrete wall increase. The greater the speed, the greater the total internal energy will be. When the ship with an initial velocity of 2.5 m/s impacts the concrete wall, the total internal energy of the concrete wall is smooth and stable for undamaged concrete wall, and the total internal energy of the ship increases by 64 MJ, which becomes stable for the rebound of the ship.

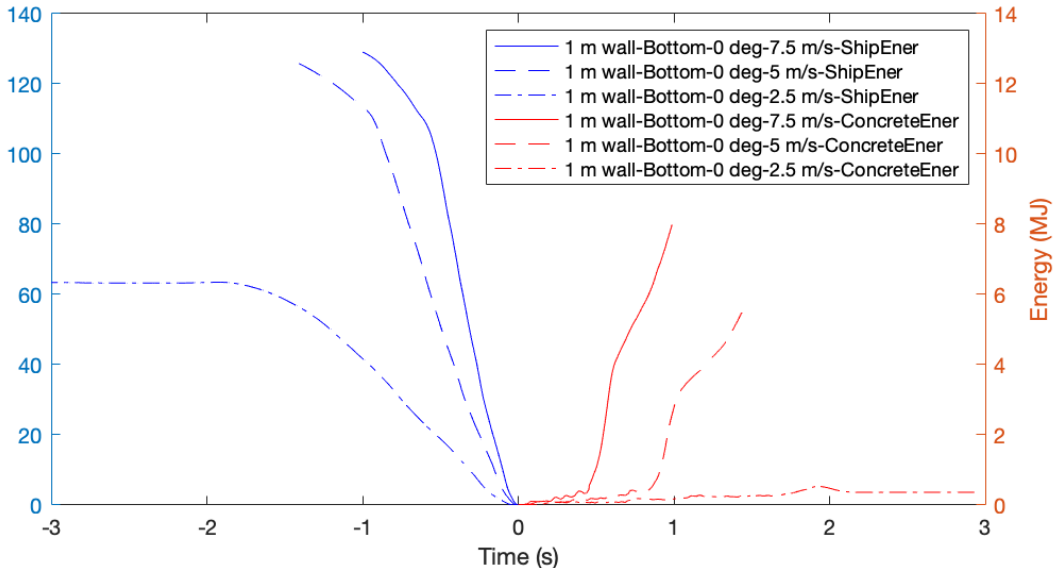

Figure 4-23 Internal energy (including eroded internal energy) of the ship and concrete wall when the ship with different initial ship velocities impacts bottom of 1 m thick wall at 0 degrees.

4.4.2.3 Structural deformation

Figure 4-39, Figure 4-24 and Figure 4-25 are shown the structural deformation of the ship, whose initial velocities of 7.5 m/s, 5 m/s and 2,5 m/s, respectively, impacting on the bottom of 1 m thick wall at 0 degrees. When the initial velocity of the ship is 7.5 m/s, the structural deformation of the ship has a small change after 0.5 s. Similarly, the structural deformation of the ship with an initial velocity of 5 m/s has small deformation after 1 s. For the ship with an initial velocity of 2.5 m/s, the structural deformation of the ship becomes larger and then the stress moves from the top to the middle of the ship.

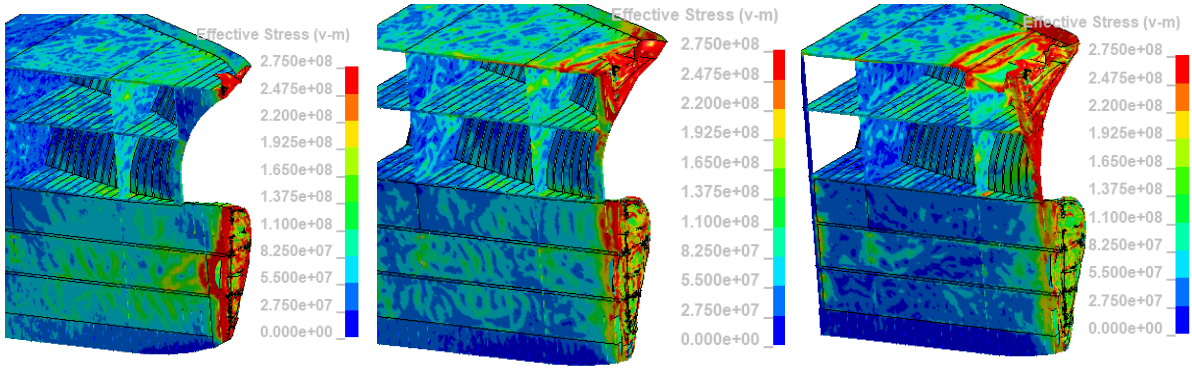

0.5 s 1 s 1.5 s

Figure 4-24 Time-varying structural deformation of the ship when the ship with an initial velocity of 5 m/s impacts bottom of 1 m thick wall at 0 degrees.

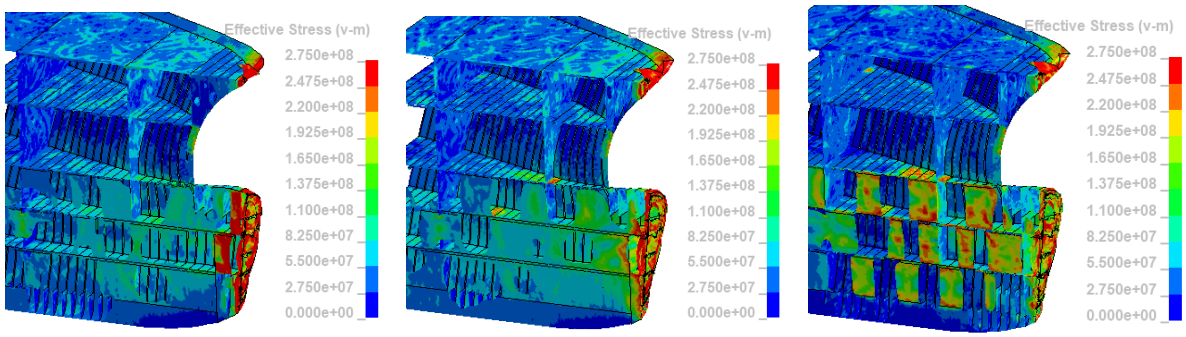

1 s 2 s 3 s

Figure 4-25 Time-varying structural deformation of the ship when the ship with an initial velocity of 2.5 m/s impacts bottom of 1 m thick wall at 0 degrees.

Figure 4-26 shows the strain and displacement in the ship direction when the ship with an initial velocity of 5 m/s impacts the bottom of 1 m thick wall at 0 degrees. After 1 s, the concrete wall is broken and the displacement in the ship direction is 0.48 m. For the ship with an initial velocity of 2.5 m/s in Figure 4-27, the contact area of the ship and concrete remains unchanged. In Figure 4-28, due to the rebound of the ship, the displacement in the ship direction increases and down. As a result, the conical shape of the concrete wall is more sensitive than the top normal column. It's dangerous for a high-speed ship to hit the bottom of column.

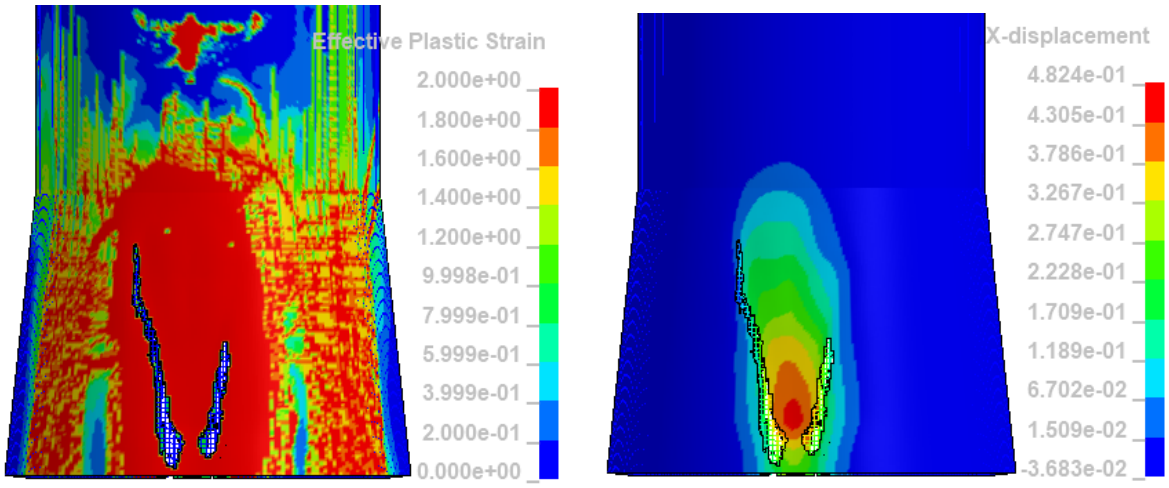

(a) (b)

Figure 4-26 Contour of (a) plastic strain at 1 s and (b) displacement at 1 s in ship direction when the ship with an initial velocity of 5 m/s impacts bottom of 1 m thick wall at 0 degrees.

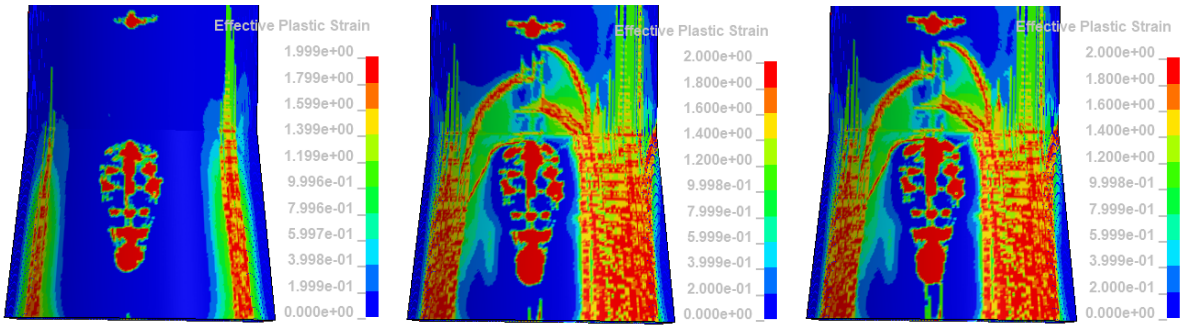

1 s 2 s 3 s

Figure 4-27 Time-varying concrete strain contour when the ship with an initial velocity of 2.5 m/s impacts bottom of 1 m thick wall at 0 degrees.

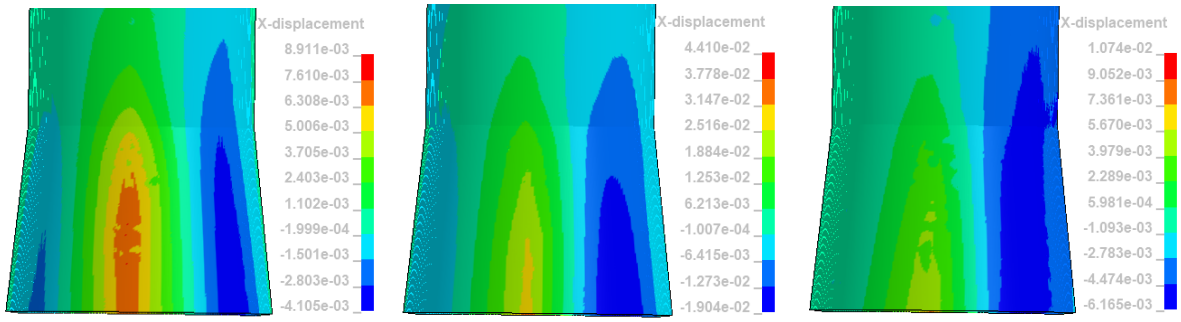

1 s 2 s 3 s

Figure 4-28 Time-varying contour of displacement in ship direction when the ship with an initial velocity of 2.5 m/s impacts bottom of 1 m thick wall at 0 degrees.

4.5 Effect of impact angle

In this section, the ship with an initial velocity of 7.5 m/s impacts SWL of the 1 m thick wall at 0 and 45 degrees.

4.5.1 Force-displacement curve

Figure 4-29 shows the force-displacement curve of bulb and forecastle when the ship with an initial velocity of 7.5 m/s impacts SWL of 1 m thick wall at 0 and 45 degrees. During the whole process, the forces of 45 degree-collision are smaller than that of 0 degree-collision. After 1 m displacement, the force of bulb-ship decreases suddenly, because the ship is snap. The force of forecastle-ship has a similar trend and the force of 45 degrees is bigger than the force of 0 degrees, because after snap of bulb, the main force on the forecastle.

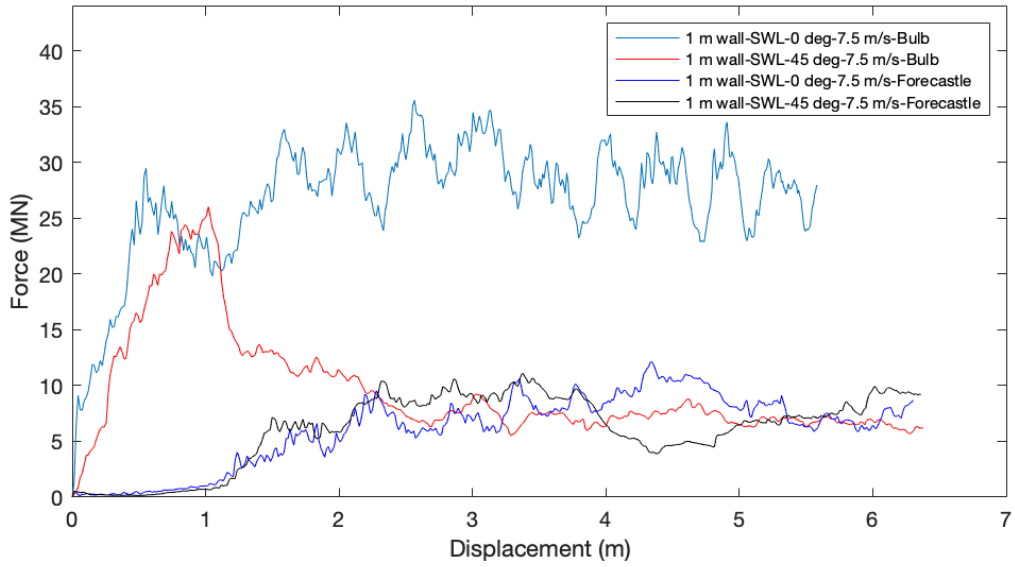

Figure 4-29 Force-displacement curve of ship bulb and forecastle when ship with initial velocity of 7.5 m/s impacts SWL of 1 m thick wall at 0 and 45 degrees.

4.5.2 Total internal energy curve

Figure 4-30 shows the internal energy of ships and concrete wall when a ship with an initial velocity of 7.5 m/s impacts 1 m thick wall at different degrees. The ship and concrete wall have the same abscissa but different ordinance. The blue ordinate is the total internal energy of the ship, and the red ordinate is the total internal energy of the concrete wall. The total internal energies of ships and concrete walls at 0 degrees angle is greater than that of the ship and concrete wall at 45 degrees angle. With the passage of time, the total energy of ships increases. When the ship impacts at 0 degree of concrete wall, the total internal energy of the concrete wall will increase with the passage of time. However, the total internal energy of the concrete wall increases to second peak in 45 degree-collision, and then keeps the flat trend, because the concrete does not strongly deform with the damage of ship.

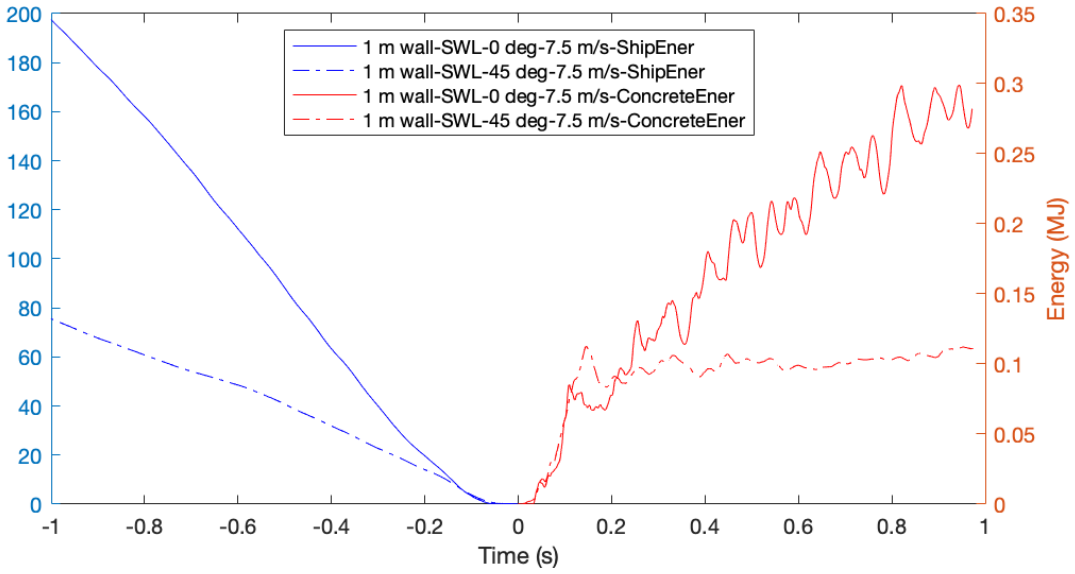

Figure 4-30 Internal energy (including eroded internal energy) of ships and concrete walls, when ship with an initial velocity of 7.5 m/s impacts SWL of 1 m thick wall at 0 and 45 degrees.

4.5.3 Structural deformation

The snapshot of ship structure deformation demonstrates in Figure 4-31. It is different from Figure 4-9 (ship impacts column at 0 degrees). 0 degree-collision damage is concentrated on the top of the ship. But 45 degree-collision makes the ship snap on the side.

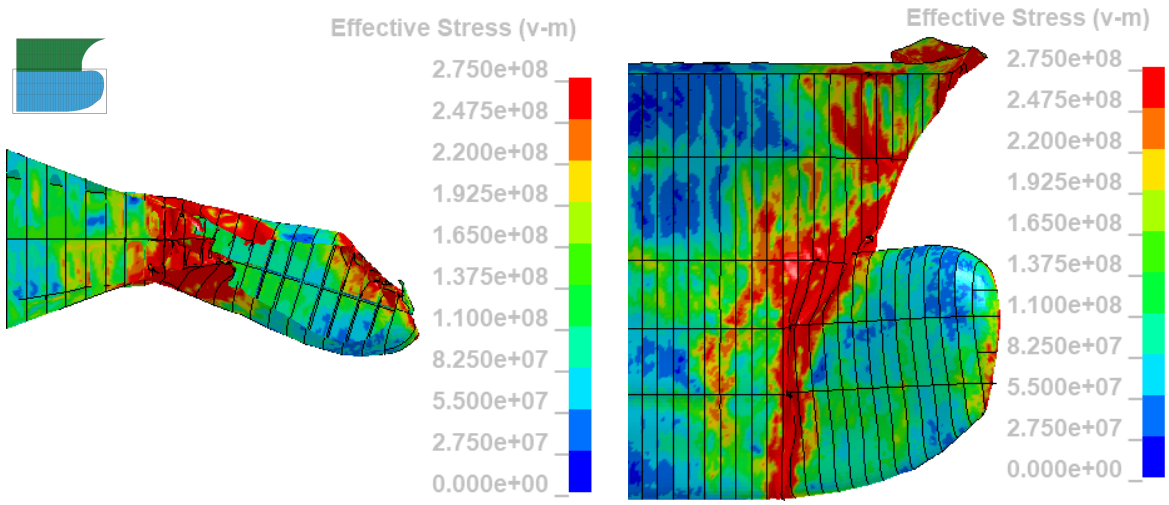

Figure 4-31 Top view (left) and side view (right) of ship structure deformation after impacting for 0.5 s, when ship with initial velocity of 7.5 m/s impacts SWL of 1 m thick wall at 45 degrees. (The picture on the top shows the cutting way)

Figure 4-32 shows the strain of concrete and displacement of concrete in the ship direction in 45 degrees-collision. The contact area of concrete strain is smaller than that in Figure 4-11 (0

degree-collision). It can be seen from Figure 4-21 (b) that the displacement of concrete in the ship direction is 0.013 m in 0 degree-collision and is 0.009 m in 45-degree-collision. Therefore, 0 degree-collision is more dangerous to concrete, and 45 degree-collision may cause danger to ship.

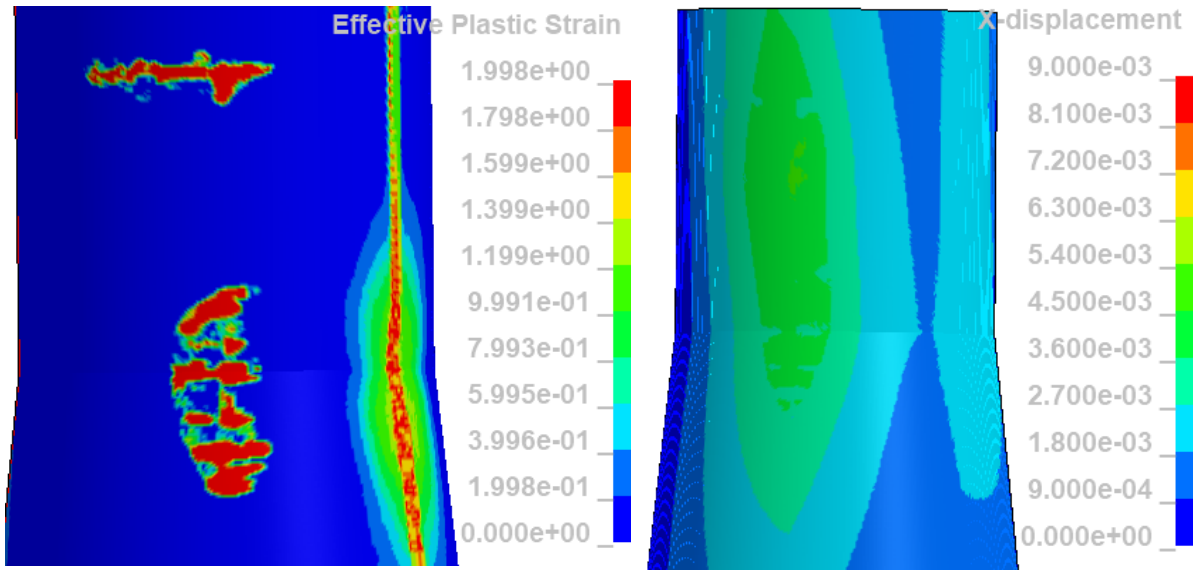

(a) (b)

Figure 4-32 Contour illustrations of (a) strain of concrete and (b) displacement in ship direction of concrete, when ship with initial velocity of 7.5 m/s impacts SWL of 1 m thick wall at 45 degrees.

4.6 Effect of impact position

In this section, the ship with an initial velocity of 7.5 m/s impacts different positions of wall with a thickness of 1 m. The positions scenarios demonstrated in chapter 0 (Figure 4-3).

4.6.1 Force-displacement curve

Figure 4-33 shows the force-displacement curves of ship bulb and forecastle when the ship with an initial velocity of 7.5 m/s impacts different position of 1 m thick wall at 0 degrees. The curve of the 1 m wall-Top-0 deg-7.5 m/s-Bulb and the curve of 1 m wall-Top1-0 deg-7.5 m/s-Bulb have a similar trend and the curve of the 1 m wall-Top1-0 deg-7.5 m/s-Bulb has larger peaks of force values. After 4.5 m displacements for the ship, the curve of the 1 m wall-Top-0 deg-7 m/s-Bulb goes down and then plunges to 1 MN, but the curve of the 1 m wall-Top1-0 deg-7.5 m/s-Bulb continues to go up and down. This is because the concrete wall in the case

of 1 m wall-Top-0 deg-7.5 m/s is broken at the beginning and then the reinforcements are damaged. The curve of the 1 m wall-Bottom-0 deg-7.5 m/s-Bulb drops down to the value of 1 MN because the rebars are damaged. For the forecastles of the ship, the force of 1 m wall-Top-0 deg-7. 5 m/s is largest at the very beginning. Because the forecastles of the ship peel off the concrete and the column damage immediately.

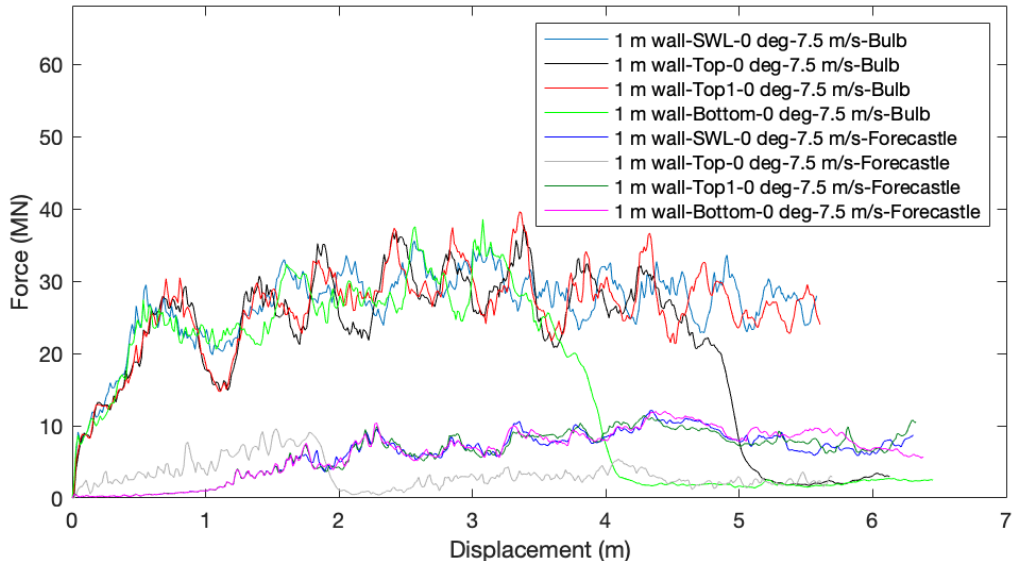

Figure 4-33 Force-displacement curve of ship bulb and forecastle when the ship with an initial ship velocity of 7.5 m/s impacts different position of 1 m thick wall at 0 degrees.

4.6.2 Total internal energy curve

The total internal energy is demonstrated in Figure 4-34. It shows the change of total energy when the ship with an initial ship velocity of 7.5 m/s impacts on different positions of 1 m thick wall at 0 degrees. The case of 1 m wall-SWL-0 deg-7.5 m/s has a large total internal energy of the ship but small total internal energy of the concrete wall. Because the concrete wall is not damaged, the total internal energy of the ship increases because of the velocity and the deformation of the ship. The case of 1 m wall-Top-0 deg-7.5 m/s and the case of 1 m wall-Bottom-0 deg-7.5 m/s have high total internal energy of concrete than other cases, because the concrete wall is damaged. Therefore, when the ship impacts the Top or the Bottom of the concrete wall, it is dangerous for the concrete column. It is necessary to avoid such collisions.

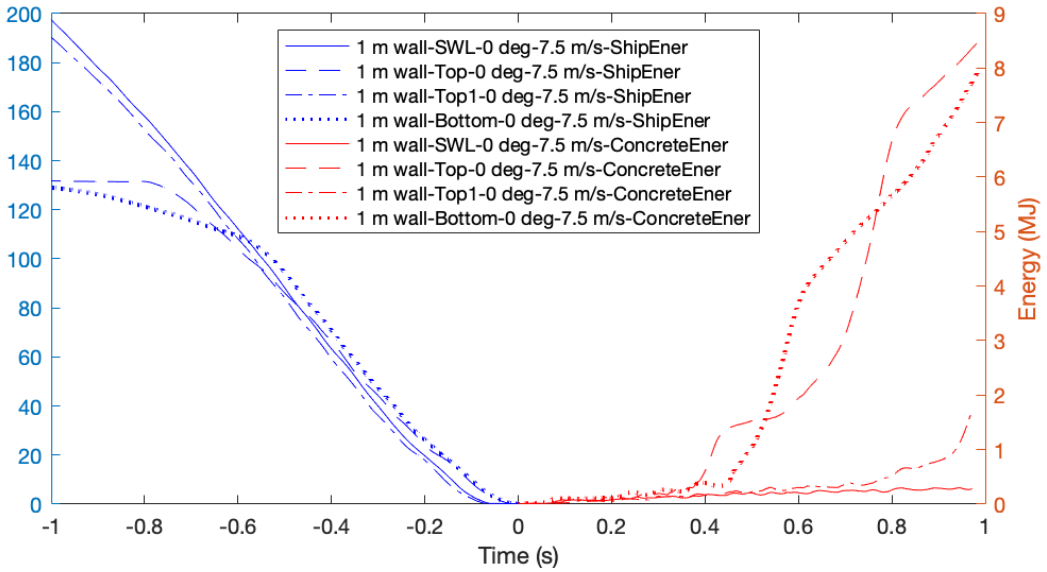

Figure 4-34 Internal energy (including eroded internal energy) of ship and concrete wall when the ship with an initial ship velocity of 7.5 m/s impacts different position of 1 m thick wall at 0 degrees.

4.6.3 Structural deformation

4.6.3.1 Ship impacts Top

Figure 4-35 shows the structural deformation of the ship when ship with an initial velocity of 7.5 m/s impacts top of 1 m thick wall at 0 degrees. As time goes on, the deformation of the bulb of the ship increases. The forecastle of the ship has stress at the beginning and then the stress decreases. The strain contours of the concrete wall change with time are shown in Figure 4-36, when the ship with an initial velocity of 7.5 m/s impacts top of 1 m thick wall at 0 degrees. The top of the concrete is damaged first, and then the part contacting with the bulb is damaged.

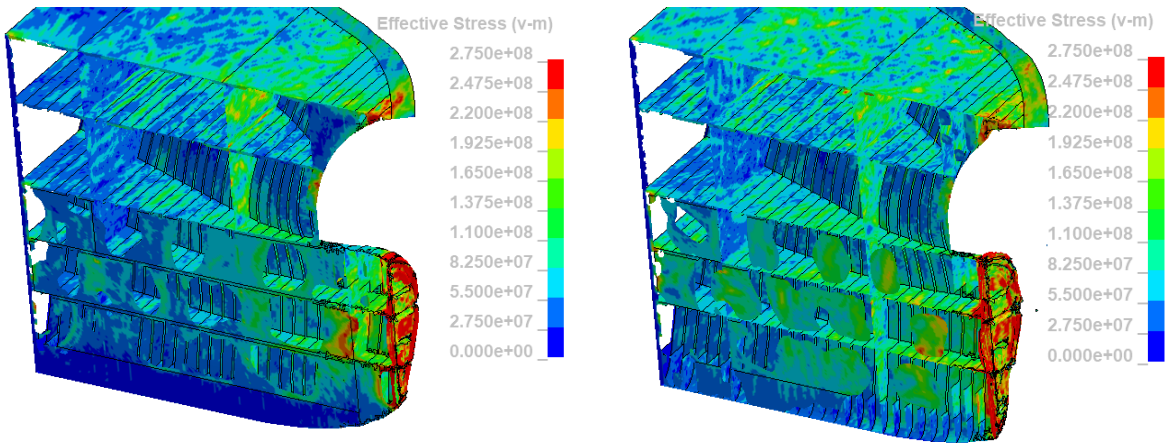

0.25 s 0.5 s

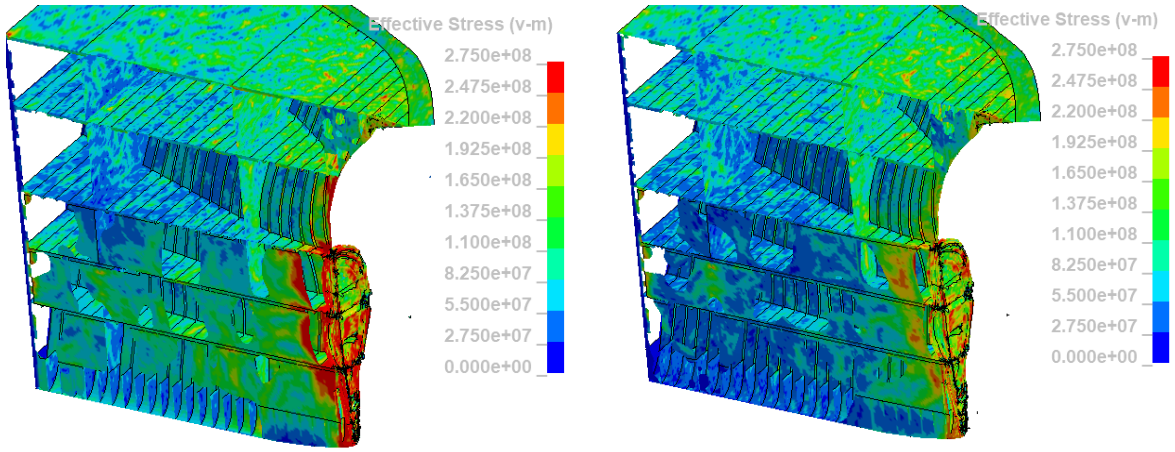

0.75 s 1 s

Figure 4-35 Time-varying structural deformation of ship when the ship with an initial velocity of 7.5 m/s impacts top of 1 m thick wall at 0 degrees.

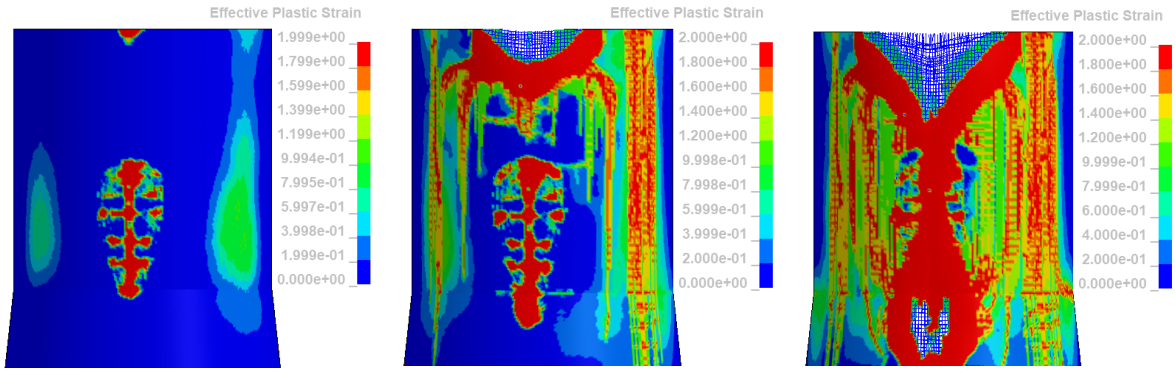

0.25 s 0.5 s 0.75 s

Figure 4-36 Time-varying strain contours of concrete wall, when ship with an initial velocity of 7.5 m/s impacts top of 1 m thick wall at 0 degrees.

4.6.3.2 Ship impacts Top1

Figure 4-37 demonstrates concrete strain and ship stress when the ship with an initial ship velocity of 7.5 m/s impacts Top1 of 1 m thick wall at 0 degrees. At 1 s, the concrete wall is not damaged, but the ship is greatly deformed. The displacement of the concrete wall in the ship direction and the axial stress of reinforcement are shown in Figure 4-38. The concrete wall is not a great deformed. As time goes on, the axial stress of rebars increases. Therefore, the column is safe when the ship crashes on the Top1 of column.

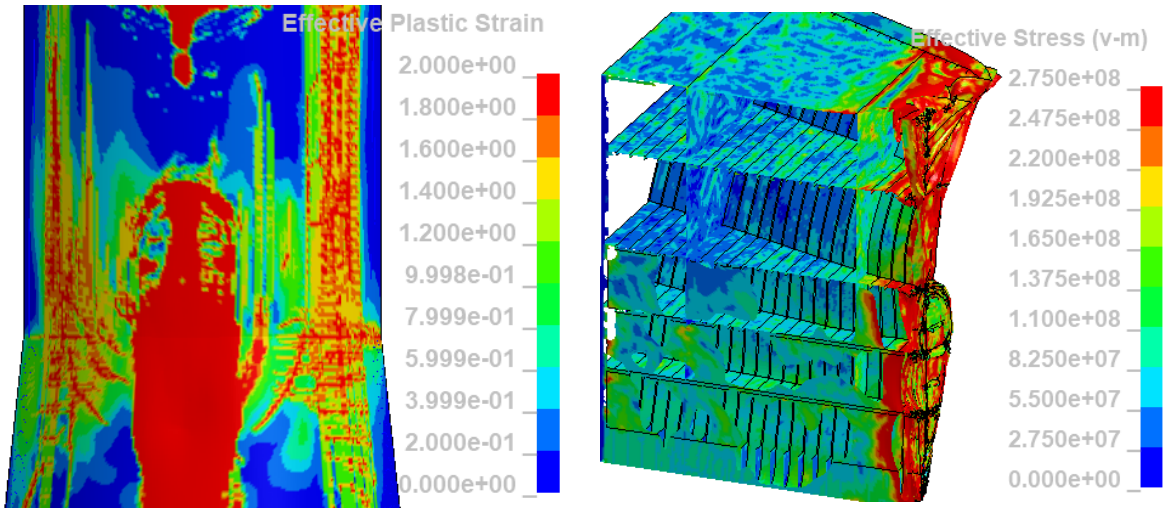

Figure 4-37 Contours of concrete strain at 1 s (left) and ship stress at 1 s (right) when ship with an initial ship velocity of 7.5 m/s impacts Top1 of 1 m thick wall at 0 degrees.

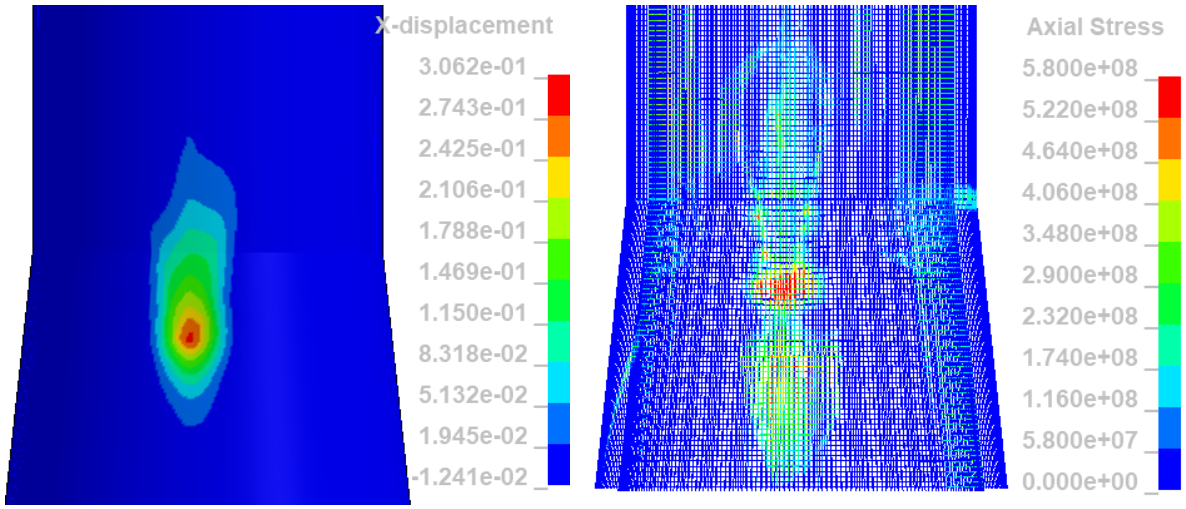

Figure 4-38 Contours of displacement in ship direction of concrete wall (left) and axial stress of rebar (right), when ship with initial ship velocity of 7.5 m/s impact Top1 of 1 m thick wall at 0 degrees

4.6.3.3 Ship impacts Bottom

Figure 4-39 shows the structural deformation of the ship when the ship with an initial velocity of 7.5 m/s impacts on the bottom of a 1 m thick wall at 0 degrees. At first, the bulb and forecastle of the ship are deformed. After 0.5 s the stress of the bulb decreases, the contact area between the ship and concrete wall increases, and the damaged area of forecastle continues to increase.

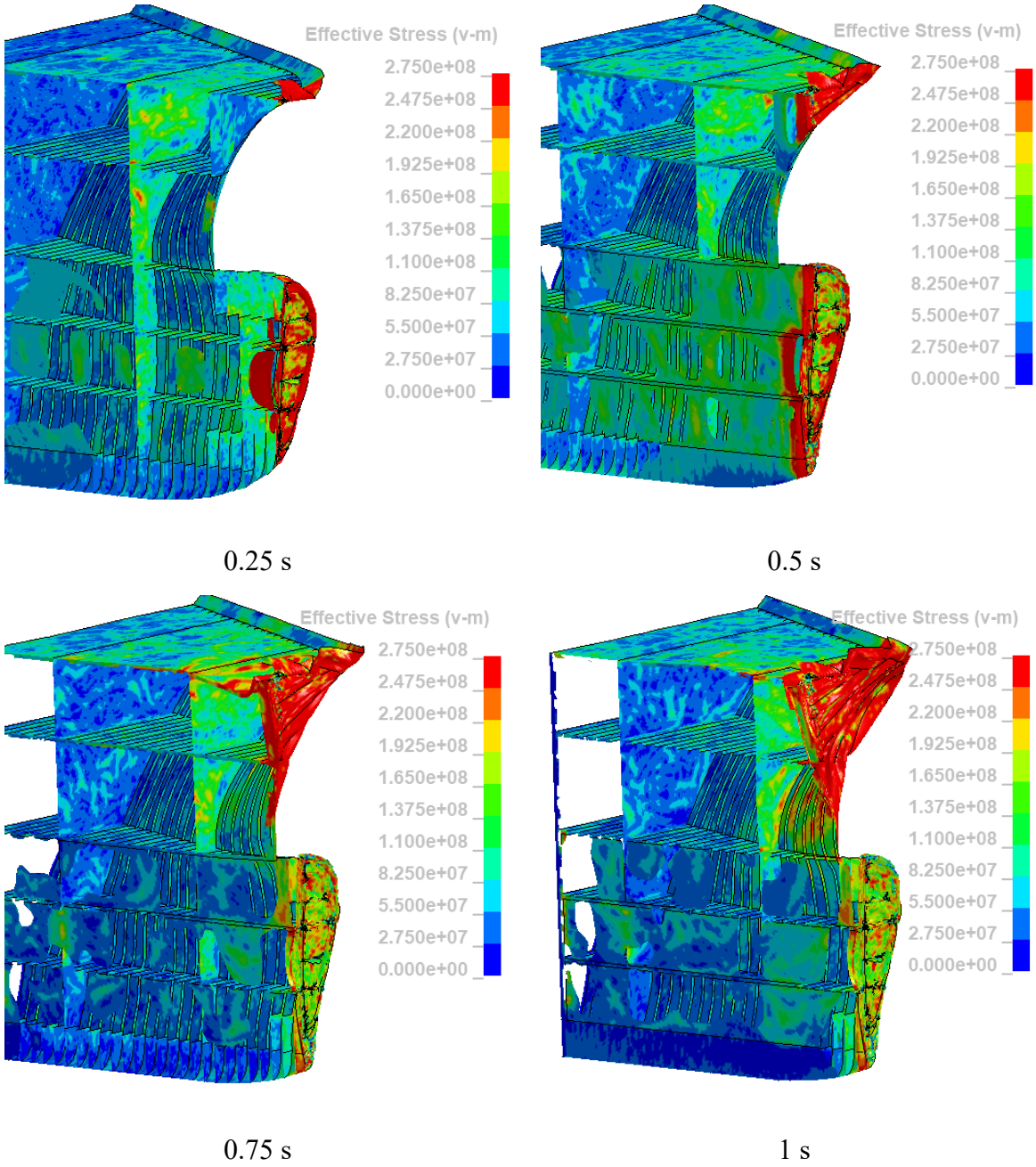

Figure 4-39 Time-varying structural deformation of ship when the ship with an initial velocity of 7.5 m/s impacts the bottom of 1 m thick wall at 0 degrees.

The time history of concrete strain and displacement in ship direction are given in Figure 4-40 and Figure 4-41. The concrete-ship contact area and the displacement in the ship direction increase over time. When displacement in the ship direction is concentrated at a small part, the concrete wall would be damaged. The deformation of the bulb is small due to the bottom of the column being damaged. As a result, it is necessary to prevent the ship from colliding with the conical part of the column. The good method is to keep the conical structure below the SWL.

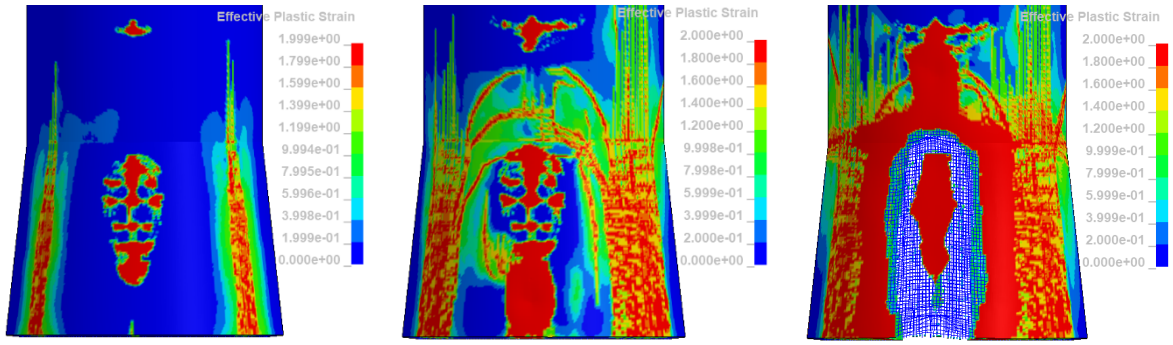

0.25 s 0.5 s 0.75 s

Figure 4-40 Time-varying concrete strain contour when ship with an initial velocity of 7.5 m/s impacts bottom of 1 m thick wall at 0 degrees.

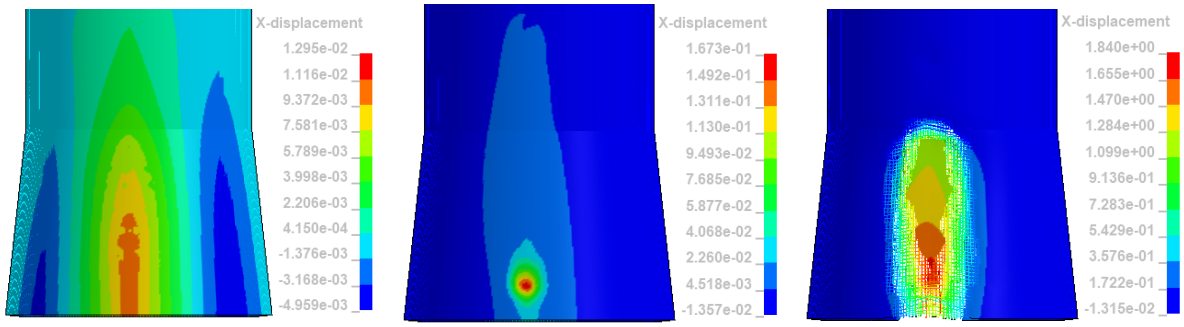

0.25 s 0.5 s 0.6 s

Figure 4-41 Time-varying displacement contours of concrete wall in ship direction, when ship with an initial velocity of 7.5 m/s impacts bottom of 1 m thick wall at 0 degrees.

4.7 Effect of strain rate

When bearing impact load, the strain rate of concrete and steel of a ship are related. Under high strain rate, the strength of concrete and steel can be improved significantly. The strain rate effect is usually defined by a dynamic increase factor (DIF).

In tension, the DIF is defined by the following equations: (Malvar & Ross, 1998)

$$TDIF = \frac{f_t}{f_{ts}} = (\frac{\dot{\varepsilon}}{\dot{\varepsilon_{ts}}})^{\delta} \text{ for } \dot{\varepsilon} \leq 1 \cdot s^{-1} \quad (4\text{-}1)$$

$$TDIF = \frac{f_t}{f_{ts}} = \beta(\frac{\dot{\varepsilon}}{\dot{\varepsilon_{ts}}})^{1/3} \text{ for } \dot{\varepsilon} > 1 \cdot s^{-1} \quad (4\text{-}2)$$

Where f_t is the dynamic tensile strength at strain rate $\dot{\varepsilon}$ in the range of in the range of 10^{-6} to $160 \cdot s^{-1}$, f_{ts} is the static tensile strength at $\dot{\varepsilon_{ts}}$, log β=6δ-2, $\delta = \frac{1}{(1+8f_c'/f_{co}')}$, f_c' is the static uniaxial compressive strength of concrete (in MPa) and f_{co}' is taken as 10 MPa.

In compression, DIF is determined by the functions given by CEB-CIP Model Code (1990) as shown below:

$$CDIF = \frac{f_c}{f_{cs}} = (\frac{\dot{\varepsilon}}{\dot{\varepsilon_{cs}}})^{1.026\delta} \text{ for } \dot{\varepsilon} \leq 30 \cdot s^{-1} \quad (4\text{-}3)$$

$$CDIF = \frac{f_c}{f_{cs}} = \gamma(\dot{\varepsilon})^{1/3} \text{ for } \dot{\varepsilon} > 30 \cdot s^{-1} \quad (4\text{-}4)$$

Where f_c is the dynamic compressive strength at strain rate $\dot{\varepsilon}$, f_{cs} is the static compressive strength at $\dot{\varepsilon_{cs}}$, log γ=6.156α-0.49, $\alpha = \frac{1}{(5+3f_{cu}/4)}$, $and\ f_{cu}$is the static cube strength (in MPa).

For steel in the ship, simple equations for calculating DIF are as follows:

$$DIF = (\frac{\dot{\varepsilon}}{10^{-4}})^{\alpha} \quad (4\text{-}5)$$

$$\alpha = 0.074 - \frac{0.04 f_y}{414} \quad (4\text{-}6)$$

Where f_y is the steel yield strength (in MPa).

4.7.1 Force-displacement curve

Figure 4-42 shows the force-displacement curve of ship bulb and forecastle when the ship with an initial ship velocity of 7.5 m/s impacts SWL of 1 m thick wall at 0 degrees and strain rates of different parts are considered. In the initial stage, the curves of ship and concrete without strain rate have the same trend as the curve of concrete with strain rate. Because of the concrete damage, the curves of 1 m wall-SWL-0 deg-7.5 m/s-Bulb-StrainRateNo and 1 m wall-SWL-0 deg-7.5 m/s-Bulb-StrainRateShip go down to 1 MN. The curve of 1 m wall-SWL-0 deg-7.5 m/s-Bulb-StrainRateConcrete goes up and down for the deformation of the ship. For the forecastle, the curve of 1 m wall-SWL-0 deg-7.5 m/s-Forecastle-StrainRateConcrete is larger than other curves because of the ship deformation.

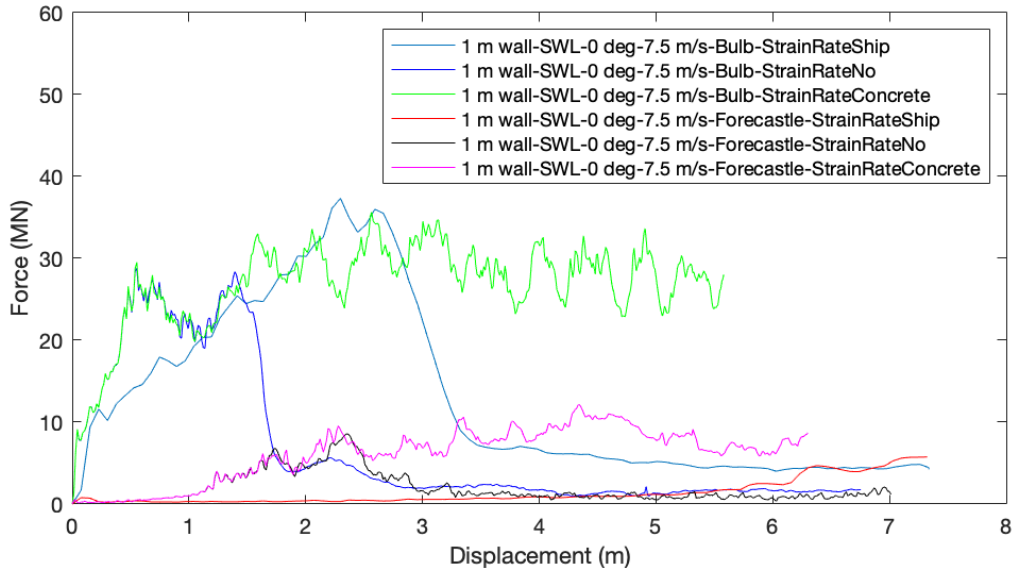

Figure 4-42 Force-displacement curve of ship bulb and forecastle when ship with an initial velocity of 7.5 m/s impacts SWL of 1 m thick wall at 0 degrees and strain rates of different parts are considered.

4.7.2 Total internal energy curve

Figure 4-43 shows the internal energy (including eroded internal energy) of the ship and concrete wall when the ship with an initial velocity of 7.5 m/s impacts SWL of 1 m thick wall at 0 degrees and strain rates of different parts are considered. The total internal energy of the ship is greater than that of the concrete wall. When the strain rate of concrete is considered, the total energy of the ship is much larger than that of other cases, but the total internal energy of concrete with a strain rate is smaller than other curves. The reason is that the concrete with strain rate improves the strength of the concrete wall, thus allowing the ship to be damaged. If the ship has strain rate, the concrete wall would been damaged.

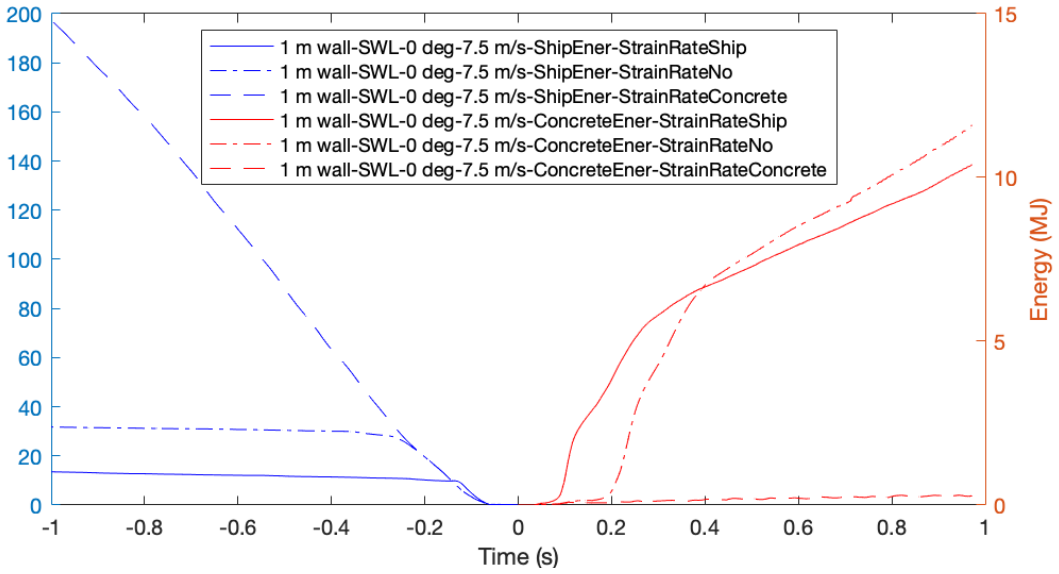

Figure 4-43 Internal energy (including eroded internal energy) of the ship and concrete wall, when ship with an initial ship velocity of 7.5 m/s impacts SWL of 1 m thick wall at 0 degrees and strain rates of different parts are considered.

4.7.3 Structural deformation

Figure 4-44 shows the time-varying structural deformation of the ship when the ship with a strain rate and an initial velocity of 7.5 m/s impacts SWL of 1 m thick wall at 0 degrees. The bulb of the ship does not deform with changes of time, but the forecastle of the ship deforms before 0.5 s.

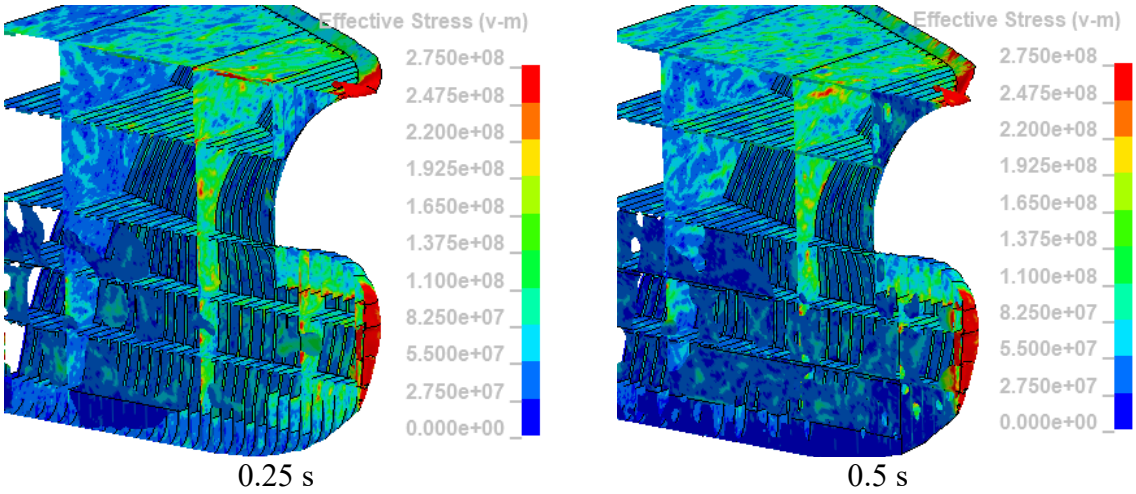

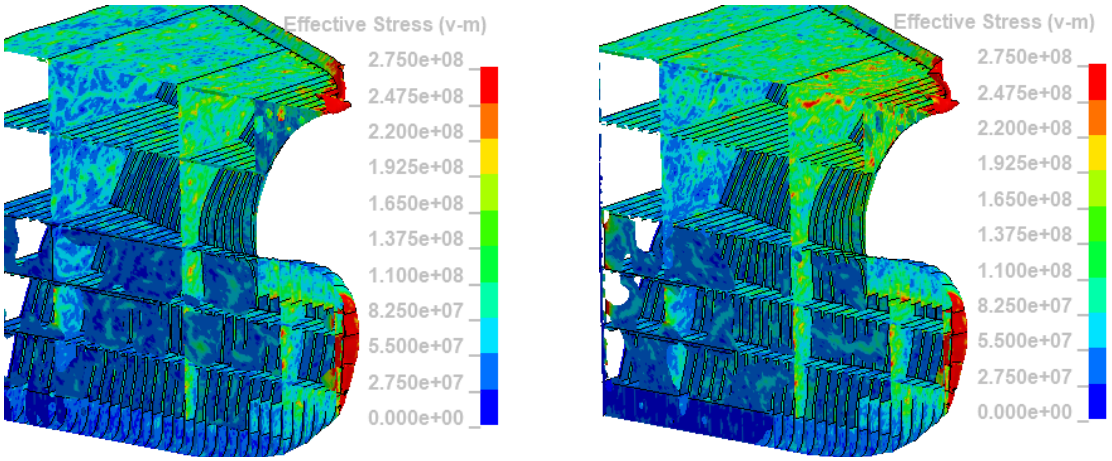

0.75 s 1 s

Figure 4-44 Time-varying structural deformation of ship when the ship with strain rate and an initial velocity of 7.5 m/s impacts SWL of 1 m thick wall at 0 degrees.

Figure 4-45 shows the time-varying structural deformation of the ship when the ship with an initial velocity of 7.5 m/s impacts SWL of 1 m thick wall at 0 degrees (The ship and concrete without strain rate). At the beginning, the ship undergoes structural deformation and the stress focuses on the top of bulb, then the ship does not deform, and the stress becomes smaller. Comparing with Figure 4-44 , Figure 4-45 and Figure 4-9, the ship with a strain rate is stronger than that ship without strain rates.

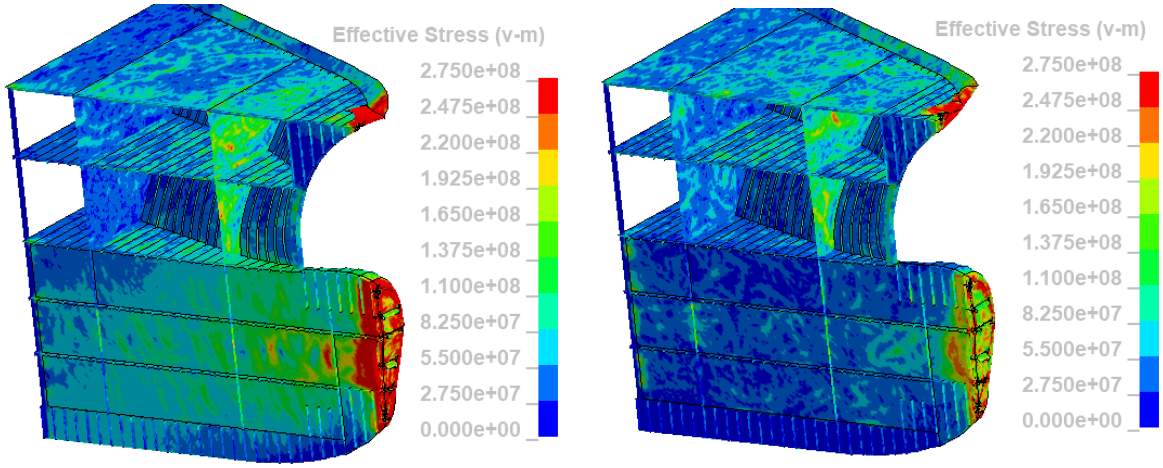

0.25 s 0.5 s

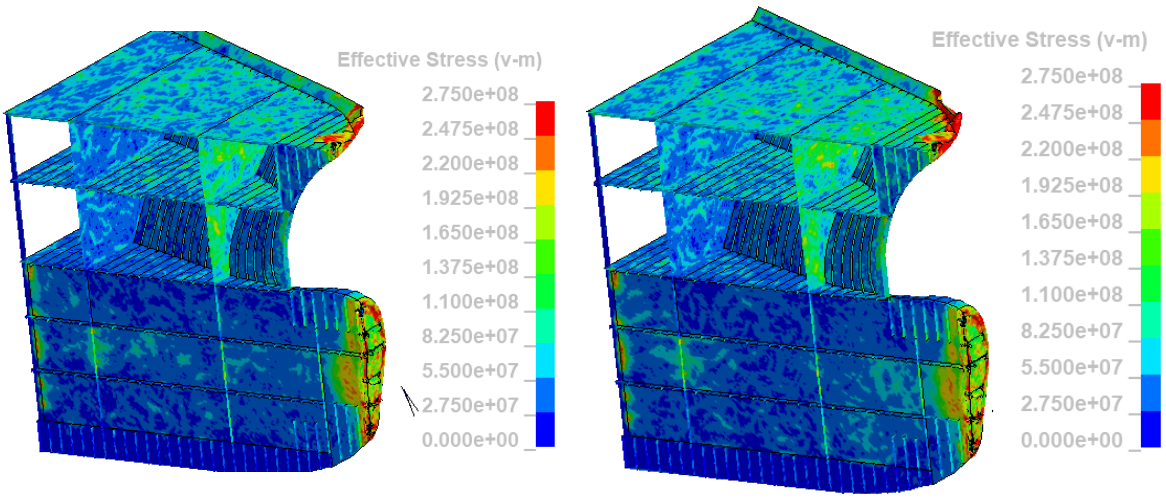

0.75 s 1 s

Figure 4-45 Time-varying structural deformation of ship when the ship with an initial velocity of 7.5 m/s impacts SWL of 1 m thick wall at 0 degrees. (The ship and concrete without strain rate)

The strain of concrete, displacement in the ship direction and axial stress show in Figure 4-46, when the ship with strain rate and an initial velocity of 7.5 m/s impacts SWL of 1 m thick wall at 0 degrees. After the ship collision, the concrete wall is damaged, the displacement in the ship direction is 1.09 m and the rebar has axial stress.

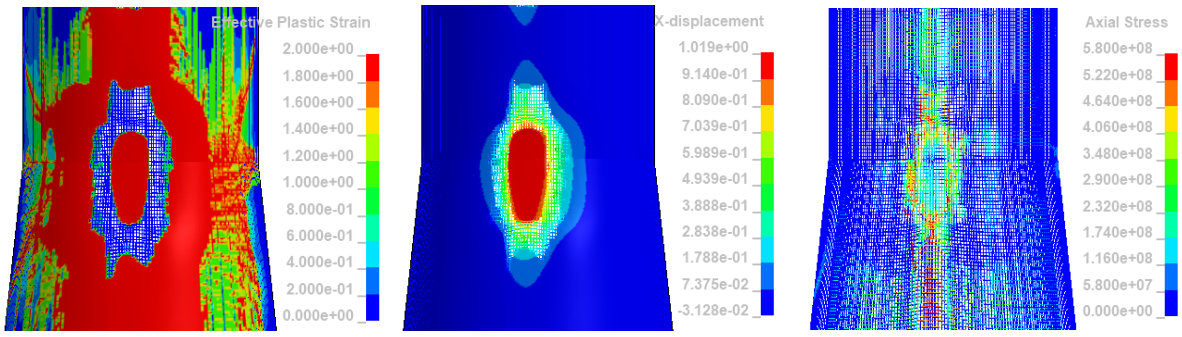

(a) (b) (c)

Figure 4-46 Contours of (a) strain of concrete wall at 0.25 s, (b) displacement of concrete wall at ship direction at 0.25 s and (c) axial stress of rebars at 0.25 s when ship with strain rate and an initial velocity of 7.5 m/s impacts SWL of 1 m thick wall at 0 degrees.

Figure 4-47, Figure 4-48 and Figure 4-49 show the strain of concrete, displacement in the ship direction and axial stress when ship with an initial velocity of 7.5 m/s impacts SWL of 1 m thick wall at 0 degrees and the ship and concrete have no strain rate. Compared with ship with strain rate, it takes more time to destroy concrete walls.

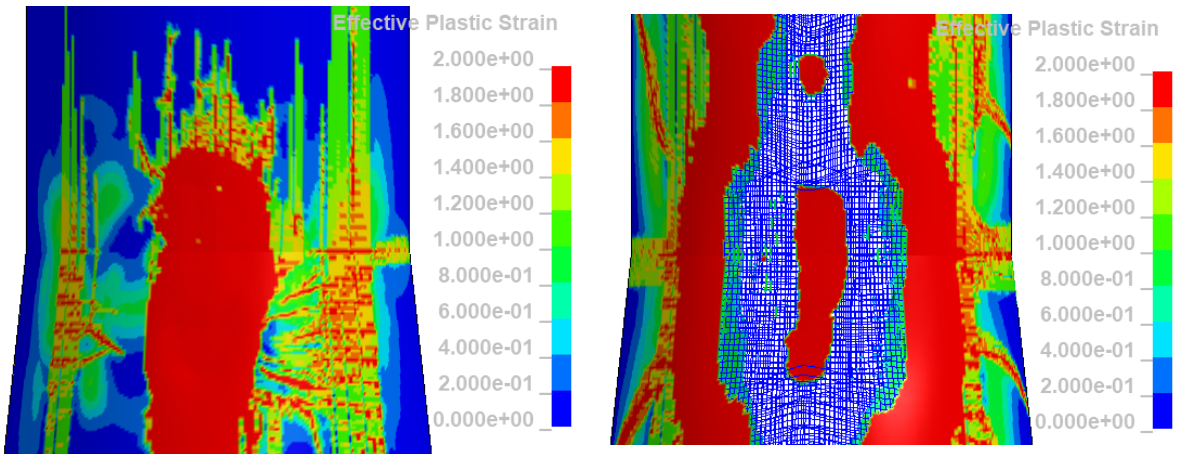

0.25 s 0.5 s

Figure 4-47 Time-varying strain contours of concrete wall when ship with an initial velocity of 7.5 m/s impacts SWL of 1 m thick wall at 0 degrees. (The ship and concrete without strain rate)

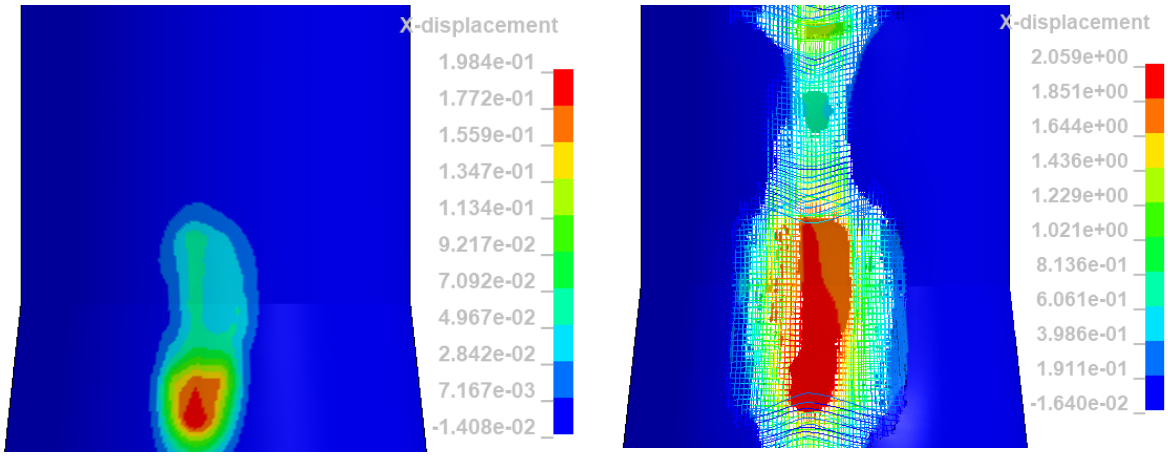

0.25 s 0.5s

Figure 4-48 Time-varying contours of displacement in ship direction of concrete wall when the ship with an initial velocity of 7.5 m/s impacts SWL of 1 m thick wall at 0 degrees. (The ship and concrete without strain rate)

Figure 4-49 shows the stress contours of rebars changes with the time. After 0.25 s, the axial stress of rebars increases gradually after concrete damage but the rebars do not break. Therefore, the strength of reinforcement steel is enough to against the collision.

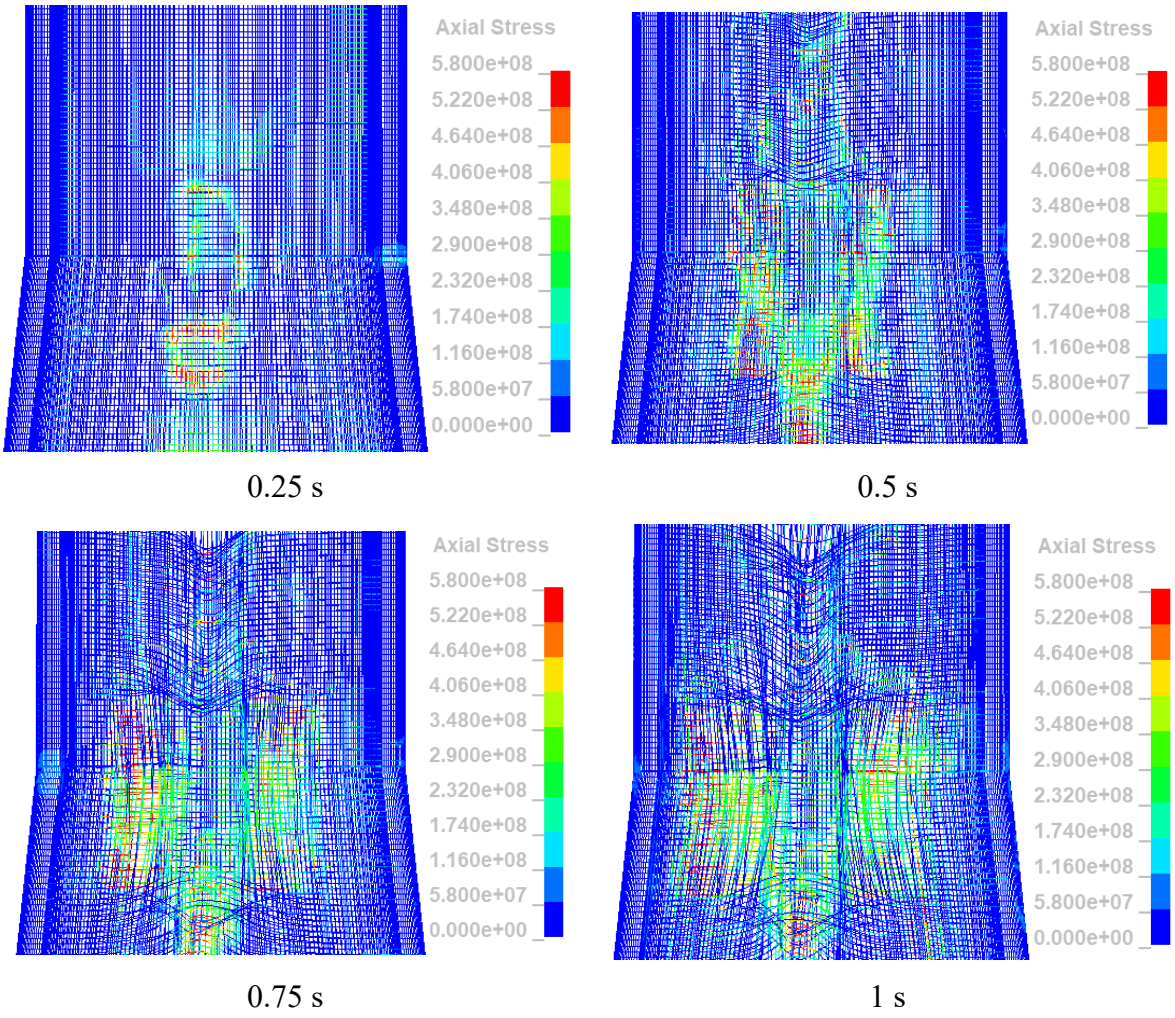

Figure 4-49 Time-varying stress contours of rebars when the ship with an initial velocity of 7.5 m/s impacts SWL of 1 m thick wall at 0 degrees. (The ship and concrete without strain rate)

Chapter 5 Global analysis and results

In this chapter, the global response of the floating offshore wind turbine is analyzed in OrcaFlex. OrcaFlex is famous for the dynamic analysis of offshore marine systems. The latest version includes a wind turbine package, which can be easily used for wind turbine analysis. Different collision scenarios between the vessel and floating offshore wind turbine in both parked and operating conditions are conducted.

5.1 Collision system and scenarios

The collision system is modeled using the constraint object and the 6D buoy object in OrcaFlex. The constraint object is used to model the non-linear stiffness spring that is connected to the vessel and only moves in its x axial direction. The corresponding force-displacement curve of the spring is input in the stiffness table. The contact between the wind turbine and the vessel is modeled via the 6D buoy object, which is connected to the spring, as shown in Figure 5-1. A force is applied to CoM of the vessel in OrcaFlex until it accelerates to a specific velocity (3 m/s, for instance), then remove the force, and a collision occurs.

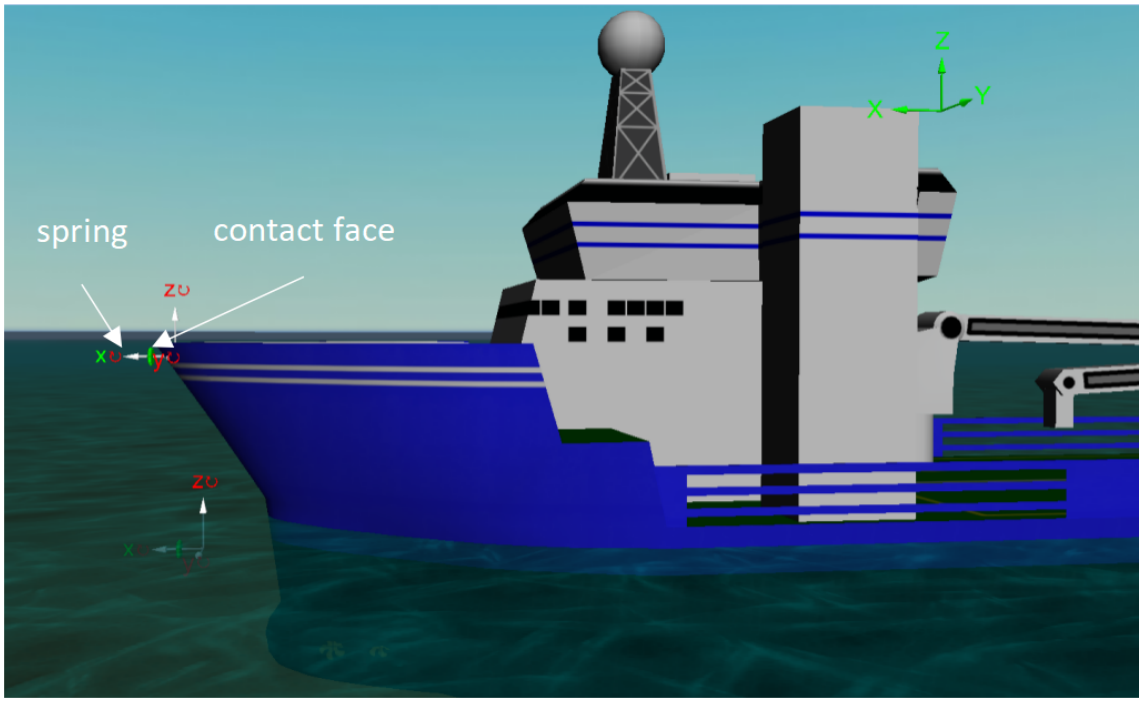

Figure 5-1 Spring and contact face in OrcaFlex

5.1.1 Vessel

Two types of vessels are selected, namely, a supply vessel and a shuttle tanker. The supply vessel model is provided by the OrcaFlex installation vessel model, with a mass of 8800 tons, a length of 103 m, a depth of 16 m, and a draft of 6.66 m, as shown in Figure 5-1. The shuttle tanker has a mass of 20000 tons. As there is no shuttle tanker model in OrcaFlex, the geometric parameters are assumed the same as supply vessel because it has little effect on the results.

The added mass of the supply vessel is provided by OrcaFlex, which is not constant but frequency-dependent, as shown in Figure 5-2. Since there is no shuttle tanker model in OrcaFlex, the added mass is assumed 40% and 10% for shuttle tanker surge and sway according to NORSOK N-003.

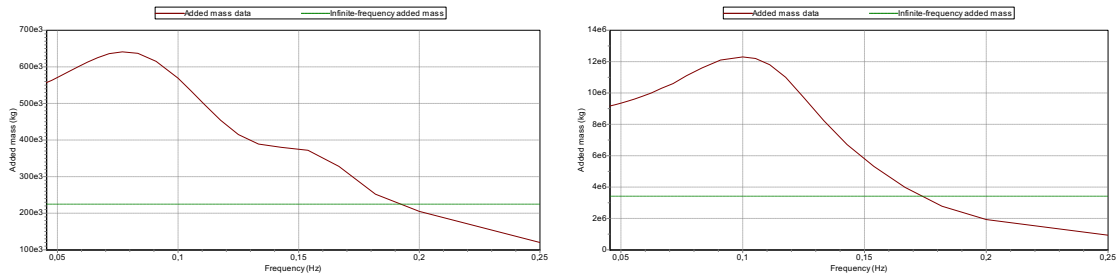

Figure 5-2 Added mass of supply vessel, surge (left) and sway (right) (OrcaFlex)

5.1.2 Spring

5.1.2.1 Spring location

For vessel bow collision, one spring is located in the center of the forecastle, and another is in the center of the bulb. The location of the bulb spring is 1.5 m below the MSL. The vertical and horizontal distances between the two springs are 8.3 m and 1.12 m, respectively. Forecastle spring engages first when the vessel bow collision occurs. For vessel side collision, the spring location is 2.4 m below the MSL.

5.1.2.2 Force-displacement curve

For the supply vessel collision, the force-displacement curves, including forecastle, bulb, and broadside, come from Martin (2020). The curves are obtained from local analysis in LS-DYNA and then simplified for global analysis. However, the simplified curves of forecastle and bulb are significantly different from the original results in Martin's paper. In the following analysis, fine curves of the supply vessel's forecastle and bulb will be used. Detailed analysis between

the fine curve and simple curve is presented in chapter 5.4.1. For the shuttle tanker, the force-displacement curves for forecastle and bulb come from LS-DYNA local analysis in chapter 4. Since the shuttle tanker side collision is not conducted in local analysis, the force-displacement curve is obtained by multiplying the force-displacement curve of the supply vessel side with a factor of 1.5 after consulting the supervisor. The force-displacement curves for the supply vessel and shuttle tanker are shown in Figure 5-3, Figure 5-4 and Figure 5-5.

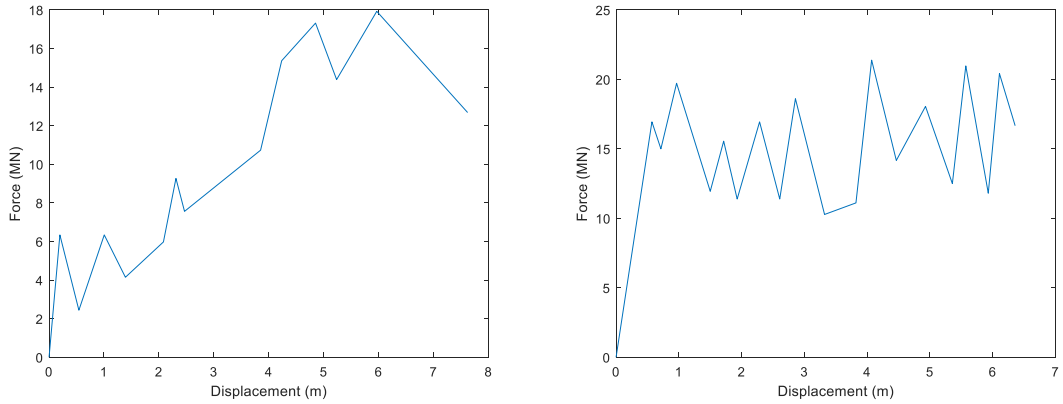

Figure 5-3 Force-displacement curves of supply vessel, forecastle (left) and bulb (right)

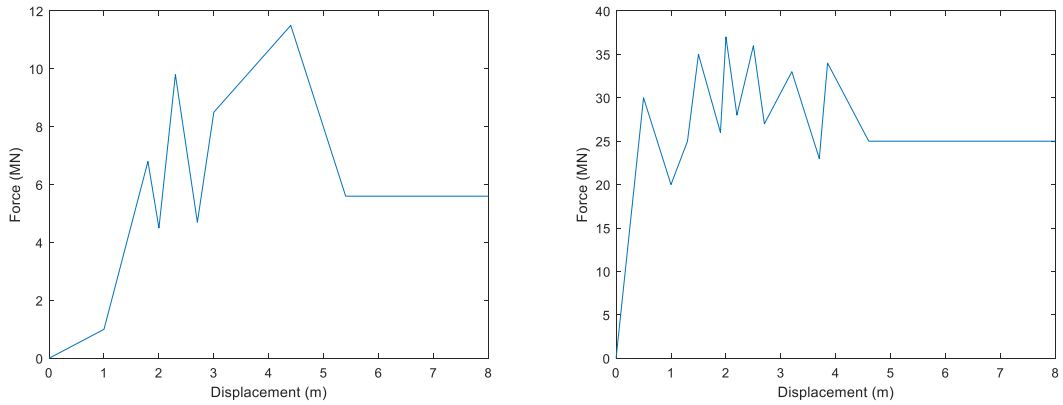

Figure 5-4 Force-displacement curves of shuttle tanker, forecastle (left) and bulb (right)

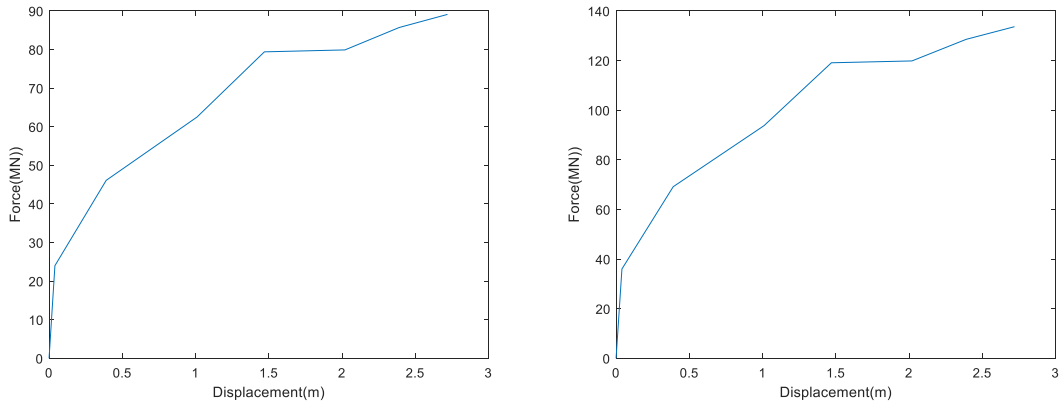

Figure 5-5 Force-displacement curves of supply vessel side (left) and shuttle tanker side (right)

5.1.3 Collision scenarios

According to NORSOK N-003 (2007), the speed should not less than 0.5 m/s and 2 m/s for Ultimate Limit State (ULS) and Accidental Limit State (ALS) design checks, respectively. The recommended impact energy for head-on and side collision is 11 MJ and 14 MJ, respectively. But the latest version suggests the minimum impact energy of 28 MJ and 50 MJ for side and head-on collision because the supply vessel size has increased (Moan, 2019). The impact energy is given:

$$E_v = 0.5(m_s + m_a)v_s^2 \tag{5-1}$$

Where, E_v is approaching ship energy, m_s is displacement of the approaching ship, m_a is added mass of the approaching ship, v_s is speed of the approaching ship.

For the wind turbine, both parked and operating conditions are considered. Rotating speed is set as rated rotating speed in operating conditions. For the vessel, both vessel head-on and side collision are considered. Collision velocity is 3 m/s, 5 m/s and 10 m/s for vessel bow collision and 2 m/s for vessel side collision. In addition, vessel impact direction and location are also considered. 36 scenarios in total are conducted, and key information is summarized in Table 5-1.

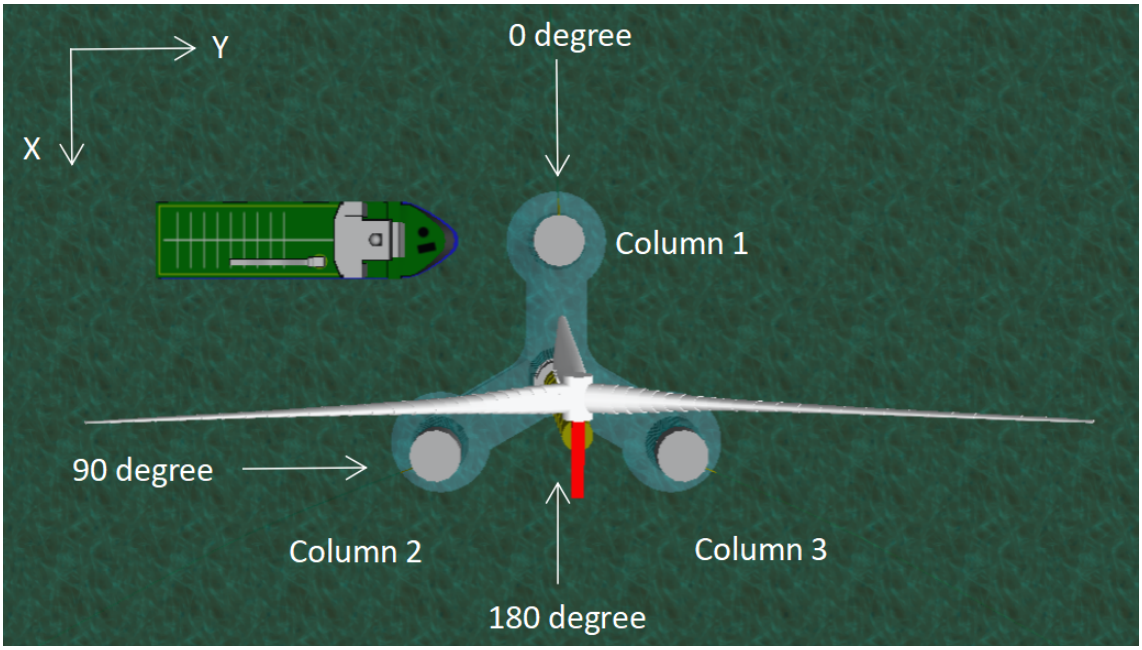

Figure 5-6 Definition of the vessel – FOWT collision scenarios

Table 5-1 Vessel collision scenarios

Case number	Ship section	Velocity (m/s)	Column	Angle (degree)
1/2/3	Supply Vessel bow	3/5/10	1	0
4/5/6	Supply Vessel bow	3/5/10	1	90
7/8/9	Supply Vessel bow	3/5/10	2	90
10/11/12	Supply Vessel bow	3/5/10	2	180
13	Supply Vessel side	2	1	0
14	Supply Vessel side	2	1	90
15	Supply Vessel side	2	2	90
16	Supply Vessel side	2	2	180
17	Supply Vessel side	2	2 and 3	180
18	Supply Vessel side	2	1 and 3	120
19/20/21	Shuttle tanker bow	3/5/10	1	0
22/23/24	Shuttle tanker bow	3/5/10	1	90
25/26/27	Shuttle tanker bow	3/5/10	2	90
28/29/30	Shuttle tanker bow	3/5/10	2	180
31	Shuttle tanker side	2	1	0
32	Shuttle tanker side	2	1	90
33	Shuttle tanker side	2	2	90
34	Shuttle tanker side	2	2	180
35	Shuttle tanker side	2	2 and 3	180
36	Shuttle tanker side	2	1 and 3	120

5.2 Wind turbine in parked condition

5.2.1 Supply vessel

5.2.1.1 Model verification

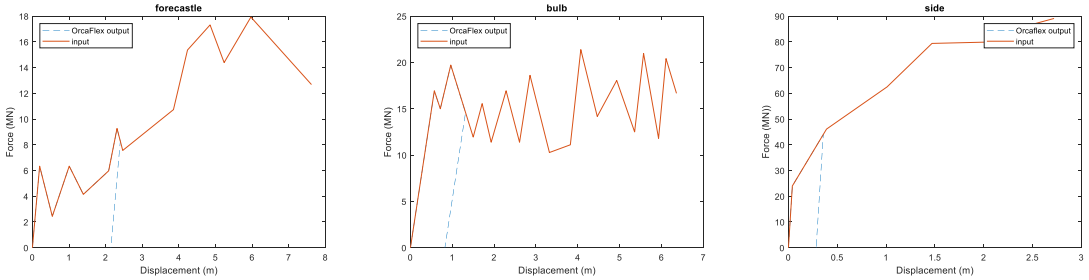

Figure 5-7 Input and OrcaFlex output force-displacement curves comparison, forecastle (left), bulb (middle) and broadside (right)

Input force-displacement curves for supply vessel forecastle, bulb and broadside are compared with output curves from OrcaFlex, as shown in Figure 5-7. The OrcaFlex output curves are in good agreement with the input curves, indicating that the collision system represents the ship correctly. The force increases linearly as displacement increases before entering the plastic zone. When unloading, force follows the same path as the loading.

5.2.1.2 Nacelle acceleration

Mechanical and electrical equipment such as gearbox and generator are in the nacelle and are sensitive to high acceleration. It is recommended to limit it to 0.2-0.3g. Otherwise, the equipment is at high risk, which will cause equipment damage and economic loss. The maximum allowable acceleration of the nacelle is 6 m/s^2 (Liu et al., 2015). Therefore, in the event of a collision, monitoring the response of the nacelle is essential.

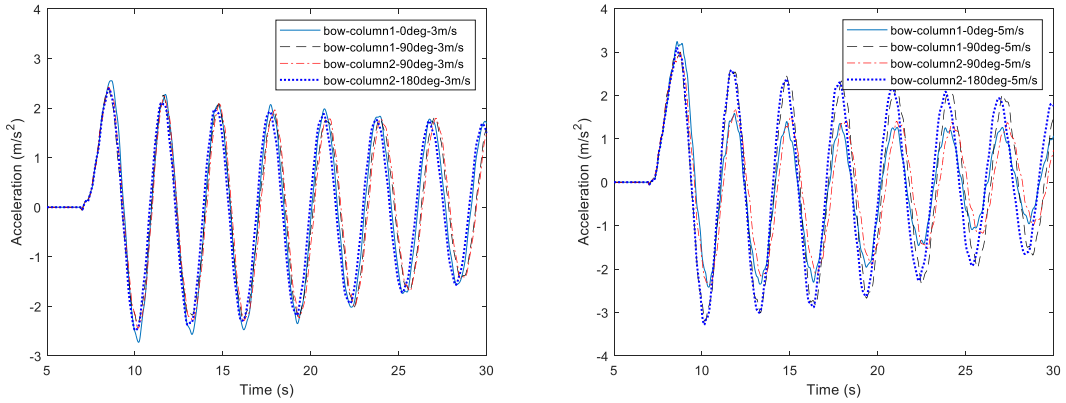

Figure 5-8 Nacelle acceleration when supply vessel hits wind turbine at the speed of 3 m/s (left) and 5 m/s (right)

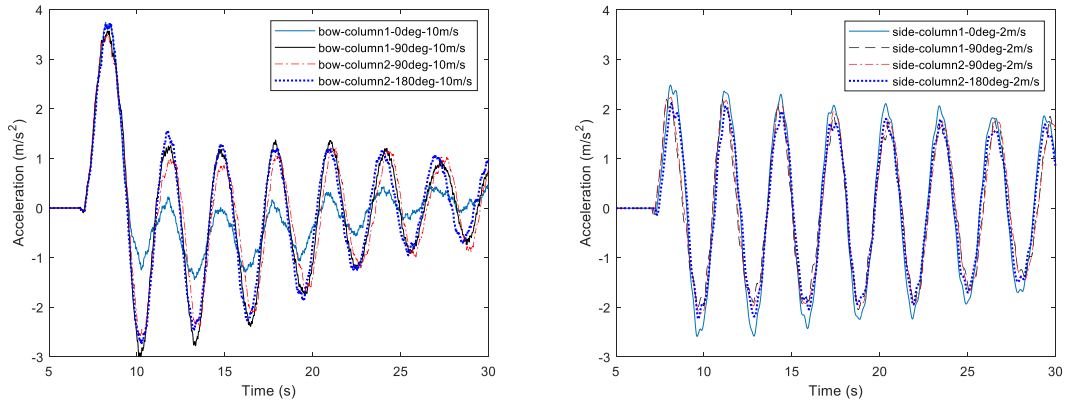

Figure 5-9 (left) Nacelle acceleration when supply vessel bow hits wind turbine at the speed of 10 m/s; (right) Nacelle acceleration when supply vessel side hits wind turbine at the speed of 2 m/s

Nacelle acceleration in all supply vessel collision scenarios exceeds 2 m/s^2, as shown in Figure 5-8 and Figure 5-9, indicating that the mechanical and electric equipment in the nacelle is in hazard condition, which may cause equipment damage and economic loss. The maximum nacelle acceleration is almost the same when the supply vessel impacts the wind turbine at a certain speed. When the supply vessel bow hits the wind turbine at different speeds, the faster the vessel, the greater the nacelle acceleration.

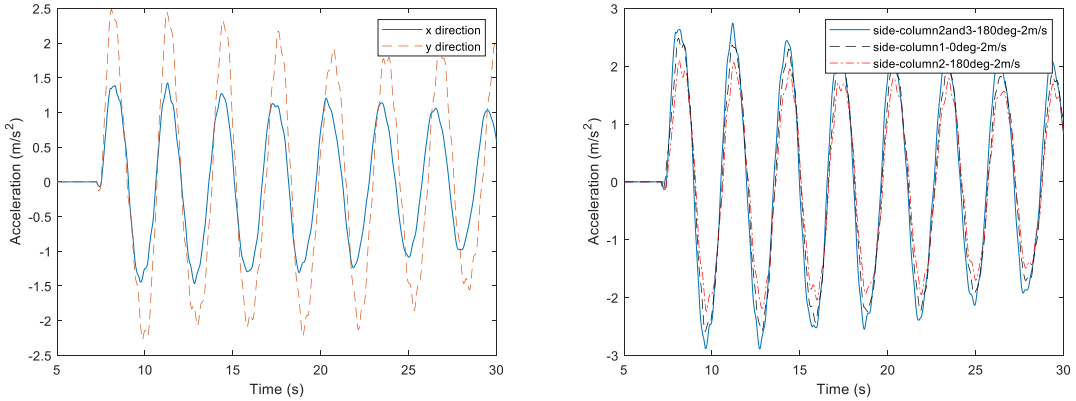

Figure 5-10 (left) The x and y component of nacelle acceleration of case supply vessel side-column 1 and 3-120 deg-2 m/s; (right) Comparison of nacelle acceleration when supply vessel side hits two columns and one column

The maximum nacelle acceleration is about 3 m/s^2 when the supply vessel side crashes into two columns. The y component of nacelle acceleration of case supply vessel side-column 1 and

3-2 m/s exceeds 2 m/s^2, as shown in Figure 5-10. Compared with the supply vessel collides with one column, nacelle acceleration is greater when it crashes into two columns.

5.2.1.3 Force and displacement

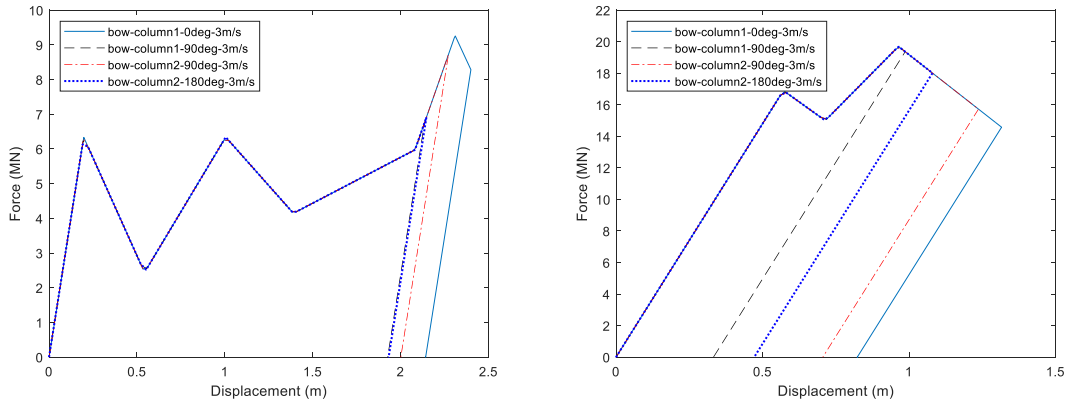

Figure 5-11 Forecastle (left) and bulb (right) force-displacement curves when supply vessel bow hits wind turbine at the speed of 3 m/s

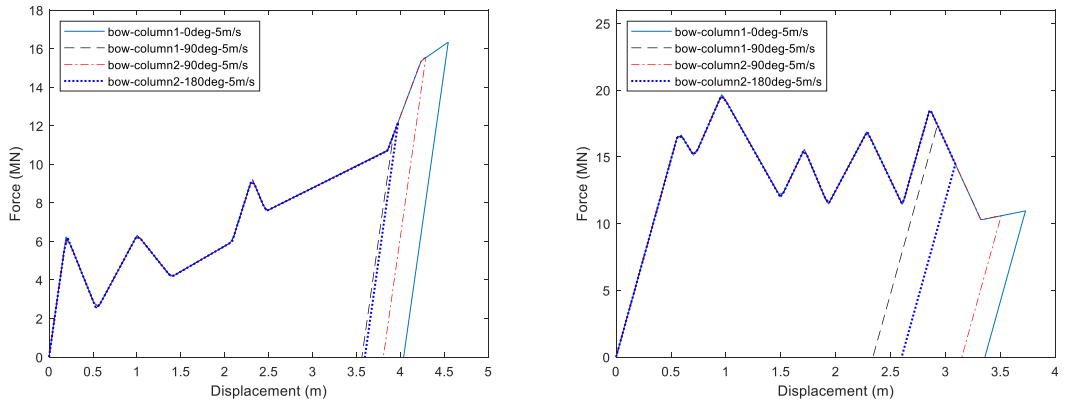

Figure 5-12 Forecastle (left) and bulb (right) force-displacement curves when supply vessel bow hits wind turbine at the speed of 5 m/s

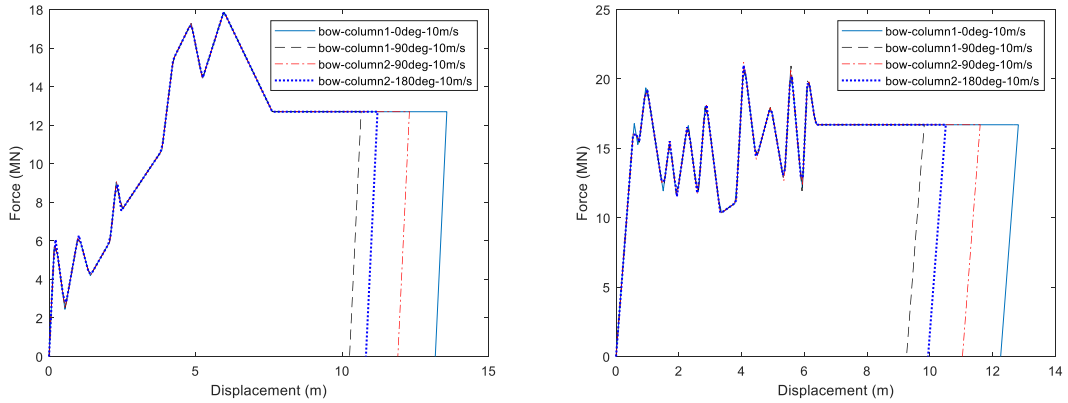

Figure 5-13 Forecastle (left) and bulb (right) force-displacement curves when supply vessel bow hits wind turbine at the speed of 10 m/s

When supply vessel bow hits the wind turbine at the speed of 3 m/s, 5 m/s and 10 m/s, the maximum forecastle force is 9.3 MN, 16.3 MN and 17.9 MN, respectively; and the maximum bulb force is 19.7 MN, 19.7 MN and 21.2 MN, respectively. When the supply vessel bow impacts the wind turbine at a certain speed, the impact direction and location have little effect on the maximum force, which explains the nacelle acceleration is almost the same when the supply vessel bow hits the wind turbine at various directions and locations.

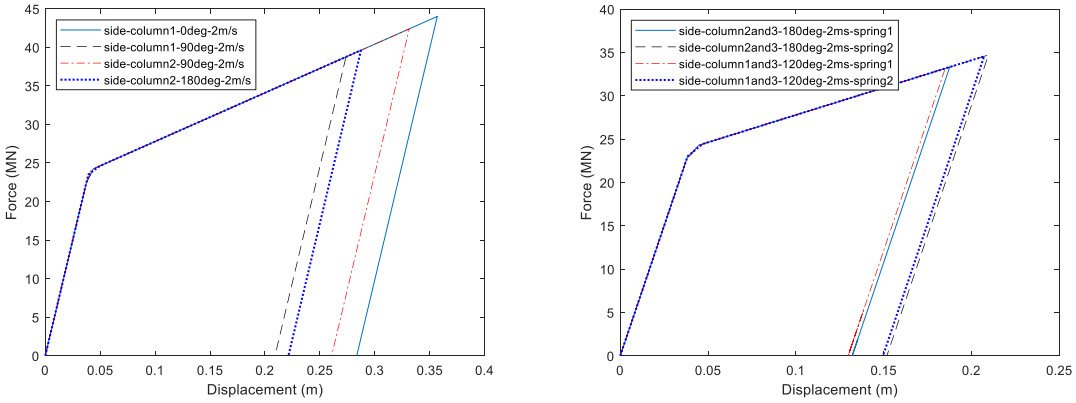

Figure 5-14 Force-displacement curves when supply vessel side crash into one column (left) and two columns (right) of wind turbine at speed of 2 m/s

When the supply vessel side hits one column at the speed of 2 m/s, the maximum force is 44.0 MN. For case supply vessel side-column 2 and 3-180 deg-2 m/s and case supply vessel side-column 1 and 3-120 deg-2 m/s, the maximum force is 34.7 MN and 34.6 MN, respectively. The resultant force is greater when the supply vessel side crashes into two columns, which

explains that the nacelle acceleration is more significant when the supply vessel side crashes into two columns compared with hitting one column.

5.2.1.4 Strain energy

Table 5-2 The kinetic energy of supply vessel and shuttle tanker

Velocity (m/s)	Supply vessel	Energy (MPa)	Shuttle tanker	Energy (MPa)
2	Side	17.6	Side	40
3	Bow	39.6	Bow	90
5	Bow	110	Bow	250
10	Bow	440	Bow	1000

Since the added mass for the supply vessel model in OrcaFlex is not constant but frequency-dependent, added mass is not included when calculating the vessel kinetic energy. Table 5-2 summarizes the kinetic energy for both supply vessel and shuttle tanker of different collision scenarios.

Table 5-3 Strain energy of supply vessel bow collision

Velocity (m/s)	Ship section	Column1-0 deg (MJ)	Column 1-90 deg (MJ)	Column 2-90 deg (MJ)	Column 2-180 deg (MJ)
3	Forecastle	11.15	9.33	9.91	9.37
	Bulb	13.89	5.55	12.10	8.15
5	Forecastle	31.15	24.07	27.44	24.46
	Bulb	48.13	35.22	45.83	39.39
10	Forecastle	156.79	119.64	140.56	126.76
	Bulb	196.36	146.28	176.03	157.73

Table 5-4 Strain energy of supply vessel side collision

Scenario	Strain energy (MJ)
Column 1-0 deg-2 m/s	9.64
Column 1-90 deg-2 m/s	6.56
Column 2-90 deg-2 m/s	8.65
Column 2-180 deg-2 m/s	7.04
Column 2 and 3-180 deg-2 m/s	Spring 1: 3.78, Spring 2: 4.45
Column 1 and 3-120 deg-2 m/s	Spring 1: 3.71, Spring 2: 4.44

The kinetic energy of the vessel is dissipated by the vessel's forecastle and bulb in the form of structural deformation during the collision. The maximum strain energy is 25.04 MJ, 79.28 MJ, and 353.15 MJ for collision speeds of 3 m/s, 5 m/s, and 10 m/s, respectively. The most energy is dissipated when the supply vessel bow hits column 1 in the 0-degree direction at a certain speed, which means this scenario is more dangerous to supply vessel and personnel on board, this also applies to supply vessel side collision and the strain energy is 9.64 MJ. The total strain energy is similar when the supply vessel side hits one column and two columns, but it is smaller for each collision location when it hits two columns.

5.2.1.5 Tower stress

The turbine tower is an unstiffened cylindrical shell with varying diameters and thicknesses from the bottom to the top. The tower is made of steel with a yield stress of 355 MPa. The tower is subjected to bending stresses due to collision-induced vibrations and axial compression from gravitational loads, and thus shall be designed against local buckling. Tower members have hollow, conical geometry, for members with a low D/t ratio, the design is in general based on material yielding, while for large ratios, the elastic buckling strength decrease. In the event of vessel impact, the turbine tower is exposed to large forces and moments. The section connected to the floater suffers the most significant risk for shell buckling. Properties for this section are given in Table 5-5.

Table 5-5 Properties of lower section of DTU 10 MW wind turbine tower

Diameter (m)	Thickness (m)	D/t	Young's modulus (GPa)	Yield strength (MPa)	Length (m)
8.3	0.038	218.42	210	355	11.5

According to DNV-RP-C202 (2013), the elastic buckling strength of an unstiffened circular cylindrical shell is given by:

$$f_E = c\frac{\pi^2 E}{12(1-v^2)}\left(\frac{t}{l}\right)^2 \tag{5-2}$$

Where, f_E is elastic buckling strength, E is young's modulus, v is passion ratio, t is thickness, l is length, and c is reduced buckling coefficient, can be calculated as:

$$c = \varphi\sqrt{1+\left(\frac{\rho\xi}{\psi}\right)^2} \tag{5-3}$$

The values for ψ, ξ and ρ are given in Table 5-6 for the most important load cases.

Table 5-6 Buckling coefficients for unstiffened cylindrical shells (DNV-RP-C202, 2013)

	ψ	ξ	ρ
Axial stress	1	$0.702Z_l$	$0.5\left(1+\frac{r}{150t}\right)^{-0.5}$
Bending	1	$0.702Z_l$	$0.5\left(1+\frac{r}{150t}\right)^{-0.5}$
Torsion and shear force	5.34	$0.856Z_l^{\frac{3}{4}}$	0.6

The curvature parameter Z_l is defined as

$$Z_l = \frac{l^2}{rt}\sqrt{1-v^2} \tag{5-4}$$

Where, r is radius.

Based on the tower segments' geometrical properties, elastic strength for axial and bending stress is 443 MPa and 498 MPa, respectively.

The knock-down factor for shape imperfections is essential both in the elastic and elastoplastic range. Modifying the elastic critical stress for plasticity is achieved by calculating the characteristic buckling strength. Critical stress is defined by

$$\sigma_{eq,cr} = \frac{\sigma_y}{\sqrt{1+\bar{\lambda}_{eq}^2}} \tag{5-5}$$

The equivalent slenderness parameter $\bar{\lambda}_{eq}^2$ is given as:

$$\bar{\lambda}_{eq}^2 = \frac{\sigma_y}{\sigma_{eq,E}}\left[\frac{\sigma_{x,sd}}{\sigma_{xE}}+\frac{\sigma_{b,sd}}{\sigma_{bE}}\right] \tag{5-6}$$

$$\sigma_{eq,E} = \sqrt[2]{(\sigma_{x,sd} + \sigma_{b,sd})^2} \quad (5\text{-}7)$$

Where, $\sigma_{eq,cr}$ is the characteristic buckling strength of a shell, $\sigma_{x,sd}$ is the design axial stress, $\sigma_{b,sd}$ is the design bending stress, σ_{xE} is elastic buckling strength for axial force, σ_{bE} is elastic buckling strength for bending moment, σ_y is yield strength for material, and $\sigma_{eq,E}$ is design equivalent von mises stress.

The utilization factor η is defined as the ratio between the equivalent stress and the critical equivalent stress. To have an adequate design with respect to the elastoplastic buckling of the tower, η should be smaller than one:

$$\eta = \frac{\sigma_{eq}}{\sigma_{eq,cr}} \leq 1 \quad (5\text{-}8)$$

Table 5-7 Von mises stress of supply vessel bow collision

Velocity (m/s)	Column 1-0 deg (MPa)	Column 1-90 deg (MPa)	Column 2-90 deg (MPa)	Column 2-180 deg (MPa)
3	149.2	142.2	145.7	151.3
5	179.9	182.9	161.3	187.7
10	206.1	193.7	190.4	193.5

Table 5-8 Von mises stress of supply vessel side collision

Scenario	Von mises stress (MPa)
Column 1-0 deg-2 m/s	139.3
Column 1-90 deg-2 m/s	122.8
Column 2-90 deg-2 m/s	123
Column 2-180 deg-2 m/s	129.6
Column 2 and 3-180 deg-2 m/s	167.2
Column 1 and 3-120 deg-2 m/s	149.1

The maximum tower stress is 151.3 MPa, 187.7 MPa, and 206.1 MPa for collision velocity of 3 m/s, 5 m/s, and 10 m/s, respectively, indicating the tower stress increase as collision speed increases. For supply vessel side collision, maximum tower stress is 139.3 MPa when the supply vessel side hits one column and 167.2 MPa when it crashes into two columns, which

means it is more serious when the supply vessel crashes into two columns. Tower stress less than yield stress in all cases.

5.2.1.6 Mooring force

Offshore mooring chains are classified into five grades according to DNVGL-OS-E302 (2015): R3, R3S, R4, R4S, and R5. The proof load is defined as the maximum tensile force applied to the mooring line without signs of defects and plastic deformation, which means the material must remain in the elastic region when loaded up to its proof load. The proof load is typically 70-80% of the minimum breaking load.

Two steel grades representing low and high strength are selected, Grade R3 with a yield stress 410MPa and Grade R5 with a yield stress 760 MPa. According to DNVGL-OS-E302 (2015), the proof load and breaking load are given by:

For Grade R3:

$$\text{proof load} = 0.0156d^2(44 - 0.08d) \quad (5\text{-}9)$$

$$\text{breaking load} = 0.0223d^2(44 - 0.08d) \quad (5\text{-}10)$$

For Grade R5:

$$\text{proof load} = 0.0251d^2(44 - 0.08d) \quad (5\text{-}11)$$

$$\text{breaking load} = 0.0320d^2(44 - 0.08d) \quad (5\text{-}12)$$

Where, d is the diameter of mooring chain.

Table 5-9 Proof load and breaking load of the mooring chain

	Grade R3 with a yield stress 410 MPa	Grade R5 with a yield stress 760 MPa
Proof load (MN)	9.67	13.83
Breaking load (MN)	13.83	19.84

Table 5-10 Mooring force of supply vessel bow collision

Velocity (m/s)	Column 1-0 deg (MN)	Column 1-90 deg (MN)	Column 2-90 deg (MN)	Column 2-180 deg (MN)
3	2.54	2.23	2.32	2.04
5	3.41	2.51	2.65	2.20
10	4.24	3.51	3.18	2.76

Table 5-11 Mooring force of supply vessel side collision

Scenario	Mooring force (MN)
Column 1-0 deg-2 m/s	2.53
Column 1-90 deg-2 m/s	2.35
Column 2-90 deg-2 m/s	2.36
Column 2-180 deg-2 m/s	2.05
Column 2 and 3-180 deg-2 m/s	2.11
Column 1 and 3-120 deg-2 m/s	2.13

The maximum mooring force is 2.54 MN, 3.41 MN, 4.24 MN for collision speed of 3 m/s, 5 m/s, 10 m/s, respectively, it increases as the impact velocity increases. When the supply vessel bow impacts the wind turbine at a certain speed, the worst scenario is that it hits column 1 in the 0-degree direction because only one mooring line withstands the load. This also applies to supply vessel collision scenarios. The maximum mooring force is 2.53 MN when the supply vessel side hits one column. The mooring force is about 2.1 MN when the supply vessel side hits two columns, which is smaller compared with supply vessel side collides with two columns because two mooring lines withstand the load. The mooring force does not exceed the proof load in all cases, which means the mooring lines can withstand the collision load.

5.2.1.7 Tower clearance

The blade tip shall keep a safe distance from the tower, it will cause serious damage to the wind turbine and significant economic loss as a consequence of a clash between the blade and tower. Conventionally, there are three methods to keep the blade tip at a safety distance from the tower: first, the shaft is tilted to increase the tower clearance, the tilt angle in this model is 5 degree; second, the blade is not perpendicular to the shaft, a pre-cone angle can increase the tower clearance, and the pre-cone angle is 2.5 degree in this model; third, the blade tip is bend to increase blade tip clearance. The tower clearance is 18.26 m for DTU 10 MW including tilt, cone and prebend, while it is 14.92 m for the OrcaFlex model, the main reason for the difference is the prebend of the blade tip. The vessel impact load will vibrate the blade and bend the tower. The blade sway would be the dominant response when ship velocity is parallel to the rotational plane, so only scenario that vessel velocity is perpendicular to the rotational plane would be considered for wind turbine parked condition.

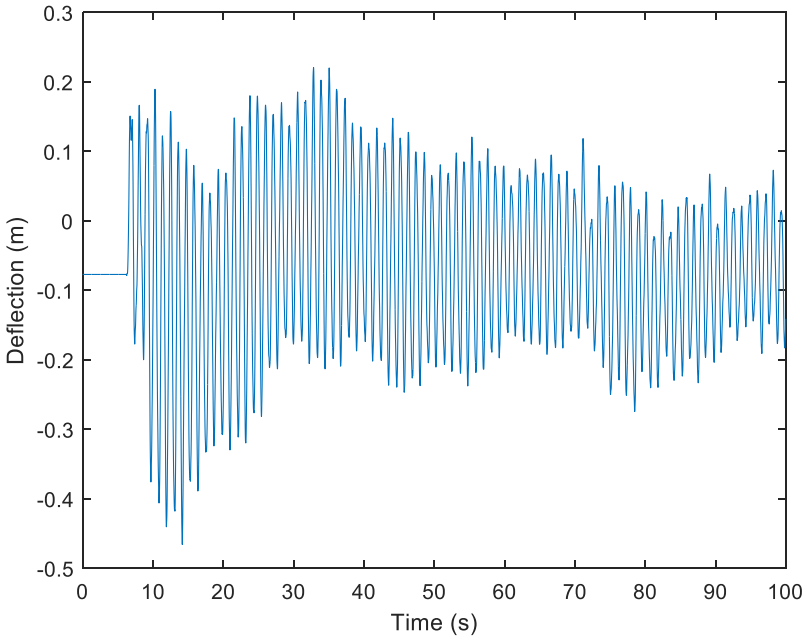

Figure 5-15 Blade deflection of case supply vessel bow-column1-0 deg-10 m/s

Figure 5-15 shows the blade deflection when the supply vessel bow impacts the wind turbine at the speed of 10 m/s, the collision will vibrate the blade and decrease the tower clearance, but the deflection is small compared with tower clearance without load and the blades keep a safe distance from the tower. The tower clearance would be more severe when the wind turbine is in operating condition because the wind load will bend the blades.

5.2.2 Shuttle tanker

5.2.2.1 Model verification

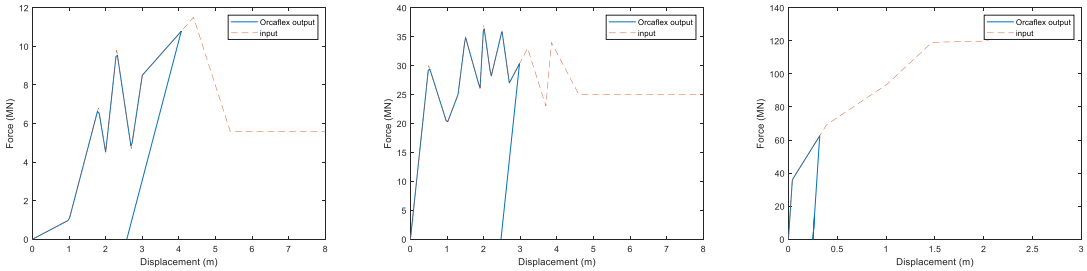

Figure 5-16 Model verification of shuttle tanker, forecastle (left), bulb (middle) and broadside (right)

Input force-displacement curves for supply vessel forecastle, bulb and broadside are compared with output curves from OrcaFlex, as shown in Figure 5-16. The OrcaFlex output curves match input curves very well, which indicates that the collision system represents the ship correctly.

5.2.2.2 Nacelle Acceleration

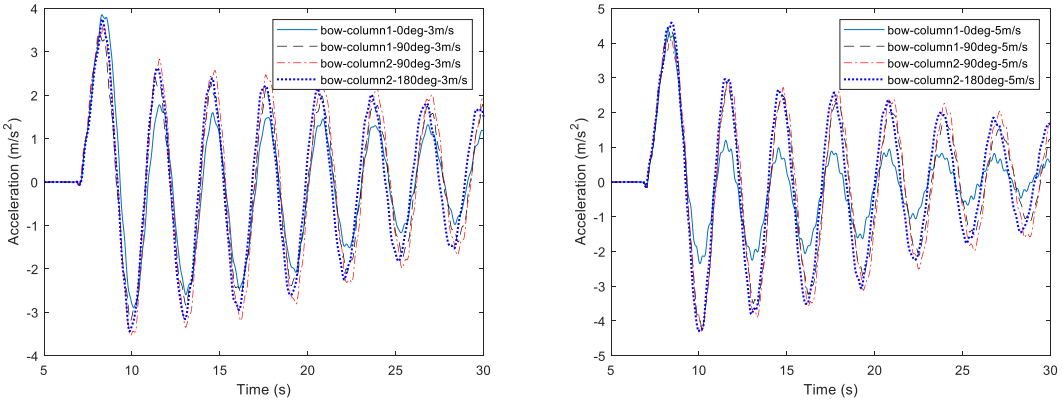

Figure 5-17 Nacelle acceleration when shuttle tanker bow hits wind turbine at the speed of 3 m/s (left) and 5 m/s (right)

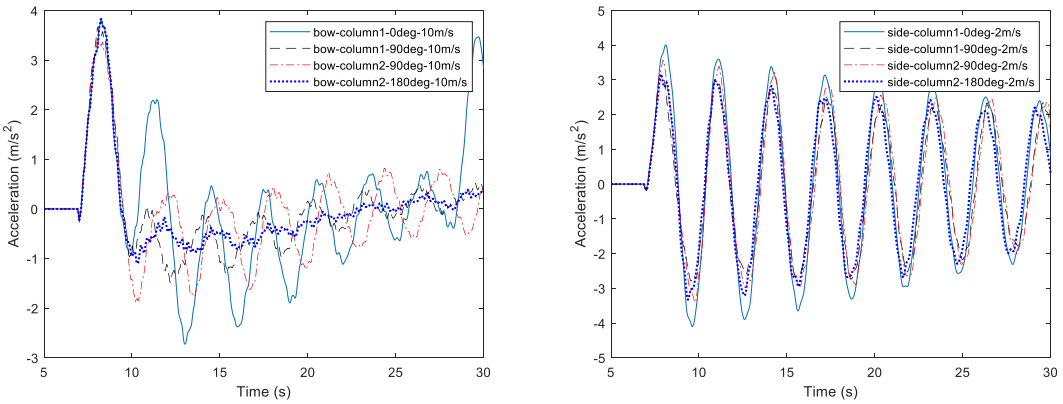

Figure 5-18 (left) Nacelle acceleration when shuttle tanker bow hits wind turbine at the speed of 10 m/s, (right) Nacelle acceleration when shuttle tanker side hits wind turbine at the speed 2 m/s (right)

Figure 5-17 and Figure 5-18 show the nacelle acceleration of the shuttle tanker bow and side collision with the wind turbine. The maximum nacelle acceleration surpasses 3 m/s^2 in all shuttle tanker collision scenarios, indicating that shuttle tanker collision poses a real threat to the wind turbine's mechanical and electrical equipment.

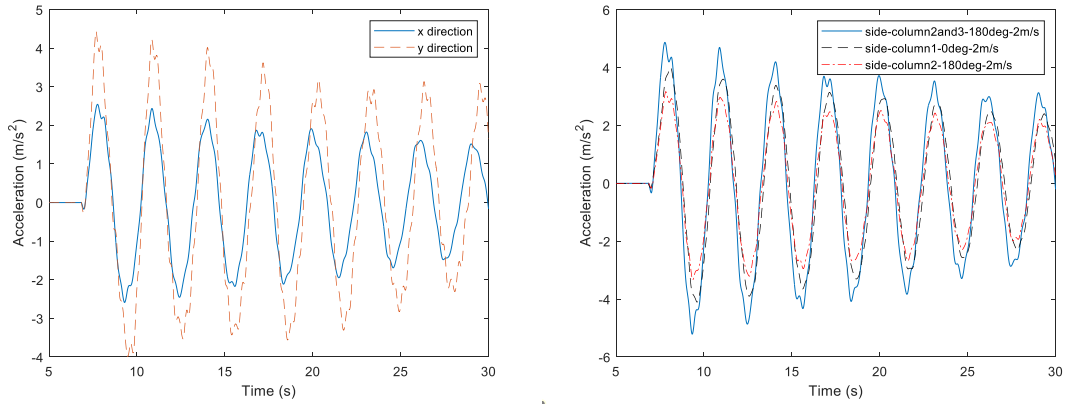

Figure 5-19 (left) Nacelle acceleration of case shuttle tanker side-column 1 and 3-120 deg-2 m/s, (right) Nacelle acceleration comparison of shuttle tanker hits two columns and 1 column.

For shuttle tanker side collision, the peak value of nacelle acceleration exceeds 5 m/s^2 when it collides with two columns, both x component and y component of nacelle acceleration exceeds 2 m/s^2 for case shuttle tanker side-column 1 and 3-120 deg-2 m/s. Comparing shuttle tanker side collision with 1 column, nacelle acceleration is greater when it crashes into two columns.

5.2.2.3 Force and displacement

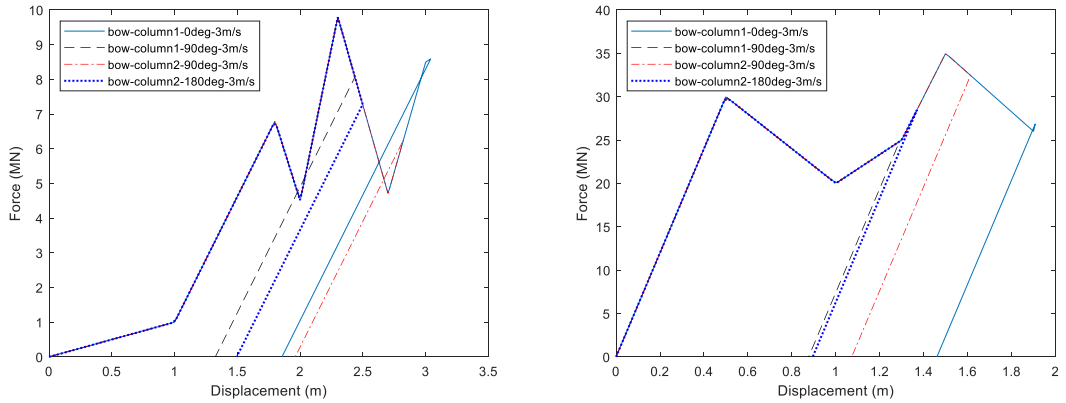

Figure 5-20 Forecastle (left) and bulb (right) force-displacement curve when shuttle tanker bow hits wind turbine at the speed of 3 m/s

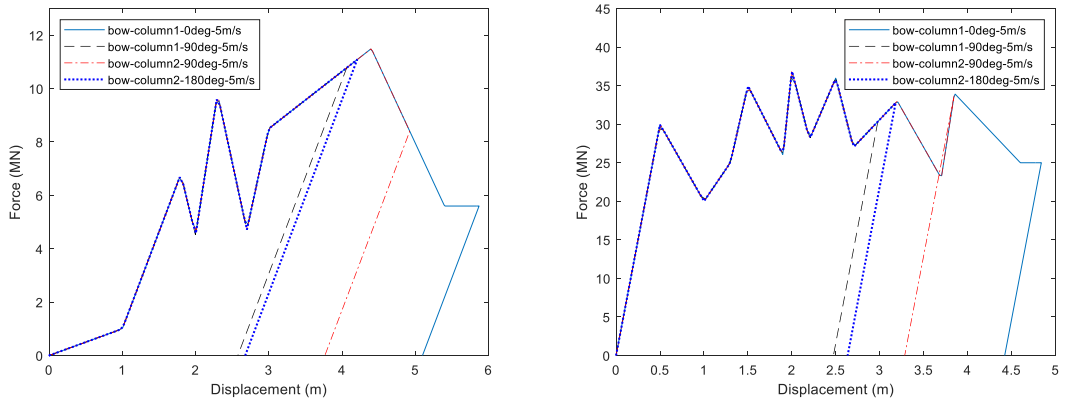

Figure 5-21 Forecastle (left) and bulb (right) force-displacement curve when shuttle tanker bow hits wind turbine at the speed of 5 m/s

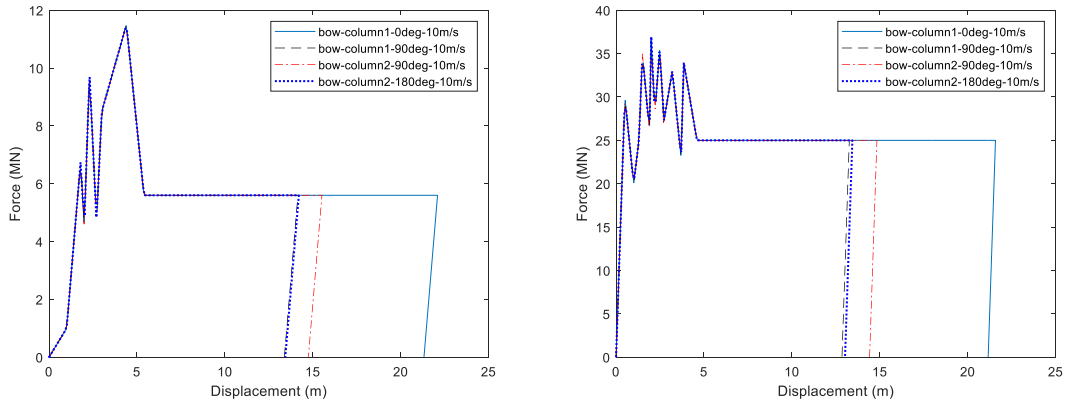

Figure 5-22 Forecastle (left) and bulb (right) force-displacement curve when shuttle tanker hits wind turbine at the speed of 10 m/s

When the shuttle tanker bow hits the wind turbine at the speed of 3 m/s, 5 m/s and 10 m/s, the maximum forecastle force is 9.8 MN, 11.5 MN and 11.5 MN, respectively; and the maximum bulb force is 34.9 MN, 36.9 MN and 36.9 MN, respectively. When the shuttle tanker bow impacts the wind turbine at a certain speed, the impact direction and location have no significant effect on the maximum force, which explains the nacelle acceleration is almost the same when shuttle vessel bow hits the wind turbine at various directions and locations.

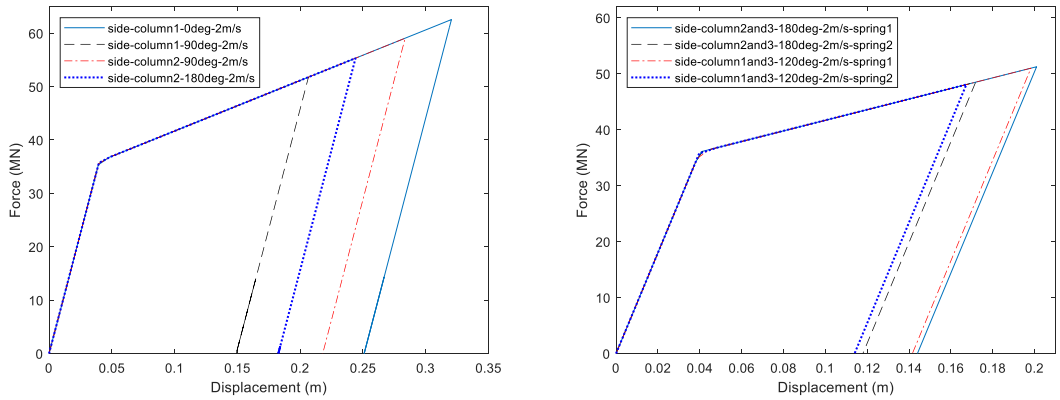

Figure 5-23 Force-displacement curve when shuttle tanker side crashes into 1 column (left) and two columns (right) at the speed of 2 m/s.

When the shuttle tanker side hits one column and two columns at the speed of 2 m/s, the maximum force is 62.6 MN. The maximum force is 51.2 MN and 51.0 MN for case shuttle tanker side-column 2 and 3-180 deg-2 m/s and case shuttle tanker side-column 1 and 3-120 deg-2 m/s, respectively. Although the maximum force is greater when the shuttle tanker side hits one column, the resultant force is greater when the shuttle tanker side crashes into two columns, which explains the nacelle acceleration is greater when the shuttle tanker side crashes into two columns compared with hitting one column.

5.2.2.4 Strain energy

Table 5-12 Strain energy of shuttle tanker bow collision

Velocity (m/s)	Ship section	Column 1-0 deg (MJ)	Column 1-90 deg (MJ)	column 2-90 deg (MJ)	column 2-180 deg (MJ)
3	Forecastle	7.03	3.63	7.77	4.94
	Bulb	39.15	21.37	27.80	21.85
5	Forecastle	34.80	14.01	26.13	15.11
	Bulb	126.65	70.80	94.18	75.94
10	Forecastle	125.68	81.98	88.94	81.52
	Bulb	545.33	337.3	376.62	341.82

Table 5-13 Strain energy of shuttle tanker side collision

Scenario	Strain energy (MJ)
Column 1-0 deg-2 m/s	12.37
Column 1-90 deg-2 m/s	6.54
Column 2-90 deg-2 m/s	10.36
Column 2-180 deg-2 m/s	8.34
Column 2 and 3-180 deg-2 m/s	Spring 1: 6.28, Spring 2: 4.98
Column 1 and 3-120 deg-2 m/s	Spring 1: 6.16, Spring 2: 4.79

The maximum strain energy is 46.18 MJ, 161.45 MJ and 671.01 MJ when the shuttle tanker bow impacts the wind turbine at the speed of 3 m/s, 5 m/s and 10 m/s, respectively. The same as supply vessel bow collision, the most energy is dissipated when shuttle tanker bow hits column 1 in the 0-degree direction, this also applies to shuttle tanker side collision. The maximum strain energy for shuttle tanker side collision is 12.37 MJ. The total energy dissipated is similar when the shuttle tanker side hits one column and two columns, but it is smaller for each collision location when it hits two columns.

5.2.2.5 Tower stress

Table 5-14 Von mises stress of shuttle tanker bow collision

Velocity (m/s)	Column 1-0 deg (MPa)	Column 1-90 deg (MPa)	Column 2-90 deg (MPa)	Column 2-180 deg (MPa)
3	210.8	182.7	207	197
5	232.5	240.3	239.4	250.5
10	267.4	197.1	186.4	191.3

Table 5-15 Von mises stress of shuttle tanker side collision

Scenario	Von mises stress (MPa)
Column 1-0 deg-2 m/s	214.8
Column 1-90 deg-2 m/s	163
Column 2-90 deg-2 m/s	183.6
Column 2-180 deg-2 m/s	183.9
Column 2 and 3-180 deg-2 m/s	270.4
Column 1 and 3-120 deg-2 m/s	250.1

The maximum tower stress is 210.8 MPa, 250.5 MPa and 267.4 MPa for collision velocity of 3 m/s, 5 m/s and 10 m/s, respectively, indicating the tower stress increase as collision speed increases. For case shuttle tanker bow-column 1-90 deg-10 m/s, case shuttle tanker bow-column 2-90 deg-10 m/s and case shuttle tanker bow-column 2-180 deg-10 m/s, tower stress looks unreasonable because it is too small. The maximum force when the shuttle tanker hits the wind turbine at the speed of 10 m/s is similar to hitting the wind turbine at the speed of 5 m/s, as shown in Figure 5-21 and Figure 5-22, which means the tower stress shall be similar. The reason for this phenomenon is unknown. But we can infer that the tower stress should be around 260 MPa. For shuttle tanker side collision, maximum tower stress is 214.8 MPa when supply vessel side hits one column and 270.4 MPa when it crashes into two columns, which means it is more serious when the supply vessel crashes into two columns. Tower stress less than yield stress in all cases.

5.2.2.6 Mooring force

Table 5-16 Mooring force of shuttle tanker bow collision

Velocity (m/s)	Column 1-0 deg (MN)	Column 1-90 deg (MN)	Column 2-90 deg (MN)	Column 2-180 deg (MN)
3	3.79	2.72	2.32	2.92
5	4.39	3.56	3.25	2.85
10	9.41	4.22	3.42	3.39

Table 5-17 Mooring force of shuttle tanker side collision

Scenario	Mooring force (MN)
Column 1-0 deg-2 m/s	3.33
Column 1-90 deg-2 m/s	2.38
Column 2-90 deg-2 m/s	2.71
Column 2-180 deg-2 m/s	2.17
Column 2 and 3-180 deg-2 m/s	2.43
Column 1 and 3-120 deg-2 m/s	2.48

The maximum mooring force is 3.79 MN, 4.39MN, 9.41MN when the shuttle tanker bow collides with the floater at the speed of 3 m/s, 5 m/s, 10 m/s, respectively. The mooring force

increases as the impact velocity increases. The most severe scenario is shuttle tanker bow hits column 1 in a 0-degree direction because only one mooring line bears the load, this also applies to shuttle tanker side collision. The maximum mooring force is 3.33 MN when the shuttle tanker side collides with one column and 2.48 MN when the shuttle tanker side hits two columns, the latter one is smaller compared with the shuttle tanker side collides with 1 column because two mooring lines withstand the load. The mooring force does not exceed the proof load in all cases.

5.3 Wind turbine in operating condition

The condition of the wind turbine has an impact on the collision results. For example, the wind load on the wind turbine and wave load on the floater push the floating wind turbine backward, thus the mooring line is at higher risk, in addition, the wind load on the blades yields greater stress on the tower. The floating wind turbine is assumed to work in the rated condition in the following analysis, the rated rotor speed is 9.6 rpm and the rated wind speed is 11.4 m/s. Wind speed increases gradually from zero to rated wind speed and then remains constant at rated wind speed. The wave is set as JONSWAP, and the H_S (significant wave height) is 3.5 m. considering the worst scenario, wind direction is set as positive x-direction (0-deg direction), because only one mooring line bears the load. The collision scenarios are the same as the parked condition.

5.3.1 Supply vessel

5.3.1.1 Nacelle acceleration

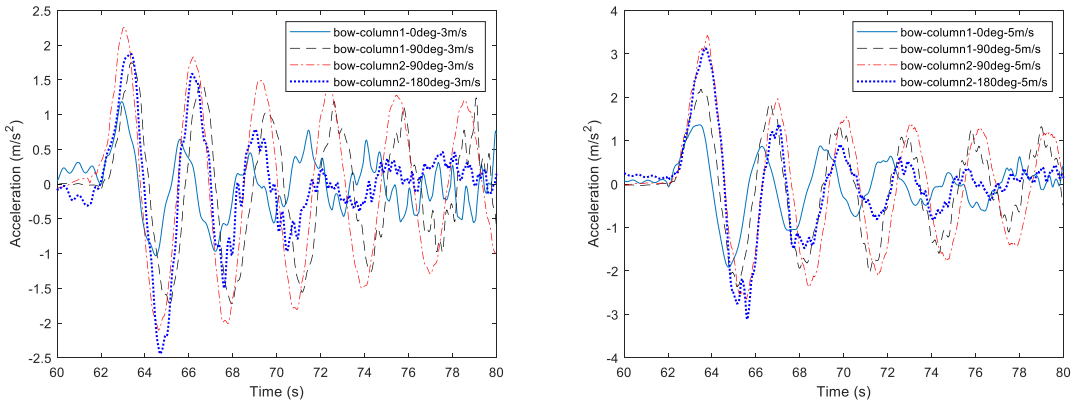

Figure 5-24 Nacelle acceleration when supply vessel bow hits wind turbine at the speed of 3 m/s (left) and 5 m/s (right)

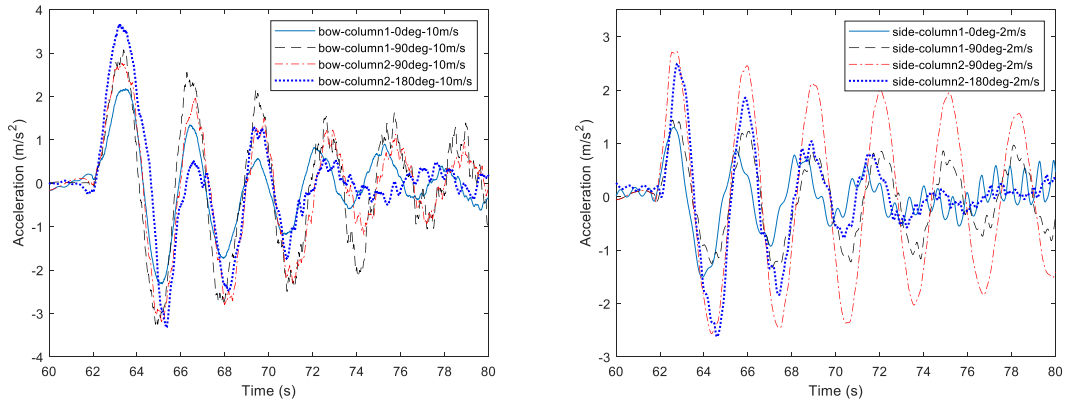

Figure 5-25 (left) Nacelle acceleration when supply vessel bow hits wind turbine at the speed of 10 m/s; (right) Nacelle acceleration when supply vessel side hits wind turbine at the speed of 2 m/s

Figure 5-24 and Figure 5-25 show nacelle acceleration when the supply vessel's bow and side collide with the wind turbine. When impact speed is 3 m/s, nacelle acceleration exceeds 2 m/s^2 only for case supply vessel bow-column 2-90 deg-3 m/s and supply vessel bow-column 2-190 deg-3 m/s. When impact speed is 5 m/s, nacelle acceleration less than 2 m/s^2 only for case supply vessel bow-column 1-0 deg-5 m/s. When impact speed is 10 m/s, nacelle acceleration exceeds 2 m/s^2 for all four cases. When the supply vessel side hits the wind turbine, nacelle acceleration exceeds 2 m/s^2 for case supply vessel side-column 2-90 deg-2 m/s and case supply vessel side-column 2-180 deg-2 m/s. The collision location and direction have a significant effect on the nacelle acceleration; generally, it is more severe to hit column 2 than column 1.

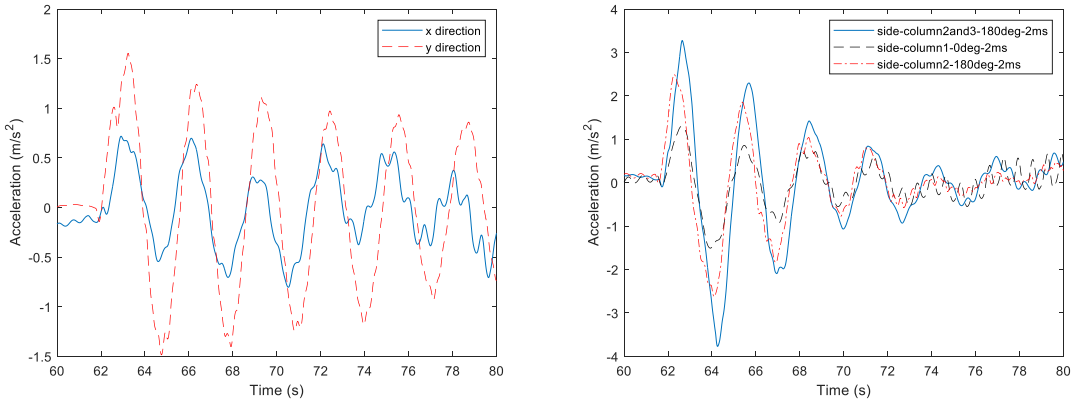

Figure 5-26 (left) Nacelle acceleration of case supply vessel side-column 1 and 3-120 deg-2 m/s; (right) Nacelle acceleration comparison when supply vessel collides with 1 column and two columns

Figure 5-26 shows x component and y component of nacelle acceleration for case supply vessel side-column 1 and 3-120 deg-2 m/s. Y component is larger than the x component, but both less than 2 m/s^2. Compared with supply vessel crashes into one column, nacelle acceleration is more extensive when it crashes into two columns.

5.3.1.2 Force and displacement

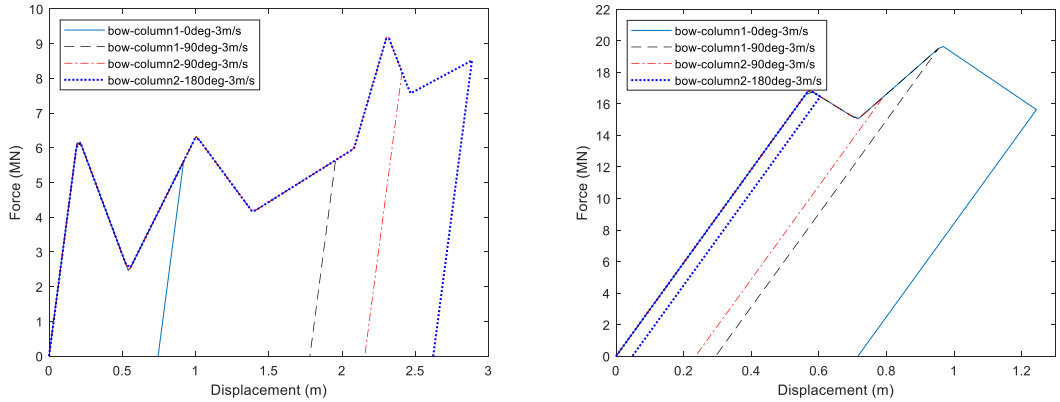

Figure 5-27 Forecastle (left) and bulb (right) force-displacement curve when supply vessel bow hits wind turbine at the speed of 3 m/s

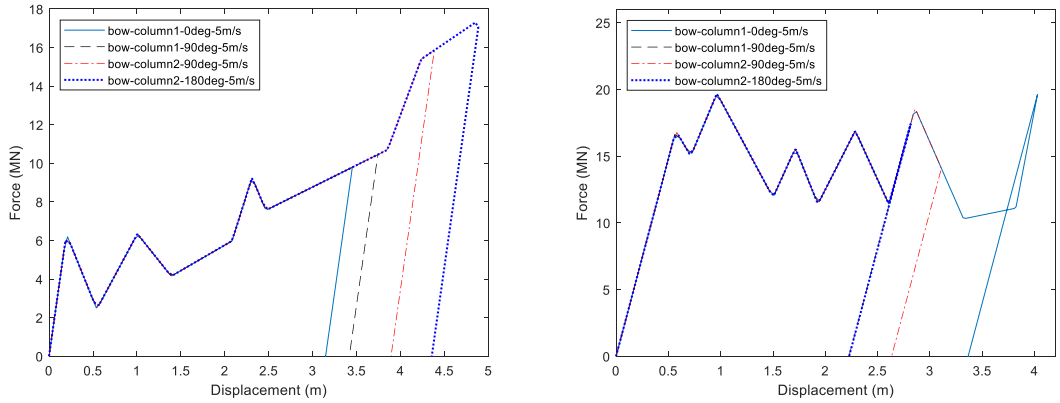

Figure 5-28 Forecastle (left) and bulb (right) force-displacement curve when supply vessel bow hits wind turbine at the speed of 5 m/s

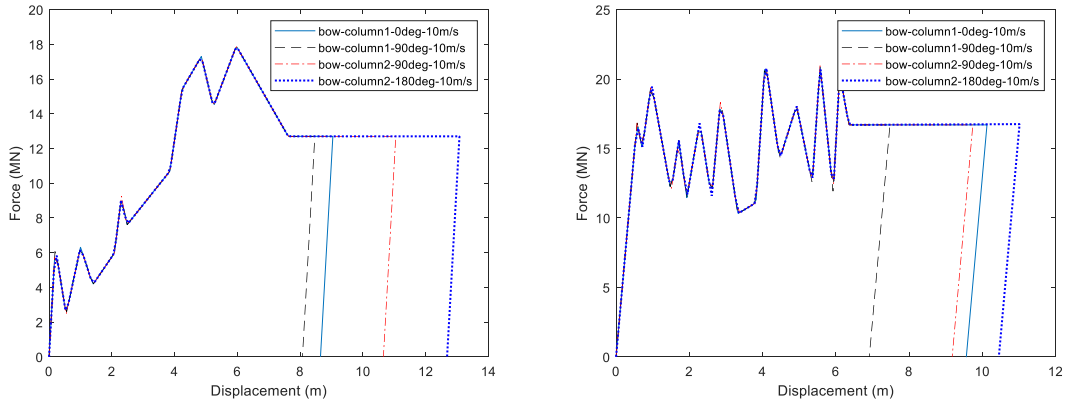

Figure 5-29 Forecastle (left) and bulb (right) force-displacement curve when supply vessel bow hits wind turbine at the speed of 10 m/s

When the supply vessel bow hits the wind turbine at the speed of 3 m/s, 5 m/s, and 10 m/s, the maximum forecastle force is 9.2 MN, 17.3 MN, and 17.9 MN, respectively; and the maximum bulb force is 19.6 MN, 19.7 MN, and 21 MN, respectively. The resultant force difference between the collision speed of 3 m/s and 5 m/s is noticeable, and the difference between the collision speed of 5 m/s and 10 m/s is not apparent.

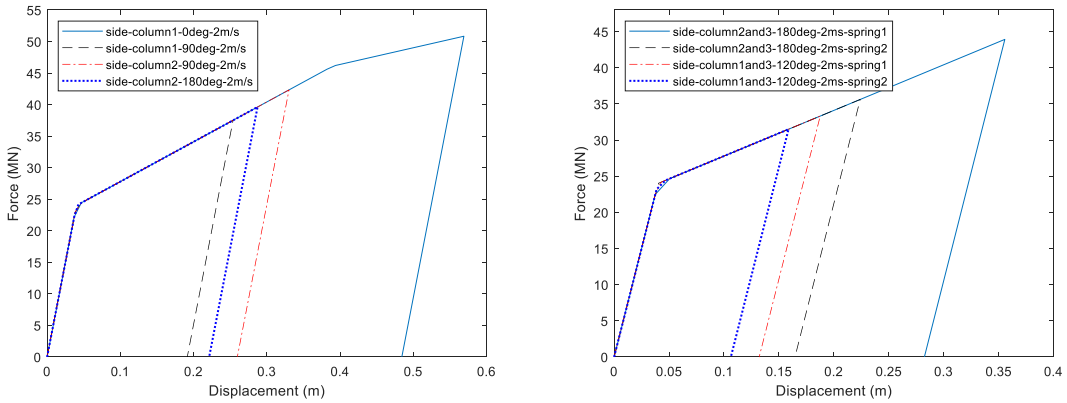

Figure 5-30 Force-displacement curve when supply vessel side crashes into one column (left) and two columns (right) at speed of 2 m/s

When the supply vessel side hits one column at the speed of 2 m/s, the maximum force is 50.8 MN. When the supply vessel side hits two columns, the maximum force is 43.9 MN and 33. 3 MN for case supply vessel side-column 2 and 3-180 deg-2 m/s and case supply vessel side-column 1 and 3-120 deg-2 m/s, respectively. Although the maximum force is greater when the supply vessel side hits one column, the resultant force is greater when the supply vessel side

crashes into two columns, explaining the nacelle acceleration is more significant when the supply vessel side crashes into two columns compared with hitting one column.

5.3.1.3 Strain energy

Table 5-18 Strain energy of supply vessel bow collision

Velocity (m/s)	Ship section	Column 1-0 deg (MJ)	Column 1-90 deg (MJ)	Column 2-90 deg (MJ)	Column 2-180 deg (MJ)
3	Forecastle	3.16	8.46	11.26	15
	Bulb	12.25	4.81	3.75	0.8
5	Forecastle	19.79	22.52	28.81	36.53
	Bulb	47.83	33.2	39.87	33.24
10	Forecastle	99.20	91.91	124.66	151.83
	Bulb	151.48	107.21	145.10	162.96

Table 5-19 Strain energy of supply vessel side collision

Scenario	Strain energy (MJ)
Column 1-0 deg-2 m/s	19.27
Column 1-90 deg-2 m/s	5.88
Column 2-90 deg-2 m/s	8.61
Column 2-180 deg-2 m/s	7.04
Column 2 and 3-180 deg-2 m/s	Spring 1: 9.59, Spring 2: 4.91
Column 1 and 3-120 deg-2 m/s	Spring 1: 3.78, Spring 2: 2.95

When the supply vessel bow impacts the wind turbine in operating condition at the speed of 3 m/s, 5 m/s, and 10 m/s, the maximum strain energy is 15.8 MJ, 69.77 MJ, and 314.79 MJ, respectively, strain energy increases as collision velocity. The forecastle energy is the smallest when the direction is in the positive x-direction and the largest in the negative direction. The wind turbine would tilt backward in operating condition, and bulb spring engages first when supply vessel bow impacts wind turbine, compared with wind turbine in parked condition. When the supply vessel side impacts one column and two columns at the speed of 2 m/s, the maximum strain energy is 19.27 MJ and 14.5 MJ, respectively. The movement of the wind

turbine has a significant impact on strain energy, especially when the wind turbine speed is opposite to vessel speed, which will cause more damage to the vessel.

5.3.1.4 Tower stress

Table 5-20 Von mises stress of supply vessel bow collision

Velocity (m/s)	Column 1-0 deg (MPa)	Column 1-90 deg (MPa)	Column 2-90 deg (MPa)	Column 2-180 deg (MPa)
3	286.1	290.9	310.6	340.1
5	321.6	285.3	320.2	408.3
10	332	338.3	316.3	436.1

Table 5-20 shows the von mises stress when the supply vessel bow impacts wind turbine in operating condition. The maximum tower stress is 340 MPa, 408 MPa, and 436 MPa when the supply vessel bow impacts the wind turbine at the speed of 3 m/s, 5 m/s, and 10 m/s, respectively. The worst scenario is that the supply vessel hits column 2 in the 180-deg direction, and tower stress exceeds yield stress when the impact speed is 5 m/s and 10 m/s.

Table 5-21 Von mises stress of supply vessel side collision

Scenario	Von mises stress (MPa)
Column 1-0 deg-3 m/s	311.6
Column 1-0 deg-5 m/s	285.2
Column 1-0 deg-10 m/s	290
Column 2-180 deg-2 m/s	350
Column 2 and 3-180 deg- 2 m/s	387.4
Column 1 and 2-120 deg-2 m/s	287.4

The maximum tower stress is 350 MPa when the supply vessel side impacts one column. The same as supply vessel bow collision, the worst scenario is that the supply vessel impacts column 2 in the 180-deg direction, exceeding yield stress. When the supply vessel side impacts two columns, the maximum tower stress is 387.4 MPa. Compared with the supply vessel side hits one column, tower stress is more considerable when the supply vessel side hits two columns in a 180-deg direction.

5.3.1.5 *Mooring force*

Table 5-22 Mooring force of supply vessel collision

Scenario	Mooring force (MN)
Bow-column 1-0 deg-3 m/s	5.15
Bow-column 1-0 deg-5 m/s	6.58
Bow-column 1-0 deg-10 m/s	7.98
Side-column 2-180 deg-2 m/s	5.68
Side-column 2 and 3-180 deg- 2 m/s	2.43
Side-column 1 and 2-120 deg-2 m/s	2.48

The wind load on the wind turbine pushes it backward, in the worst scenario, the wind blows from positive x-direction (0-deg direction), and only one mooring line bears the load. Table 5-22 summarizes the mooring force. The maximum mooring force is 5.15 MN, 6.58 MN, and 7.98 MN when the supply vessel bow hits the wind turbine at the speed of 3 m/s, 5 m/s, and 10 m/s, respectively. When the supply vessel bow hits the wind turbine, the mooring force increases as the collision velocity increases. When the supply vessel side hits one column, the maximum mooring force is 5.68 MN. The maximum mooring force is 2.48 MN when the supply vessel side hits two columns, which is relatively small compared with the supply vessel side hits 1 column because two mooring lines bear the load. Mooring forces in all scenarios do not exceed the proof load, indicating that the mooring line is capable of withstanding the collision load.

5.3.1.6 *Tower Clearance*

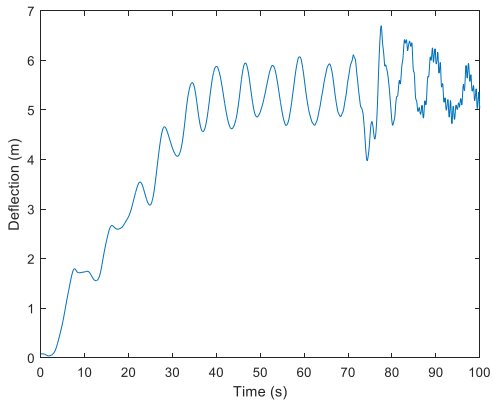

Figure 5-31 Blade deflection in operating condition

Figure 5-31 shows the blade deflection when an operating wind turbine is impacted by a supply vessel. The wind turbine blades bend as wind speed increases, and the blade deflection is about 6 m when the wind turbine operating at rated power condition. When the supply vessel hits the wind turbine at 65 s, the maximum blade deflection is about 6.7 m. The blade deflection increases because collision load bends the tower and vibrates the blades, but the increment is small. Though the wind load bends the blades, the blade deflection is relatively small compared with tower clearance under no load, and the risk of blades hitting the tower is minimal.

5.3.2 Shuttle tanker

5.3.2.1 Nacelle acceleration

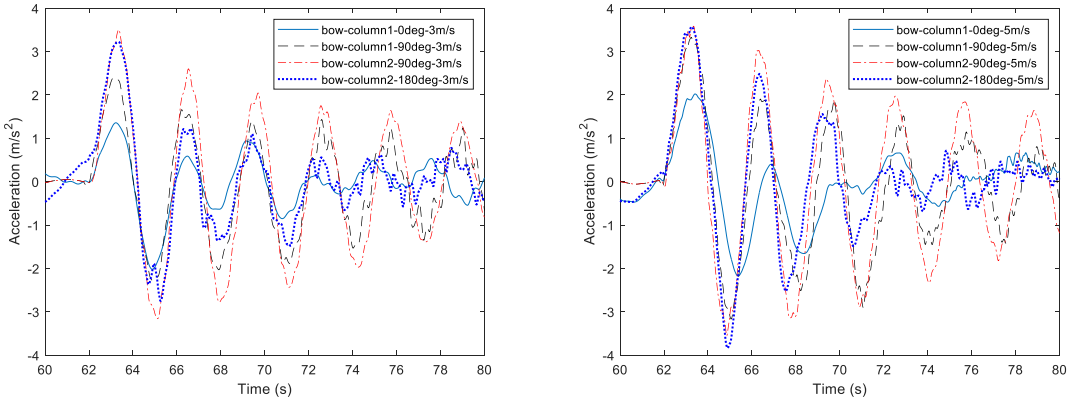

Figure 5-32 Nacelle acceleration when shuttle tanker bow hits the wind turbine at the speed of 3 m/s (left) and 5 m/s (right)

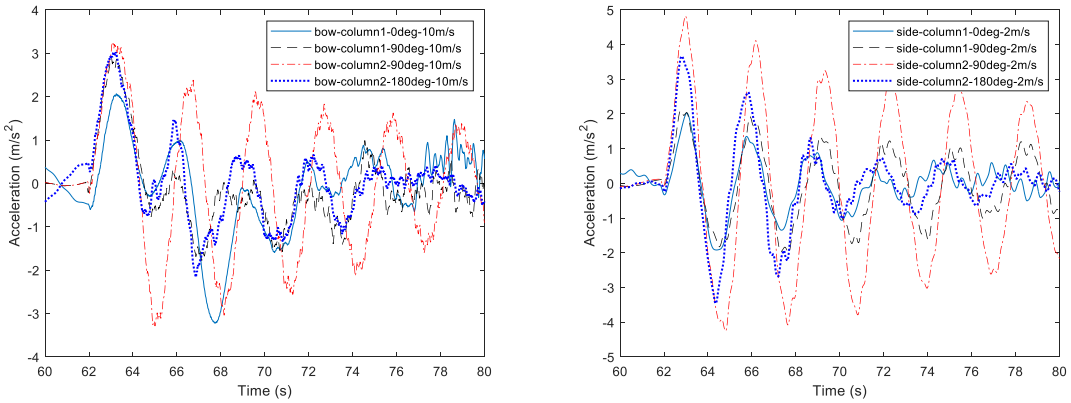

Figure 5-33 (left) Nacelle acceleration when shuttle tanker bow hits the wind turbine at the speed of 10 m/s; (right) Nacelle acceleration when shuttle tanker side hits the wind turbine at the speed of 2 m/s

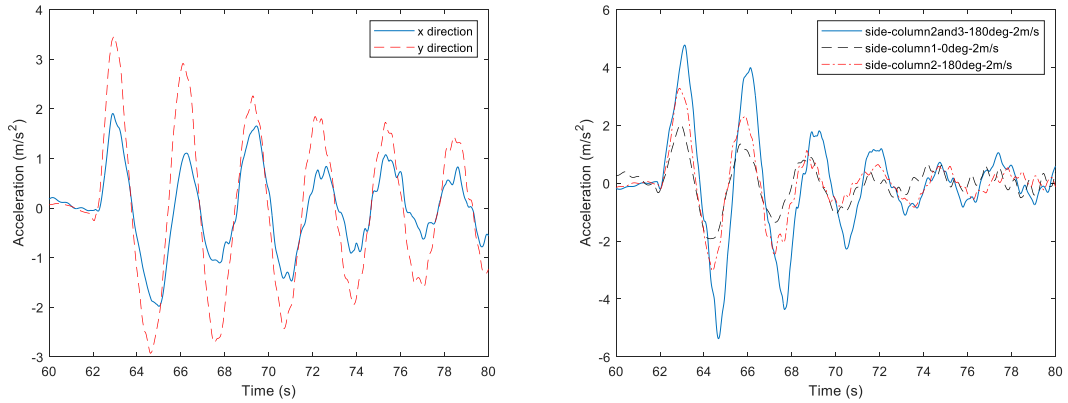

Figure 5-34 (left) Nacelle acceleration of case shuttle tanker side-column 1 and 3-120 deg-2 m/s; (right) Nacelle acceleration comparison of shuttle tanker side hits 1 column and two columns

Figure 5-32 and Figure 5-33 shows nacelle acceleration when the shuttle tanker impacts the wind turbine in operating condition at various speeds. Nacelle acceleration exceeds 2 m/s^2 in all cases, indicating the collision poses a threat to mechanical and electrical equipment in the nacelle. When the shuttle tanker side crashes into two columns, nacelle acceleration exceeds 5 m/s^2. Compared with the shuttle tanker hitting one column, nacelle acceleration is more significant when it crashes into two columns, as shown in Figure 5-34.

5.3.2.2 Force and displacement

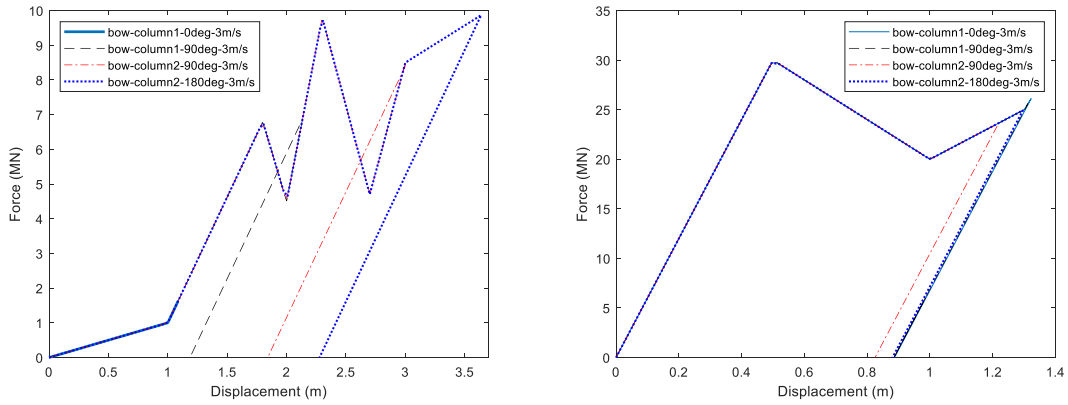

Figure 5-35 Forecastle (left) and bulb (right) force-displacement curve when shuttle tanker bow hits wind turbine at the speed of 3 m/s

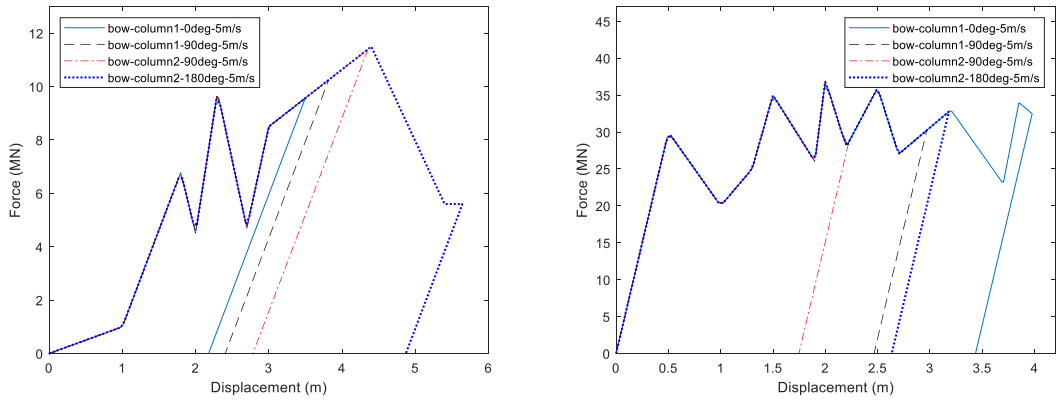

Figure 5-36 Forecastle (left) and bulb (right) force-displacement curve when shuttle tanker bow hits wind turbine at the speed of 5 m/s

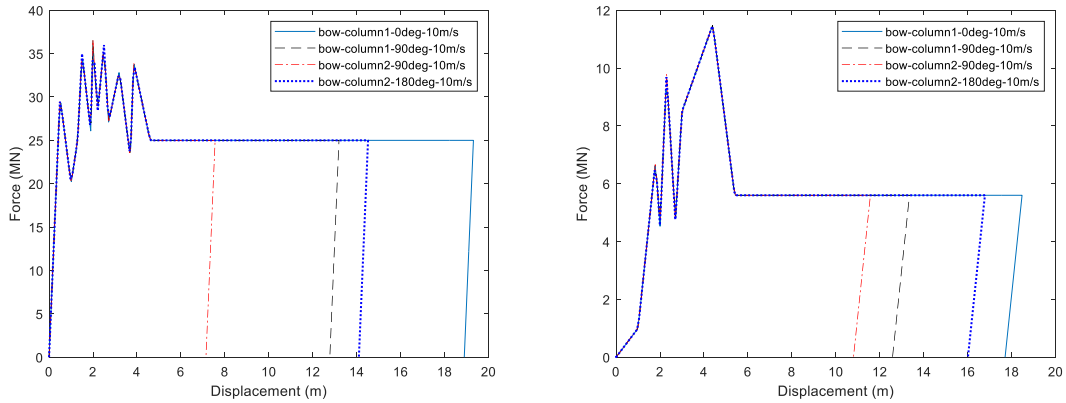

Figure 5-37 Forecastle (left) and bulb (right) force-displacement curve when shuttle tanker bow hits wind turbine at the speed of 10 m/s

When supply vessel bow hits the wind turbine at the speed of 3 m/s, 5 m/s and 10 m/s, the maximum forecastle force is 9.9 MN, 11.5 MN and 11.5 MN, respectively; and the maximum bulb force is 30.0 MN, 36.9 MN and 36.9 MN, respectively.

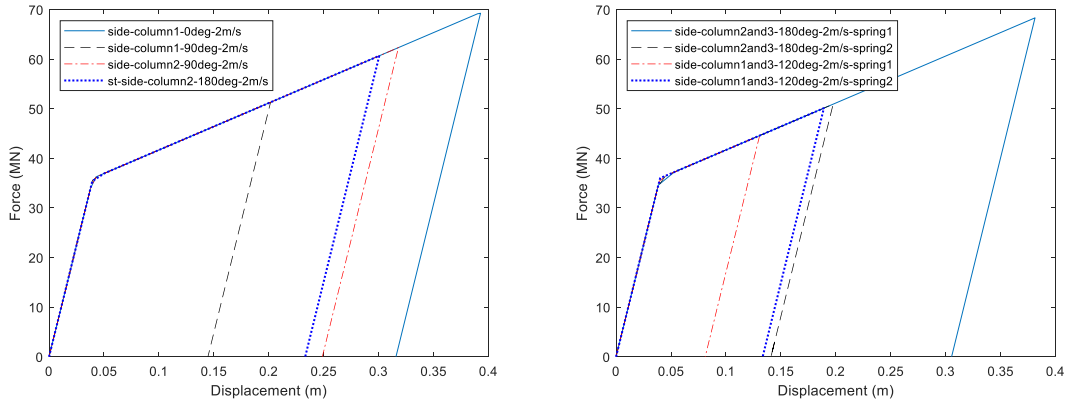

Figure 5-38 Force-displacement curve when shuttle tanker side crashes into one column (left) and two columns (right) at the speed of 2 m/s

When the shuttle tanker side hits one column and two columns at the speed of 2 m/s, the maximum force is 69.3 MN. The maximum force is 68.3 MN and 50.1 MN for case shuttle tanker side-column 2 and 3-180 deg-2 m/s and case shuttle tanker side-column 1 and 3-120 deg-2 m/s, respectively. Although the maximum force is greater when shuttle tanker side hits one column, the resultant force is greater when the shuttle tanker side crashes into two columns, which explains the nacelle acceleration is greater when the shuttle tanker side crashes into two columns compared with hitting one column.

5.3.2.3 Strain energy

Table 5-23 Strain energy of shuttle tanker bow collision

Velocity (m/s)	Ship section	Column 1-0 deg (MJ)	Column 1-90 deg (MJ)	Column 2-90 deg (MJ)	Column 2-180 deg (MJ)
3	Forecastle	0.6	2.26	6.9	10.92
	Bulb	21.64	21.59	20.12	21.47
5	Forecastle	9.96	12.19	16.3	33.53
	Bulb	99.19	70.59	48.46	75.94
10	Forecastle	105.36	76.70	66.76	95.90
	Bulb	488.44	335.51	194.63	368.7

Table 5-24 Strain energy of shuttle tanker bow collision

Scenario	Strain energy (MJ)
Column 1-0 deg-2 m/s	166.43
Column 1-90 deg-2 m/s	63.12
Column 2-90 deg-2 m/s	122.29
Column 2-180 deg-2 m/s	112.69
Column 2 and 3-180 deg-2 m/s	Spring 1:159.25, spring 2:61.24
Column 1 and 3-120 deg-2 m/s	Spring 1:32.68, spring 2: 57.47

When the shuttle tanker bow impacts the wind turbine in operating condition at the speed of 3 m/s, 5 m/s and 10 m/s, the maximum strain energy is 32.39 MJ, 109.15 MJ and 593.8 MJ, respectively, strain energy increases as collision velocity. The forecastle energy is the smallest when the direction is in the positive x-direction and the largest in the negative direction. The wind turbine would tilt backward in operating condition, bulb spring engages first when the shuttle tanker bow impacts wind turbine, compared with wind turbine in parked condition. When the shuttle tanker side impacts one column and two columns at the speed of 2 m/s, the maximum strain energy is 166.43 MJ and 220.49 MJ, respectively. The movement of the wind turbine has a great impact on strain energy, especially when the wind turbine speed is opposite to vessel speed, it will cause more damage to the vessel.

5.3.2.4 Tower stress

Table 5-25 Von mises stress of shuttle tanker bow collision

Velocity (m/s)	Column 1-0 deg (MPa)	Column 1-90 deg (MPa)	Column 2-90 deg (MPa)	Column 2-180 deg (MPa)
3	323.3	287	351.9	419.6
5	321.3	320.1	408.9	465.7
10	382.5	303.8	385.7	415.3

Table 5-26 Von mises stress of shuttle tanker side collision

Scenario	Von mises stress (MPa)
Column 1-0 deg-2 m/s	318.1
Column 1-90 deg-2 m/s	298.1
Column 2-90 deg-2 m/s	359.2
Column 2-180 deg-2 m/s	412.1
Column 2 and 3-180 deg-2 m/s	456.6
Column 1 and 3-120 deg-2 m/s	368.4

When the shuttle tanker bow impacts the wind turbine in operating condition at the speed of 3 m/s, 5 m/s and 10 m/s, the maximum tower stress is 419 MPa, 465 MPa and 415 MPa, respectively. The maximum tower stress is 412 MPa when the shuttle tanker side impacts the wind turbine in operating condition at 2 m/s. Tower stress of case shuttle tanker bow-column 1-90 deg-10 m/s, case shuttle tanker bow-column 2-90 deg-10 m/s and case shuttle tanker bow-column 2-180 deg-10 m/s is too small and the reason is unknown, but we can infer that tower stress when shuttle tanker bow impacting wind turbine at the speed of 10 m/s is almost the same as that at the speed of 5 m/s because the maximum force is the same and the error may come from wind turbine motion under wind and wave load. When the shuttle tanker impacts the wind turbine in operating condition, the worst scenario is that it hits column 2 in the 180-deg direction. The tower stress is 456 MPa when shuttle tanker side impacts column 2 and 3 in the 180-deg direction, compared with case shuttle tanker side-column 2-180 deg-2 m/s, tower stress is greater when it crashes into two columns.

5.3.2.5 Mooring force

Table 5-27 Mooring force of shuttle tanker collision

Scenario	Mooring force (MN)
Bow-column 1-0 deg-3 m/s	8.33
Bow-column 1-0 deg-5 m/s	11.76
Bow-column 1-0 deg-10 m/s	18
Side-column 2-180 deg-2 m/s	7.99
Side-column 2 and 3-180 deg-2 m/s	5.19
Side-column 1 and 2-120 deg-2 m/s	7.2

Table 5-27 shows the mooring forces of the worst scenarios when the shuttle tanker collides with the wind turbine. It increases as collision velocity increases. The mooring force is relatively small when the shuttle tanker side impacts two columns, for case shuttle tanker side-column 2 and 3-180 deg-2 m/s, the collision direction is opposite to wind turbine movement, for case shuttle tanker side-column 1 and 3-120 deg-2 m/s, a large portion of force component is in the y-direction and only a small portion of force component in the x-direction. For case shuttle tanker bow-column 1-0 deg-5 m/s, mooring force exceeds the proof load of 'Grade R3 with a yield stress 410 MPa', which is 9.67 kN, a mooring line with higher Grade and yield stress should be used.

5.4 Discussion

5.4.1 The simple and fine force-displacement curve

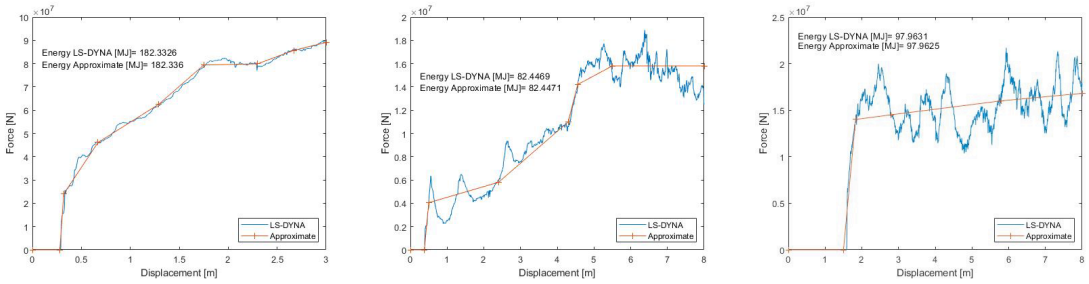

Figure 5-39 Side (left), forecastle (middle) and bulb (right) force-displacement curves of supply vessel (Martin, 2020)

Figure 5-39 shows the LS-DYNA output curves and simplified curves Martin used. There is an apparent difference between the force-displacement curves, resulting in deviations in collision simulation results. A comparison between the simple curve and fine curve is discussed in this section, Figure 5-40 shows a comparison of the fine curve and simple curve.

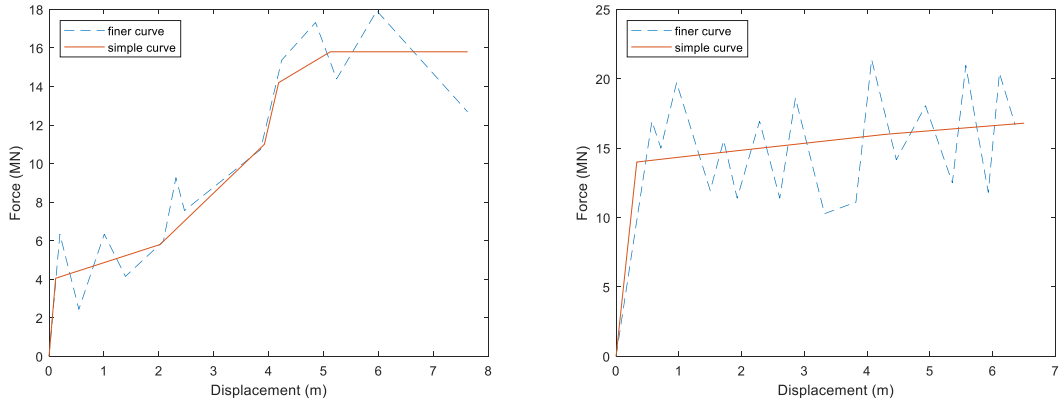

Figure 5-40 Comparison of force-displacement curves, forecastle (left) and bulb (right)

The supply vessel bow collision at the speed of 3 m/s is selected for the analysis. Four scenarios, as described below, are carried out.

(1) supply vessel bow-column 1-0 deg-3 m/s

(2) supply vessel bow-column 1-90 deg-3 m/s

(3) supply vessel bow-column 2-90 deg-3 m/s

(4) supply vessel bow-column 2-180 deg-3 m/s

5.4.1.1 Model verification

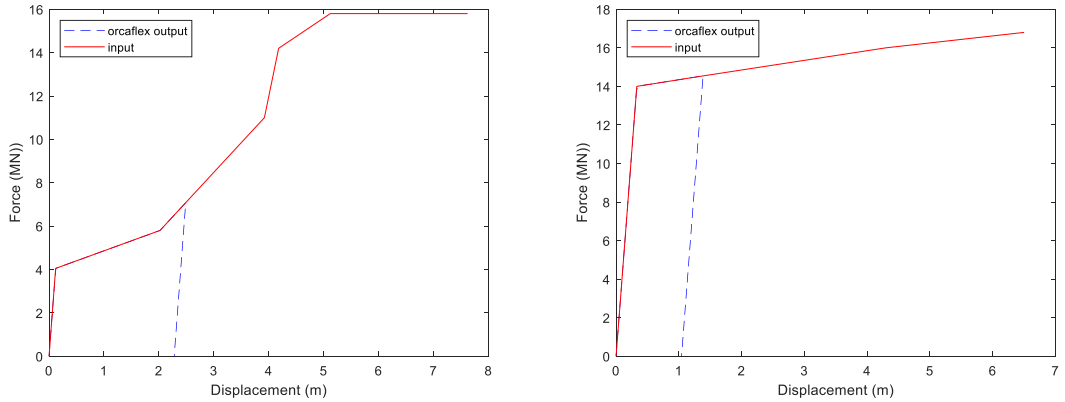

Figure 5-41 Input and OrcaFlex output force-displacement curves comparison for simple curve, forecastle (left) and bulb (right)

As the model verification has been done for the fine force-displacement curve in the previous section, Figure 5-41 displays the model verification just for simple curves, including supply vessel forecastle and bulb. The OrcaFlex output force-displacement curves are in good agreement with input curves, indicating the model is correct and the collision system represents the ship correctly. The unloading path follows the same path as the loading.

5.4.1.2 *Force and displacement*

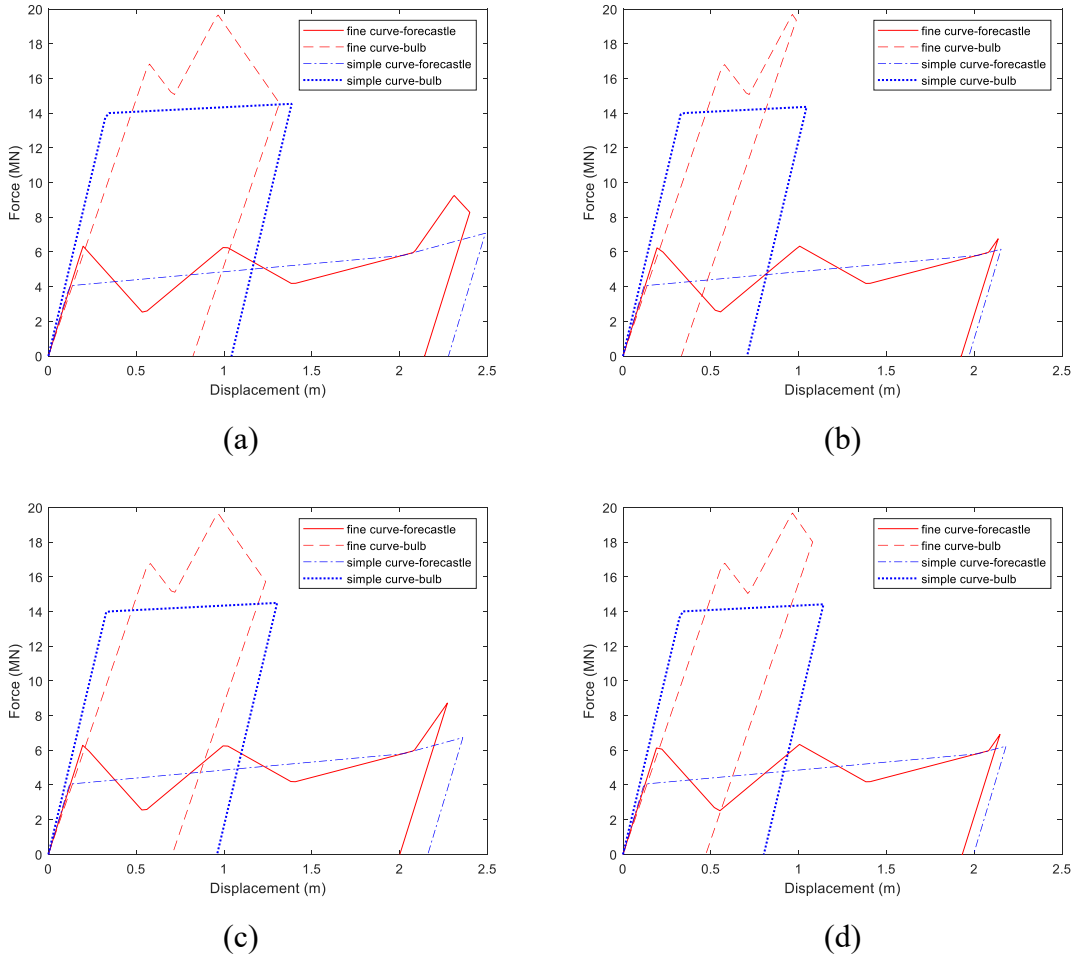

Figure 5-42 Force-displacement curves comparison of the simple curve and fine curve, (a) case supply vessel bow-column 1-0 deg-3 m/s; (b) case supply vessel bow-column 1-90 deg-3 m/s; (c) case supply vessel bow-column 2-90 deg-3 m/s; (d) case supply vessel bow-column 2-180 deg-3 m/s

Figure 5-42 shows the force-displacement comparison of vessel forecastle and bulb between the simple and fine curve. In all four scenarios, it is evident that the maximum displacement is different. For both the vessel forecastle and bulb, the fine curve results in shorter displacement but greater force, leading to a greater nacelle acceleration and bending stress to the tower. In addition, a larger force means greater damage to the floater and may break the columns.

5.4.1.3 *Strain energy*

Table 5-28 Comparison of strain energy between the fine curve and simple curve when supply vessel bow impacts the wind turbine at the speed of 3 m/s

Curve	Ship section	Column1-0 deg (MJ)	Column 1-90 deg (MJ)	Column 2-90 deg (MJ)	Column 2-180 deg (MJ)
Simple curve	Forecastle	11.87	9.83	11.06	9.99
	Bulb	14.88	10.02	13.69	11.40
Fine curve	Forecastle	11.15	9.33	9.91	9.37
	Bulb	13.89	5.55	12.10	8.15

Table 5-28 shows the stain energy dissipated in different scenarios. Compared with the fine curve, the strain energy of the simple curve is greater, and the differences in strain energy between the simple curve and the fine curve are 1.71 MJ, 4.97 MJ, 2.74 MJ, and 3.87 MJ, respectively. The error is most significant for case supply vessel bow-column 1-90 deg-3 m/s, about 25 %.

5.4.1.4 Velocity

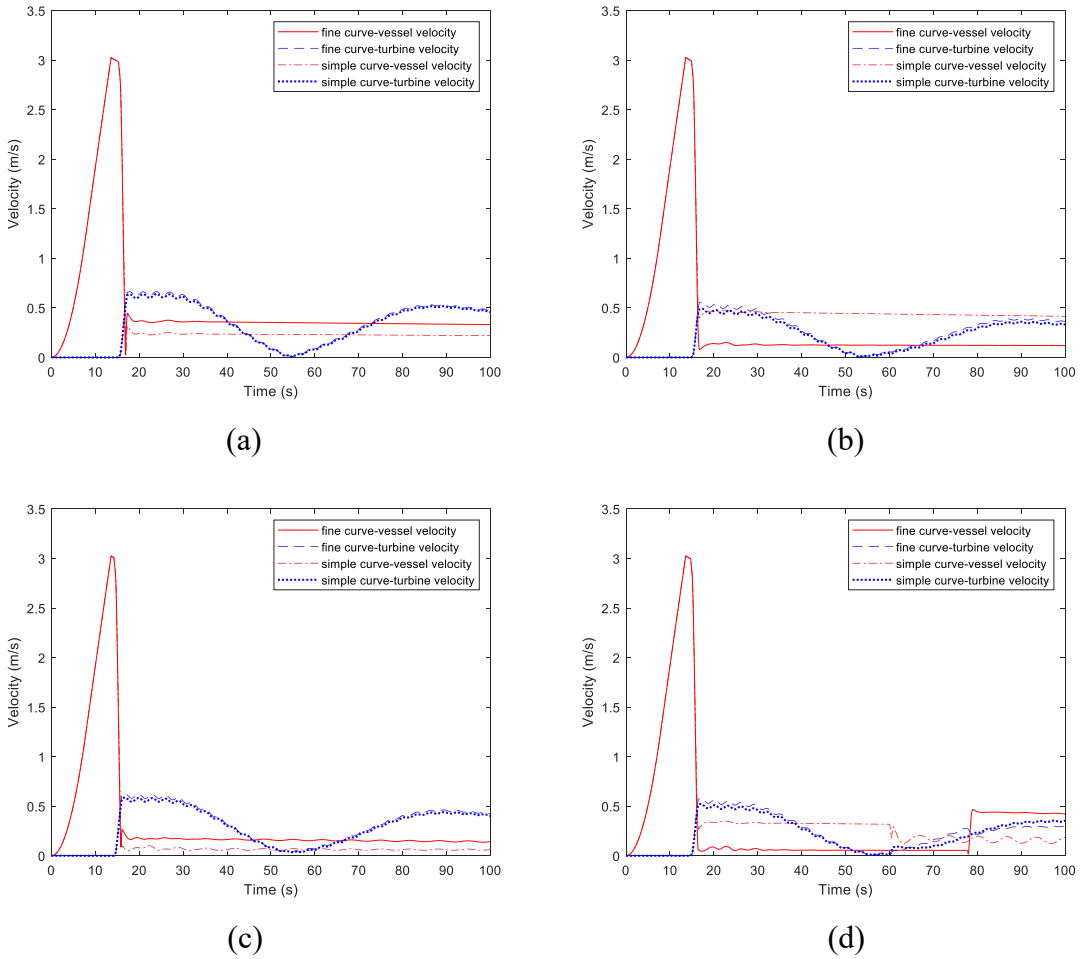

Figure 5-43 Supply vessel and wind turbine velocity comparison before and after collision between the simple curve and fine curve, (a) case supply vessel bow-column 1-0 deg-3 m/s; (b) case supply vessel bow-column 1-90 deg-3 m/s; (c) case supply vessel bow-column 2-90 deg-3 m/s; (d) case supply vessel bow-column 2-180 deg-3 m/s

Figure 5-43 shows the velocity of the supply vessel and wind turbine before and after the collision. In all four scenarios, the wind turbine velocity is almost the same for both the simple curve and fine curve. The velocity of the vessel decreases sharply after the collision. There is a slight difference between the two curves, but the deviation can also be neglected since we care more about the motion of the wind turbine.

5.4.1.5 Acceleration

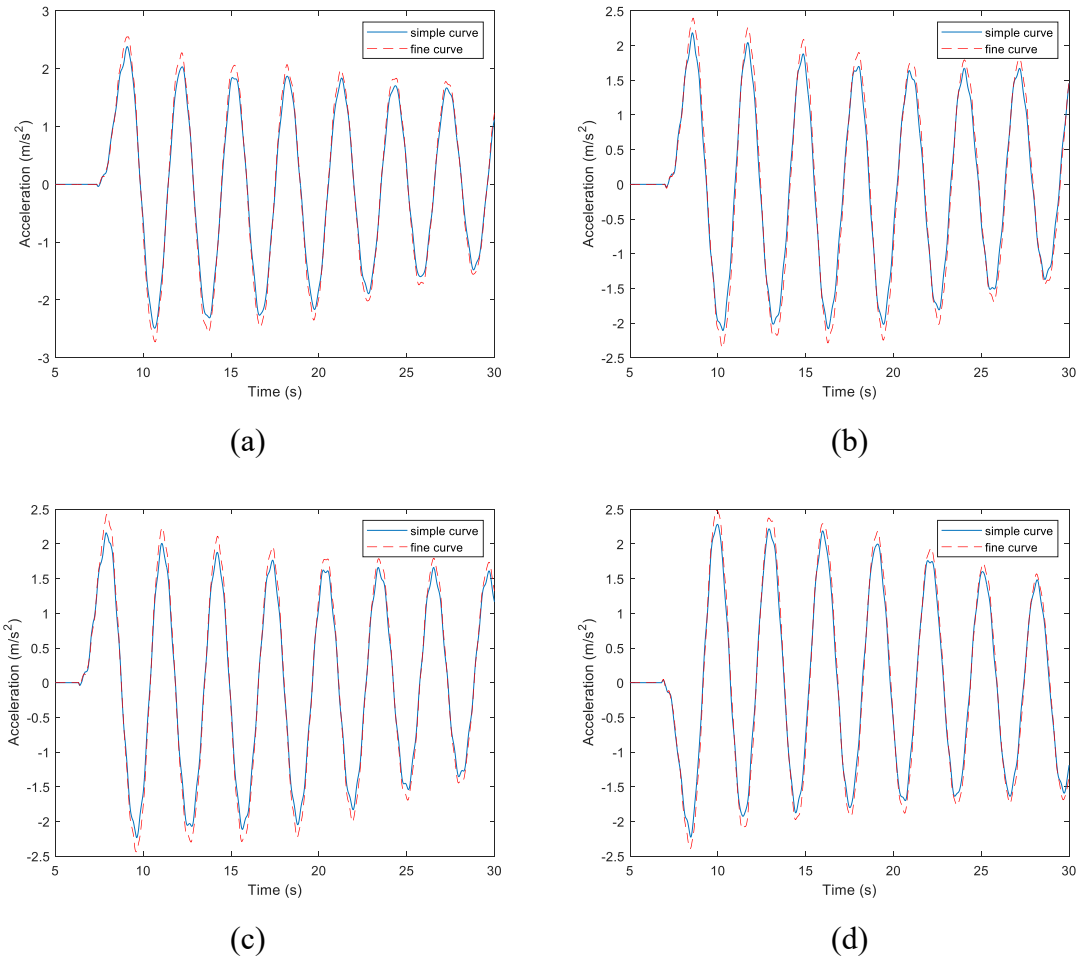

Figure 5-44 Nacelle acceleration comparison between the simple curve and fine curve, (a) case supply vessel bow-column 1-0 deg-3 m/s; (b) case supply vessel bow-column 1-90 deg-3 m/s;

(c) case supply vessel bow-column 2-90 deg-3 m/s; (d) case supply vessel bow-column 2-180 deg-3 m/s

Figure 5-44 shows the nacelle acceleration comparison of the simple curve and fine curve. The nacelle acceleration of the fine curve is larger than that of the simple curve because the maximum force of the fine curve is larger than that of the simple curve, as shown in Figure 5-42.

5.4.1.6 Mooring line force

Table 5-29 Comparison of mooring force between the simple curve and fine curve when supply vessel bow impacts the wind turbine

Force-displacement curve	Bow-column 1-0 deg-3 m/s (MN)	Bow-column 1-90 deg-3 m/s (MN)	Bow-column 2-90 deg-3 m/s (MN)	Bow-column 2-180 deg-3 m/s (MN)
Simple curve	2.50	2.35	2.30	2.04
Fine curve	2.54	2.23	2.32	2.04

Table 5-29 shows the mooring force comparison of the fine curve and simple curve, and there is no obvious difference. The mooring force is related to the wind turbine velocity. Wind turbine would be pulled back by the mooring after it reaches the maximum displacement. As Figure 5-43 shows, wind turbine velocity is almost the same after the collision for both the fine curve and simple curve, which means the maximum mooring line force would be the same.

5.4.1.7 Tower stress

Table 5-30 Comparison of von mises stress between the simple curve and fine curve when supply vessel bow impacts the wind turbine

Force-displacement curve	Bow-column 1-0 deg-3 m/s (MPa)	Bow-column 1-90 deg-3 m/s (MPa)	Bow-column 2-90 deg-3 m/s (MPa)	Bow-column 2-180 deg-3 m/s (MPa)
Simple curve	137.2	129.8	134.4	140.1
Fine curve	149.2	142.2	145.7	151.3
Deviation	12	12.4	11.3	11.2

Von mises stress of the fine curve is greater than that of the simple curve, as shown in Table 5-30, and the deviation is about 12 MPa. This is reasonable because the force is greater for the fine curve, as shown in Figure 5-42

The simple curve can represent the ship correctly to some degree: the velocity of the wind turbine and vessel after the collision is similar for fine curve and simplified curve, which also applies to mooring force. However, due to the larger collision force, the fine force-displacement curve gives a larger nacelle acceleration and tower stress, and the strain energy also differs. Therefore, the fine force-displacement curve will be used in this paper to obtain more accurate results.

5.4.2 Collision location horizontal offset

In this section, the impact of the horizontal offset of collision location on the response of the wind turbine will be analyzed because the collision can be eccentric. The collision location will be offset from the centerline by 1 m, 2 m, and 3 m, respectively. Two scenarios, namely case supply vessel-column 1-0 deg-3 m/s and case supply vessel bow-column 2-90 deg-3 m/s, are conducted. Then the results will be compared with the scenario without offset.

5.4.2.1 Nacelle acceleration

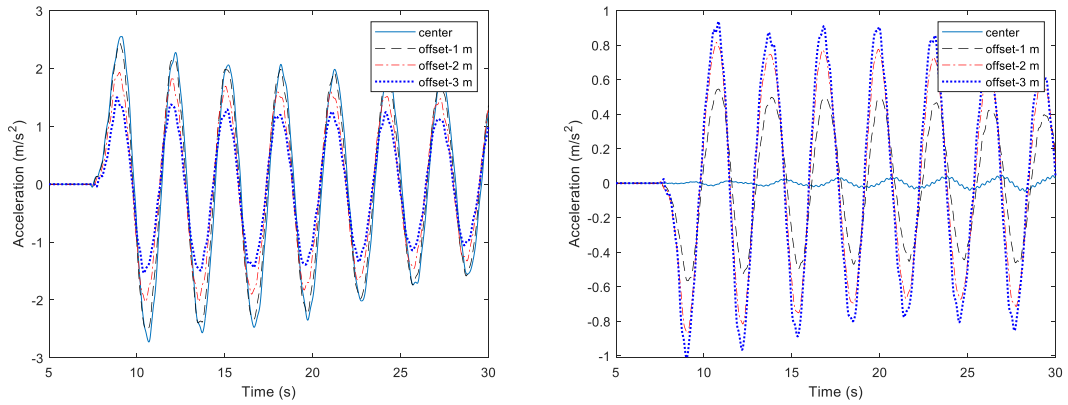

Figure 5-45 Nacelle acceleration comparison of case supply vessel bow-column 1-0 deg-3 m/s at different horizontal locations, x component (left) and y component (right)

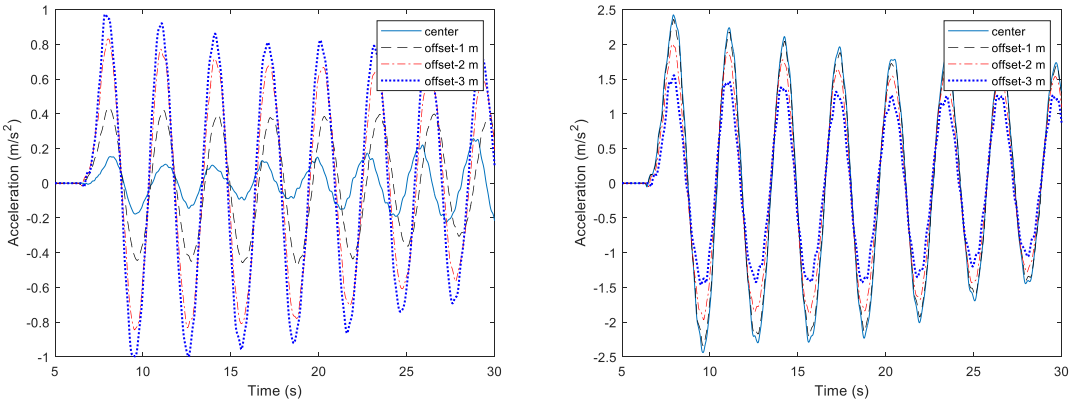

Figure 5-46 Nacelle acceleration comparison of case supply vessel bow-column 2-90 deg-3 m/s at different horizontal locations, x component (left) and y component (right)

As the offset distance increases, for both case bow-column 1-0 deg-3 m/s and case bow-column 2-90 deg-3 m/s, the nacelle acceleration decreases in the direction parallel to the vessel speed and increases in the direction perpendicular to the vessel speed, as shown in Figure 5-45 and Figure 5-46. There is no force component perpendicular to vessel speed when the supply vessel impacts the wind turbine in the center of the column, and the force component perpendicular to vessel speed increases as offset distance increases. Offset distance at the initial stage has little effect on the nacelle acceleration, and there is no significant difference between an offset distance of 1 m and without offset. However, there is an obvious difference between an offset distance of 1 m and 2 m. Moreover, the nacelle acceleration in the direction parallel to vessel speed exceeds 2 m/s^2 when offset 1 m and without offset, but it less than 2 m/s^2 when offset 2 m and 3 m. Nacelle acceleration in the direction perpendicular to vessel speed increases as offset distance increases, but it less than 1 m/s^2.

5.4.2.2 Force and displacement

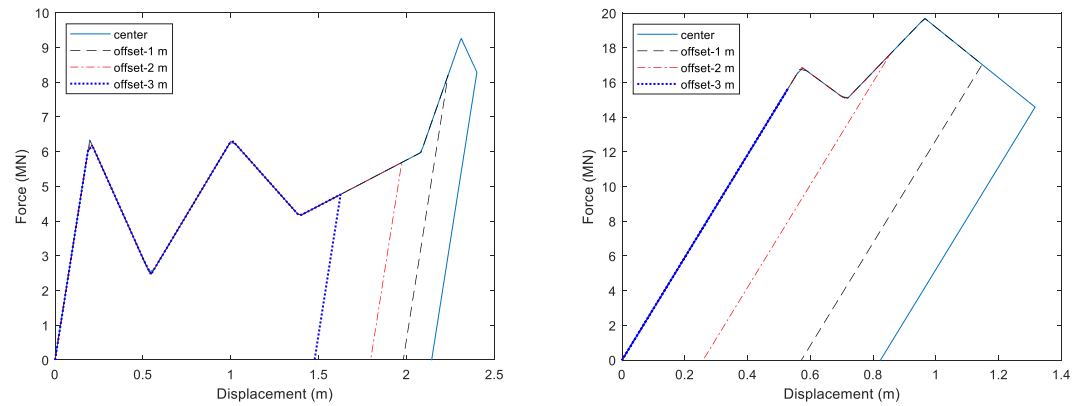

Figure 5-47 Forecastle (left) and bulb (right) force-displacement curves comparison of case supply vessel bow-column 1-0 deg-3 m/s at different horizontal locations

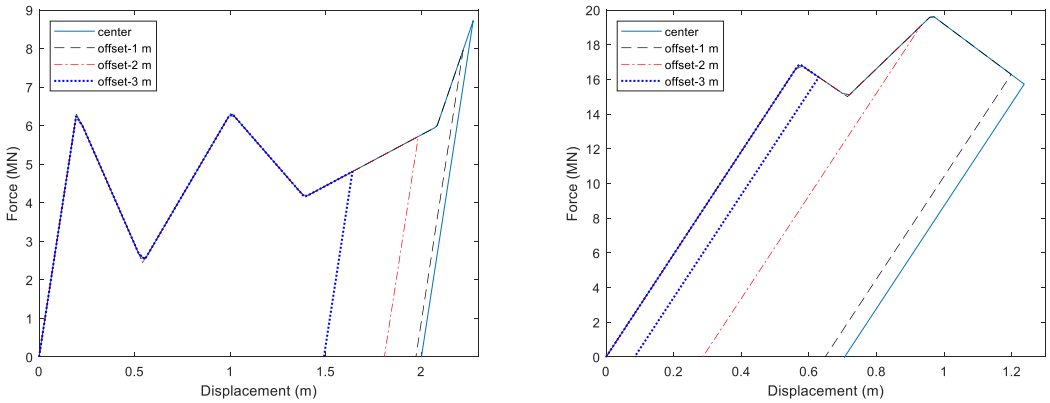

Figure 5-48 Forecastle (left) and bulb (right) force-displacement curve comparison of case supply vessel bow-column 2-90 deg-3 m/s at different horizontal locations

Figure 5-47 and Figure 5-48 show the force-displacement curve. In case supply vessel bow-column 1-0 deg-3 m/s, when there is no offset and offset distance is 1 m, the maximum forecastle force is 9.3 MN, 8.2 MN, respectively, and the maximum bulb force is the same, which is 19.6 MN; when the offset distance is 2 m and 3 m, the maximum forecastle force is the same, which is 6.3 MN, and the maximum bulb force is 17.6 MN and 15.7 MN, respectively. In case supply vessel bow-column 2-90 deg-3 m/s, when without offset and offset distance is 1 m, the maximum forecastle force is 8.7 MN and 8.0 MN, respectively, and the maximum bulb force is the same, which is 19.6 MN; when offset distance is 2 m and 3 m, the maximum forecastle force is same, which is 6.3 MN, and the maximum bulb force is 19.1 MN and 16.9 MN, respectively. Compared with the case without offset, there is no significant difference in force when offset distance is 1 m, but there is a difference when offset distance is further increased, which explain why there is no significant difference in nacelle acceleration when offset 1 m but an obvious difference when the offset is further increased. This also applies to displacement.

5.4.2.3 Strain energy

Table 5-31 Comparison of strain energy when supply vessel bow impact wind turbine at different horizontal locations

Scenario	Ship section	Center (MJ)	Offset 1 m (MJ)	Offset 2 m (MJ)	Offset 3 m (MJ)
Column 1-0	Forecastle	11.15	9.74	8.55	6.88
deg-3 m/s	Bulb	13.89	9.90	4.14	0
Column 2-90	Forecastle	9.91	9.67	8.62	6.95
deg-3 m/s	Bulb	12.10	11.18	4.65	1.39

Both forecastle and bulb strain energy decrease as the offset distance increases, as shown in Table 5-31, strain energy of bulb decreases rapidly compared with forecastle. For case supply vessel bow-column 1-0 deg-3 m/s, bulb strain energy is 0 MJ when offset 3 m because it is elastic deformation. Strain energy decreases by 13.89 MJ for the bulb and 4.27 MJ for the forecastle. For case supply vessel bow-column 2-90 deg-3 m/s, strain energy decrease by 10.71 MJ for the bulb and 2.96 MJ for the forecastle. This is reasonable, the displacement and force decrease as offset distance increases, as shown in Figure 5-47 and Figure 5-48, which means less damage is made to the vessel.

5.4.2.4 Velocity

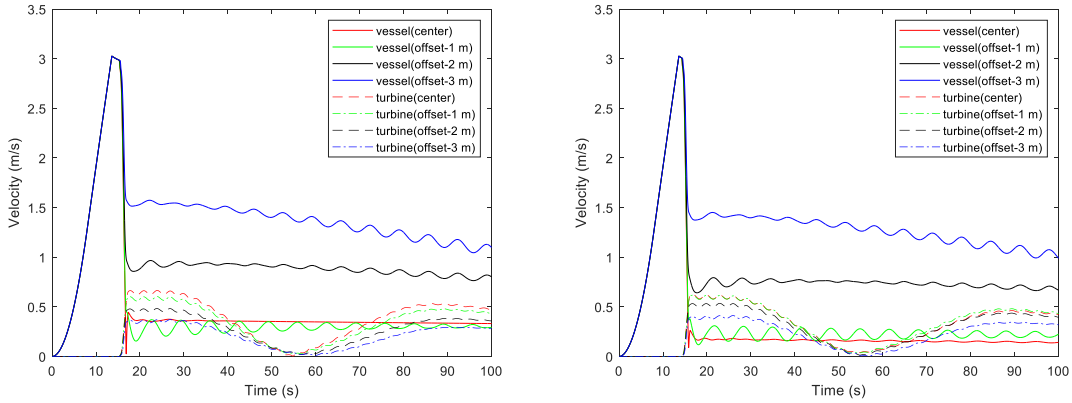

Figure 5-49 Velocity of vessel and wind turbine before and after the collision when supply vessel impacts wind turbine at different horizontal locations. (left) Case supply vessel bow-column 1-0 deg-3 m/s and (right) case supply vessel bow-column 2-90 deg-3 m/s

Figure 5-49 shows the velocity of the vessel and wind turbine before and after the collision. There is no obvious difference for the wind turbine but a significant difference for the vessel velocity. The vessel velocity decreases from 3 m/s to 1.5 m/s for case offset 3 m, and to 0.4 m/s and 0.2 m/s for case supply vessel bow-column 1-0 deg-3 m/s and case supply vessel bow-column 2-90 deg-3 m/s when offset 3 m.

5.4.2.5 Tower stress

Table 5-32 Comparison of von mises stress when supply vessel impacts wind turbine at different horizontal locations

Scenario	Center (MPa)	Offset 1 m (MPa)	Offset 2 m (MPa)	Offset 3 m (MPa)
Supply vessel bow-column 1-0 deg-3 m/s	149.2	144.2	121.2	101.2
Supply vessel bow-column 2-90 deg-3 m/s	145.7	143.6	130.6	113.4

Table 5-32 shows the von mises stress comparison, which decreases as the offset distance increases. There is no significant difference when the offset distance is 1 m, but when the offset distance is further increased, there will be an obvious difference, which can be explained by the maximum force shown in Figure 5-47 and Figure 5-48.

5.4.2.6 Mooring force

Table 5-33 Comparison of mooring force when supply vessel impacts wind turbine at different impact location

Scenario	Center (MN)	Offset 1 m (MN)	Offset 2 m (MN)	Offset 3 m (MN)
Supply vessel bow-column 1-0 deg-3 m/s	2.54	2.42	2.21	2.04
Supply vessel bow-column 2-90 deg-3 m/s	2.32	2.41	2.34	2.15

Table 5-33 shows the mooring force. There are no obvious differences because the mooring force is greatly dependent on the kinetic energy of the wind turbine. Figure 5-49 shows that wind turbine velocity is almost the same after collision.

5.4.3 Collision location vertical offset

In the previous section, the horizontal offset effect of collision location is analyzed, and the vertical offset effect of collision location would be investigated in this section. The collision location may offset vertically due to the vessel draft and wave. The draft will increase when the vessel is fully loaded. Besides, the vessel and wind turbine will move up and down along with the wave, affecting the collision location. The case supply vessel bow-column 1-0 deg-3 m/s is chosen, and the wind turbine is in parked condition. A total of five cases are considered. The spring locations of the basic case are described in chapter 5.1.2. The vessel hits the wind turbine only with the forecastle or bulb in the two extreme cases. In the other two cases, the spring locations of the forecastle and bulb are moved downward 1 m and 2 m.

5.4.3.1 Nacelle acceleration

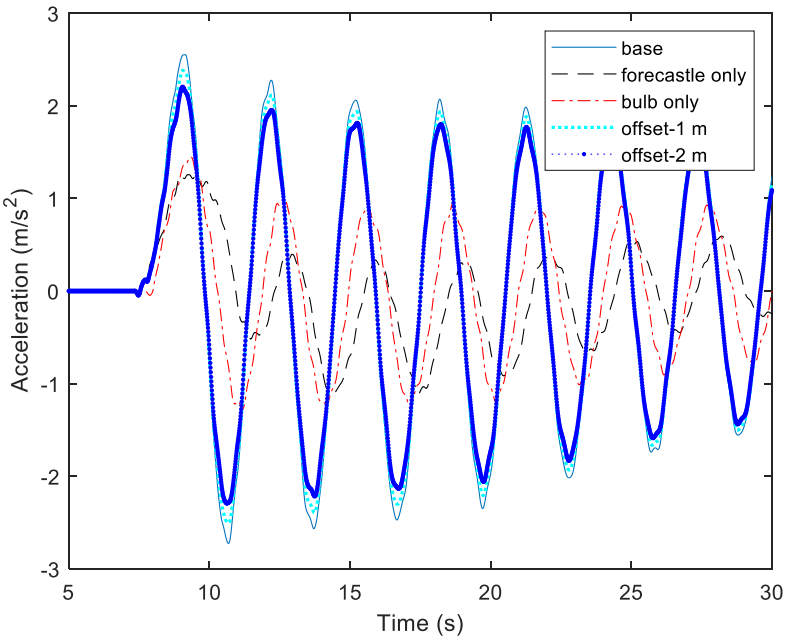

Figure 5-50 Comparison of acceleration of case supply vessel bow-column 1-0 deg-3 m/s when supply vessel impacts wind turbine at different vertical locations

When the supply vessel bow hits the wind turbine with only the forecastle or bulb, the nacelle acceleration is around 1.2 m/s^2. When the supply vessel hitting wind turbine with both forecastle and bulb, nacelle acceleration is more than 2 m/s^2. Nacelle acceleration is obviously more significant when the supply vessel bow hits the wind turbine with the forecastle and bulb, as shown in Figure 5-50. When comparing the cases of 'base', 'offset-1 m', and 'offset-2 m',

it is found that the offset distance has a relatively little effect on the nacelle acceleration, but the nacelle acceleration decreases as the offset distance increases.

5.4.3.2 Force and displacement

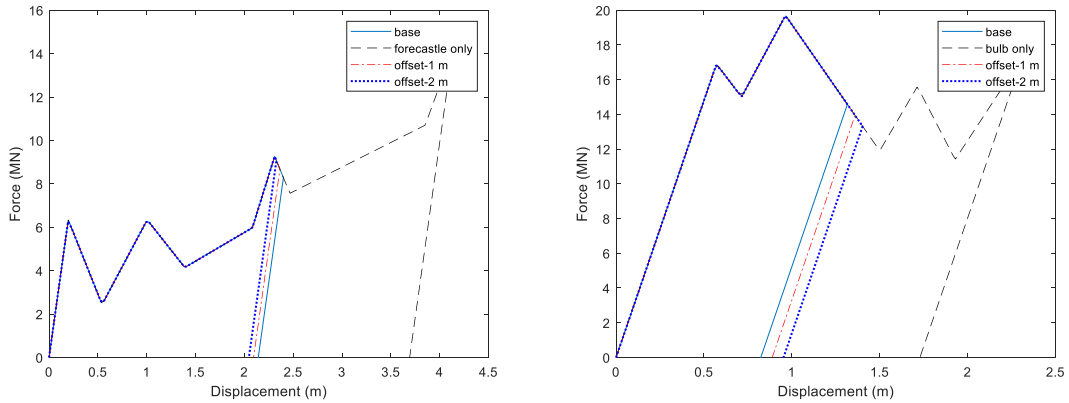

Figure 5-51 Forecastle (left) and bulb (right) force-displacement curves comparison of case supply vessel bow-column 1-0 deg-3 m/s when supply vessel impacts wind turbine at different vertical locations

Figure 5-51 shows the force-displacement curves comparison for forecastle and bulb. Compared with the supply vessel hits the wind turbine with both forecastle and bulb, both the displacement and force are much larger when the vessel hits wind turbine just with forecastle. The maximum bulb force is the same, but the displacement is larger when the supply vessel hits the wind turbine just with bulb. It explains that the nacelle acceleration is much smaller when the vessel hits wind turbine with just a forecastle or bulb because the resultant force is much smaller.

5.4.3.3 Turbine and vessel motion

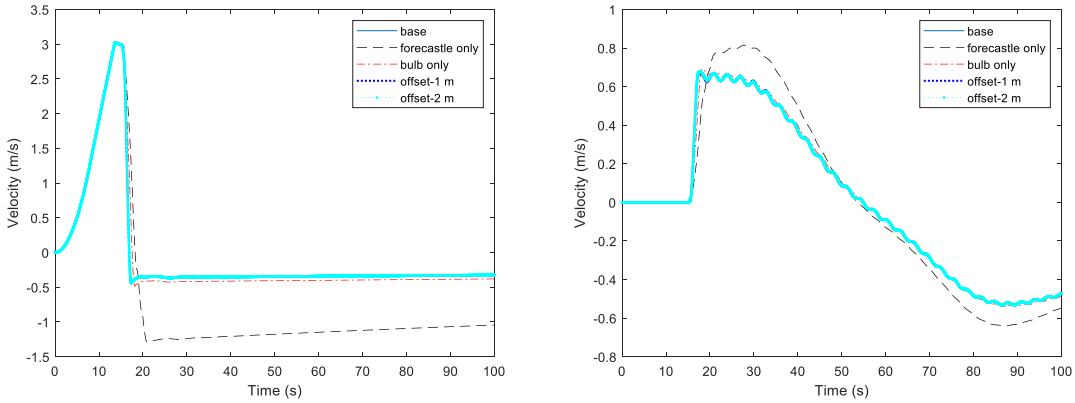

Figure 5-52 Vessel (left) and wind turbine (right) velocity comparison before and after collision of case supply vessel bow-column 1-0 deg-3 m/s when supply vessel impacts wind turbine at different vertical locations

Figure 5-52 shows the velocity of the vessel and wind turbine before and after the collision. The vessel velocity in all scenarios is negative after the collision, which means the vessel is rebounded after the collision. When the supply vessel hits the wind turbine with just the forecastle, the maximum velocity after collision is 1.28 m/s, which is larger than the other four cases. The wind turbine velocity is slightly larger when the vessel hits with just a forecastle.

5.4.3.4 Strain energy

Table 5-34 Comparison of strain energy of case supply vessel bow-column 1-0 deg-3 m/s when supply vessel impacts wind turbine at different vertical locations

Energy	Base (MJ)	Forecastle only (MJ)	Bulb only (MJ)	Offset 1 m (MJ)	Offset 2 m (MJ)
Forecastle	11.15	25.77		10.74	10.32
Bulb	13.88		26.21	14.81	15.69

Table 5-34 shows the strain energy dissipated by vessel forecastle and bulb during the collision in the form of structural deformation. The total energy dissipated by the vessel is almost the same, which means more damage is made to the forecastle or bulb when the vessel hits with just a forecastle or bulb.

5.4.3.5 Tower stress

Table 5-35 Comparison of von mises stress of case supply vessel bow-column 1-0 deg-3 m/s when supply vessel impacts wind turbine at different vertical locations

Stress	Base (MPa)	Forecastle only (MPa)	Bulb only (MPa)	Offset 1 m (MPa)	Offset 2 m (MPa)
Von mises stress	149	101.4	90.5	138.9	128

Table 5-35 shows the von mises stress of the tower. The von mises stress is much smaller when the supply vessel hits the wind turbine with just a forecastle or bulb. As Figure 5-51 shows, the

resultant force is much smaller compared with vessel hits wind turbine with both forecastle and bulb. Tower stress decreases slightly as offset distance increases, which is in accordance with nacelle acceleration.

5.4.3.6 Mooring force

Table 5-36 Comparison of mooring force of case supply vessel bow-column 1-0 deg-3 m/s when supply vessel impacts wind turbine at different vertical locations

	Base (MPa)	Forecastle only (MPa)	Bulb only (MPa)	Offset 1 m (MPa)	Offset 2 m (MPa)
Mooring force	2.54	2.67	2.49	2.54	2.53

The mooring forces are almost the same for all the cases, as shown in Table 5-36, because the wind turbine velocity after the collision has no obviously difference.

5.4.4 Comparison between parked condition and operating condition

In this section, a comparison between the parked condition and operating condition would be present. Supply vessel bow collision at a speed of 5 m/s is selected.

5.4.4.1 Nacelle acceleration

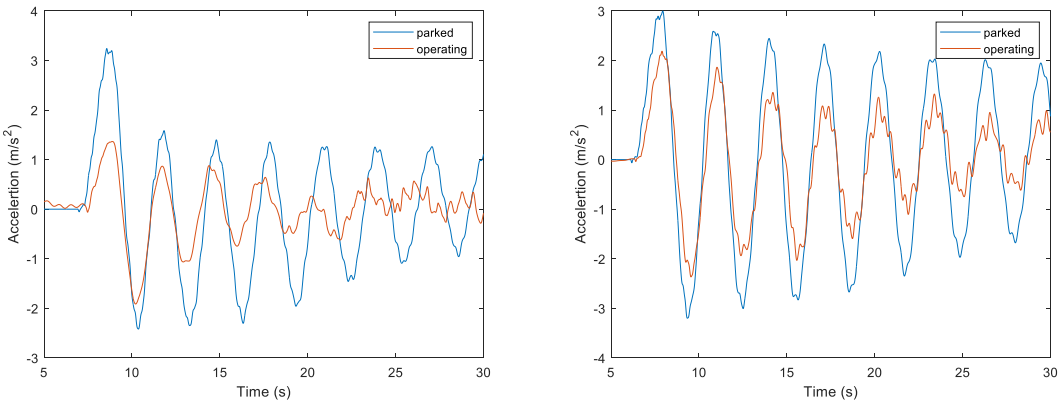

(a) (b)

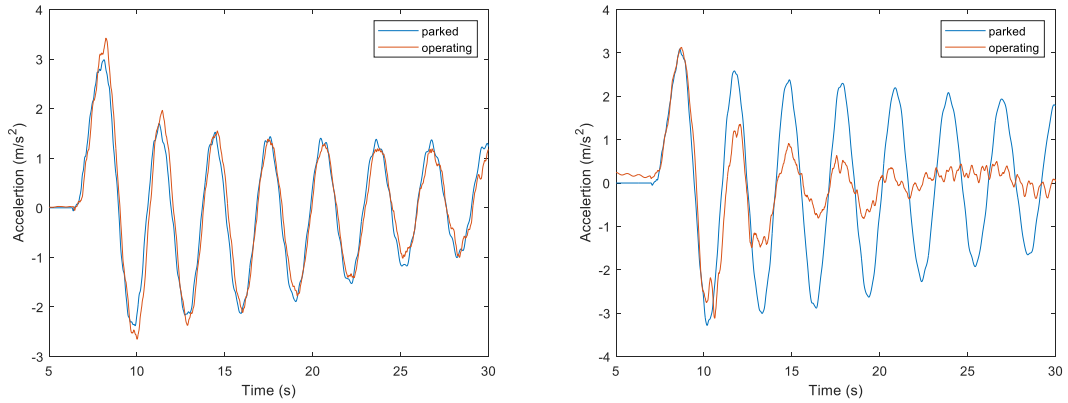

(c) (d)

Table 5-37 Nacelle acceleration comparison of supply vessel bow collision with FOWT in the parked condition and operating condition. (a) case supply vessel bow-column 1-0 deg-5 m/s; (b) case supply vessel bow-column 1-90 deg-5 m/s; (c) case supply vessel bow-column 2-90 deg-5 m/s; (d) case supply vessel bow-column 2-180 deg-5 m/s

In parked condition, maximum nacelle acceleration is the same for all four cases and exceeds 3 m/s^2. In operating condition, collision direction and location have a great impact on the nacelle acceleration, it less than 2 m/s^2 for case supply vessel bow-column 1-0 deg-5 m/s and the worst scenario is supply vessel bow hits column 2.

5.4.4.2 Force and displacement

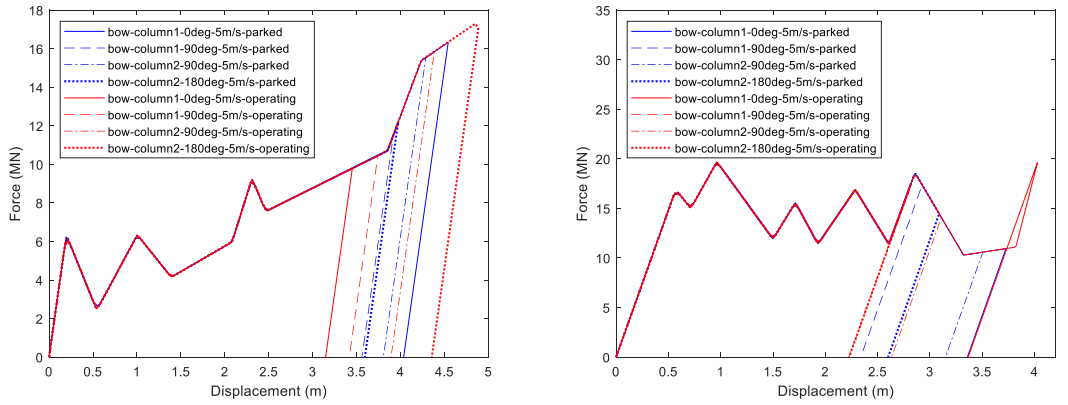

Table 5-38 Force-displacement curve for supply vessel bow collision with FOWT in the parked and operating condition at the speed of 5 m/s, forecastle (left) and bulb (right)

There is a slight difference in force and displacement between parked condition and operating condition when supply vessel speed is perpendicular to wind speed, force and displacement

differ between parked condition and operating condition when vessel speed is parallel to wind speed because wind turbine will tilt backward under wind load, as shown in Figure 5-53, compared with the parked condition, more energy will be dissipated by bulb when supply vessel hits column 1 in 0-deg direction and by forecastle when supply vessel impact column 2 in 180-deg direction.

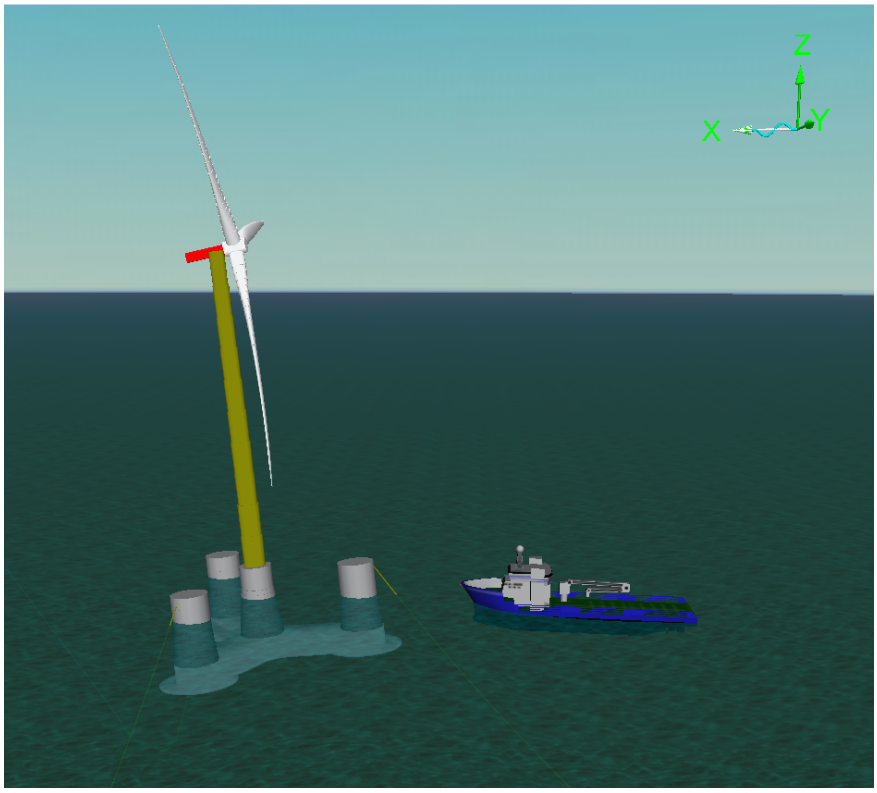

Figure 5-53 Wind turbine tilts backward under wind load

5.4.4.3 Tower stress

Table 5-39 Comparison of von mises stress in parked condition and operating condition

scenario	Parked condition (MPa)	Operating condition (MPa)
Supply vessel bow-column 1-0 deg-5 m/s	179.9	321.6
Supply vessel bow-column 1-90 deg-5 m/s	182.9	285.3
Supply vessel bow-column 2-90 deg-5 m/s	161.3	320.2
Supply vessel bow-column 2-180 deg-5 m/s	187.7	408.3

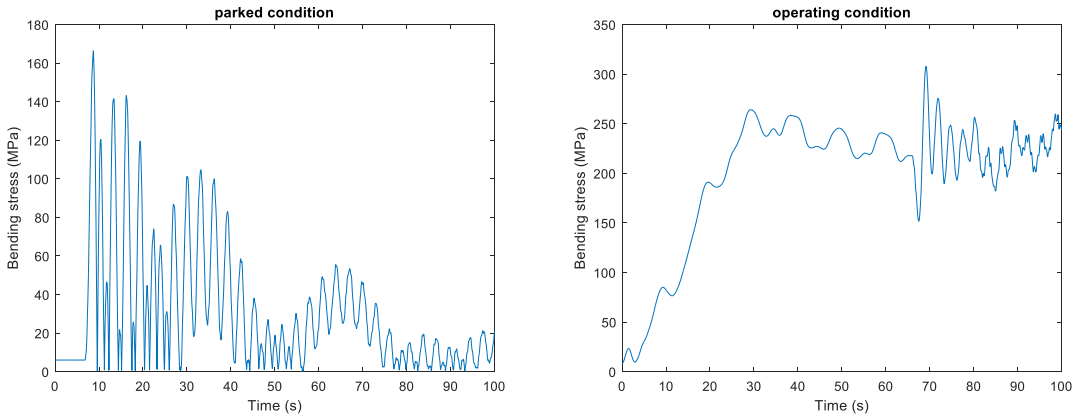

Figure 5-54 Tower stress comparison when supply vessel bow impact wind turbine in parked condition (left) and operating condition (right) at the speed of 5 m/s

In parked condition and operating condition, the maximum tower stress is 187.7 MPa and 408 MPa, respectively. Tower stress does not exceed yield stress in parked condition. Compared with the parked condition, tower stress in operating condition is much larger, the minimum value is 285.3 MPa and the utilization factor is above 0.8. Wind load has a great impact on tower stress because wind turbine blades generate thrust force and bend the tower.

5.4.4.4 Mooring force

Table 5-40 Comparison of mooring force in parked condition and operating condition

scenario	Parked condition (MN)	Operating condition (MN)
Supply vessel bow-column 1-0 deg-5 m/s	3.41	6.58
Supply vessel bow-column 1-90 deg-5 m/s	2.51	4.87
Supply vessel bow-column 2-90 deg-5 m/s	2.65	4.9
Supply vessel bow-column 2-180 deg-5 m/s	2.20	4.77

The mooring force of FOWT is different between parked condition and operating condition because wind load and wave load push FOWT backward until the maximum displacement is reached, then the mooring line pulls it back. In both parked condition and operating condition, the worst scenario is the supply vessel bow-column 1-0 deg-5 m/s, because only one mooring line bears the load, and the vessel collision makes the situation worse in operating condition.

5.4.4.5 Tower clearance

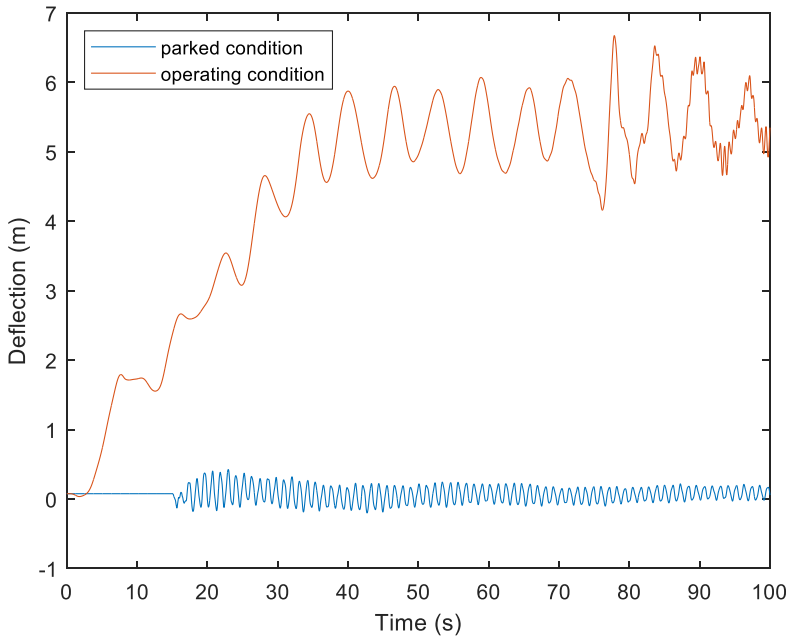

Figure 5-55 Blade deflection comparison when supply vessel bow impacts wind turbine in parked and operating condition at the speed of 5 m/s

Vessel collision cause blades to vibrate slightly, but it is negligible compared to deflection caused by wind load, as shown in Figure 5-55, blades deflect gradually as wind speed increases until reaching rated wind speed, blade deflection increases slightly when the collision occurs.

5.4.4.6 Strain energy

Table 5-41 Strain energy comparison between the parked condition and operating condition

Scenario	Ship section	Parked condition (MJ)	Operating condition (MJ)
Supply vessel bow-column 1-0 deg-5 m/s	Forecastle	31.15	19.79
	Bulb	48.13	47.83
Supply vessel bow-column 1-90 deg-5 m/s	Forecastle	24.07	22.52
	Bulb	35.22	33.2
Supply vessel bow-column 2-90 deg-5 m/s	Forecastle	27.44	28.81
	Bulb	45.83	39.87
Supply vessel bow-column 2-180 deg-5 m/s	Forecastle	24.46	36.53
	Bulb	39.39	33.24

There is no significant difference for total energy dissipated by supply vessel forecastle and bulb between parked condition and operating condition of the wind turbine. In operating condition, the wind turbine tilts backward under wind load, which may affect the strain energy distribution by forecastle and bulb. For example, compared with the parked condition, bulb engages earlier when the collision occurs for case supply vessel bow-column 1-0 deg-5 m/s, which means more energy dissipated by bulb while less energy dissipated by forecastle.

5.4.5 Environmental load

It is crucial to analyze the dynamic response of the wind turbine subjected to the vessel collision in cut-out wind speed conditions, that is, 25 m/s. In high wind speed, the rotor speed can be limited by pitching the blades to feather, decreasing the lift force and drag force to prevent blades over speed and crash with the tower. When the wind speed ranges from rated wind speed and cut-out wind speed, the wind turbine still works in rated condition. Therefore, in this section, the wind speed is set as rated wind speed, 11.4 m/s, and wind direction is in the positive x-direction. The wave profile is set as JONSWAP, and the H_S (significant wave height) is 8.31 m. The wave direction is the same as the wind direction. The supply vessel bow collision with the wind turbine at the speed of 3 m/s is performed.

5.4.5.1 Nacelle acceleration

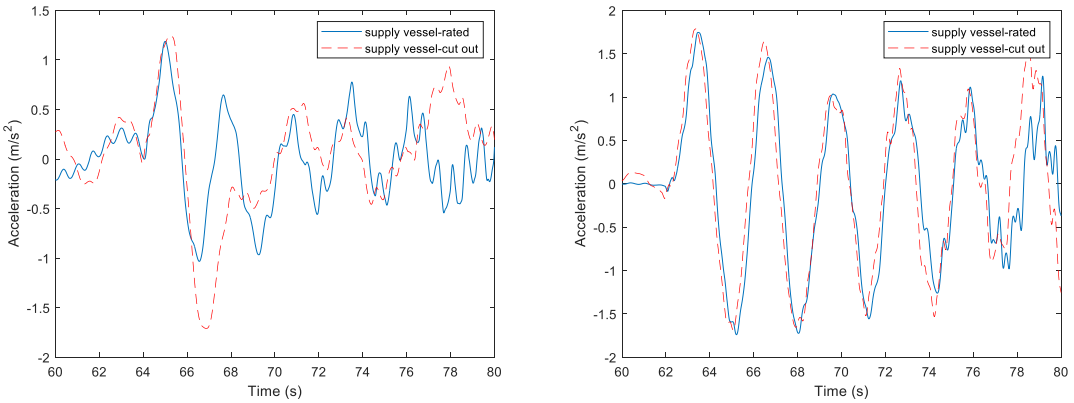

(a) (b)

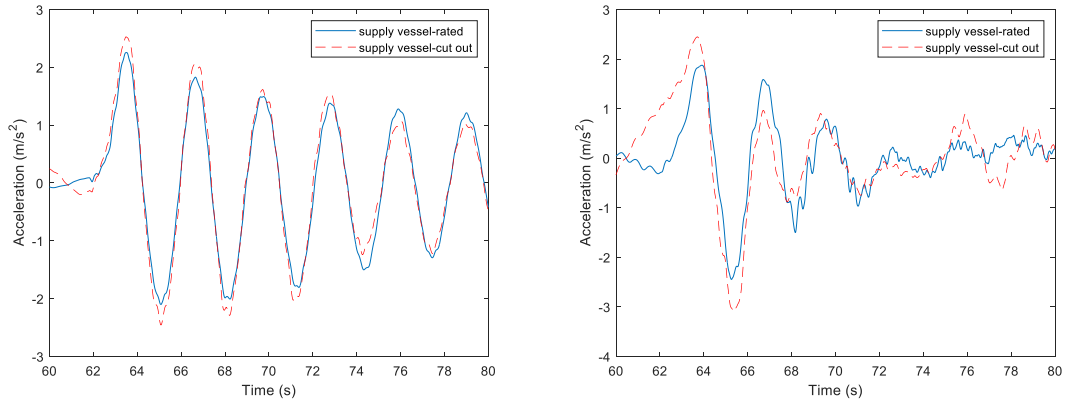

(c) (d)

Figure 5-56 Nacelle acceleration comparison when supply vessel hits wind turbine at the speed of 3 m/s in rated (Hs=3.5) and cut-out (Hs=8.31) conditions, (a) case supply vessel bow-column 1-0 deg-3 m/s; (b) case supply vessel bow-column 1-90 deg-3 m/s; (c) case supply vessel bow-column 2-90 deg-3 m/s; (d) case supply vessel bow-column 2-180 deg-3 m/s

Figure 5-56 displays the nacelle acceleration when the supply vessel bow hits the wind turbine in cut-out condition and rated condition. There is no difference for nacelle acceleration between cut-out condition and rated condition when supply vessel direction parallel to blade rotating plane. However, it affects nacelle acceleration slightly when vessel direction perpendicular to rotating plane, and nacelle acceleration increases slightly for case supply vessel bow-column 1-0 deg-3 m/s and case supply vessel bow-column 2-180 deg-3 m/s.

5.4.5.2 Force and displacement

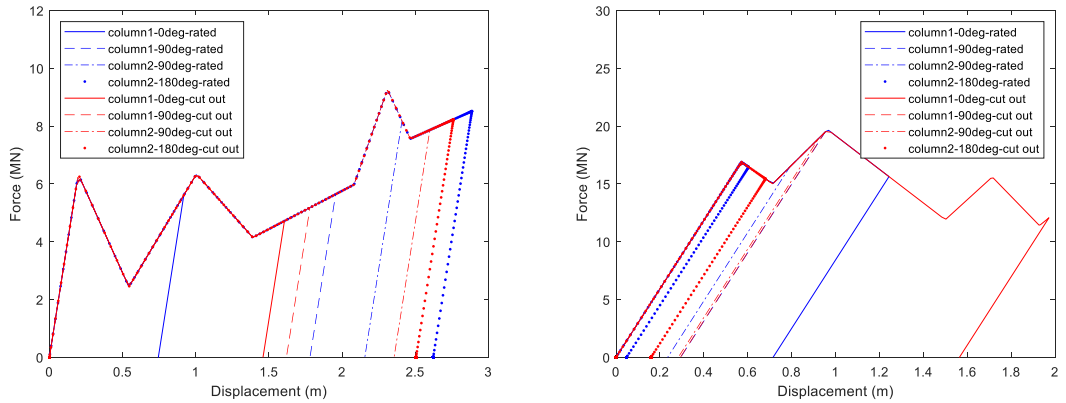

Figure 5-57 Force-displacement curves when supply vessel bow hits wind turbine at the speed of 3 m/s in rated (Hs=3.5 m) and cut-out (Hs=8.31 m) conditions, forecastle (left) and bulb (right)

Wind turbine tilts backward under wind load and wave load, bulb engages first in the event of a collision for case supply vessel bow-column 1-0 deg-3 m/s, as shown in Figure 5-57, bulb displacement is the largest while forecastle displacement is the least. For case supply vessel bow-column 2-180 deg-3 m/s, on the contrary, bulb displacement is the least while forecastle displacement is the largest. Compared with the rated condition, it has the greatest impact on case supply vessel bow-column 1-0 deg-3 m/s, both forecastle and bulb displacement have doubled.

5.4.5.3 Strain energy

Table 5-42 Comparison of strain energy when supply vessel bow hits wind turbine at the speed of 3 m/s in rated (Hs=3.5 m) and cut-out (Hs=8.31 m) conditions

Environmental condition	Ship section	Column 1-0 deg (MJ)	Column 1-90 deg (MJ)	Column 2-90 deg (MJ)	Column 2-180 deg (MJ)
Cut-out condition	Forecastle	6.8	7.59	12.81	14.02
	Bulb	23.8	4.79	4.6	2.58
Rated condition	Forecastle	3.16	8.46	11.26	15
	Bulb	12.25	4.81	3.75	0.8

When the supply vessel bow impacts the wind turbine at the speed of 3 m/s in cut-out condition, the maximum strain energy is 30.6 MJ. Compared with the rated condition, strain energy dissipated by the forecastle and the bulb in cut-out condition is similar. In the case supply vessel bow-column 1-0 deg-3 m/s, since the displacement is doubled, as shown in Figure 5-57, the strain energy is also doubled in cut-out condition.

5.4.5.4 Tower stress

Table 5-43 Comparison of tower stress when supply vessel bow hits wind turbine in rated (Hs=3.5 m) and cut-out (Hs=8.31 m) condition at the speed of 3 m/s

	Column 1-0 deg (MPa)	Column 1-90 deg (MPa)	Column 2-90 deg (MPa)	Column 2-180 deg (MPa)
Cut-out condition	313.4	327.2	355.6	372.9
Rated condition	286.1	290.9	310.6	340.1

When the supply vessel bow impacts the wind turbine at the speed of 3 m/s in the rated and cut-out conditions, the maximum tower stress is 372.9 MPa and 340.1 MPa, respectively. Compared with the rated condition, the tower stress is greater in the cut-out condition due to the larger wave load.

Table 5-44 Comparison of mooring force when supply vessel bow hits wind turbine in rated (Hs=3.5 m) and cut-out (Hs=8.31 m) condition at the speed of 3 m/s

Condition	Mooring force (MN)
Cut-out condition	5.15
Rated condition	6.8

The same as rated condition, the worst scenario is case supply vessel bow-column 1-0 deg-3 m/s because only one mooring line bears the load. The maximum mooring force is 6.8 MN and 5.15 MN in cut-out condition and rated condition, respectively. Mooring force is more significant in cut-out conditions because the greater wave load pushes the wind turbine further. But the mooring force is still less than the proof load, which means it can withstand the collision load.

Chapter 6 Conclusions

This paper presents a case study of ship collision with a semi-submersible floating wind turbine. The local collision analysis found that the thickness of the wall should be larger than 1 m, because the 0.5 m thick wall is brittle. When the ship with different initial velocities impacts the 1 m thick wall, only the ship will deform if the collision energy is small. As increases of the speed, the structural deformation of the ship increases. If the collision energy is large enough, the structural deformation will concentrate on the concrete wall, and the deformation of the ship will decrease. For the deformation of the ship, both the bulb and forecastle are deformed, but most of the collision energy is dissipated through the deformation of the ship bulb structure. When the ship impacts 1 m thick wall at 45 degrees, there is a side crack in the bulb of the ship. The ship is more likely to be deformed and the concrete wall is safer. For various collision positions, the forecastle of the ship peeling on the top of the column is dangerous. The conical structure at the bottom of the column is sensitive to a collision, especially at high speed. It is necessary to avoid the conical structure from emerging from the water. The strain rates have an effect on the strength of structures. The reinforcements in the concrete wall are subjected to small axial stress before the concrete failure.

Global analysis of the collision between vessel and FOWT in parked conditions and operating conditions is conducted. Depending on FOWT condition (parked or operating), ship type (8800-ton supply vessel or 20000-ton shuttle), collision type (head-on or sideways), collision direction, collision location, and collision speed, multiple scenarios are conducted. The nacelle acceleration, tower stress, tower clearance, strain energy, and mooring force are obtained. Generally, nacelle acceleration in almost all scenarios exceeds the limitation of 2 m/s^2, which may cause damage to electrical equipment and economic loss. Tower stress does not exceed yield stress in parked conditions, but it may exceed yield stress in operating conditions. Compared with the blade deflection caused by wind load, the vessel collision has little impact on the blade deflection. Blades keep a safe distance from the tower in both parked and operating conditions. The worst case for the mooring line is that the vessel impacts column 1 in a 0-deg direction because only one mooring line bears the load. Compared with the parked condition, the mooring line bears a greater load in the operating conditions. The mooring force exceeds the proof load of steel Grade R3 when the shuttle tanker bow impacts the wind turbine at the speed of 5 m/s. Thus, mooring lines with a higher steel grade shall be used. Then the effect of

collision location is discussed. It has a significant effect when the vertical offset distance is more than 2 meters from the column centerline. The nacelle acceleration and tower stress are smaller when the vessel impacts the wind turbine with only the forecastle or bulb. Compared with the simple force-displacement curve, the fine curve results in larger tower stress and nacelle acceleration and shall be used to obtain more accurate simulation results. The collision between the vessel and wind turbine in cut-out conditions is also simulated. When the collision direction is parallel to wave direction, the tower stress and nacelle acceleration are more significant.

Chapter 7 Recommendation for further work

The local analysis and global analysis for collision between a FOWT and the vessel have been conducted in this paper, more work can be done in the future.

For local analysis:

1 The material model of **MAT_72R3* in LS-DYNA in LS-DYNA has been used in this study. According to (Jiang & Zhao, 2015), the RC structure can be simulated by other material models, such as **MAT_CSCM_CONCRETE_MODEL* (MAT 159), **MAT_SCHWER_MURRAY_CAP_MODEL* (MAT 145) and so on. These material models can be compared with *MAT_72R3 model and can be used as effect material model analysis in further work

2 The conical structure of the column is brittle. In the future work, there will be some suggestions, such as redesigning the cone into a cylinder, increasing the thickness of the cone structure, and changing concrete to other anti-corrosion materials.

For global analysis:

1 Blade pitch is not considered in this paper. According to Bak et al. (2013), the pitch angle is zero in the rated condition (wind speed is 11.4 m/s), and the blades start to pitch when the wind speed is above the rated wind speed. The wind speed is assumed to be 11.4 m/s in the operating conditions in this paper. The dynamic response of the wind turbine in cut-out condition is studied in chapter 5.4.5. However, the wind speed is assumed to be 11.4 m/s instead of 25 m/s because the wind turbine works in rated condition when the wind speed ranges from 11.4 m/s to 25 m/s. There are some errors in this assumption. Besides, the wind turbine will pitch the blades to reduce the thrust force in extreme environmental conditions such as typhoon. Thus, to obtain more accurate simulation results in high wind speed conditions, the dynamic response of the wind turbine considering the pitch angle shall be investigated.

2 When shuttle tanker bow impacts the wind turbine at the speed of 10 m/s, the simulation results of the tower stress and nacelle acceleration seem to be incorrect, which are is smaller compared with the results when vessel impacts the wind turbine at the speed of 5 m/s. The reason is unknown and further work is needed.

Nacelle acceleration, tower stress, and mooring force are not included in the local analysis, and the deformation of the column is not considered in the global analysis due to the drawback of software. Therefore, a comprehensive software tool is needed for the collision analysis of the FOWT.

Reference

Amdahl, J., & Holmas, T. (2011). High energy ship collisions with jacket supported offshore wind turbines.

American Bureau of Shipping. (2013). Guidance Notes on Accidental Load Analysis and Design for Offshore Structures

AS, D. N. V. (2013). Buckling Strength of Shells. Recommended Practice DNV-RP-C202.

Asian, S., Ertek, G., Haksoz, C., Pakter, S., & Ulun, S. (2016). Wind turbine accidents: A data mining study. IEEE Systems Journal, 11(3), 1567-1578.

Bachynski, E. E., & Moan, T. (2012). Design considerations for tension leg platform wind turbines. Marine Structures, 29(1), 89-114.

Bak, C., Zahle, F., Bitsche, R., Kim, T., Yde, A., Henriksen, L. C., ... & Hansen, M. (2013). Description of the DTU 10 MW reference wind turbine. DTU Wind Energy Report-I-0092, 5.

Bathe, K.-J. (2014). Finite element procedures (2nd ed). Prentice-Hall.

Bela, A., Le Sourne, H., Buldgen, L., & Rigo, P. (2017). Ship collision analysis on offshore wind turbine monopile foundations. Marine Structures, 51, 220-241.

Bhattacharya, S. (2019). Design of foundations for offshore wind turbines. Wiley.

Caithness windfarm information forum. Summary of Wind Turbine Accident data to 31 March 2021. http://www.caithnesswindfarms.co.uk/AccidentStatistics.htm

DIN, E. (2004). 10025-2 Hot Rolled Products of Structural Steels—Part 2: Technical Delivery Conditions for Non-Alloy Structural Steels. Brussels, Belgium: European Committee for Standardisation.

Ding, H., Zhu, Q., & Zhang, P. (2014). Dynamic simulation on collision between ship and offshore wind turbine. Transactions of Tianjin University, 20(1), 1-6.

DNV-RP-C204. (2010). DNV-RP-C204: Design Against Accidental Loads.

DNV, G. (2010). Design against accidental loads. DNV-RP-C204, Det Norske Veritas AS.

DNVGL. DNVGL OS E302, Offshore mooring chains. 2015.

DNVGL. DNVGL ST 0119, Floating wind turbine structures. 2018.

Du Beton C. E. I., CEB-FIP model code 1990, Bull. d'Inform. 213 (1993) 48–50.

Echeverry, S., Márquez, L., Rigo, P., & Le Sourne, H. (2019, October). Numerical crashworthiness analysis of a spar floating offshore wind turbine impacted by a ship. In Developments in the Collision and Grounding of Ships and Offshore Structures: Proceedings of the 8th International Conference on Collision and Grounding of Ships and Offshore Structures (ICCGS 2019), 21-23 October 2019, Lisbon, Portugal (p. 85). CRC Press.

Europe, W. (2017). Floating offshore wind vision statement. Wind Europe: Brussels, Belgium.

Fang, H., Mao, Y., Liu, W., Zhu, L., & Zhang, B. (2016). Manufacturing and evaluation of large-scale composite bumper system for bridge pier protection against ship collision. composite Structures, 158, 187-198.

Furnes, O., & Amdahl, J. (1980). Ship collisions with offshore platforms. Intermaritec'80.

GL, L. B. D. (2015). Qualification of innovative floating substructures for 10MW wind turbines and water depths greater than 50m.

Hallquist, J. O. (2006). LS-DYNA theory manual. Livermore software Technology corporation, 3, 25-31.

Han, Z., Li, C., Deng, Y., & Liu, J. (2019). The analysis of anti-collision performance of the fender with offshore wind turbine tripod impacted by ship and the coefficient of restitution. Ocean Engineering, 194, 106614.

Hao ertong, Liu yingzhou, Liu chungguang. Damage and dynamic response analysis of offshore wind turbine with monopile foundation subjected to ship impact.Journal of Dalian University of Technology.2014.09,vol.54,No.5

Hao, E., & Liu, C. (2017). Evaluation and comparison of anti-impact performance to offshore wind turbine foundations: Monopile, tripod, and jacket. Ocean engineering, 130, 218-227.

IEA (2020), Offshore Wind, IEA, Paris. https://www.iea.org/reports/offshore-wind

Jiang, H., & Zhao, J. (2015). Calibration of the continuous surface cap model for concrete. Finite Elements in Analysis and Design, 97, 1-19.

John O., H. (2006). LS-DYNA Theory Manual—March 2006.

Kvitrud, A. (2011, January). Collisions between platforms and ships in Norway in the period 2001-2010. In International Conference on Offshore Mechanics and Arctic Engineering (Vol. 44342, pp. 637-641).

Le Sourne, H., Barrera, A., & Maliakel, J. B. (2015). Numerical crashworthiness analysis of an offshore wind turbine jacket impacted by a ship. Journal of Marine Science and Technology, 23(5), 694-704.

Liu, C., Hao, E., & Zhang, S. (2015). Optimization and application of a crashworthy device for the monopile offshore wind turbine against ship impact. Applied Ocean Research, 51, 129-137.

Malvar, L. J., & Ross, C. A. (1998). Review of strain rate effects for concrete in tension. ACI Materials Journal, 95, 735-739.

Mander, J. B., Priestley, M. J. N., & Park, R. (1988). Observed stress-strain behavior of confined concrete. Journal of structural engineering, 114(8), 1827-1849.

Martin Rypestøl. (2020). Analysis of Floating offshore wind turbine subjected to ship collisions. Master's Thesis, Norwegian University of Science and Technology, June 2020

Minorsky, V. U. (1958). An analysis of ship collisions with reference to protection of nuclear power plants (No. NP-7475). Sharp (George G.) Inc., New York.

Moan, T., Amdahl, J., & Ersdal, G. (2019). Assessment of ship impact risk to offshore structures-New NORSOK N-003 guidelines. Marine Structures, 63, 480-494.

Moulas, D., Shafiee, M., & Mehmanparast, A. (2017). Damage analysis of ship collisions with offshore wind turbine foundations. Ocean Engineering, 143, 149-162.

N-003, NORSOK (2017). Actions and action effects. 3rd ed. NORSOK STANDARD.

Offshorewind.biz. (2016). https://www.offshorewind.biz/2016/05/26/three-rescued-after-fishing-boat-hits-wind-turbine-off-walney-island/

Offshorewind.biz. (2020). https://www.offshorewind.biz/2020/04/24/three-injured-after-ctv-hits-wind-turbine-at-german-offshore-wind-farm/

Papadopoulos, M. P., Apostolopoulos, C. A., Alexopoulos, N. D., & Pantelakis, S. G. (2007). Effect of salt spray corrosion exposure on the mechanical performance of different technical class reinforcing steel bars. Materials & design, 28(8), 2318-2328.

Pegalajar-Jurado, A., Bredmose, H., Borg, M., Straume, J. G., Landbø, T., Andersen, H. S., ... & Lemmer, F. (2018, October). State-of-the-art model for the LIFES50+ OO-Star Wind Floater Semi 10MW floating wind turbine. In Journal of Physics: Conference Series (Vol. 1104, No. 1, p. 012024). IOP Publishing.

Pire, T., Echeverry Jaramillo, S., Rigo, P., Buldgen, L., & Le Sourne, H. (2017). Validation of a simplfied method for the crashworthiness of offshore wind turbine jackets using finite elements simulations. Progress in the Analysis and Design of Marine Structures, 497-505.

Pire, T., Le Sourne, H., Echeverry, S., & Rigo, P. (2018). Analytical formulations to assess the energy dissipated at the base of an offshore wind turbine jacket impacted by a ship. Marine Structures, 59, 192-218.

Ramírez, L., Fraile, D., & Brindley, G. (2020). Offshore wind in Europe: Key trends and statistics 2019.

Sha, Y., Amdahl, J., & Liu, K. (2019). Design of steel bridge girders against ship forecastle collisions. Engineering Structures, 196, 109277.

Song, M., Jiang, Z., & Yuan, W. (2021). Numerical and analytical analysis of a monopile-supported offshore wind turbine under ship impacts. Renewable Energy, 167, 457-472.

Song, M., Shi, W., Ren, Z., & Zhou, L. (2019). Numerical study of the interaction between level ice and wind turbine tower for estimation of ice crushing loads on structure. Journal of Marine Science and Engineering, 7(12), 439.

Standard, B. (2004). Eurocode 2: Design of concrete structures—. Part 1-1: General rules and rules for buildings, 230.

Standard, N. (2007). NORSOK N-003, Actions and Action Effects.

Veritas, B. (2019). Classification and certification of floating offshore wind turbines.

Wind energy in Europe 2020 Statistics and the outlook for 2021-2025 https://windeurope.org/intelligence-platform/product/wind-energy-in-europe-in-2020-trends-and-statistics/

Wind energy in Europe: Outlook to 2020 September 2017

Yu, W., Müller, K., Lemmer, F., Bredmose, H., Borg, M., Sanchez, G., & Landbo, T. (2017). Public Definition of the Two LIFES50+ 10MW Floater Concepts. LIFES50+ Deliverable, 4.

Yu, Z., & Amdahl, J. (2018). A review of structural responses and design of offshore tubular structures subjected to ship impacts. Ocean Engineering, 154, 177-203.

Zhang, Y., Hu, Z., Ng, C., Jia, C., & Jiang, Z. (2021). Dynamic responses analysis of a 5 MW spar-type floating wind turbine under accidental ship-impact scenario. Marine Structures, 75, 102885.

Zhou, L., Ding, S., Song, M., Gao, J., & Shi, W. (2019). A Simulation of Non-Simultaneous Ice Crushing Force for Wind Turbine Towers with Large Slopes. Energies, 12(13), 2608.